UNIVERSITY OF BIRMINGHAM

MODEL BASED CONTROL FOR A MODERN AUTOMOTIVE DIESEL ENGINE

By

CHENG TAN

A thesis submitted to

The University of Birmingham

for the degree of

DOCTOR OF PHILOSOPHY

The University of Birmingham

School of Mechanical Engineering

August, 2015

ABSTRACT

The dynamic performance of a turbocharged diesel engine during transient operation has been studied in the present work. Based on the experimental results, a novel real-time control oriented diesel engine model was developed. In addition, an advanced fast predictive control approach was proposed and validated in a hardware-in-the-loop (HIL) simulation platform.

For appropriate analysis of data obtained from engine transient operation, four alternative automated filtering methods, namely fast Fourier transform (FFT), low-pass, linear and zero-phase filtering were implemented on the cycle-by-cycle in-cylinder pressure. Furthermore, the techniques to process instantaneous emission data and align the transient data from different analyzers were developed. In the experimental study, the effects of engine speed and exhaust gas recirculation (EGR) have been investigated through load increase tests at a constant engine speed between 1000 rpm to 2000 rpm with different EGR calibrations. The main findings, including spikes of pressure drop between the intake and exhaust manifold, drop of oxygen concentration and deteriorated emission behaviours are reported. In addition, the sensitivity of fuel properties on the effects of engine dynamic performance has been studied using hydrotreated vegetable oil (HVO) blends.

The control-oriented diesel engine model was developed in Simulink with a fixed simulation step. The model is capable of simulating the main engine parameters such as the oxygen concentration, EGR mass flow, intake air mass flow, maximum in-cylinder temperature and IMEP in both steady state and transient operation of engine performance. Three main parts,

the air path model, combustion model and dynamic emission behaviour model constitute the engine model. Due to the simple structure, the model can run as a real-time simulator for engine control strategy development, reducing the experimental time and cost on real engine testing.

The novel predictive control approach, model predictive control (MPC), was developed for EGR and variable-geometry turbocharger (VGT) control in the air system of a turbocharged diesel engine. The oxygen concentration oriented control was designed and implemented in the real-time engine model. Compared with the conventional PID control method, MPC presents a good tracking performance of reference values with a shorter response time. Additionally, a great potential for emission abatement is illustrated. The HIL simulation platform was developed to present the real-time capability of the model-based control strategy. Small differences of outputs response between the pure model and the actual control unit are found in the validation results, proving that the developed MPC control can be implemented in real vehicle application.

ACKNOWLEDGEMENT

First and foremost, I would like to give my great thanks to my supervisor Professor Hongming Xu for his guidance and encouragement throughout my PhD study. The support from my associate supervisor Professor Miroslaw L. Wyszynski is also appreciated. In addition, I would like to thank Professor Akbar Ghafourian for his great help and Ben Neaves from Jaguar Land Rover for his invaluable advice.

I acknowledge the support of Advantage West Midlands and European Regional Development Fund, Jaguar Land Rover and Shell Global Solutions. Without their equipments and financial supports, I could not finish my PhD study.

Great thanks go to the laboratory technicians - Carl Hingley, Jack Garrod, Lee Gauntlett and Peter Thornton - for their support with test facilities. I am also grateful to Dr. Arumugam Sakunthalai Ramadhas, Dr. Guoxiang Lu, Dr. Xiao Ma, Dr. He Ma, Dr. Fan Zhang, Dr. Dai Liu, Dr. Changzhao Jiang and Dr. Chongming Wang for their generous help and technical support. I also acknowledge the English writing support from Mrs. Janet Hingley.

Special thanks go to my friends and colleagues at the University of Birmingham: Jianyi Tian, Powen Tu, Daliang Jing, Haichun Ding, Ziman Wang, Soheil Zeraati Rezaei, Tawfik Badawy and Yunfan Zhang for their great supports in my study and social life.

Finally, I would like to express my sincere gratitude to my parents from the bottom of my heart for their unconditional support and encouragement. Last but not least, I want to give

my most special thanks to my fiancée Chen Peng. Her understanding and encouragement are the greatest motivation during my PhD study.

CONTENTS

LIST OF ABBREVIATIONS

ACD	Adaptive Critic Design
AFR	Air-Fuel Ratio
BSNOx	Brake Specific NOx
BSFC	Brake Specific Fuel Consumption
CFD	Computation Fluid Dynamics
CI	Compression Ignition
CLD	Chemi-Luminescence Detector
CO	Carbon Dioxide
COP	Conformity Of Production
COV	Coefficient Of Variation
CVT	Continuously Variable Transmission
DOC	Diesel Oxidation Catalyst
DPF	Diesel Particulate Filter
ECU	Engine Control Unit
EGR	Exhaust Gas Recirculation
F&E	Filling and Emptying
FFT	Fast Fourier Transform
FID	Flame Ionisation Detector
GDI	Gasoline Direct Injection
GHV	Gross Heat Value
HC	Hydrocarbon
HCCI	Homogeneous Charge Compression Ignition
HIL	Hardware-In-the-Loop
HR50	50% of the cumulative Heat Release occurs
HRmax	maximum Hear Release rate
HVO	Hydrotreated Vegetable Oil
IC	Internal Combustion
IMEP	Indicated Mean Effective Pressure

IVC	Intake Valve Close
LPV	Linear Parameter Varying
LTC	Low Temperature Combustion
MIL	Model-In-the-Loop
MIMO	Multi-Input-Multi-Output
MPC	Model Predictive Control
MVM	Mean-Value Model
NARMAX	Nonlinear AutoregRessive Moving Average with eXogenous
PCCI	Premixed Charged Compression Ignition
PEM	Prediction Error Minimization
PM	Particulate Mass
PMP	Particle Measurement Programme
PMT	Photo Multiplier Tube
PN	Particle Number
ppm	parts per million
PRBS	Pseudo-Random Binary Sequence
QP	Quadratic Program
RCCI	Reactivity Controlled Compression Ignition
RME	Rapeseed Methyl Ester
RoHR	Rate of Heat Release
SCR	Selective Catalytic Reduction
SI	Spark Ignition
SME	Soy Methyl Ester
TDC	Top Dead Centre
TWC	Three-Way Catalysts
VGT	Variable-Geometry Turbocharger
VPR	Volatile Particle Remover
VVT	Variable Valve Timing
WLTP	Worldwide Harmonized Light Vehicles

LIST OF SYMBOLS

h_0	Specific stagnation enthalpy
k	Control interval
$\dot{m}_{in}$	Mass flow through intake valve
$\dot{m}_{out}$	Mass flow through exhaust valve
m_{φ}	Fuel injected amount per cycle
n_y	Number of plant output variables
p	Prediction horizon
p_{cr}	Critical pressure where the flow achieves a sonic condition
p_{im}	Intake manifold pressure
p_{em}	Exhaust manifold pressure
$p_{m\varphi}$	Fuel mean effective pressure
r_c	Compression ratio
s_j^y	Scale factor for j^{th} plant
u	Internal energy
w	Measured disturbance
$w_{i,j}^y$	Tuning weight for j^{th} plant output at i^{th} prediction horizon step
$\hat{y}$	Simulated model output
$\bar{y}$	Mean of the measured data sequence
z_k	Optimization problem decision
H_l	Lower heating value
I_p	Pump cell current
$J(\cdot)$	Cost function for optimization
L	Rod
M	Molar mass of intake air

P	In-cylinder pressure
$\dot{Q}_{ht}$	Heat Transfer
R	Ideal gas constant
$T_{\max}$	Maximum in-cylinder temperature
V	Instantaneous volume
V_c	Clearance volume
V_d	Cylinder displacement volume
X_{Oim}	Oxygen mass fraction in the intake manifold
X_{Oem}	Oxygen mass fraction in the exhaust manifold
$[N_2]_e$	Equilibrium concentration of nitrogen
$[NO]$	Species concentration of NO
$[O_2]_e$	Equilibrium concentration of oxygen
ϕ	EGR valve position
γ	Specific heat capacity ratio
λ	Stoichiometric air-fuel ratio
η_e	Combustion efficiency
θ	Current crank angle
ω_e	Engine speed
ω_t	Turbocharger speed
$\psi(\cdot)$	Flow function
$\| \ \|$	Euclidean distance

LIST OF FIGURES

LIST OF TABLES

LIST OF PUBLICATIONS

1. **Tan, C**., Xu, H., Ma, H., Tian, J. et al., "A Study of Methodology for the Investigation of Engine Transient Performance," SAE Technical Paper 2014-01-2714, 2014, doi:10.4271/2014-01-2714.

2. **Tan, C**., Xu, H., Ma, H., and Ghafourian, A., "Investigation of VVT and spark timing on combustion and particle emission from a GDI Engine during transient operation," SAE Technical Paper 2014-01-1370, 2014.

3. **Tan, C**., Xu, H., Shuai, S., Ghafourian, A. et al., "Investigation on Transient Emissions of a Turbocharged Diesel Engine Fuelled by HVO Blends," SAE Int. J. Engines 6(2):2013, doi:10.4271/2013-01-1307.

4. **Tan, C**., Xu, H., A. Ramadhas, et al., "Effects of EGR Dynamic Behaviour During Transient Operation on Performance and Emission of a Diesel Engine" Prepared to submit.

5. **Tan, C**., Xu, H., Ma, H., et al., "Dynamic emission model for on-board control of turbocharged diesel engine" Prepared to submit.

CHAPTER 1 INTRODUCTION

1.1 Background

After the successful application of internal combustion (IC) engines by Nikolaus Otto (1876) and his counterpart Rudolf Diesel (1892), IC engines have become the most important power source for automotives during the last 140 years (Alagumalai 2014). Although the development of alternative fuel vehicles including electric, hybrid and solar powered cars has been rapid during this recent decade, some critical issues such as the limited power storage and high costs still hinder their wider application (Hannan, Azidin, and Mohamed 2014). Meanwhile, many emerging technologies are being developed and implemented on modern automotive engines to further improve the energy conservation efficiency and reduce the emissions. Accordingly, IC engines are forecasted to remain the main power plant of vehicles in the 21st century (Gurney, Ahammad, and Ford 2009).

1.1.1 Challenges of Fuel Economy and Emission Legislation

With the growth of the global population and the car ownership rate, there is a rising concern about the increasing energy demand and environmental pollution from vehicles. As shown in Figure 1-1, it is estimated that the total demand for road transportation energy will increase steadily in the next two decades. Even though the share of new energy supplies,

especially biofuels, shows continuous growth, fossil fuels will still be used by the majority. Considering that fossil fuels are non-renewable resources, in order to meet the growing energy demand, improving the fuel economy becomes an essential issue for the automotive industry.

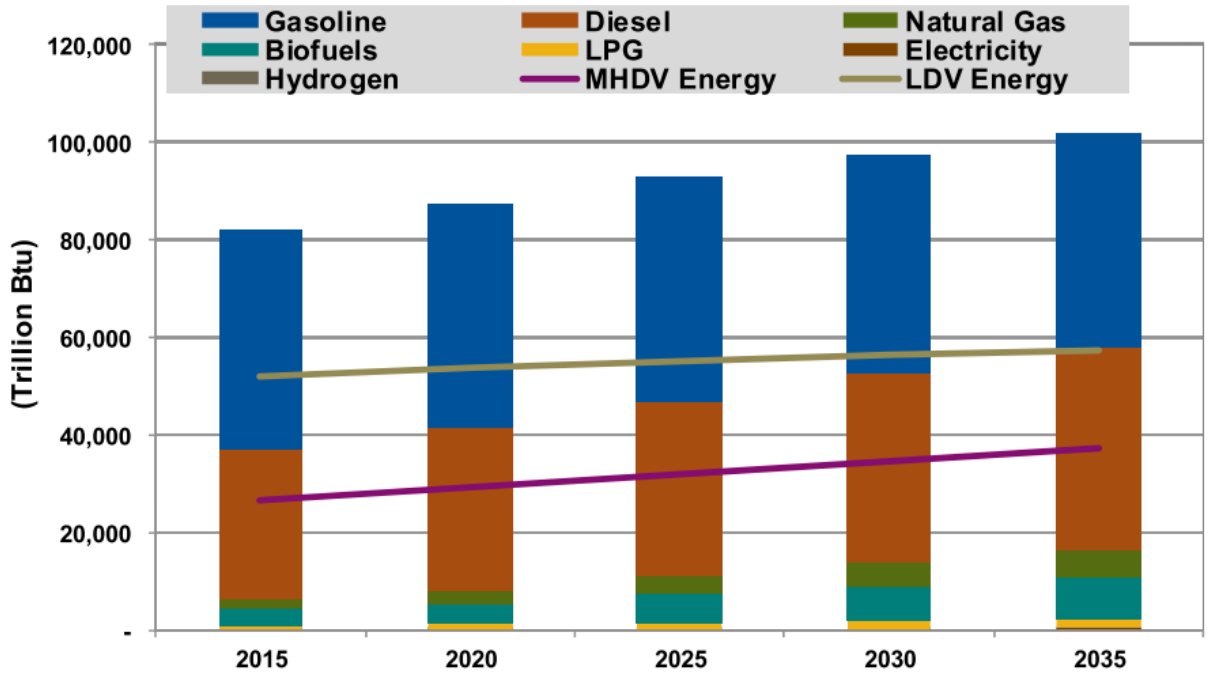

Figure 1-1 Annual Road Transportation Sector Energy Consumption by Fuel Type, Global Market (Navigant Research 2014)

In addition, the emissions from vehicles have drawn much attention from the general population and governments in recent years. The European Union introduced its first emission regulation in 1992 which included carbon dioxide (CO), hydrocarbon (HC), nitrogen oxide (NOx) and particulate matter (PM). As the concerns about the vehicle exhaust gas increase, the standard has become more and more stringent. The detailed EU emission regulation for diesel passenger cars is listed in Table 1-1. It is observed that each item of emissions has been largely reduced, i.e. the particulate matter limit in Euro 6 decreased

over 96% compared with that in Euro 1. Apart from the mass-based limit, the particle number limit was proposed in Euro 5b, elaborating the regulation of particulate matter.

Table 1-1 European Emission Regulation for Diesel Passenger Cars

Stage	Date	CO	HC+NOx	NOx	PM	PN
		g/km				#/km
Euro 1†	1992.07	2.72(3.16)	0.97(1.13)	-	0.14(0.18)	-
Euro 2,IDI	1996.01	1.0	0.7	-	0.08	-
Euro 2, DI	1996.01	1.0	0.9	-	0.10	-
Euro 3	2000.01	0.64	0.56	0.50	0.05	-
Euro 4	2005.01	0.50	0.30	0.25	0.025	-
Euro 5a	2009.09	0.50	0.23	0.18	0.005	-
Euro 5b	2011.09	0.50	0.23	0.18	0.005	6.0×10^{11}
Euro 6	2014.09	0.50	0.17	0.08	0.005	6.0×10^{11}
† Values in brackets are conformity of production (COP) limits						

Source: https://www.dieselnet.com/standards/eu/ld.php

Traditionally, the study of engine efficiency and emission behaviour has focused on the steady-state performance. However, the majority of driving consists of engine transient operation and the fuel economy and exhaust emissions during transient conditions are much worse compared with those in the steady state (Constantine D. Rakopoulos and Giakoumis 2009a). As a result, the new European driving cycle (NEDC) as a representative cycle is designed to simulate driving scenarios and test the emissions' level. In addition, a new driving cycle called worldwide harmonized light vehicles test procedures (WLTP) is being developed and is projected to be implemented in the near future. It will cover all possible driving situations and be much more aggressive compared with the NEDC; it

proposes a higher requirement for automotive manufacturers to pass the standard (Tutuianu et al. 2013). Accordingly, it is important to further research the potential of efficiency improvement and emission abatement for internal combustion engines, especially during transient operation.

1.1.2 Development of Diesel Engine Technologies

The diesel engine has been widely used in ground vehicle applications due to its high efficiency and power output. Compared with the early diesel engines, the modern counterparts are much smaller, lighter and quieter through the remarkable efforts of many generations of researchers and engineers. As mentioned in the last section, the primary challenges for IC engines now are the increasing demand for fuel economy and the stringent emission standards. Over the past ten years, a tremendous growth in the development of advanced technologies has been implemented in diesel engines.

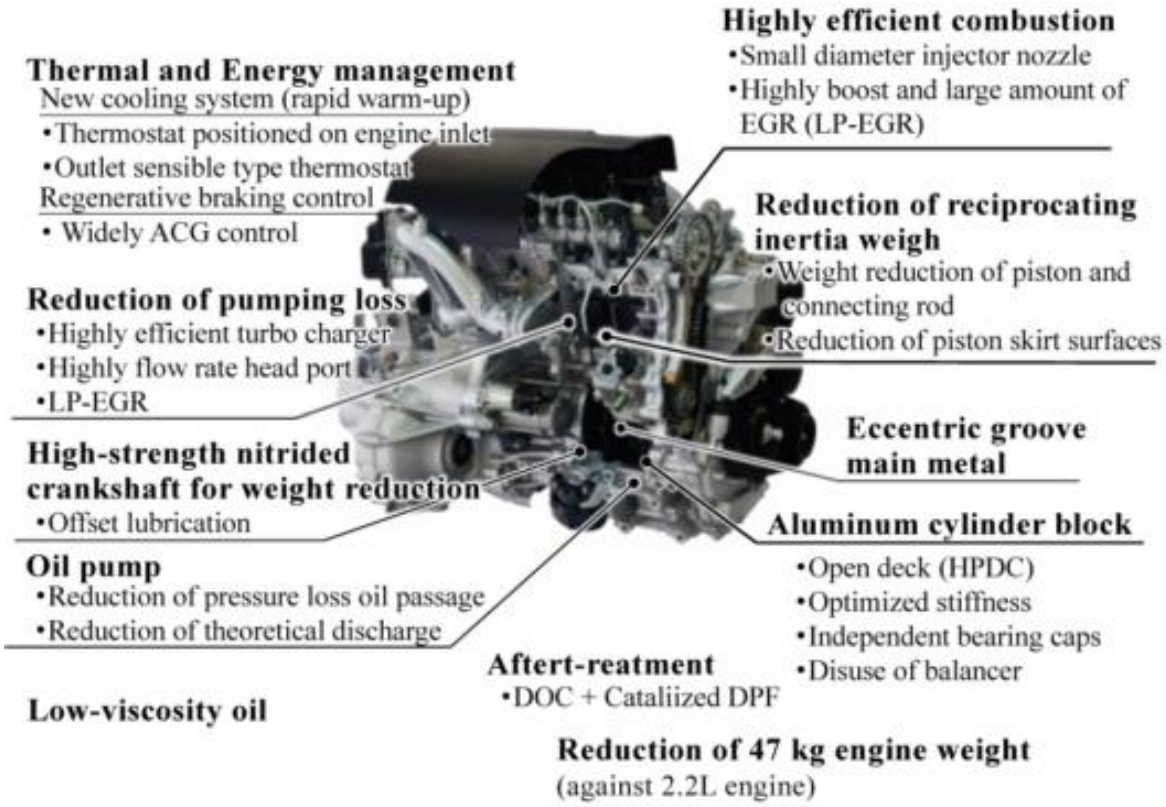

Figure 1-2 Key Technologies for Downsizing a Diesel Engine (Nishio et al. 2013)

Figure 1-2 shows a new generation of a downsized diesel engine featuring a variety of technologies. The high pressure common rail injection system with small diameter injector nozzles contributes to the highly efficient combustion. The dual EGR system consisting of a high pressure loop EGR (HP-EGR) and low pressure loop EGR (LP-EGR) provides the low pumping loss and NOx reduction simultaneously. The advanced turbocharger is utilized to raise the charging efficiency; thereby improving the fuel economy. As for the exhaust after-treatment system, the diesel oxidation catalyst (DOC) is capable of reducing over 90% HC plus CO and the DPF can decrease more than 95% PM and PN (Tim Johnson 2008). Combining these technologies, a diesel engine can become rather clean and highly efficient. Meanwhile, to control the diesel engine with more and more components and an

increasingly sophisticated structure, a powerful engine control unit (ECU) is being developed and approaches to optimize the control of engine parameters are required.

1.1.3 Diesel Engine Modelling and Control

Mathematical models have been developed and utilized to analyse the working process of IC engines for a long time. The rapid development of modern computers largely increases the computational capability and promotes the wide application of engine modelling. In addition, as the diesel engine continuously increases in complexity with a proliferation of engine sensors and control actuators, the engine modelling can not only facilitate the engine performance investigation and save the experimental costs, but also guide the development of engine control strategies (C. M. Atkinson et al. 2009). As shown in Figure 1-3, with the evolution of emission legislations and the emerging control technologies, a variety of modelling techniques have been proposed. Generally, the computation cost and simulation accuracy is a trade-off (Millo, Rolando, and Andreata 2011); as a result, the designation of modelling techniques is dependent on the specific sub-system structure and purpose.

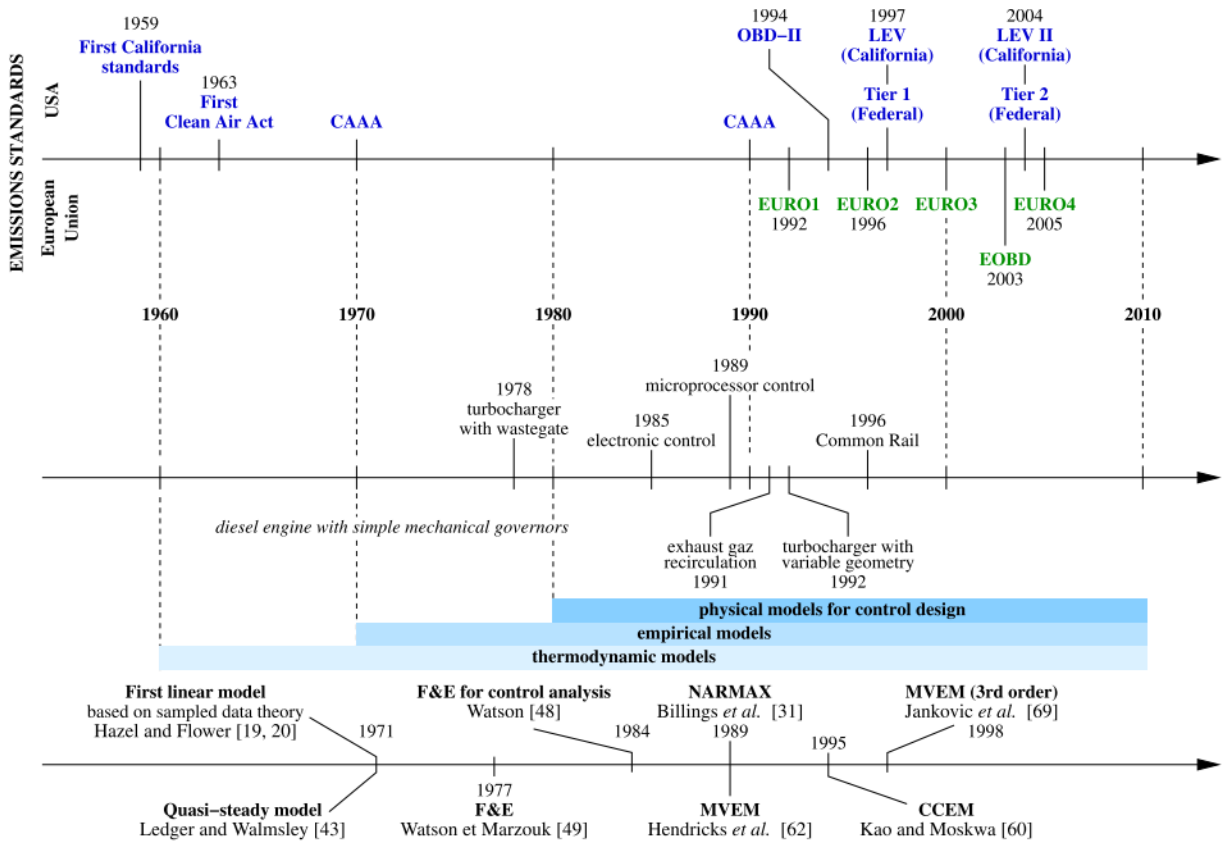

Figure 1-3 From top to bottom: Evolution of Regulations, Diesel Engine Control Technologies, Modelling Trends and Evolution of Modelling Techniques for Control (Grondin et al. 2004)

Meanwhile, with the increase of engine complexity, the technical demand for engine control has been greatly increased. Table 1-2 lists the control parameters of diesel engines in recent generations. It is clearly shown that the number of control parameters is growing and the proper control of modern diesel engines is critical and difficult. Many novel control strategies such as fuzzy logic control, neural network control and model predictive control have been developed for diesel engines (García-Nieto et al. 2008) (Omran, Younes, and Champoussin 2009) (Black et al. 2010b). However, there is a gap between the research and the complete application onto real engines due to various limitations. In other words, it is important to develop an approach to implement an advanced control strategy in diesel engine control.

Table 1-2 Diesel Engine Control Degree of Freedom (C. M. Atkinson et al. 2009)

Year	Number of Actuators	Description of Independent Control Parameters
2001	1	Injector valve
2004	3	Injector valve EGR valve VGT
2007	6	2 Injector valves EGR valve VGT Inlet throttle HC doser
2010	7	2 Injector valves EGR valve Turbo-compound engagement Inlet throttle HC doser Urea doser
2015+	10+	2 Injector valves EGR valve Turbo-compound engagement Inlet throttle HC doser Urea doser VVT

Furthermore, the difficulty of transient engine control has dramatically increased due to the growth of engine control parameters and their complex interaction. It is reported that a conventional control method, such as PID control, has met its limitations with a highly inter-coupled complicated air system (Anderson et al. 2012). Thus, there is a need to realize a better engine transient performance with the new control methodology.

1.2 Objectives and Approaches

In this study, a turbocharged modern V6 diesel engine equipped with a common rail injection and EGR cooling system was tested. The main purpose of the research is to investigate the engine dynamic performance during transient operation and develop an advanced fast predictive control approach based on a novel real-time engine model. To achieve the research objectives, the primary approaches are listed below:

- Developing the techniques for appropriate post-processing of experimental data obtained from engine transient operation.
- Conducting experimental study of dynamic performance on a turbocharged diesel engine with varied test sequences and different engine calibrations.
- Constructing a control-oriented real time engine model with basic physical insight and simple structure based on the dynamic experimental data.
- Implementing the MPC in the air system of a diesel engine and validating the control strategy on a new HIL simulation platform.

1.3 Thesis Outline

This thesis is divided into eight chapters. A summary of each chapter is presented.

Chapter 1 - Introduction

This chapter states the background and motivation of the research. Also, a brief introduction of approaches in the study is given.

Chapter 2 - Literature Review

The literature relevant to the study is reviewed in this chapter. Firstly, a review of the development in modern diesel engines is discussed. Next, the previous research on the system delay features and deteriorated emission behaviour during engine transient operation is presented. Furthermore, the representative control-oriented modelling approaches and emerging control strategies for diesel engines are discussed. Finally, the application of HIL on engine control is reviewed.

Chapter 3 - Development of the Experimental System

The experimental system used in this study is introduced in this chapter. Detailed information about the turbocharged diesel engine is given and the set up of the engine operating system is described. Also, the experimental test facilities for engine performance measurement are introduced.

Chapter 4 - Development of Methodology for Engine Transient Analysis

Alternative automated approaches to process the in-cylinder pressure and related combustion parameters for engine transient operation are proposed and compared. Detailed methods to process the instantaneous emission data, compensate for the analyser's delay and aligning the transient data is developed.

Chapter 5 - Analysis of Diesel Engine Transient Operation

The dynamic performance of a turbocharged diesel engine is investigated. The specific effects of gas exchange process during transient operation on engine combustion and emission behaviour are discussed at varied engine speeds and calibrations with conventional diesel and alternative fuel.

Chapter 6 - Real-time Diesel Engine Modelling

This chapter introduces the modelling approaches for the real-time control-oriented diesel engine; which include the air system, combustion and dynamic emission model. The validation results and analysis are also given.

Chapter 7 - Model-based Fast Predictive Control

The development of a model predictive control approach applied on the air system of a diesel engine is presented. The oxygen concentration oriented control is proposed and compared with conventional EGR rate; MPC and PID control are also compared and analysed. Finally, the validation of the control strategy is conducted on a HIL simulation platform.

Chapter 8 - Conclusions and Future Work

This chapter summarises the main findings and achievements in this research. Finally, some recommendations for future work are provided.

CHAPTER 2 LITERATURE REVIEW

The aim of this chapter is to review the literature which is relevant to the study in this thesis. The scope of discussion covers major developments in modern diesel engines, transient operation investigation, control-oriented modelling, engine control strategies and approaches to HIL simulation.

2.1 Modern Diesel Engines

Compression ignition (CI) engines were invented by Rudolf Diesel in 1895 and have become the dominant powertrain in heavy and light duty vehicles. Compared with their spark ignition (SI) counterparts, diesel engines have the significant advantage on thermal efficiency due to their higher compression ratio and fuel lean operation. In addition, incremental innovations in engine combustion, emissions abatement and input fuels have resulted in sophisticated but increasingly efficient and clean, modern diesel engines (Bonilla et al. 2014). Four main categories of the modern diesel engine development will be introduced respectively.

2.1.1 Gas Exchange Process

In four-stroke cycle engines, the gas exchange process involves the intake and exhaust, which are to remove the burned gases and admit the charge for the next cycle (Heywood 1988). To maximize the induction of air and retain the mass within the cylinder, new technologies are developed and applied.

Turbocharging, as one approach to boost the intake air through a compressor driven by an exhaust gas turbine, has been commonly used in modern diesel engines (Stone 1999). The pressurised air at the inlet increases the mass flow rate of air; thereby allowing the corresponding augmentation of the fuel flow rate and enhancing the power output. To suit the wide range of engine operation points with varied boost pressure, VGT have been designed, which can regulate the exhaust gas by using pivoted nozzle vanes. 'Ultra boost', proposed by Bath University, is reported to demonstrate a 35% reduction in fuel consumption by extremely boosting the intake air pressure (Turner et al. 2014). Also, Chadwell and Walls proposed a new kind of turbocharger, SuperTurbo, which was coupled with a continuously variable transmission (CVT) and able to act as a supercharger at low engine speed (Chadwell and Walls 2010).

Furthermore, a variable valve timing (VVT) mechanism, the process of varying the timing of valve lift events, has been more and more applied to diesel engines (Hansen, Kyritsis, and Lee 2009). Facing the increasingly stringent emission legislation and high fuel economy demand, diesel engines are required to precisely control the air charge in the mass flow rate and pressure. VVT can largely improve the compromises of valve timing in high engine

speed versus low engine speed and full load versus part load. In addition, significant emission reduction was realized by employing low temperature combustion (LTC) with the VVT technique (Yutaka Murata et al. 2008) (Y. Murata et al. 2006).

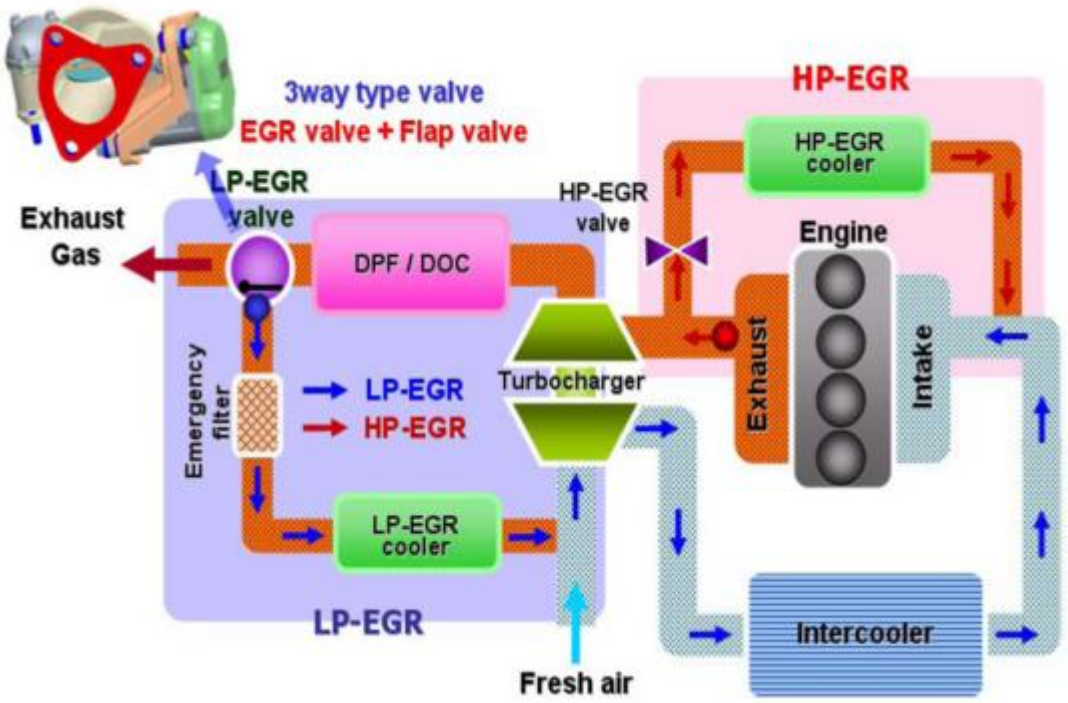

Figure 2-1 **Schematic of Dual Loop EGR System**(Nam, Yu, and Cho 2011)

EGR is in widespread use in diesel engines for NOx emission reduction. By introducing a certain fraction of exhaust gases into the intake manifold, some O_2 in the intake air is replaced by CO_2 or O_2, resulting in lower flame temperature and a significant reduction in NOx (Ladommatos, Abdelhalim, and Zhao 2000). However, the application of EGR causes a particulate emission penalty, an increase of specific brake fuel consumption and the debasement of lubrication oil and engine durability (Maiboom, Tauzia, and Hétet 2008) (Benajes et al. 2008) (Jacobs, Assanis, and Filipi 2003). Accordingly, many efforts have been made to solve the issue. Akihama used a high EGR rate under stoichiometric condition to reduce the particulate and NOx emissions simultaneously (Akihama et al. 2001). Also, a dual

loop EGR system (low pressure EGR and high pressure EGR) was proposed as illustrated in Figure 2-1. A part of the exhaust air is made to flow back to upstream of the turbocharger as a supplement for high pressure EGR. The addition of low pressure EGR provides high flexibility in the air path and has presented improvement of fuel economy and emissions (Nam, Yu, and Cho 2011) (Heuwetter et al. 2011) (Yunyu et al. 2014).

2.1.2 Combustion Process

At the end of the compression stroke, the combustion process is initiated by the injection of liquid fuel and its spontaneous ignition after atomization and vaporization. In typical diesel combustion, the start is determined by the injection timing; the premixed combustion occurs at the local fuel-air mixture with a high equivalence ratio after a small period called ignition delay; diffusive combustion follows at the spray periphery. Emerging technologies are being investigated to increase the thermal efficiency and abate emissions.

The common rail system features a high-pressure fuel rail supplying individual solenoid valves. It allows precise control of injection pressure, fuel injected quantity and injection timings while achieving multiple injections within one cycle (Carlucci et al. 2003). In a review of Wolfgang's work, the experiment showed the possibility to improve the emissions by varying fuel injection pressure and realizing a pilot injection (Boehner and Hummel 1997). Generally, higher injection pressure results in small spray droplets and shorter injection periods, which improve the fuel atomization and provides more efficient utilization (C. Park, Kook, and Bae 2004) (Jindal et al. 2010). The pilot injection increases the temperature and pressure of the mixture in the combustion chamber; thereby shortening the ignition delay

of the main injection and reducing the fraction of fuel burned in the premixed phase (Mancaruso, Merola, and Vaglieco 2008). Meanwhile, the post injection (a small amount of fuel being injected after the main injection event) is reported to provide a high temperature late in the cycle and promote the soot oxidation (Dec and Kelly-Zion 2000).

Also, different combustion strategies such as homogeneous charge compression ignition (HCCI), premixed charge compression ignition (PCCI) and reactivity controlled compression ignition (RCCI) have been studied by many researchers. HCCI is characterised by the fact that the mixture of air and fuel is compressed and auto-ignites at multiple sites within the combustion chamber (Yao, Zheng, and Liu 2009). Although a remarkable reduction of NOx and particulate matter can be achieved by large amounts of EGR with a lean air-fuel ratio (Iida and Igarashi 2000), HCCI engines have two main disadvantages. First, there is the difficulty in combustion phasing control since the auto-ignition is affected by many factors but no direct method for controlling the start of combustion is available (Stanglmaier and Roberts 1999). Additionally, they produce high HC and CO emissions due to low in-cylinder temperature, which is inevitable at a lean mixture and high EGR rate condition (Dec 2009). In PCCI combustion, fuel is injected early in the compression stroke, forming a long mixing period for a lean mixture and ignited by a second injection with a small amount of fuel (Lu, Han, and Huang 2011). The conditions for HCCI and PCCI combustion have been illustrated in Figure 2-2. Similar to HCCI, PCCI reduces the emissions primarily by lowering the combustion temperature. Accordingly, the operation range of PCCI is also limited with high THC and CO emissions. In addition, a new dual fuel engine combustion technology, RCCI, was proposed by Wisconsin University (Kokjohn et al. 2011). In the experiments, the utilization of gasoline and diesel can achieve remarkably high thermal efficiency and near

zero levels of NOx and particulate emissions (Splitter, Reitz, and Hanson 2010) (Splitter et al. 2011). However, due to the complicated fuel strategy, there is a long way for RCCI to go before it is applied in real vehicles, especially for transient operation.

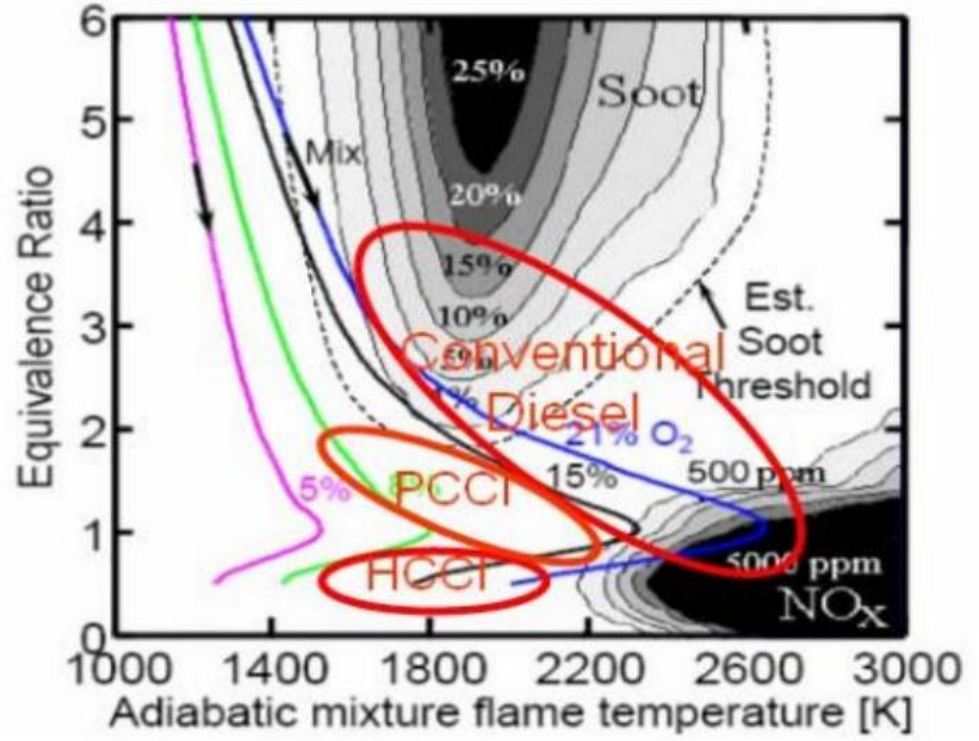

Figure 2-2 Diagram of ϕ-temperature Ranges for NOx and Soot Formation at the Regions for Conventional, HCCI and PCCI Combustion (Kim et al. 2008)

2.1.3 Emissions Control

One of the biggest challenges for modern diesel engines lies in the control of regulated emissions. Since a lean combustion mode is adopted in diesel engines at most operation ranges, a large amount of O_2 is contained in the exhaust gas. Thus, dissimilar to gasoline engines, three-way catalysts (TWC), the mature and effective approach which relies on a stoichiometric mixture to carry out both oxidation and reduction reactions, cannot be

applied in diesel engines (York et al. 2010). Various emission control strategies have been developed, which can be classified into two aspects: in-cylinder and exhaust after-treatment techniques.

For in-cylinder techniques, the representative methods are EGR and multiple injections with optimized control strategies on injection timings and quantities. The application of EGR has been introduced in section 2.1.1 discussing the gas exchange process. The main idea lies in lowering the combustion temperature and decreasing the intake oxygen concentration, two factors dominating the formation of NOx (Heywood 1988). The multiple injections and the new combustion modes realized by combining EGR and different injection strategies have been presented in the section on the combustion process. As shown in Figure 2-2, many researchers have employed various methods to achieve operation regions with low NOx and soot emissions (Natti and Henein 2012) (Choi et al. 2005) (Chiara and Canova 2009) (Cong et al. 2011).

In order to meet the increasingly stringent emission legislation, a number of exhaust after-treatment techniques have been developed to further reduce emissions. For modern diesel engines, the main issues of tailpipe emissions concern NOx and particulate matter. There is a trade-off between NOx and PM in most conditions and these two emissions are the primary goal of after-treatment techniques. The most common NOx after-treatment technology is selective catalytic reduction (SCR). The technology of SCR uses ammonia (NH_3) derived from the rapid hydrolysis of on-board urea as the reductant to reduce NOx. To achieve high NOx conversion efficiency, the system requires above 300^{o}C exhaust temperature and optimized hydrogen addition for various exhaust conditions (T V Johnson

2009). In the case of particulate emission abatement, the diesel particulate filter (DPF) and DOC are representative methods. DPF is efficient in reducing particulate matter (as high as 95-98%), both in mass and number (Tim Johnson 2008). The soot particles are trapped when the exhaust gases flow through the honeycomb structured device consisting of ordered square channels. Meanwhile, DOC is widely used to control diesel particulate emissions through oxidizing CO, HC and organic fraction (SOF) to harmless products (Ambs and McClure 1993).

2.1.4 Alternative Fuels

Alternative fuels are gaining more and more attention as sustainable energy supplies (Hansen, Kyritsis, and Lee 2009). In light of the environmental consideration and price rise of traditional fossil fuel, the European Union has issued a 10 percent minimum target for renewable energy consumption in the transportation sector by 2020. For diesel engines, most of the popular alternative fuels are derived from natural lipid feedstock such as algal, vegetable oils and animal fats, called biodiesel. Since various biodiesels from different feedstocks have varied fuel properties, numerous experiments have been conducted to test the performance, emissions and durability of engines fuelled with biodiesel or its blend.

Previous tests have shown that at full and partial loads, losses of engine power were observed ranging between 3% to 10%, mainly due to the lower gross heat value of combustion (GHV) of biodiesels (Kaplan, Arslan, and Sürmen 2006) (Çetinkaya et al. 2005). Also, many experimental studies on the fuel economy of biodiesel indicated that a small increase of brake specific fuel consumption (BSFC) was found and the increasing rate was

close to the reduction of the heating value (Canakci 2005) (Dai Liu 2014). For the emission behaviours, most results presented that biodiesel fuels had slightly increased NOx and the most common explanations are the advanced injection and increased injection pressure caused by higher bulk modulus and viscosity (Nabi, Akhter, and Shahadat 2006) (Lapuerta et al. 2005). Meanwhile, significantly reduced partide emissions were reported by most researchers (Monyem and H. Van Gerpen 2001) (Cardone et al. 2002) (Lapuerta et al. 2005). The reasons for this were investigated and summarized: the oxygen content of biodiesel fuels contributed to convert carbon to CO or CO_2 rather than soot (Frijters and Baert 2006); aromatics which are considered as the soot precursors are not contained in biodiesel fuels (Lapuerta, Armas, and Ballesteros 2002); the earlier start of combustion due to the high cetane number or advanced injection, which promotes the soot oxidation with a longer high-temperature period in the combustion (Cardone et al. 2002); the lower final boiling point of biodiesel fuels caused better vaporization (Lapuerta, Armas, and Ballesteros 2002).

2.2 Diesel Engine Transient Operation

Engine steady-state operation has been widely investigated and calibrated with the development of the techniques mentioned above and the mature engine calibration methods. However, the majority of an automotive engine operating pattern is transient operation and the exhaust emissions during transient periods, such as cold start, acceleration and deceleration, are a primary source of pollution. This problem has attracted the attention of engine researchers and designers in recent years. Detailed measurement and analysis of engine behaviour under transient operating conditions are required to improve engine calibration. The performance and emissions of turbocharged diesel engines

under transient operation are significantly worse than those under steady conditions. Higher particulate matter and HC emissions are produced because of the difficulties in optimizing the transient response of the intake, injection and combustion systems (Wijetunge et al. 1999). The system delay features and emission behaviours in transient operation are reviewed in the following sections.

2.2.1 System Delay in Transient Operation

The delay of air supply and engine power increase is the most notable issue for turbocharged diesel engines transient operation. The fundamental study was initially conducted by Watson who compared a naturally aspirated engine with a turbocharged engine of the same displacement during rapid accelerations to full load, full speed conditions (Watson and Janota 1982). It was found that the fuel delivery responded rapidly but the boost pressure of the turbocharged engine built up slowly and the development of the air flow of both engines was close; thereby resulting in the transient torque deficit. Detailed measurement carried out by Catania also proved that the fuel injection system was able to instantaneously adapt to the new steady state position within a few cycles (Catania et al. 1996).

The causes of the system delay in transient operation have been investigated by many researchers and can be classified into three aspects: mechanical, thermal and fluid dynamic phenomena (Constantine D. Rakopoulos and Giakoumis 2009a). The friction losses and inertia of a turbocharger are the main mechanical factors; while the thermal contributor mainly indicates the heat transfer to the cylinder walls and exhaust manifold surfaces. The

detailed contributors of the system delay are illustrated in Figure 2-3. Although only a small amount of research has been reported on the improvement of the mechanical and thermal aspects, many researchers claimed that the delay from fluid inertia and EGR effects, which accounted for the primary role of the delay, could be reduced (Alberer and del Re 2009) (Yunyu et al. 2014). First, it was reported that the adoption of a VGT largely improved the engine transient response by closing down the vane aggressively; thereby accelerating the compressor and compensating for the effect of rotational inertia (Wijetunge et al. 1999) (Filipi, Wang, and Assanis 2001). Also, the optimal closed loop control of EGR was developed and proved its effectiveness in lower NOx emissions and equivalent PM emission levels during transient conditions (Yokomura et al. 2004).

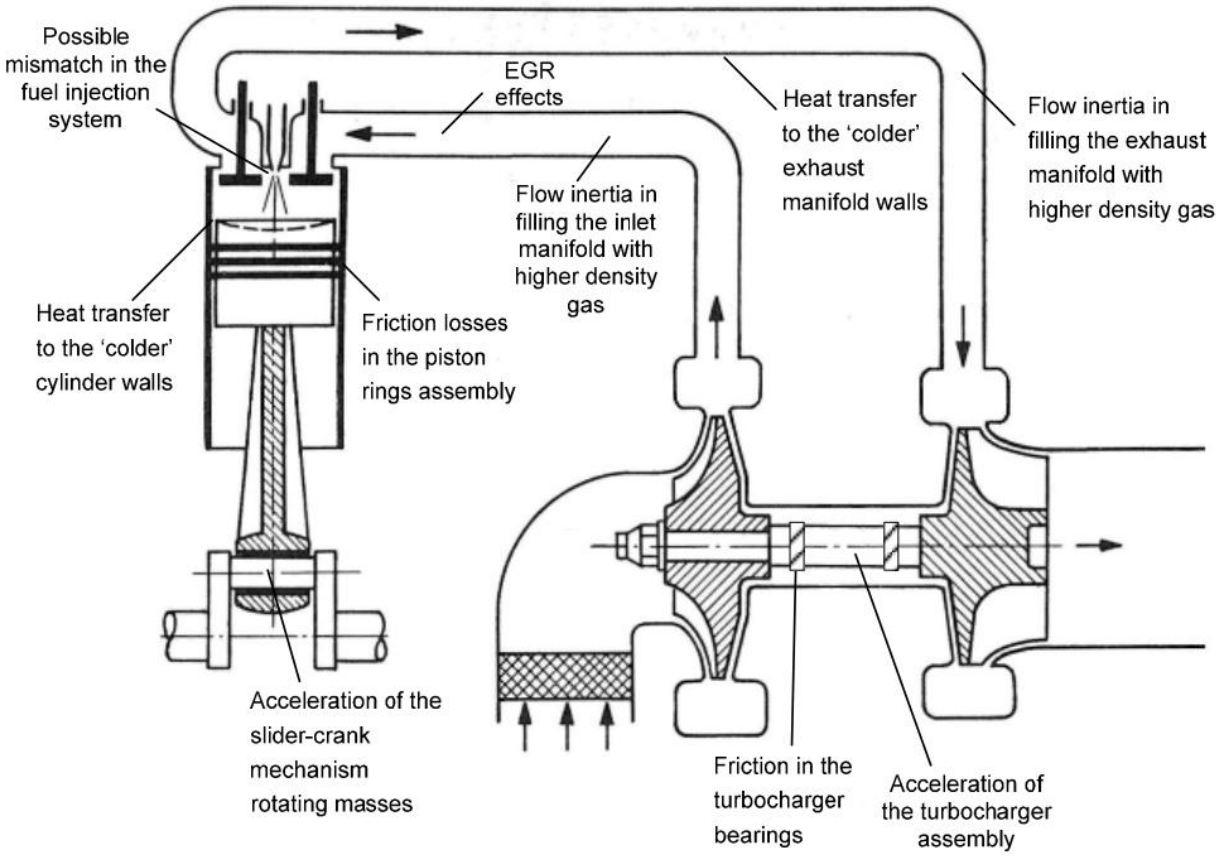

Figure 2-3 Schematic Illustration of the Main Contributions to the System Delay during Transient Operation of a Turbocharged Diesel Engine (Constantine D. Rakopoulos and Giakoumis 2009a)

2.2.2 Transient Emission Characteristics

Due to the system delay of a turbocharged diesel engine, gaseous and particulate emissions during transient operation have presented rather high values compared with those in a steady state (C.D. Rakopoulos and Giakoumis 2006). Research on the transient emission characteristics of a turbocharged engine initially was carried out by simulation and indirect measurement. Arcoumanis and Jou predicted the formation of NO based on the cylinder local temperature and the heat release rate which were derived from measured cylinder

pressure during transient operation (Arcoumainis and Jou 1992). Conventional slow response analyzers were used to measure transient emissions and then they were recovered by reconstruction techniques for analysis (Chan 1996). However, these methods were not convenient and the results were hard to prove.

Detailed research on transient emission characteristics has been made possible by the application of fast response exhaust gas analyzers. With the highly dynamic gas analyzers, even cycle-by-cycle emissions could be detected to study misfire during cold start (Davis and Peckham 2007). The load tip-in tests with different acceleration periods at constant engine speed were conducted and significant increases of both NOx and particulate emissions were observed when the ramp-up time became shorter (Hagena, Filipi, and Assanis 2010). Varied VGT settings were tested in full-load transient experiments and it was indicated that the opening of the VGT could lower the back pressure but not improve the emissions (Black et al. 2010a). In both speed transient and load transient tests, the rapid change in EGR and intake charge composition were primarily responsible for the transient emissions (Glewen et al. 2011). Specifically, as the load increases, the in-cylinder temperature rises due to more fuel being injected. The prolonged duration of diffusion combustion and oxygen deficiency caused by system lag contributes to the soot formation. Meanwhile, the EGR valve normally shuts rapidly to help boost the turbo, which results in an overshoot of NOx (Kang and Farrell 2010).

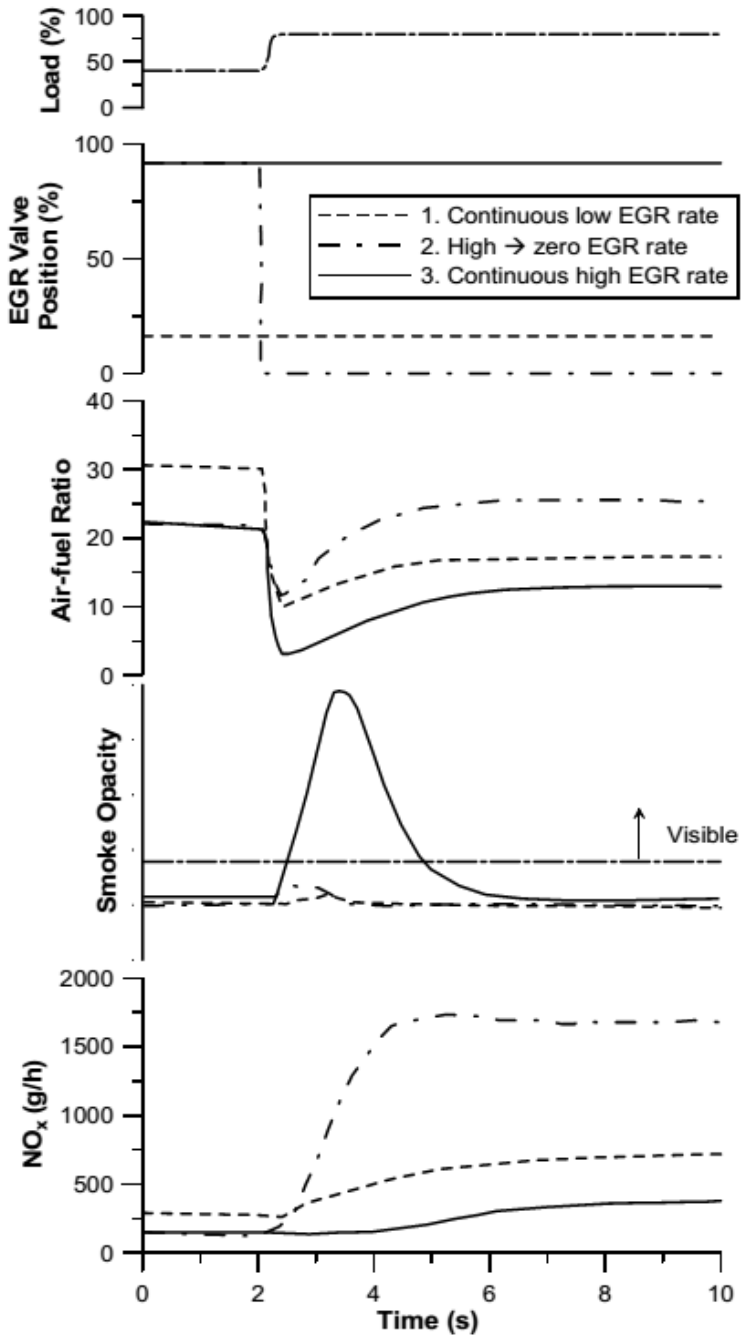

Figure 2-4 Typical Profiles of NOx and Smoke During Load Step Tests (Yokomura et al. 2004)

As shown in Figure 2-4, the different EGR strategies were compared and it was indicated that the air-fuel ratio was a key parameter to determine the emission behaviours. Also, the trade-off between NOx and particulate emissions still existed even during transient

operation (Yokomura et al. 2004). From the perspective of control, a better control of the air-fuel ratio is a promising approach to optimize the transient emissions.

2.3 Control-oriented Modelling of Diesel Engines

Engine modelling has become a critical tool in the engine control design due to the increasing complexity of diesel engines. For various modelling approaches, although computation fluid dynamics (CFD) multi-dimensional modelling normally provides the best accuracy, the high cost of computation hinders its application for engine control purposes (Ma, Xu, and Wang 2011); therefore CFD modelling is not included in this section. A number of representative diesel engine modelling approaches, classified as thermodynamic models, empirical models and semi-physical approximate models are introduced and compared.

2.3.1 Thermodynamic Models

The thermodynamic model is based on equations of energy and mass conservation. In order of complexity, three types of modelling techniques: (i) quasi-steady, (ii) filling and emptying and (iii) multi-zone models are classified (Heywood 1988).

Quasi-steady Models

Quasi-steady models have been applied on engine components of which transient responses can be assumed equal to a sequence of steady points. This technique represents the engine thermodynamics by basic crankshaft and turbocharger dynamics and empirical

relations (Grondin et al. 2004). The method was proposed by Ledger who simulated the brake torque of a turbocharged diesel engine based on a simple function of fuel injection quantity per cycle m_f and engine speed N (Ledger, Benson, and Furukawa 1973):

$$bmep = k_1 m_f - k_2 N \qquad \textbf{Equation 2-1}$$

Where k_1 and k_2 indicate constants obtained from experimental data.

Although the structures are simple, this method has been widely used in the simulation of engine power, air mass flow and exhaust temperature (Filipi, Wang, and Assanis 2001). It was found that combustion parameters from one engine cycle during transients could be considered as quasi-steady (Assanis et al. 2000). Apart from the gas flow and combustion, quasi-steady models were used to estimate the emissions on the basis of engine speed and load and provided a rough guidance of trends (Kirchen, Obrecht, and Boulouchos 2009).

In brief, the quasi-steady model is suitable for real-time simulation due to its short running time. However, the accuracy of a quasi-steady model is low when the system is complex and intermediate processes are oversimplified. The other main disadvantage lies in its poor compatibility. It is difficult to transpose one quasi-steady model to other engines since the empirical relation in the model strongly relies on the experimental data.

Filling and Emptying Method

In order to overcome the drawbacks of quasi-steady models, diesel engine models with the filling and emptying (F&E) method, also called zero-dimensional models, were developed

(Watson and Marzouk 1977). In these models, the engine components are treated as a series of control volumes with the assumption that the gas mixture in each volume is at uniform state. Accordingly, the detailed process such as fuel droplet vaporization and spatial variation of mixture are ignored (Kumar, Kumar Chauhan, and Varun 2013). The schematic of a typical filling and emptying method model of in-cylinder simulation is shown in Figure 2-5, which involves heat transfer $\dot{Q}_{ht}$; mass flow through intake and exhaust valve $\dot{m}_{in}$ and $\dot{m}_{out}$; work of the piston W_{pist} and combustion heat release Q_{combt}. The model is able to simulate the combustion process based on the first law of thermodynamics (Watson and Janota 1982):

$$\frac{dT_{cyl}}{dt} = \frac{\left(\sum\left[\frac{dQ}{dt}\right]_{ht} + \sum\left(h_0 \frac{dm}{dt}\right)_{in} - \sum\left(h_0 \frac{dm}{dt}\right)_{out} + \frac{dQ_{comb}}{dt} - u\frac{dm}{dt}\right)\frac{1}{m} - \frac{RT_{cyl}}{V_{cyl}}\frac{dV_{cyl}}{dt} - \frac{\partial u}{\partial \phi}\frac{d\phi}{dt}}{\frac{\partial u}{\partial T_{cyl}}}$$

Equation 2-2

Where u represents the internal energy per unit mass of gas and h_0 indicates the specific stagnation enthalpy.

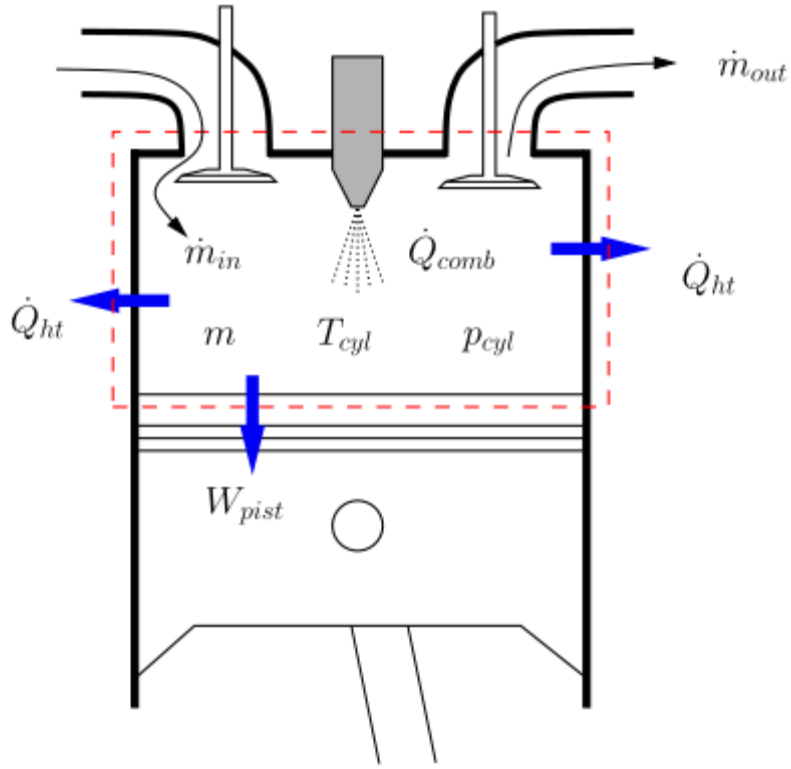

Figure 2-5 Schematic of the Filling and Emptying Method Model of an Engine Cylinder

Also, the F&E method has been widely employed for engine manifolds modelling (C D Rakopoulos, Michos, and Giakoumis 2005) (Chung, Kim, and Sunwoo 2005) (August et al. 2008) (Wahlstrom and Eriksson 2011). In these models, the manifold volume and heat loss from the surface of the manifold could be considered. Although the effect of pressure wave was ignored, it was reported that most models showed acceptable accuracy at common diesel engine operating speeds.

Mean-value Models

Mean-value models (MVM) were proposed based on the filling and emptying method and quasi-steady models (Kao and Moskwa 1995). Compared to the F&E method, the significant feature of MVM involves a minimum set of differential equations to reduce the computation

cost for engine control design. In MVM, time is the independent variable and time scale is up to one engine cycle; discrete cycles of the engine are neglected with the assumption that all processes and effects are spread out over the engine cycle (Guzzella and Onder 2010). In a review of the literature, MVM has widespread use for simulation of a turbocharged diesel engine (Jankovic, Jankovic, and Kolmanovsky 2000) (Jung 2003) (Haiyan 2006) (L.Eriksson 2007). For different purposes, the number of states in these models varied. Most of mean-value diesel engine models designate the intake and exhaust manifold pressure, turbocharger and compressor mass flow dynamics as states. In Wahlstrom's work, an eight-state model was proposed, including the intake and exhaust manifold pressure p_{im}, p_{em}; the oxygen mass fraction in the intake and exhaust manifold X_{Oim}, X_{oem}; the turbocharger speed w_t and three states presenting the EGR and VGT dynamics $\tilde{u}_{EGR1}$, $\tilde{u}_{EGR2}$ and $\tilde{u}_{VGT}$ (Wahlstrom and Eriksson 2011). The model structure is illustrated in Figure 2-6 and the results indicated that the temperature state in the model had minor effects on the dynamic behaviour.

In spite of the simplicity, mean-value engine models are able to capture most of the fundamental characteristics of transient engine operation, especially the air system dynamics (Cieslar et al. 2014). As a result, this method has been commonly adopted for the engine control design of turbocharged diesel engines.

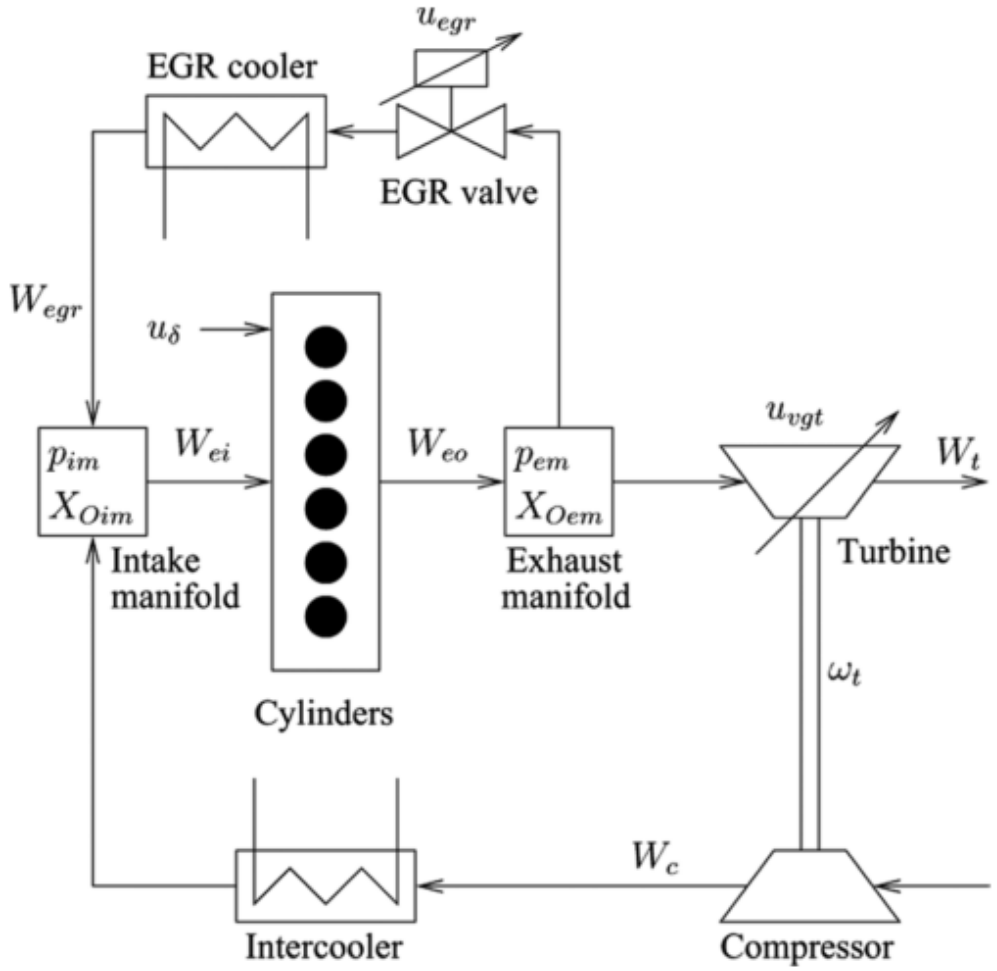

Figure 2-6 A Mean-value Model Structure of a Turbocharged Diesel Engine

Multi-zone Models

Multi-zone models of diesel engines were developed for the purpose of accurate prediction and study on engine combustion and emission pollutants. Compared with the approaches mentioned previously, multi-zone models consider the spatial and temporal variation of concentration and temperature within the control volume (Kouremenos, Rakopolous, and Karvounis 1987). As a result, detailed analysis of air-fuel distribution and calculation of gas composition is achievable. A number of research studies presented that the important combustion parameters such as heat release rate, IMEP and heat transfer could be

simulated by multi-zone models; meanwhile, NOx and soot emissions of diesel engines were predicted based on the related parameters (Kuleshov 2009) (Boretti 2012) (Visakhamoorthy et al. 2012).

Although the detailed mechanisms in multi-zone models enhance the accuracy of engine simulations, especially the combustion process and emission formation, rare direct application has been found on engine control strategy development, due to its complication and the huge computational time required. It was reported that the multi-zone models can be used to calibrate the mean-value models (Catania, Finesso, and Spessa 2011).

2.3.2 Non-thermodynamic Models

Non-thermodynamic models, also called "black-box" models were developed for complex systems with the minimum level of understanding. In these models, no fundamental principles are involved and the input-output behaviours purely rely on the experimental data (Grondin et al. 2004). Linear and non-linear "black-box" models are introduced in the following sections.

Linear "Black-box" Models

Due to the complexity of thermodynamic models, linear non-thermodynamic engine models were employed for initial controller design. These models are constructed based on identification of recorded data with adequate model structures such as the state-space and transfer function. It was reported that the pseudo-random binary sequence (PRBS) signal

could be added to the fuel rack position and record this signal and engine speed; thereby obtaining the discrete linear model (Jiang 1994). In addition, the step response fitting was employed in Winterbone's work (Winterborne, Thiruarooran, and Wellstead 1977). The model was a transfer function G(s) with a delay term, represented as:

$$G(s) = \frac{Y(s)}{U(s)} = K \exp(-Ts) \frac{s+c}{(s+a)(s+b)} \frac{ab}{c} \qquad \textbf{Equation 2-3}$$

Where s indicated the Laplace variable; K, T, a, b and c were the model parameters identified to fit the observed step response.

The major advantage of linear "black-box" models is its short running time due to its simplicity. However, these models are only acceptably accurate in a certain operating range. Considering the strong nonlinearity of turbocharged diesel engines, the utilization is restricted.

Nonlinear "Black-box" Models

With the fast development of computer science, powerful computation capability facilitates the optimal identification techniques for nonlinear engine models. Two important approaches have been developed, i.e. nonlinear autoregressive Moving average with exogenous Input (NARMAX) models and neural networks.

Billings reported a NARMAX model of a diesel engine with the nonlinear difference equation (Billings, Chen, and Backhouse 1989):

$$
\begin{aligned}
y(t) = &-a_0 + a_1 y(t-1) + a_2 u(t) \\
&+ a_3 u(t-1) + a_4 y^2(t-1) \\
&+ a_5 y(t-1)u(t) - a_6 y(t-1)u(t-1) \\
&- a_7 u^2(t) - a_8 u^2(t-1)
\end{aligned}
$$

Equation 2-4

Where u indicated the fuel rack position and y represented the engine speed; a_n was obtained by the identification based on dynamic experimental data. This method is able to capture the dynamics effectively even when the system is complex and with little physical insight.

Meanwhile, neural network models have been commonly used for engine model development (Garg, Diwan, and Saxena 2012). With sufficient data from engine experiments, neural networks are capable of learning the complex, multi-dimensional and non-linear relationships between designated variables (C. Atkinson and Mott 2005). It was reported by He that a neural network engine model was able to predict the combustion parameters and emissions based on the inputs like engine speed, engine load, injection pressure, etc. The general schematic of the model is shown in Figure 2-7 (He and Rutland 2002). Furthermore, Alonso discussed the effect of the selection of the number of neurons in the model on the accuracy of the outputs and suggested that a larger number of neurons are required when the relationships are complex (Alonso et al. 2007). For example, the process of emission formation in a diesel engine is far more complicated than the fuel consumption.

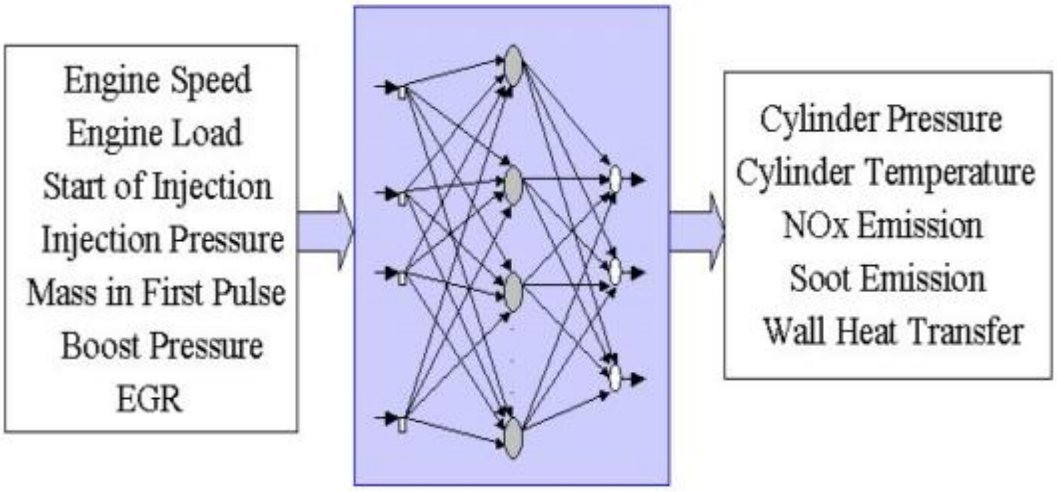

Figure 2-7 Schematic of a Feedforward Neural Network Engine Model (He and Rutland 2002)

Although the nonlinear "blackbox" models are rather powerful and computationally efficient, especially the neural networks, they are not perfect for engine modelling. The biggest issue of these models is over-fitting. The over-fitting derives from the inaccuracies of transient data and errors in synchronizing various parameters; as a result, the models would learn non-existent correlation and show poor accuracy in the extrapolation (I. Brahma and Chi 2011b). Also, due to the heavy dependence on the experimental data, "black-box" models are application-specific and the compatibility is poor.

2.3.3 Semi-physical Approximate Models

Semi-physical models which combine the characteristics of both thermodynamic and non-thermodynamic models are built based on equations with physical insight; while the parameters in these models are measured or estimated by identification (Grondin et al. 2004). It was found that the semi-physical models failed to capture the detailed complicated combustion during transient operation (C. D. Rakopoulos and Giakoumis 2006). However,

this method is an emerging and promising tool for on-line estimation of engine emissions and many related research studies have been explored (Grahn et al. 2012) (W. Park et al. 2013) (Finesso, Misul, and Spessa 2014) (Quérel, Grondin, and Letellier 2015). Quérel proposed a semi-physical model of NOx emissions based on the main phenomena in NOx formation and presented a good correlation with experimental data (Quérel et al. 2013). A semi-physical particulate matter emissions model, acting as a function of significant engine operating variables, was developed (Finesso, Misul, and Spessa 2014). It was reported that the air-fuel ratio and value of the chemical energy release at the end of the main injection were the dominant variables to predict the PM emissions.

2.3.4 Comparison of Different Modelling Approaches

After the review of all these modelling approaches, the trade-off between computation cost and fidelity is exhibited. It is easy to understand that the simulation time would increase when the model structure becomes more complex, to ensure higher accuracy. Also, a simple structure and high compatibility are difficult to achieve simultaneously. The advantage on the computing time offered by models with a simple structure such as quasi-steady and the F&E method, is paid through their heavy dependence on empirical correlations; this is difficult to properly describe during transients (Guzzella and Onder 2010). In other words, there is no approach perfectly suitable for all the cases of engine modelling. Currently, a complete turbocharged diesel engine model includes the air path, in-cylinder combustion and exhaust emissions simulation; each subsystem of the engine has varied characteristics and complexity. As a result, a mixture of thermodynamic, “black-box” and semi-physical sub-models has been more and more adopted in diesel engine modelling (Millo, Rolando,

and Andreata 2011). The detailed development of one turbocharged diesel engine with various modelling approaches for its subsystems will be introduced in Chapter 6.

In addition, it has been reported that the trend of engine modelling is to include more physical knowledge inside the model-based control design (Grondin et al. 2004). The semi-physical models are considered as a good compromise between simplicity and genericity (D'Ambrosio et al. 2014).

2.4 Emerging Control Strategies

Many studies have been conducted to explore the new control strategies for turbocharged engines. Since the key factors determining the transient performance of a turbocharged diesel engine lie in the air path, i.e. the engine air-supply and EGR management as mentioned in the previous section, this review will focus on the application of these control strategies to the air management system of engines. Three types of representative control strategies, namely the fuzzy logic control, neural network control and model predictive control are introduced.

2.4.1 Fuzzy Logic Control

Due to the simple heuristic nature, tolerance to noise and the absence of the need of mathematical derivation, the fuzzy logic control strategy has been adopted in the air management of turbocharged diesel engines (R.S.Wijetunge et al. 2000). It is a control

structure emulating the method of humans making decisions at a certain set of circumstances (Pedrycz 1989). In order to implement the fuzzy logic control, the desired behaviour of actuators such as the VGT and EGR valves is required to be identified; a significant number of classes of inputs which normally indicate the errors are defined; and then the rule determining the controller could be summarized (Omran, Younes, and Champoussin 2009). Arnold proposed a fuzzy multivariable approach to simultaneously regulate the intake pressure and the air mass flow by controlling the VGT, EGR valve and throttle (J. F. Arnold et al. 2006) (J.-F. Arnold, Langlois, and Chafouk 2009). The structure of the controller is illustrated in Figure 2-8. It was reported that the fuzzy controller could provide effective control of the engine gas charge shown by the experimental and simulation results.

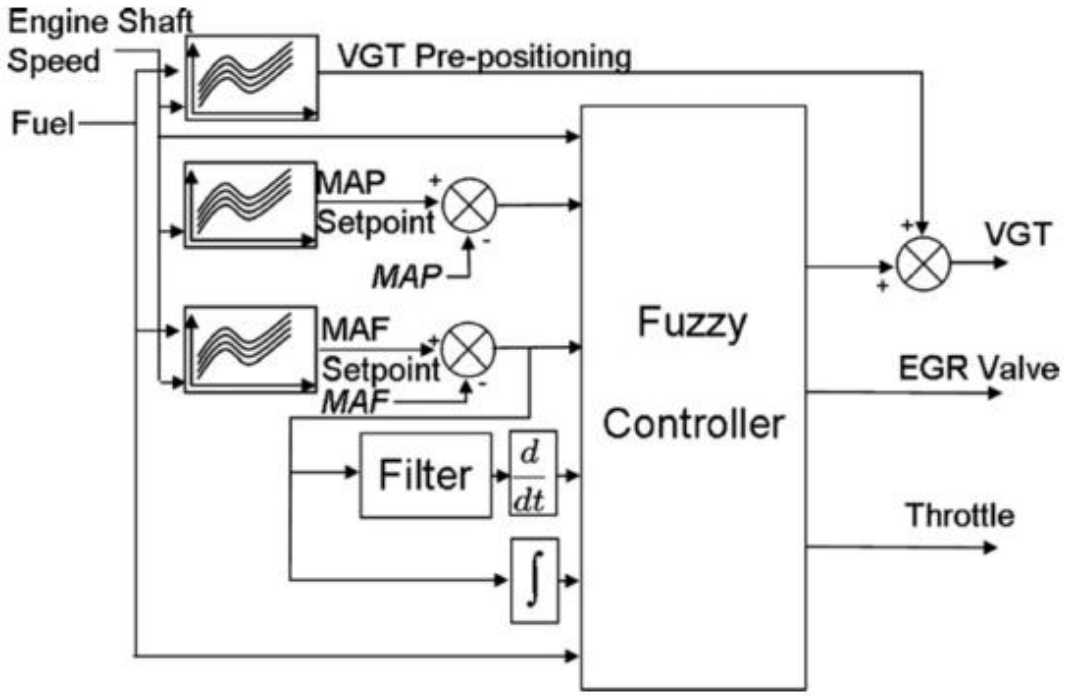

Figure 2-8 Typical Structure of the Fuzzy Controller for Air Management (J.-F. Arnold, Langlois, and Chafouk 2009)

The structure of fuzzy logic control is simple so that the computational requirements are low and close to conventional PID control (J.-F. Arnold, Langlois, and Chafouk 2009). However, this strategy relies on the full understanding of the actuator's behaviour, thereby determining the logic rule, which largely restricts the application to complex systems. In addition, a large amount of tuning is required to improve the control results.

2.4.2 Neural Network Control

As introduced in the previous section, neural networks have been commonly used to identify and represent the input-output correlation for engine modelling. Based on the powerful learning capability of neural networks, the neural network controller has been exploited and applied to some engine control scheme design (Black et al. 2010b).

Omran proposed a methodology to obtain optimal control schemes and apply a neural network controller online to the engine (Omran, Younes, and Champoussin 2009). First, one complete engine model was developed and validated; next, the optimization process was defined and the optimization algorithm was adopted to search optimal control variables during dynamic courses; finally, the neural network with a feed-forward back-propagation algorithm was trained by the optimal control database and integrated into the real-time engine simulation. The proposed controller showed an apparent reduction in opacity over the ETC test cycle compared with the original control strategy. Liu developed an approach involving adaptive critic designs (ACDs) for engine control based on neural networks (Derong Liu et al. 2008). The schematic of the proposed neural network controller is shown

in Figure 2-9. The control references were set as air-fuel ratio (AFR) and torque (TRQ); Q(t) implied the critic network outputs function, which evaluated the control results.

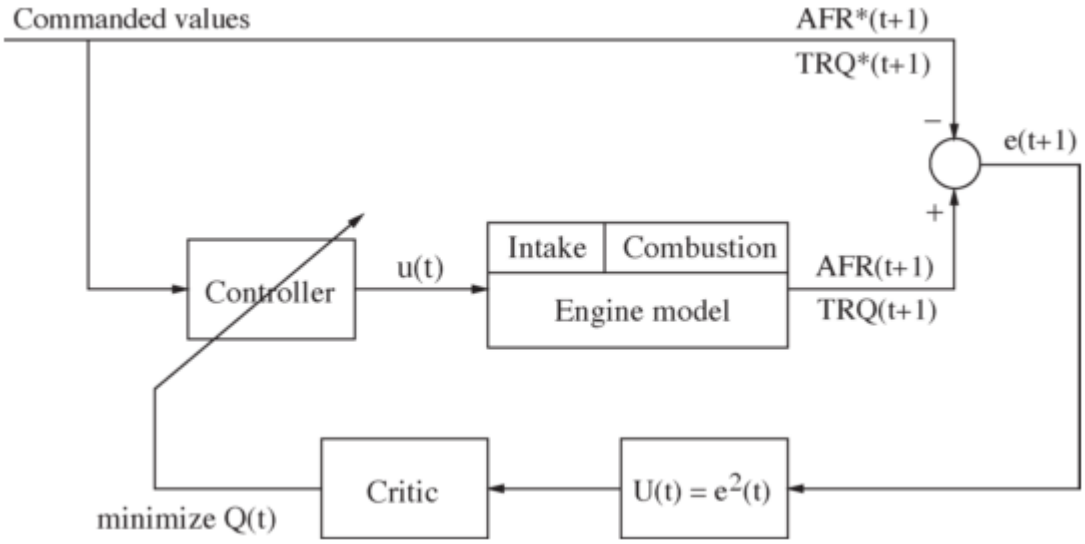

Figure 2-9 Structure of the Neural Network Engine Controller with Adaptive Critic Designs

(Derong Liu et al. 2008)

It was reported that the neural network controller was capable of realizing optimal control with low computation cost and good performance in a certain operation range (Nakayama et al. 2008). However, this method inherited the issues of neural networking modelling, i.e. limited robustness guarantees in the extrapolation and heavy dependence on a large amount of experimental data.

2.4.3 Model Predictive Control

Model Predictive Control is an emerging control framework based on optimisation (Maciejowski 2001). In light of the input/output constraints included and the high applicability to multi-input-multi-output (MIMO) systems, MPC has been applied to

increasingly complex diesel engines by many researchers. The basic idea of MPC is to solve an optimal control problem of a finite horizon at each control interval. Nonlinear and linear MPC approaches of diesel engines will be reviewed respectively.

Nonlinear MPC

Since the conventional control methods are not able to directly incorporate performance specification and constraints in a nonlinear system, the idea of nonlinear MPC was proposed (García-Nieto et al. 2008). The main difference from linear MPC lies in that the quadratic program (QP) of nonlinear MPC (NMPC) is required to be refreshed at each sampling instant (P Ortner et al. 2009). Herceg applied nonlinear MPC to the air path of a turbocharged diesel engine and showed the improved transient behaviour in the simulation; the setpoints were the intake manifold p_i^s, exhaust manifold pressure p_x^s and compressor power p_c^s; while constraints were considered based on actuator limits and mechanical limits (Herceg et al. 2006). The basic control structure is presented in Figure 2-10. Similarly, based on a linear parameter varying (LPV) engine model, Ortner developed a nonlinear MPC controller for a diesel engine air path and the reference was the air mass flow and boost pressure (P Ortner et al. 2009).

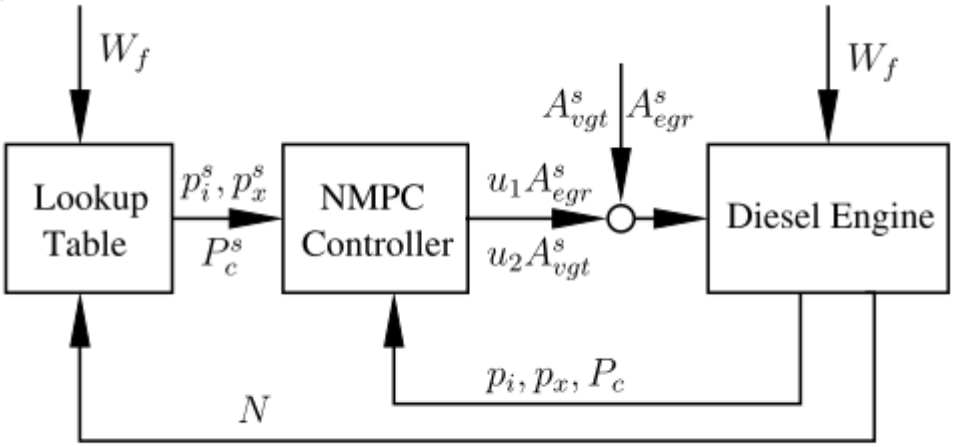

Figure 2-10 Structure of a Nonlinear MPC Diesel Engine Controller (Herceg et al. 2006)

Although the nonlinear MPC shows an excellent tracking performance in the simulation, the biggest issue is its high computational complexity. As a result, nonlinear MPC is inapplicable to the real-time control currently.

Linear MPC

Due to the limitation that the standard linear MPC cannot directly deal with the nonlinear system, one approach has been proposed to implement MPC on engine transient control based on the identified local prediction models. One methodology of model-based control for the air path of diesel engines was developed by the Johannes Kepler University (Peter Ortner and Re 2007). First, a mean value model of the engine air path was constructed. Note that the model should have physical insight and be able to reflect the nonlinearity of the engine such as the dead zone, hysteresis and delays. Next, local linear models were identified in divided operating regions. Then, the optimal control problem was represented in a quadratic program so that MPC could be adopted to track the setpoints, the mass air flow and intake pressure. Cieslar proposed one model-based approach to the turbocharged

diesel engine air path (Cieslar et al. 2014). A Ricardo WAVE 1-D engine simulation model acted as the model plant; a MVM was used for the MPC formulation and an engine simulator; a simple driveline model was included to predict the longitudinal motion of the vehicle. The schematic of the control system is shown in Figure 2-11.

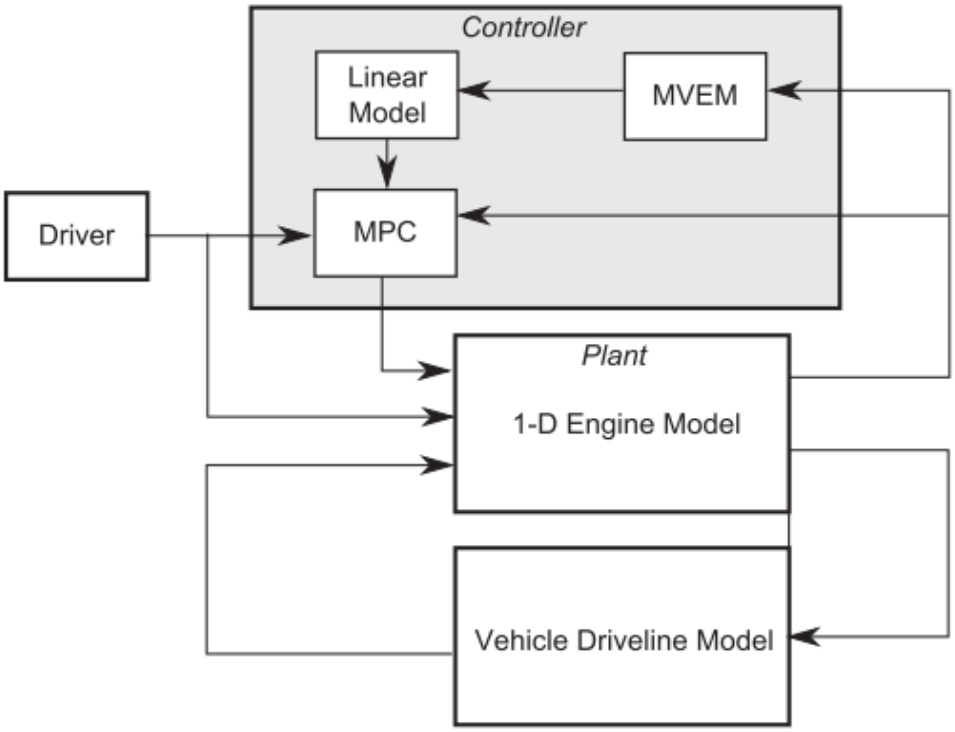

Figure 2-11 Structure of a Linear MPC Control System (Cieslar et al. 2014)

Furthermore, a new concept, explicit MPC (EMPC) was proposed (Bemporad 2001). It solves the quadratic program offline and stores the resulting piecewise affine control laws in a look-up table, so that only a linear control law rather than a complete quadratic minimization problem needs solving at each instant. The application of explicit MPC on turbocharged diesel engines was reported (Zhao et al. 2014). The main process of EMPC and standard MPC is the same, while the major difference in the implementation procedure is illustrated in Figure 2-12. It was reported that EMPC showed significantly lower computation cost and is applicable for fast-speed systems.

In summary, the possibility of a systematic means to the development of modern automotive engines control with an explicit treatment of constraints was found to be a key advantage of MPC, over the conventional procedures (Stewart and Borrelli 2008).

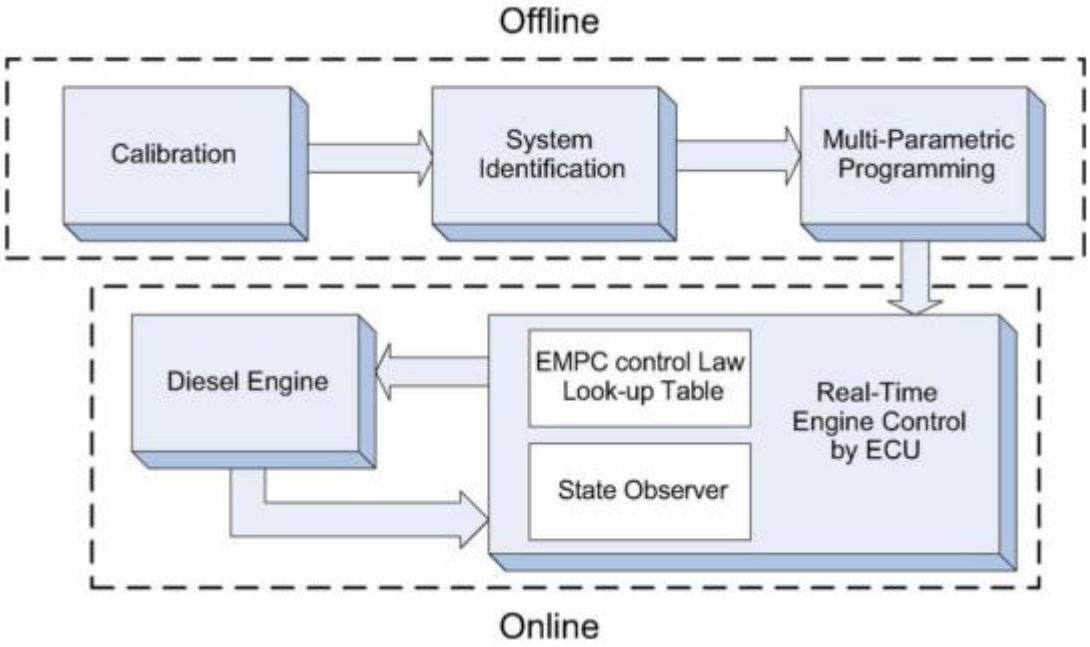

Figure 2-12 Implementation Procedure of Explicit MPC on Diesel Engines (Zhao et al. 2014)

2.5 Approach to Hardware-in-the-Loop

Hardware-in-the-loop is a form of real-time simulation, adopted in the development and calibration of complex control systems. It differs from the pure real-time simulation by the addition of a real component in the loop (Bullock et al. 2004). The typical structure of HIL simulation is shown in Figure 2-13. A plant model is implemented in the HIL system and an electronic control unit (ECU) is connected through I/O signals. Although the most effective way to test the control strategy is to implement it on the real plant, the HIL simulation plant has the advantage of flexibility, safety and low cost.

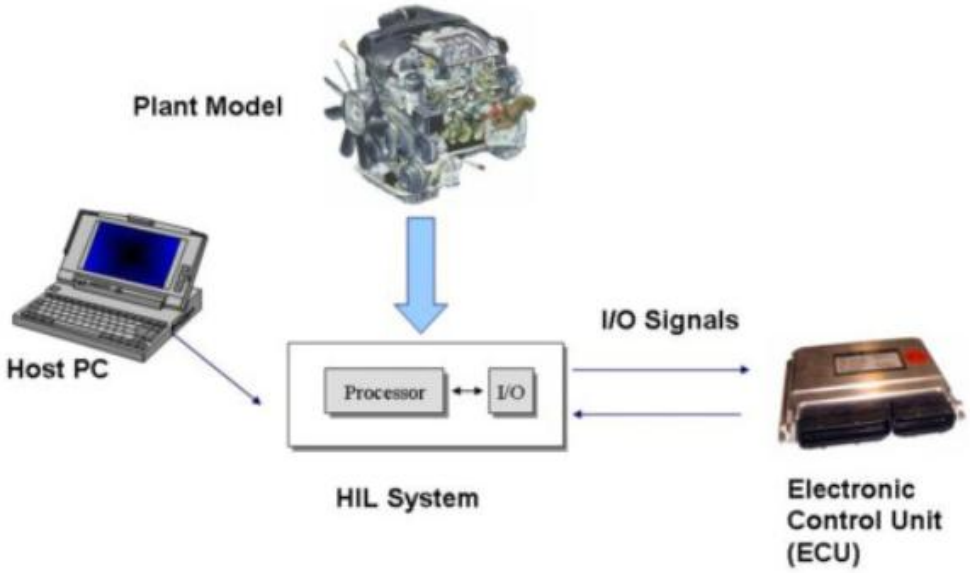

Figure 2-13 Typical Structure of a HIL System

Due to the increasing number of control actuators in modern diesel engines, HIL has been more and more applied to the engine control development. Maroteaux developed a physical combustion engine model which was coded in S-functions Simulink blocks and implemented on a HIL simulation (Maroteaux and Saad 2013). The detailed set up of the system is shown in Figure 2-14. In the approach, some real engine actuators were controlled by the ECU and used as components in the loop, while other actuators were modelled by Simulink; one signal failure generator was included to simulate the failure situation; the ECU with embedded software was connected to the test bench. The whole system was able to work as a real car so that the control strategies of the engine could be validated and tuned. In addition, commercial engine models such as GT-POWER were reported to be implemented in a HIL simulation successfully; which largely facilitated the application of HIL in the automotive industry (Nanjundaswamy et al. 2011).

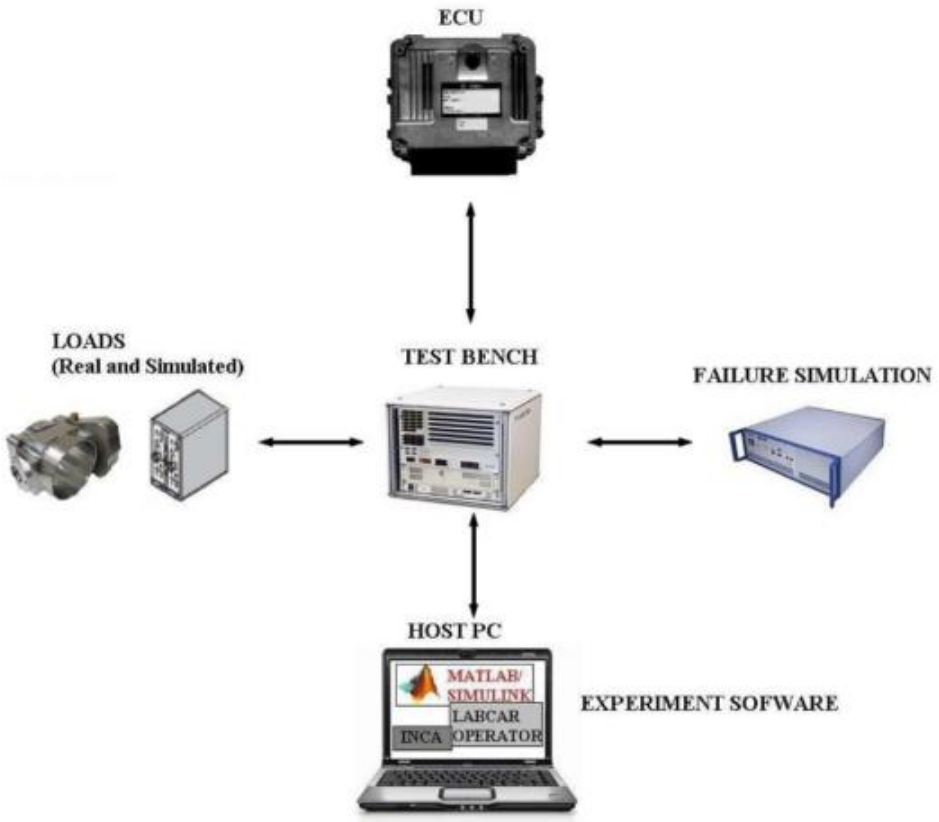

Figure 2-14 Set up of a HIL Real-time Simulation for Engine Control Development (Saad et al. 2011)

In brief, HIL simulation is efficient and desirable for transient engine control. It has been proved that the implementation of HIL is useful in the validation of real-time models and control strategies. One HIL platform was developed for real-time engine control by the author and will be introduced in Chapter 7.

2.6 Summary

In summary, this literature review focuses on major developments in modern diesel engines, transient operation investigation, control-oriented modelling and engine control strategies. Also, the approaches to HIL simulation for engine control development are discussed.

From the literature review, the main findings are summarized as the following:

1. Modern diesel engines have become increasingly efficient and clean with the help of emerging technologies in gas exchange, in-cylinder combustion, emissions abatement and input fuels. Meanwhile, proper control of the progressively complex system is vital and desired.
2. The exhaust emissions caused by engine transient operation are a major source of pollution so that detailed measurement and analysis of engine behaviour under transient operating conditions are required to improve engine calibration. It is indicated that the system delay of a turbocharged diesel engine is the dominant contributor to this issue.
3. The modelling of engines has a long history and many approaches have been exploited for the development of engine control strategies. For a complete turbocharged diesel engine model, a number of subsystems have varied characteristics and complexity so that different approaches should be adopted. The semi-physical model is a promising method and considered as a good compromise between simplicity and genericity.
4. Many new control strategies for the air path of turbocharged engines have been developed to improve the transient engine control. Although the simulation results are fine, a real-time controller which can be directly implemented to engine operation is still desired. Among the emerging techniques, MPC has proven to have appropriate robustness and computation cost.
5. HIL simulation has been successfully implemented to engine control development. It is essential to validate the real-time capability and control performance with a HIL platform.

CHAPTER 3

DEVELOPMENT OF THE EXPERIMENTAL SYSTEM

This chapter introduces the test facilities and set up of the experimental system used in this study. The specification of a turbocharged diesel engine, the set up of the engine test bench and operating system and the equipment to measure the engine performance are all presented.

3.1 Introduction

The test bench of this study was built for the engine cold start research. The primary feature of this test bench is one complete conditioning system which was installed to control the temperature of the input fuel, air, engine coolant and lubricant oil down to -20°C. Most of the experiments conducted by the author were in ambient conditions (20°C) but the capability of temperature control contributed to the repeatability and accuracy of the experiment results.

Although the test bench and operating system were initially set up by Jaguar Land Rover, AVL and a previous PhD research student Dr Dai Liu, the author was responsible for maintaining the facilities and conducting the upgrade work for engine transient tests during his study. The maintenance included minor engine components' failure fixing and facility

consumables replacement such as engine coolant and filters of the emission analyzers; while the upgrade work involved reconfiguration of the control system, setting up of automatic transient manoeuvres and installation of additional measurement facilities.

3.2 Engine Specification

The Jaguar Lion V6 3.0 Litre diesel engine used in the investigation is shown in Figure 3.1.

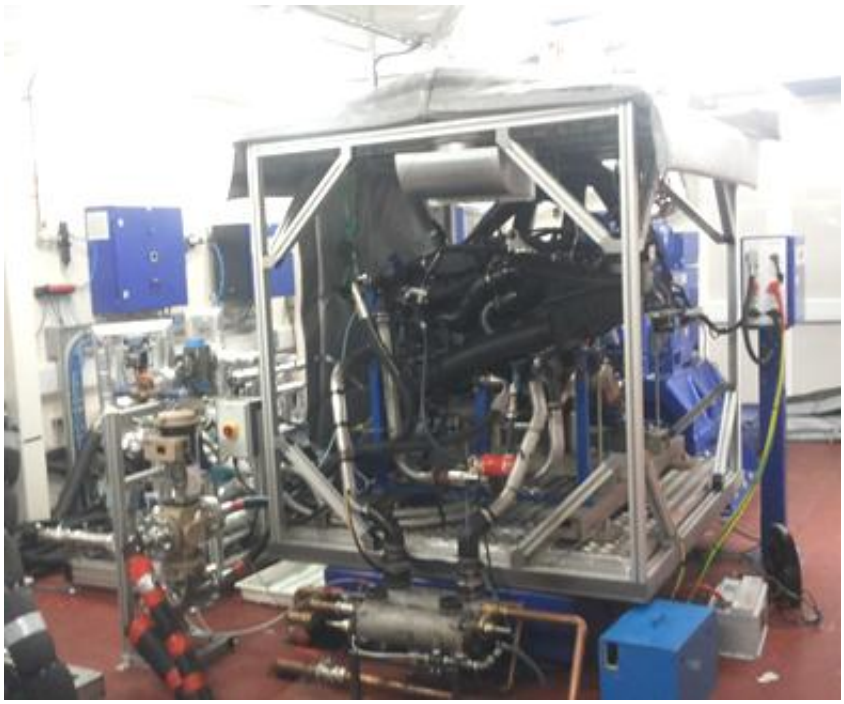

Figure 3-1 Jaguar 3.0L Lion V6 Engine

This engine is a modern diesel engine equipped with common rail injection, parallel sequential twin variable geometry turbochargers and a dual camshaft. High pressure EGR with a water cooler is employed to supply low temperature exhaust gas into the intake manifold with fast response. Also, a multiple injection strategy is adopted including two pilot injections, one main injection and one post injection for better engine combustion performance and high efficiency of emission after-treatment. During the engine operation

after warm up, the temperature of the engine coolant and oil is maintained at 90°C (±2°C); meanwhile the engine combustion air is fixed at 20°C. The schematic of the engine set-up is shown in Figure 3-2.

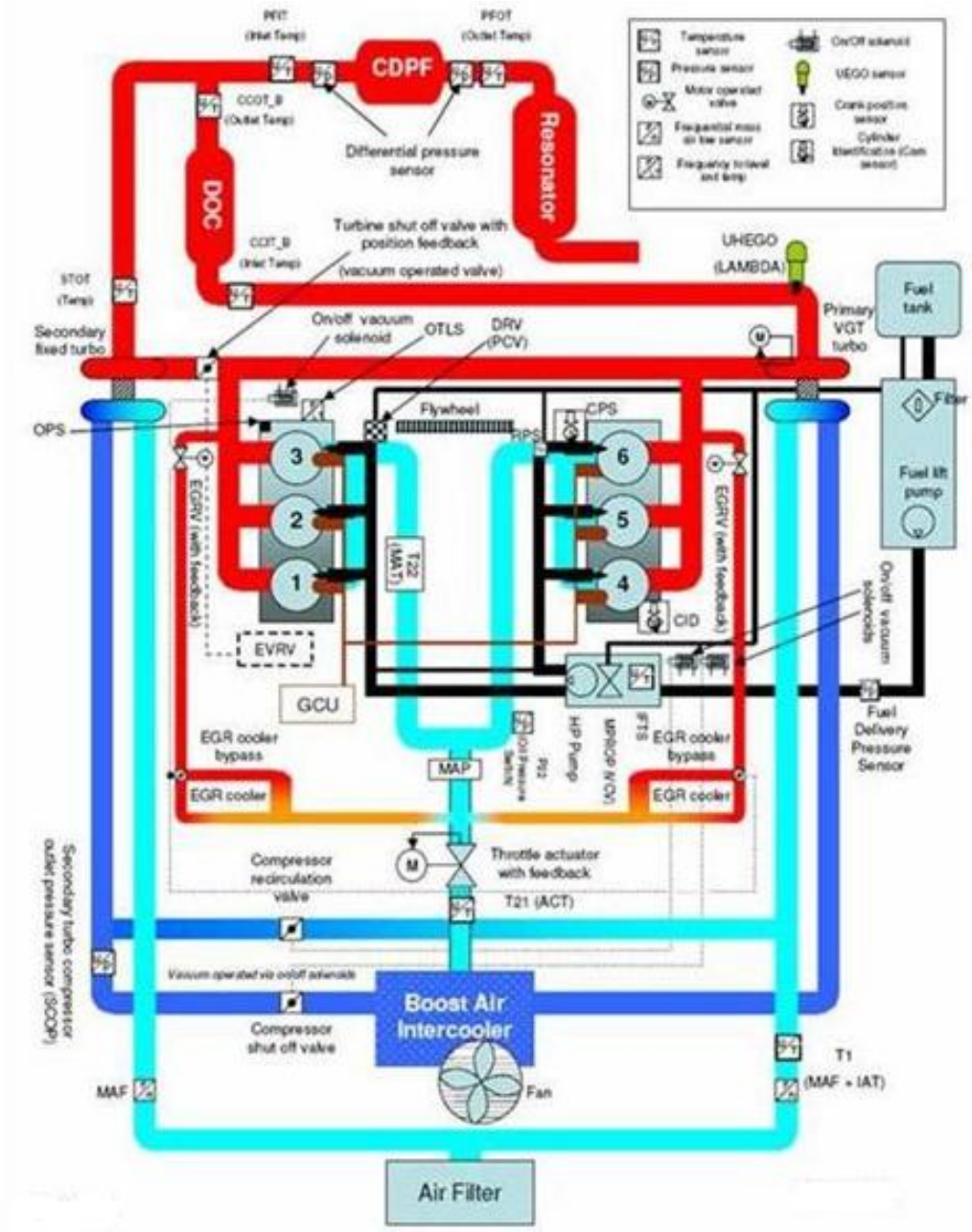

Figure 3-2 Schematic of the Original Engine Set-up (Dai Liu 2014)

The detailed technical data of the engine is supplied in Table 3-1.

Table 3-1 Specifications of the Jaguar V6 Engine

Engine Type	Euro 5 Diesel	**Max Cylinder Pressure**	173 bar
Stroke	90 mm	**Max Power**	199 kW @ 4000 rpm
Bore	84 mm	**Max Torque**	600 Nm @ 2000 rpm
Swept Volume	2993 cc	**Max Speed**	5000 rpm @ no load
Compression Ratio	16.1 : 1	**Blow-by Limit**	90 Litres/min

3.3 Operating and Control System

The engine operating and control system is essential for engine experimental study, especially for transient tests. This test bench is capable of full simulation of the transient duty cycle such as the new European driving cycle (NEDC) which is converted from on-board vehicle test and various transient manoeuvres designed by the researcher. The complete testing system with the diagnostics arrangement is illustrated in Figure 3-3. Three major parts: dynamometer, conditioning system and engine operating system will be introduced respectively.

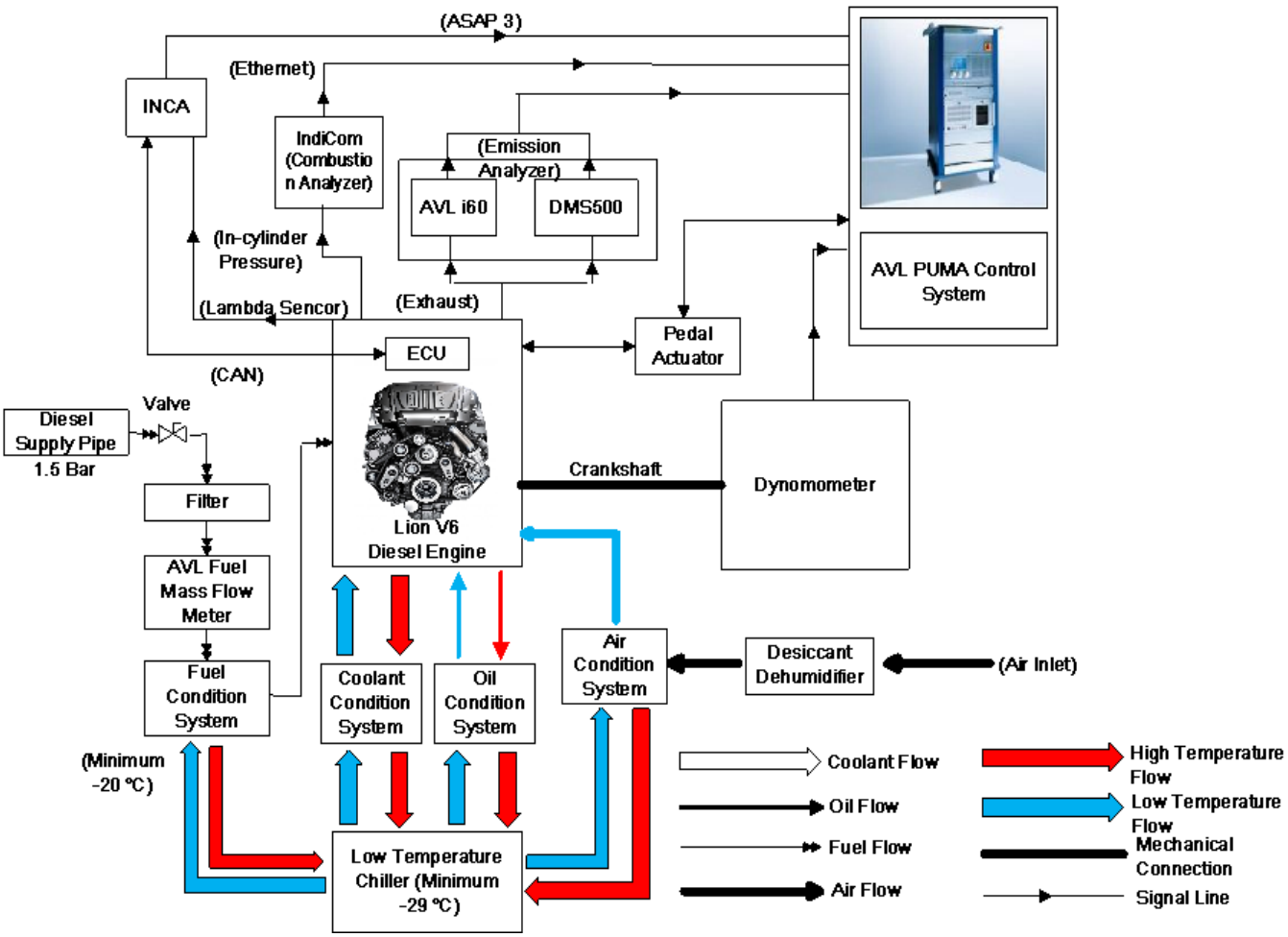

Figure 3-3 Layout of the Test Cell Arrangement

3.3.1 Dynamometer

The dynamometer used in this investigation is supplied by AVL. It is an AC machine with a squirrel cage rotor mounted with a torque flange, shown in Figure 3-4.

Figure 3-4 Transient Dynamometer in the Test Cell

The torque and speed of the dynamometer are controlled by a control cabinet which is connected to the main unit of the AVL PUMA system. The dynamometer controller has two modes, speed mode and torque mode. The speed mode indicates that the speed is settled directly and determined by the frequency of the AC motor, while the engine adjusts the fuel flow rate to achieve the desired load through the acceleration pedal (Zhang 2013). In contrast, the torque mode means that the torque is maintained by the AC motor while the engine accelerates to the desired speed. In this study, the speed mode is adopted due to its better dynamic performance and smaller fluctuation. In addition, for engine transient control, the torque flange utilized has been well calibrated and has low rotor weight and mass moments of inertia. Table 3-2 shows the specifications of the dynamometer.

Table 3-2 Specification of the Dynamometer on the Test Bench

Model	Dynodur 270	**Characteristic Tolerance**	<± 0.10 %
Nominal Torque	485 Nm	**Linearity Deviation**	<± 0.05 %
Nominal Power	270 kW	**Temperature Effect per 10K on the Output Signal**	<± 0.05 %
Maximum Speed	10000 rpm	**Temperature Effect per 10K on the Zero Signal**	<± 0.05 %
Mass Inertia	0.31 kgm^2	**Relative Standard Deviation of the Reproducibility**	<± 0.03 %

The absorbed performance curve of this dynamometer is illustrated in Figure 3-5.

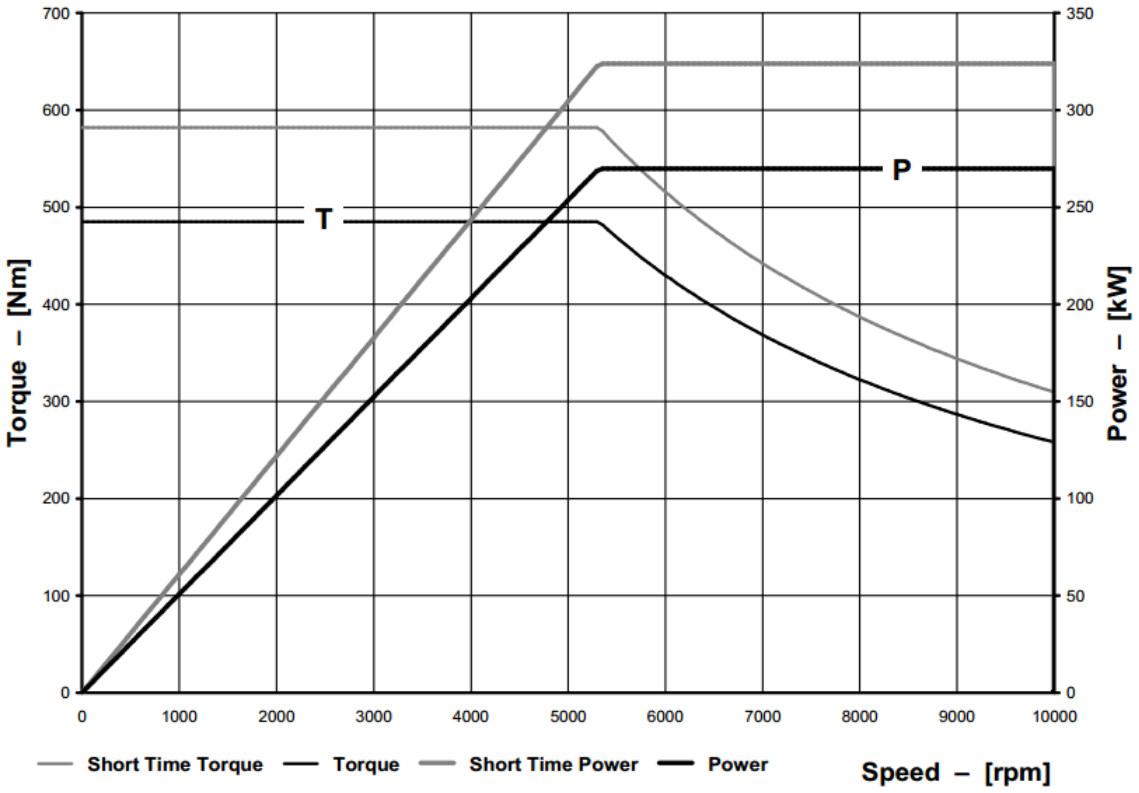

Figure 3-5 Engine Dynamometer Performance Curve of AVL Dynodur 270

3.3.2 Conditioning System

In this test cell, the low temperature circuit of the conditioning system is supplied by chilled water from a 1500 litre tank. As illustrated in Figure 3-3, the cooling water is distributed to the fuel, air, engine coolant and lubricant oil conditioning system respectively. In the cold testing mode, the chilled water needs to be cooled down to -29°C first, which takes approximately 8 hours; then the circulating to each conditioner is started. The detailed setting of cold testing can be found in Dai Liu's thesis (Dai Liu 2014). For this study, only the ambient testing mode was used and the long chilling process was unnecessary. The introduction of the separate conditioner will follow in the next section.

Fuel Conditioning System

A fuel temperature control unit, AVL 753C, was installed for the conditioning of the input fuel. First, the diesel fuel was supplied from an external tank at ambient temperature; then two fuel filter units (coarse filter and fine filter) were used to filter the diesel in order to protect the measuring equipment from soiling and subsequent damage; subsequently a fuel regulator was set at 1.5 bar to stabilize the fuel flow; a fuel mass flow meter was connected after the regulator for the precise fuel consumption measurement; finally, the fuel entered the conditioning system to achieve the desired temperature for the engine testing. The loop of the fuel conditioning system is shown in Figure 3-6. Apart from the cooling capability, one heat unit was integrated with the conditioning system. As a result, the temperature range of this fuel conditioner could be set between -20 to 80°C; however, the achievable fuel temperature depends on the cooling water temperature and the amount of heat retained in

the engine return fuel. At ambient mode, the temperature stability of the fuel conditioner is ±0.1 K, which provides a stable fuel temperature for the engine and improves the measurement accuracy of the experimental study.

Figure 3-6 Arrangement of Fuel Conditioning System

Engine Coolant and Oil Conditioning System

There are two modules designed to provide cooling capability to the engine coolant and oil with the supply of chilled water respectively. The circuit of the conditioning system is shown in Figure 3-7. Each module has one heat exchanger and one flow control valve in the loop. Through a PID controller on the flow valve, the temperature can be maintained at the desired value. As mentioned previously, in the ambient testing mode, the desired temperatures of the engine coolant and oil were set at 90°C. Considering the engine could be damaged at excessive high temperatures, a limit alarm is activated during the engine operation in case of the failure of the conditioning system. When the temperature of the engine coolant or oil is over 100°C, the system would automatically enter a stage called 'cold run' which means the engine would run at idling. This procedure would ensure the circulation of coolant and oil which would cool down the engine components, thereby protecting the engine.

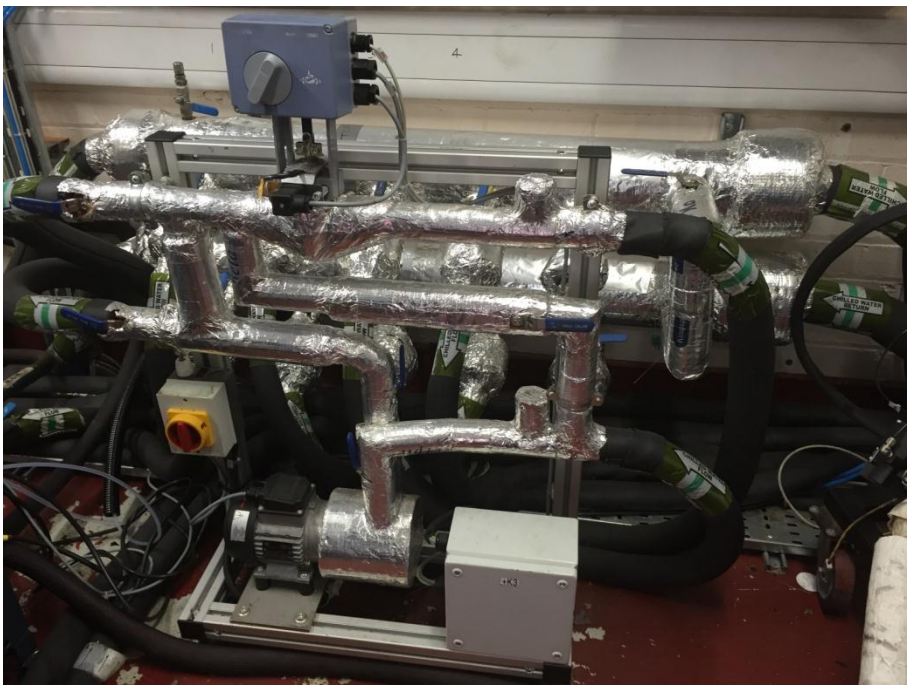

(a)

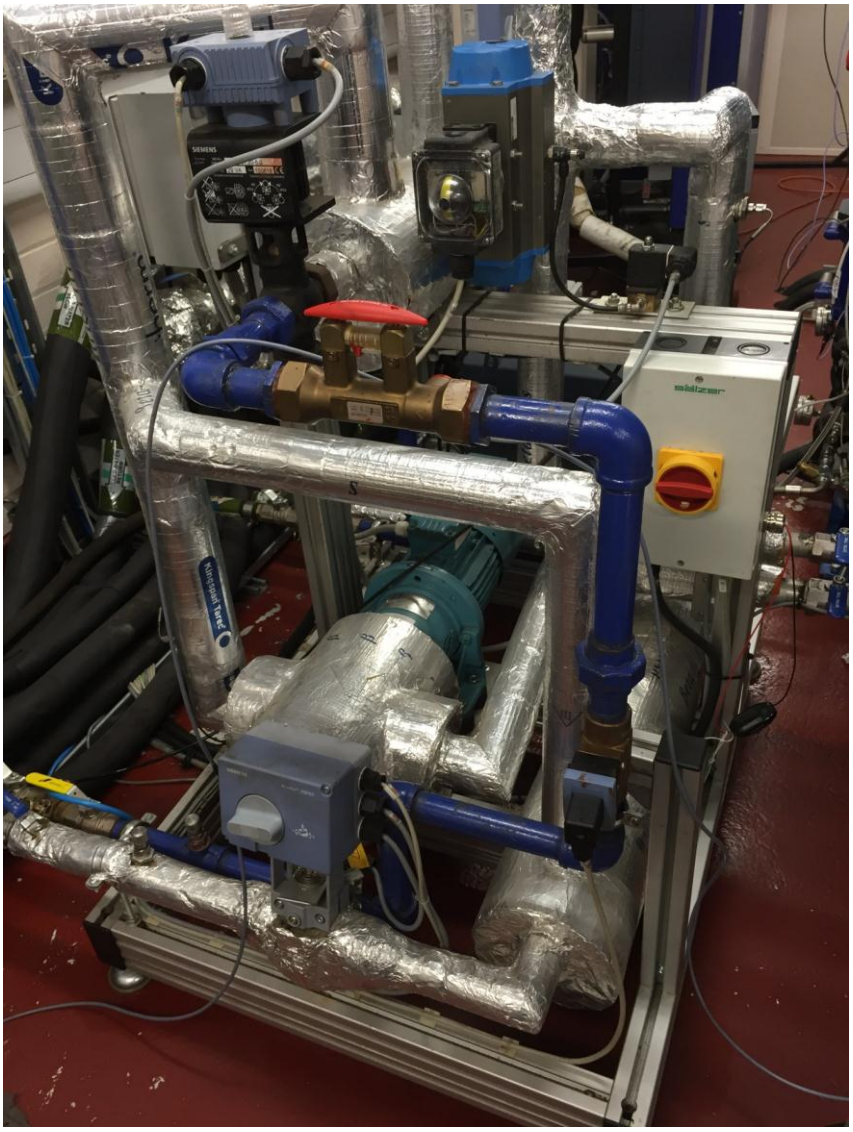
(b)

Figure 3-7 Circuit of Conditioning System: (a) Engine Coolant; (b) Lubricant Oil

Air Conditioning System

The temperature of the engine combustion air was controlled by an AVL CONSYSAIR 1600 unit. In addition, one dehumidifier was installed to adjust the relative humidity of the intake air according to the varied testing requirements. Independently from the engine operation condition, the desired temperature and humidity can be controlled at the given range with proper accuracy (±0.5°C and 3% relative humidity).

Figure 3-8 Engine Combustion Air Conditioning System

For the ambient testing mode, the intake air temperature was maintained at 20°C and the dehumidifier was kept off since the ambient temperature conditioning did not involve a serious humidity issue. The temperature control capability is essential for long periods of experimental study such as driving cycle tests. Without the air conditioning system, the temperature of the intake air would increase with the increase of the testing time; as a result, the engine performance would deviate from the desired values.

3.3.3 Engine Operating System

The AVL PUMA Open system is utilized to operate the whole test cell including the engine, dynamometer, conditioning system and emission analysers. It acts as the core of the testing system for control, monitoring and data acquisition.

For the engine and dynamometer operation, the data transfer process has been presented in Figure 3-9. The demand values such as speed and torque are calculated and transferred to the output modules. Through the Fast-Front End Module Digital Analogue Converter illustrated as number 3, the digital demand values from the PUMA system are converted into analogue quantities (current/voltage); thereby controlling the actuators. Meanwhile, the PC board PCI illustrated as number 2 in the figure is set up to transfer all the signals between the PUMA system and the FEM modules. Similarly, the conditioning system is controlled through this method and can be adjusted by tuning the PID parameters.

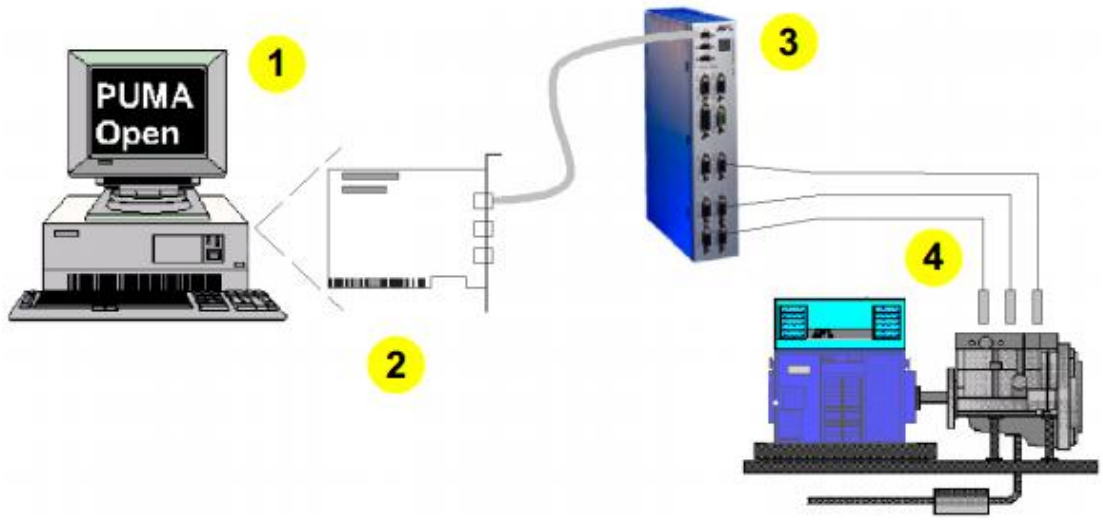

Figure 3-9 Data Transfer between PUMA System and Test Bench

In addition, the monitoring data of the test bench components such as speed, frequencies, time period and events can be acquired through a unit called a Fast-Front End Module Controller. Accordingly, in the PUMA system, all the important parameters are monitored during the tests based on the real-time data communication capability of this system.

Furthermore, calibration software entitled INCA from ETAS was installed in another desktop which was integrated with a CAN bus interface card ES580. Based on INCA, the information from the ECU was acquired and stored; meanwhile, some engine management parameters could be controlled such as the EGR rate, boost pressure, rail pressure, injection timing, etc. In order to monitor the information from the ECU in the PUMA system, ASAP3 communication was set up through Ethernet. Therefore, the PUMA system is used as a data acquisition centre to record the experimental results from different sources.

3.4 Engine Performance Measurements

To capture the dynamic engine performance, there are a number of measurement facilities installed and used in the test bench. The measurement equipment was maintained and calibrated regularly.

3.4.1 In-cylinder Pressure Measurement

The in-cylinder pressure is measured by Kistler piezoelectric pressure transducers which have been fitted in the head of the cylinders (Kistler 2007). The pressure transducer uses a

piezoelectric crystal achieving high sensitivity in the operating temperature range and generates an electrical charge at 160 kHz. The measuring range is 0 to 250 bar, meeting the requirement of the investigation. Also, one AVL angle encoder was installed to provide pulses at every crank angle degree as a clock input and one pulse every cycle to determine the top dead centre (TDC).

A multi-channel indicating system, AVL IndiModuls 621, was connected to the pressure transducers and the encoder for receiving the signals. The module was linked to a desktop which has the interface software IndiCom to present and record the in-cylinder pressure and related cycle-based values such as IMEP, peak in-cylinder pressure and the crank angle position, where 50% of the cumulative heat release occurs (HR50). In this study, the frequency of the in-cylinder pressure was set at every crank angle degree. Similarly to INCA, the data from IndiCom can be transferred to the PUMA system through Ethernet. However, due to the high frequency of the crank angle based in-cylinder pressure (around 5-12 kHz at normal engine operation), only cycle-based parameters were recorded in the PUMA system.

3.4.2 Fuel Mass Flow Measurement

In order to measure the engine fuel consumption, an AVL 735S fuel meter was installed in the test cell as illustrated in Figure 3-6. Fundamentally, this fuel meter is a Coriolis flow meter which is able to provide an instantaneous fuel consumption measurement. Integrated with the AVL 753C fuel conditioning unit, the system can have high accuracy and temperature stability. Before each test, an accuracy check and calibration were conducted. During the experiments, the fuel mass flow measurement system was monitored in the

PUMA system remotely to ensure proper running. In addition, the continuous gas bubble separation was set to avoid inaccuracy from bubbles in the fuel. The technical data of the fuel measurement system is listed below.

Table 3-3 Technical Data of Fuel Mass Flow Measurement System

Ambient Temperature	5 - 50 °C
Fuels:	Otto (EN228), Diesel (EN590), up to 6% Biodiesel and 20% alcohol
Fuel Circulation Capacity:	Standard 240 L/h, optional 450 L/h
Pressure Control:	Feed pressure: 0 – 6 bar Turn pressure: 0 – 0.5 bar
Temperature Stability:	< 0.02 °C
Heating Power:	1.6 kW
Cooling Power:	1.6 kW at 10 °C spread and 0.5 bar cooling water differential pressure
Interfaces:	2× RS232
Power Consumption:	0.4 kW

3.4.3 Additional Oxygen Concentration Measurement

The accurate measurement of oxygen concentration is important to analyse the combustion and emission behaviour; however, only one oxygen sensor is installed downstream of the turbine in a conventional diesel engine for diagnostics, due to the cost and durability. Between the cylinders and the measuring point, the exhaust gas has to go through the exhaust pipes, exhaust manifold, turbine and a last small junction pipe. Each of these components has an influence on the gas pressure, temperature and composition, thereby

affecting the accuracy of the oxygen sensor. To minimize the transport and mixing delays, one additional oxygen sensor was positioned at the exhaust manifold upstream of the EGR valve. It should be noted that this change is only for experimental study because the oxygen sensor is not recommended for large temperature gradients and high pressure (Alberer and Re 2010). Moreover, another additional oxygen sensor was fitted in the intake manifold close to its pressure sensor. The data of the oxygen concentration in the intake and exhaust manifolds is able to provide specific information which is essential for the control of engine combustion.

The oxygen sensors used in this study were Bosch LSU 4.9 wideband sensors. With an internal heater, the sensor reaches operating temperature within 20 seconds and has a response time of less than 100 milliseconds. As a result, the value from this sensor can be considered as instantaneous and is able to reflect the dynamic characteristics of air. To acquire the data, one MoTeC LTC (Lambda to CAN) monitor was connected to both the lambda sensors and CAN interface. The specific wiring diagram is shown in Figure 3-10. Basically, the data is first read by the MoTeC LTC and then transferred to the CAN signal which is received by the INCA and the PUMA system.

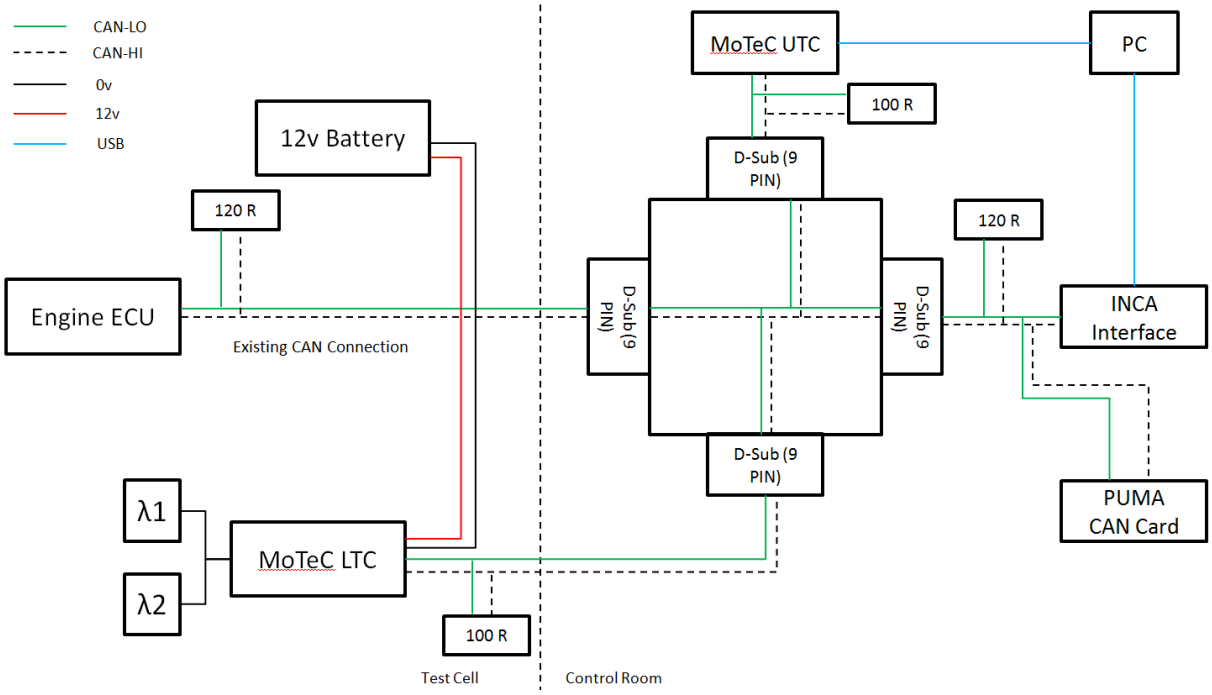

Figure 3-10 Wiring Diagram of Engine ECU and Lambda Sensors

In addition, considering the high pressure dependency of the sensor, proper compensation is necessary. The method of compensation lies in the re-calibration of the pump cell current, I_p. Fundamentally, the oxygen sensor measures the pump current while the oxygen compensation or the lambda is determined by a look-up table supplied by the manufacturer (Bosch 2014). The dependency of I_p on working pressure is illustrated in Figure 3-11 and the specific deviation of the sensor output signal is listed as below:

$$I_p(p) = \frac{I_p(p_0)\cdot(k+p_0)\cdot p}{p_0\cdot(k+p)} \qquad \textbf{Equation 3-1}$$

Where the factor k is dependent on rich or lean combustion and described as k_{lean} which is 0.47 bar and k_{rich} which is 0.39 bar; p is the measured working pressure and p_0 is the default pressure 1 bar.

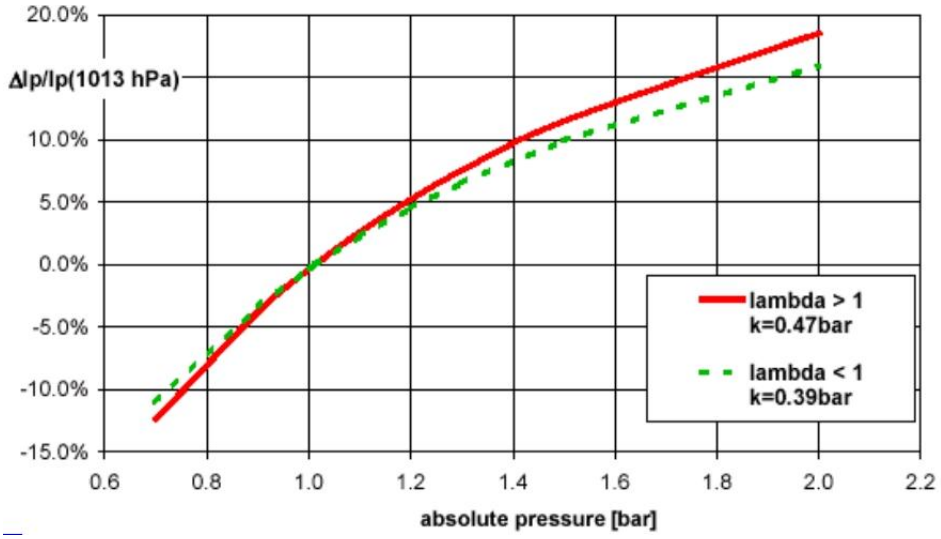

Figure 3-11 Deviation of the Pump Current of Oxygen Sensor from Pressure

Based on the instantaneous value of the intake air pressure and exhaust pressure, the compensated value of the pump current can be acquired by this method. Then, the accurate oxygen concentration is obtained based on the look-up table from the manual of the Bosch lambda sensor (Bosch 2014).

3.4.4 Gas Emission Measurement

In this study, the gas emission measurement focuses on NOx and HC due to the primary challenge of the legislation. The sample point of the measurement locates downstream of the turbine and before the DPF. In order to capture the dynamic characteristics of the emission behaviour, two different kinds of emission measurement equipment, a Cambustion FID/CLD fast analyser and an AVL AMA i60 gas tower are used.

Cambustion Fast NOx and Fast FID Analyzer

The ultra-fast response analysers CLD500 and HFR500 were installed in the test bench for NOx and HC emissions respectively. The analysers are shown in Figure 3-12.

Figure 3-12 Cambustion CLD500 Fast NOx and HFR500 Fast FID Analyser

The Cambustion CLD500 is a chemi-luminescence detector used for the NO or NOx concentration measurement, featuring a short time response as low as 2 ms $T_{10\text{-}90\%}$ (Cambustion 2013). As the location of the detectors in the remote sample heads is positioned close to the sample point in the engine, the mixing and transport delay of the sample are minimized. The principle of the CLD500 is illustrated in Figure 3-13. The NO from the sample gas and the O_3 from the ozone reacts in the chamber, emitting light. The

photons produced are detected by a photo multiplier tube (PMT) and then the voltage is outputted based on the photon counter.

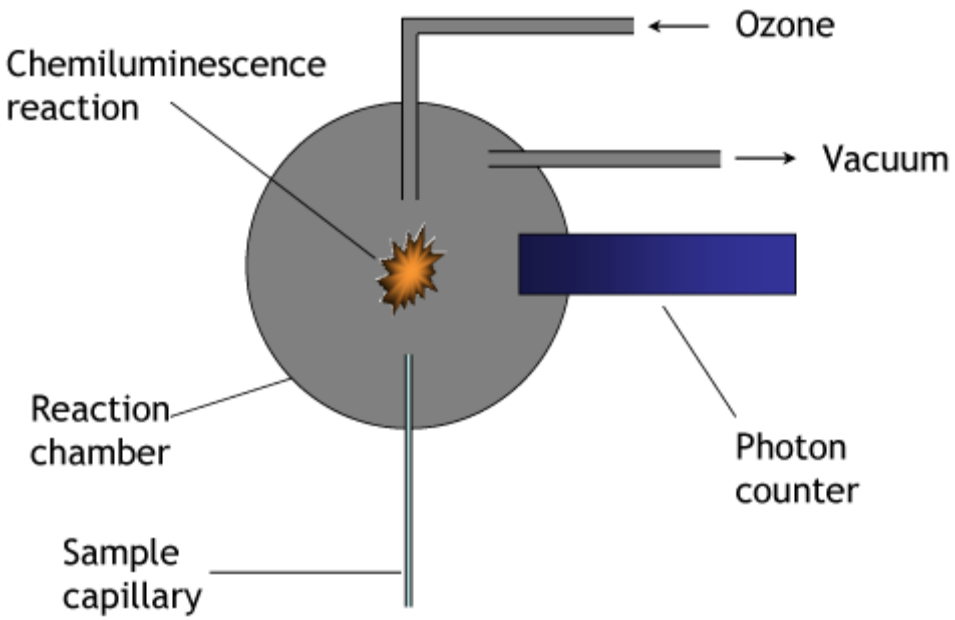

Figure 3-13 Principle of the CLD500 Analyzer

Source: http://www.cambustion.com/products/cld500/cld-principles

Similarly, the Cambustion HFR500 is a flame ionisation detector (FID) used for total hydrocarbon measurement with a short time response of 0.7 ms $T_{10\text{-}90\%}$ (Cambustion 2012). The HFR500 FID detector is also housed in the remote sample head and located close to the sample point. The basic principle of the HFR500 is shown in Figure 3-14. There is a hydrogen flame in the chamber provided by fuel gas and air. The hydrocarbons in the sample gas produce ions when they are burned in the flame. Then the ion collector is used to detect the ions and the current across the collector can indicate the rate of ionisation; thereby obtaining the concentration of HC in the sample gas.

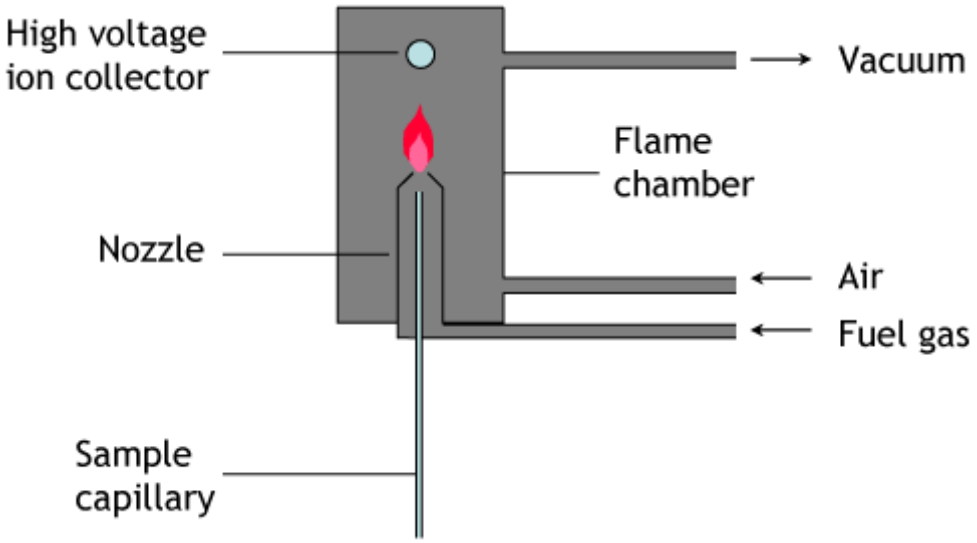

Figure 3-14 Principle of the HFR500 Analyzer

Source: http://www.cambustion.com/products/hfr500/fast-fid-principles

AVL AMA i60

The AVL AMA i60 emission bench is used to measure the gaseous toxic substances in the test cell as well, as shown in Figure 3-15. It combines basic functions for performing a gaseous emission measurement including CO, CO_2, NOx, HC and O_2. A computer is equipped to control and monitor the emission bench meanwhile the instantaneous data is transferred to the PUMA system directly through Ethernet at 10 Hz. The system was automatically calibrated by span and zero calibration gas before each testing.

Figure 3-15 AVL AMA i60 Emission Bench

Due to the long sample line, an air filter, sample flow regulator and pump are required for this gas emission bench; as a result, the response time of the i60 is much longer compared with the emission outputs from the Cambustion gas analysers. However, in light of the stable condition after the regulation, the accuracy and repeatability of the i60 is better. In addition, the integrated data acquisition system with PUMA facilitates the synchronization of data from the emission analysers and other engine measurement facilities. The selected specification of AVL AMA i60 is listed in Table 3-4.

Table 3-4 Specification of AVL AMA i60

Component	NOx	THC	O_2
Measurement principle	CLD	FID	Magneto-pneumatic detection (MPD)
Range (DSR)	0-50 -10000ppm	0-10-500ppmC 0-1000-50000ppmC	O_2 0-1-25%
Repeatability (zero)	<±0.5% FS	<±0.5% FS	<±0.5% FS
Repeatability (span)	<±0.5% RS	<±0.5% RS	<±0.5% RS
Drift (Zero)	<±0.5%FS/8h	<±1%FS/8h	<±1%FS/8h
Drift(span)	<±0.5%FS/8h	<±1%FS/8h	<±1%FS/8h
Noise	<±1%FS	<±1%FS	<±1%FS
Linearity	<±1%FS or <±2%RS	<±1%FS or <±2%RS	<±1%FS or <±2%RS
T90	NO: within 1.5 sec NOx: within 2.0 sec	<1.5sec	<2.5 sec
Sample flow rate	1.5 l/min	1.5 l/min	1.0 l/min

In the table, FS indicates full scale and RS means relative saturation.

3.4.5 Particulate Matter Measurement

Besides the gaseous emissions, particulate emissions were measured in this test cell, using the Cambustion DMS500, which can measure time-resolved particle number (PN) and their spectral weighting in the 5 nm to 1000 nm size range with a time response of 200 ms (Giakoumis et al. 2012). The equipment is presented in Figure 3-16.

Figure 3-16 DMS500 Fast Particulate Spectrometer

One dilution system of the DMS500 is fitted to avoid particle condensation and block the sample line before the sample gas enters the particle classifier. The dilution consists of two stages: first, the sample gas is diluted in the heated sampling head which is close to the engine sample point at the dilution ratio of 5:1; next, a rotating disk diluter is involved and the further dilution ratio can be controlled at the range of 200:1 to 1:1 by adjusting the speed of the rotating disk (Cambustion 2011). This controllable dilution is essential since the proper particle concentration of the diluted sample gas may vary during the engine transient operation.

After the suitable dilution, an aerosol charger and particle electrical classifier in the DMS500 is utilized to separate the particles. The particles in the diluted gas are charged and then

enter the classifier containing a high voltage electrode. Based on the electrical mobility, the charged particles can be accurately classified in the electrode rings and the numbers of particles are acquired through the charge quantities. The principle is illustrated in Figure 3-17.

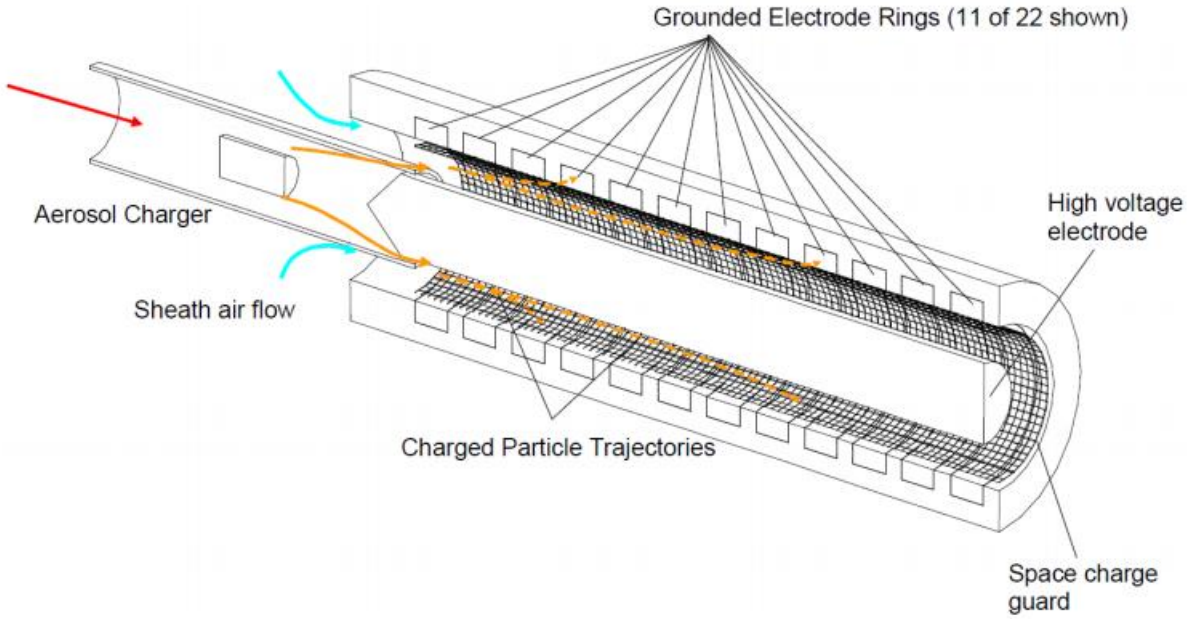

Figure 3-17 DMS500 Particle Classifier and Charger (Zhang 2013)

The DMS500 allows the nucleation and accumulation modes to be processed separately, enabling a particle measurement programme (PMP) comparable number concentration measurements without the use of a volatile particle remover (VPR). Particulate mass (PM) was determined by the calculation of DMS at real-time particle mass concentration. Since the nucleated particulates are sensitive to the sampling condition and the proportion of the total PM is small (Burtscher 2005), only the accumulation mode mass was considered in this study. The real-time particle number and particulate mass were measured and recorded to illustrate the effect of transient operation on particulate matter.

3.5 Summary

This chapter introduces the experimental system developed for this study. One Jaguar V6 diesel engine was used and fitted in the test bench. The operating and control system was set up to run the engine in the designed transient manoeuvres with a powerful transient dynamometer. The advanced conditioning system was adopted and provided the capability of temperature control during the experiments. The AVL PUMA system and INCA software were utilized to monitor and record the data from the testing facilities.

A number of engine performance measurement facilities were integrated in the test bench. Considering the focus of this study is on transient operation, all of the facilities are capable of measuring instantaneous data and have a relatively short response time. The measurements such as in-cylinder pressure, oxygen concentration, NOx, HC and particulate matter are crucial for the transient investigation and development of engine modelling.

CHAPTER 4

DEVELOPMENT OF METHODOLOGY FOR ENGINE TRANSIENT ANALYSIS

In this chapter, the techniques developed for the appropriate post-processing of data obtained from engine transient operation are introduced. Four alternative automated approaches have been developed and applied on the in-cylinder pressure data diagnostics for the analysis of combustion characteristics. The methods to calculate the cycle-by-cycle heat release rate and comparison of different filtering techniques are then presented. Detailed methods to process high-frequency instantaneous emission data, to compensate for the analysers' intrinsic delay and to align the transient data are developed. Finally, the transient data quality is discussed.

4.1 Introduction

The objective of the present study is to develop a methodology for the measurement and processing of data during transient engine tests. The main issues concerned are the noise and time alignment of data; whereas in steady state operation, because of data averaging, these issues don't cause any significant problems in the interpretation of the data. Noise levels compared to signal strengths are low enough for typical data processing methods to be used. However, these methods eliminate some high-frequency fluctuations which may

contain data on the intrinsic combustion instability of fuels. Particularly, apart from the diesel engine, data from one gasoline engine is used as a reference. The detailed information of the gasoline direction injection (GDI) engine is supplied in the Appendix. The unprocessed data presents some characteristic differences of combustion behaviour during transient operation for these two fuels. The time alignment issue is significant in emission measurements for transient operation and it arises from two delay times; one is associated with the sensors' response time and the other is the transport delay time.

4.2 Combustion Diagnostic Data Processing

The classic combustion diagnostic in engine studies relies on in-cylinder pressure which provides the most important information on the burning rate and overall engine performance. High-frequency components in the pressure signal cannot be observed with a low sampling frequency; meanwhile a high sampling frequency introduces digitization noise, deteriorating the quality of the signal (Syrimis and Assanis 2003). The purpose of filtering is to produce a physical representation of the in-cylinder pressure for combustion analysis. The most common method to filter the in-cylinder pressure is to average the data from 100 to 200 cycles in steady state experiments. Considering the different requirement of a transient experiment, cycle-by-cycle variation cannot be neglected due to the possible incomplete combustion or knock phenomenon during tests, so that the averaging method is unsuitable. Thus, proper filtering of engine in-cylinder pressure data is necessary in the transient tests because of the high frequency of the signals and inherent pressure oscillations.

4.2.1 Filtering

Two series of in-cylinder pressure traces from gasoline and diesel engine tests are used to study the filtering effectiveness of the in-cylinder pressure for combustion analysis during transient operation. For the gasoline engine test, the engine load was increased from 60 to 120 Nm at a constant speed of 1500 rpm and the spark timing was advanced from 25° BTDC (Before Top Dead Centre) to 35° BTDC. For the diesel engine test, the load was increased from 60 to 240 Nm with advanced two pilot injections at 1500 rpm as well. Furthermore, one test was operated in the gasoline engine when the engine was driven by the motor at 1500 rpm without combustion for the comparison and analysis of the pressure signal. The in-cylinder pressure sensors used in both tests were Kistler piezoelectric transducers with a natural frequency of 130 kHz. The data of the successive in-cylinder pressures during the load transient tests at a constant engine speed were recorded at a frequency of every crank angle degree (around 9 kHz considering an engine speed of 1500 rpm). The MATLAB programming language is used to write the filtering code because of the availability of a range of analytical tools and its ability to process large amounts of data automatically.

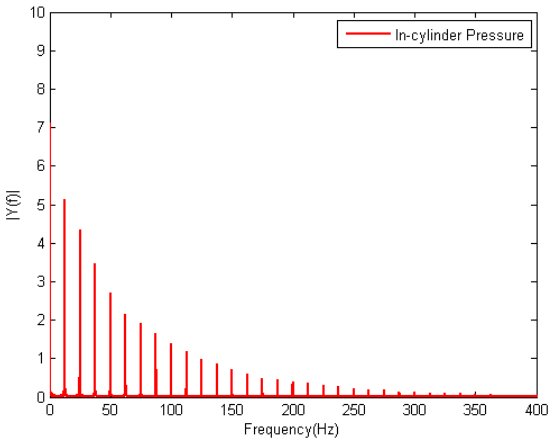

(a)

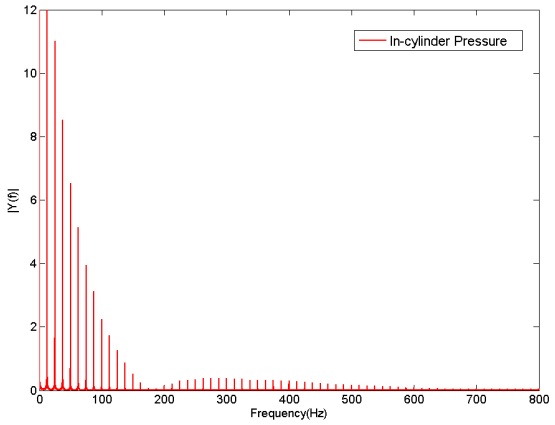

(b)

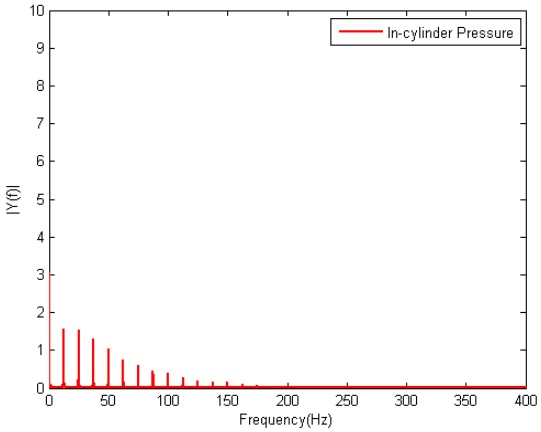

(c)

Figure 4-1 FFT Power Spectrum of the In-cylinder Pressure Signal during the Load Increase Experiment

(a) Gasoline Engine; (b) Diesel Engine; (c) Engine with No Combustion

First, FFT on the in-cylinder pressure data of each test was conducted to examine its spectral characteristics. As shown in Figure 4-1, the constant engine speed of 1500 rpm which means 12.5 Hz as an engine firing frequency, determined the spectrum of the in-cylinder pressure. The power at 12.5 Hz was the highest in all the cases. The higher frequency components are higher harmonics of the pressure wave in the cylinder. It is found that the shapes of the FFT power spectrum of these tests are different. In the gasoline engine case and the 'no combustion' case, the power was reduced gradually when the frequency increased. However, in the diesel engine case, the power becomes very low in the range about 180 Hz and then increases until 300 Hz. This phenomenon is expected to be a result of multiple combustions within one cycle in the diesel tests. When the frequency is even higher, this would be expressed in the in-cylinder pressure profile as fluctuation in the shape. The sources of fluctuation could be classified into three aspects:

1. Noise from the instruments including the pressure transducer and cable
2. Engine vibration
3. Intrinsic instability of combustion.

The main objective of filtering the in-cylinder pressure is to remove the noise from the first two aspects and achieve good visualization while retaining the important information of the combustion analysis. As shown in Figure 4-2, when the engine is purely driven by the motor and no combustion occurred, the noise is found in the whole cycle. Therefore, when the frequency is very high and the related power becomes very low, it is reasonable to assume those components as noise and can be neglected with little effect on the heat release analysis.

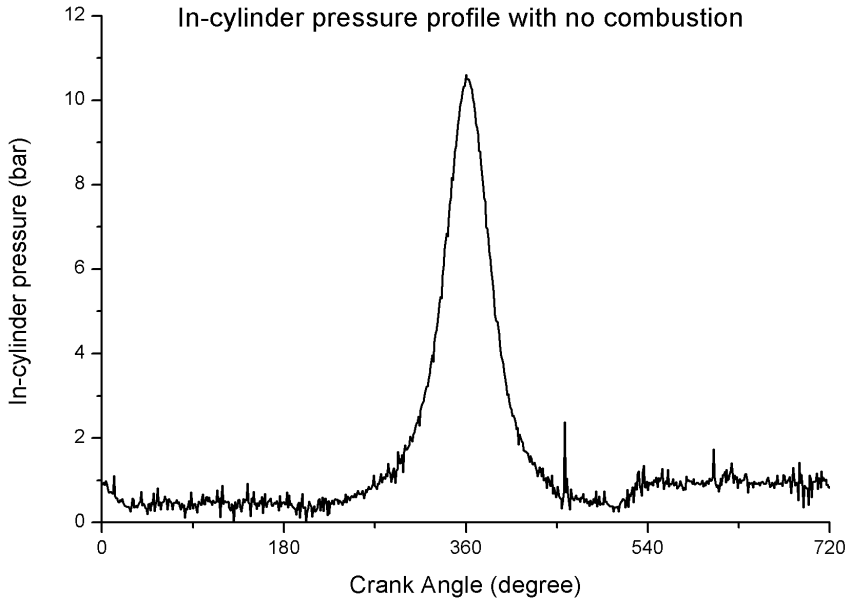

Figure 4-2 In-cylinder Pressure Profile @1500 rpm with No Combustion

To explore the proper filtering method for the in-cylinder pressure of the transient engine tests, four simple alternatives of filtering techniques are presented and compared in the next section.

FFT Filtering

As discussed above, the in-cylinder pressure trace is normally accompanied with low power higher harmonics and noise, which should be removed for the combustion analysis. FFT filtering method is employed by defining a cut-off frequency of the filter and removing Fourier components with frequencies higher than the cut-off frequency. Based on the information from Figure 4-1, the cut-off frequency of the gasoline engine case is set at 400Hz for these tests and the frequency of the diesel engine case is 800Hz.

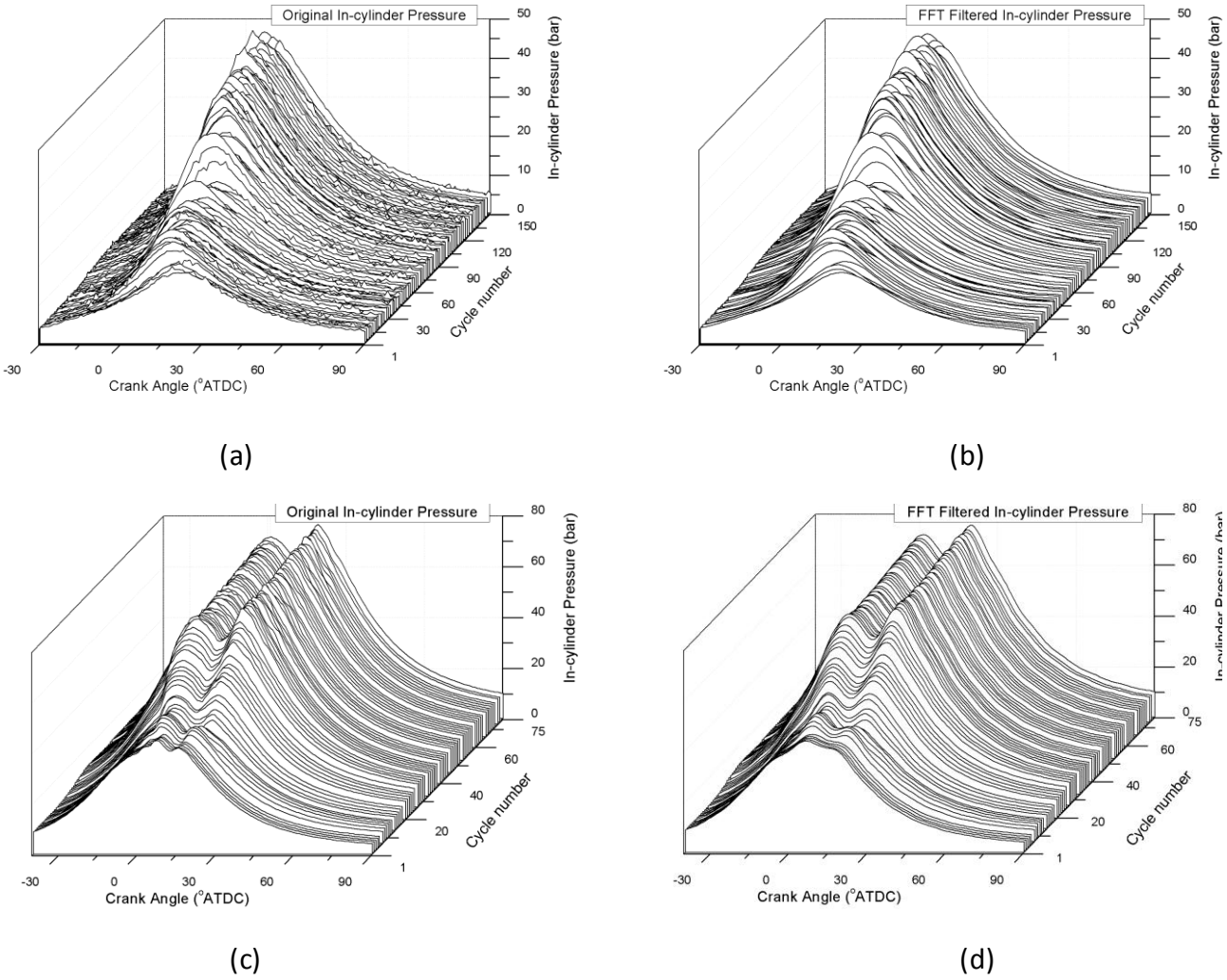

Figure 4-3 The In-cylinder Pressure during the Load Increase Experiment (a) Original Signal in Gasoline Engine; (b) FFT Filtered Signal in Gasoline Engine; (c) Original Signal in Diesel Engine; (d) FFT Filtered Signal in Diesel Engine.

Figure 4-3 presents the original and FFT filtered in-cylinder pressure traces of the gasoline engine and the diesel engine during the load increase test. In the gasoline engine case, it is obvious that the original data has a number of inherent pressure oscillations and they are most probably the noise from instruments and engine vibration. The FFT filtering smoothened out the data properly and kept the main characteristic of each cycle. In the diesel engine case, since the data is collected from the combustion analyser AVL Indicom, it was already filtered once before generating the outputs. The original pressure seems acceptable and the FFT filtered data was excessively smooth, especially the peak of the pressure.

Low-pass Filtering

In terms of noise elimination of the signal, low-pass filtering is one of the most common signal processing methods used. Therefore, Butterworth low-pass filters were applied on the in-cylinder pressure trace during the load transient tests. The filter order was set at 2 and the cut-off frequencies were set the same as the FFT filter, 400Hz and 800Hz.

Due to the intrinsic characteristic of the low-pass filter, the phase of the filtered in-cylinder pressure is found to be retarded in comparison with the original signal. However, the phase delay is constant for each cycle owing to the crank-angle based pressure data. Thus, the low-pass filtered data has been shifted afterwards to fit the crank angle degree for combustion analysis. The low-pass filtering largely smoothens out the pressure data of the gasoline engine and diesel engine as shown in Figure 4-4. Nevertheless, the distortion of the profile is apparent; it is caused by the frequency response of the Butterworth filter being flat

in the pass band. Detailed comparison and discussion of different filters are presented in a later section.

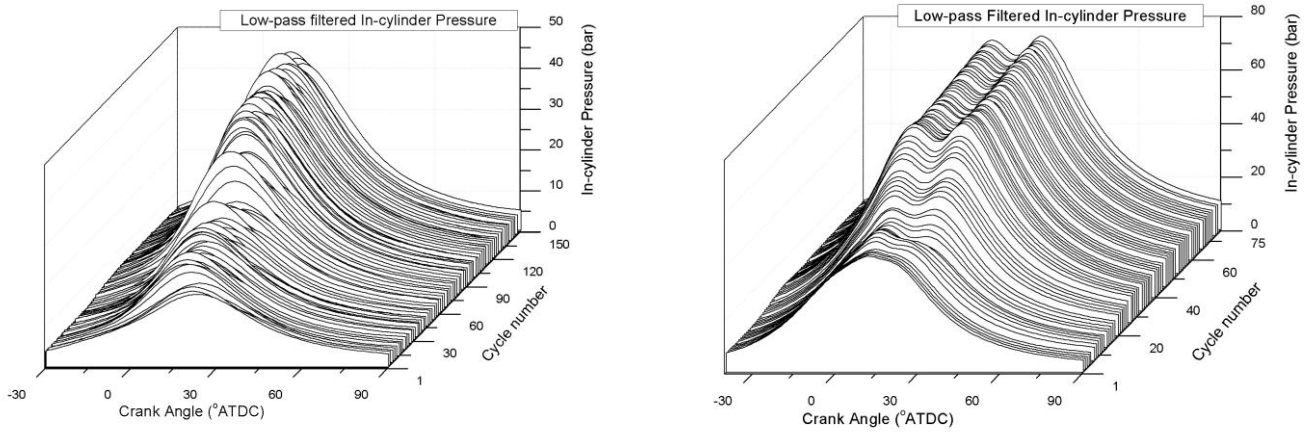

(a) (b)

Figure 4-4 The Low-pass Filtered In-cylinder Pressure during Load Increase Experiment (a) Gasoline Engine; (b) Diesel Engine.

Linear Filtering

The LTI (Linear Time-Invariant) filter is a common method of signal processing and a FIR (Finite-duration Impulse Response) filter was employed for the in-cylinder pressure profiles processing. Basically, the filter was used to find a running average of the pressure signal in order to reduce the noise. Its input-output relation is:

$$y(n) = \sum_{k=0}^{M} b_k x(n-k) \qquad \textbf{Equation 4-1}$$

Where y(n) represents the n_{th} value of the output array; similarly x(n-k) means the $(n-k)_{th}$ value of the input array; M is the filter order, set as 4 in this study and the coefficient b_k is 1/5 correspondingly. The outputs of the linear filter present a phase delay relative to the original data which is determined by the order of the filter. In order to calculate the heat

release rate correctly, the filtered data was shifted afterwards. In Figure 4-5(a), it is found that the in-cylinder pressure during the combustion period was smooth after the linear filtering while the fluctuation is apparent when the pressure is lower in other periods.

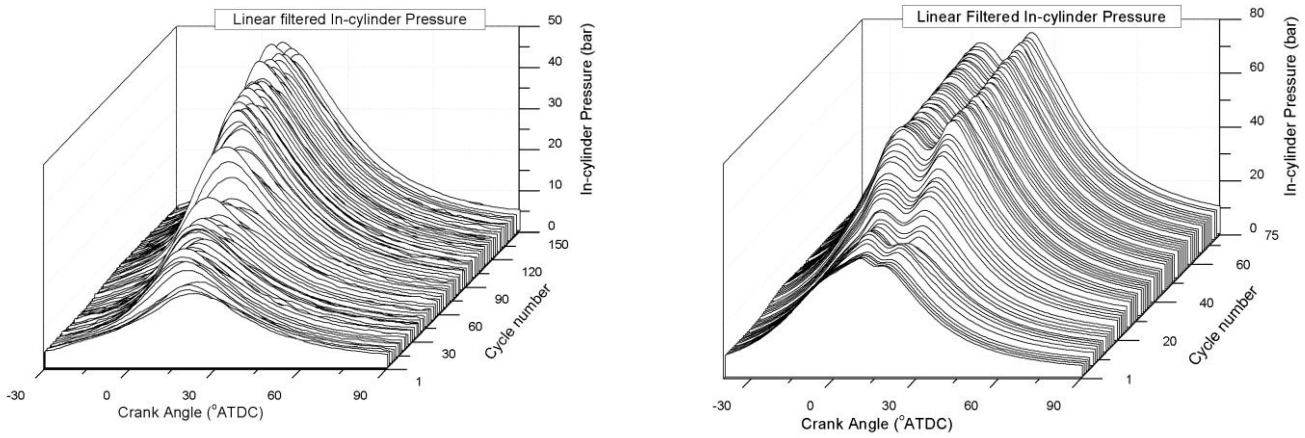

(a) (b)

Figure 4-5 The Linear Filtered In-cylinder Pressure during Load Increase Experiment (a) Gasoline Engine; (b) Diesel Engine

Zero-phase Filtering

Zero-phase filtering is one of the useful filtering methods to process a digital signal (function name, filtfilt, in the MATLAB program). The data was filtered in both forward and reverse directions. The result of this filtering has precisely zero phase distortion and magnitude modified by the square of the filter's magnitude response. The filter could be described by the difference equation:

$$y(n) = \sum_{k=0}^{B} b_k x(n-k) - \sum_{k=0}^{A} a_k y(n-k) \qquad \textbf{Equation 4-2}$$

Where y(n) represents the filter output; x(n-k) means the input value; $\{a_k, b_k\}$ are the filter coefficients. The filter was set as an FIR filter with filter order of 2.

The zero-phase filtering has an advantage for in-cylinder pressure data processing and experimental data analysis. It is capable of processing data for each individual cycle because it does not rely on periodicity of the engine combustion, which is important for FFT and low-pass filtering. The in-cylinder pressure profiles after the zero-phase filtering are presented in Figure 4-6. Similarly to the linear filter used, the output of the filtering signal depends on the values of the adjacent data points. Due to the nature of transient experiments, the tendency of change in the in-cylinder pressure is important. In this study, two data points before and two data points afterwards are considered in the filtering due to the set filter order.

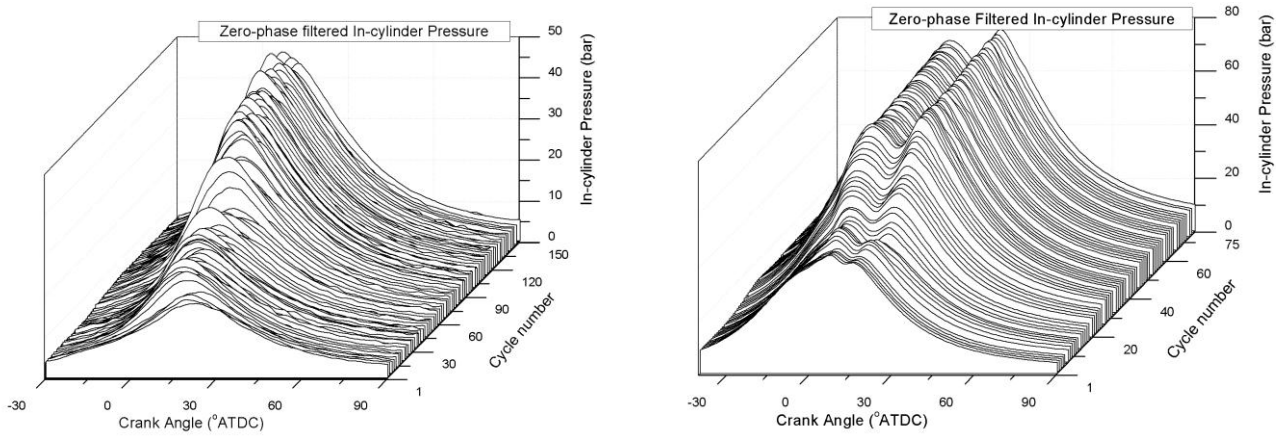

(a) (b)

Figure 4-6 The Zero-phase Filtered In-cylinder Pressure during Load Increase Experiment (a) Gasoline Engine; (b) Diesel Engine

In general, the four automated filtering techniques are all capable of largely smoothing the pressure data and removing the main fluctuation. The cycle-by-cycle profiles are clearly presented and show the main trend of change during the engine transient tests. Since the

engine combustion analysis is mainly dependent on the study of the heat release rate calculated by the in-cylinder pressure, the detailed comparison and discussion of the effect of filtering techniques on combustion analysis will follow later.

4.2.2 Heat Release Analysis

The engine rate of heat release (RoHR) is calculated from in-cylinder pressure traces for each consecutive cycle during the transient tests where the quasi-steady state is assumed for each engine cycle. The present analysis is based on the first law of thermodynamics (Heywood 1988). Considering the amount of heat loss to the surroundings is much lower than the net heat release during the load change tests, due to the slow rate of heat transfer compared to the heat release rate, heat transfer and crevice effects are neglected in the calculation.

$$\frac{dQ_n}{dt} = \frac{\gamma}{\gamma - 1} P \frac{dV}{dt} + \frac{1}{\gamma - 1} V \frac{dP}{dt} \qquad \textbf{Equation 4-3}$$

Where γ is the specific heat capacity ratio; P is the in-cylinder pressure and V is the instantaneous volume.

Since the value of a specific heat capacity ratio depends on the gas mixture composition, it is calculated by an equilibrium program. Specifically, the adiabatic process is assumed in the compression stroke and most of expansion stroke. Due to the assumption of the adiabatic process, the polytropic index is calculated by the pressure data of every cycle when air prior to combustion and burned gases individually are considered as γ. Although the specific heat

capacity ratio obtained in this method cannot reflect the composition at any given location in the cylinder, it can reflect the variation of properties during the transient operation.

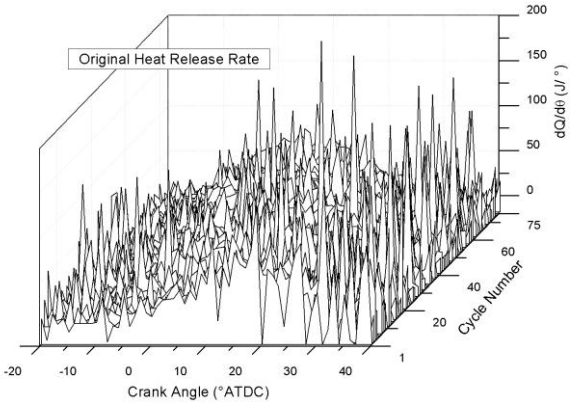

(a)

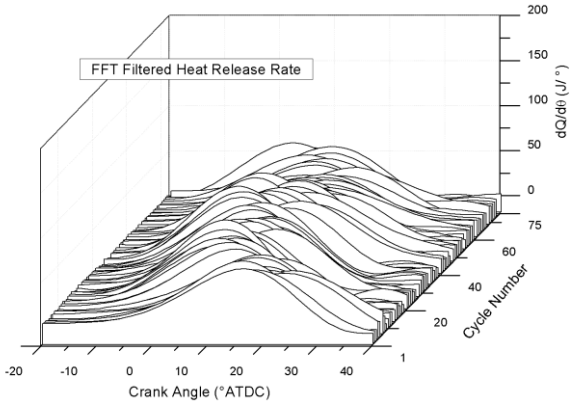

(b)

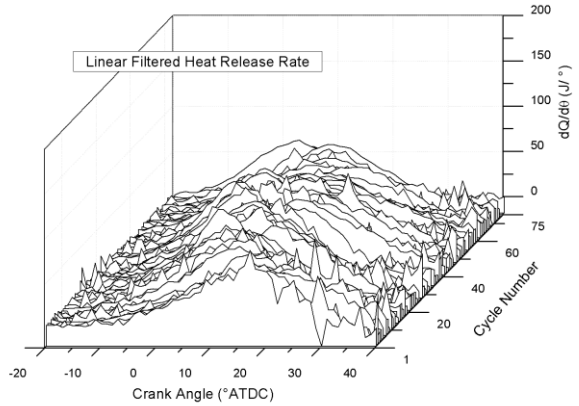

(c)

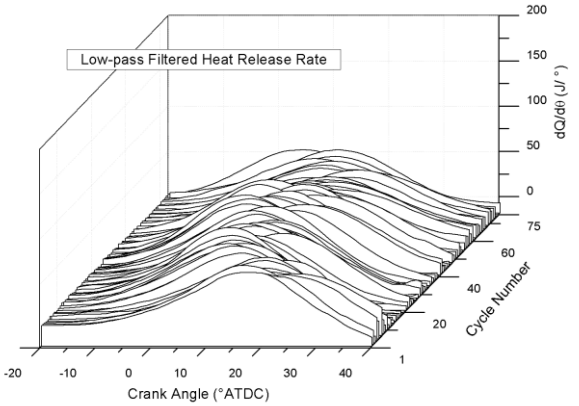

(d)

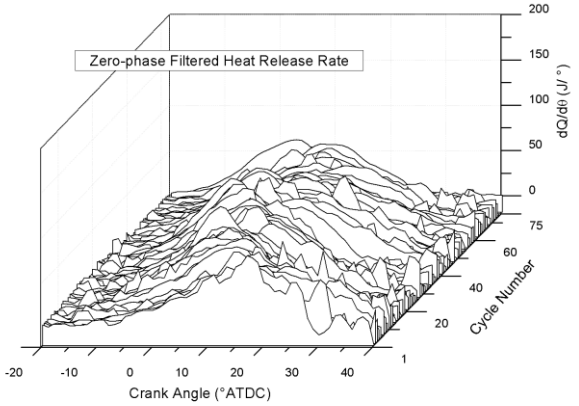

(e)

Figure 4-7 Calculated Cycle-by-cycle Heat Release Profiles in the Gasoline Engine; (a) Based on Original Pressure Data; (b) FFT Filtered Pressure; (c) Low-pass Filtered Pressure; (d) Linear Filtered Pressure; (e) Zero-phase Filtered Pressure.

The calculated cycle-by-cycle RoHR profiles with different filtering of the gasoline engine tests are presented in Figure 4-7. The RoHR profiles based on the FFT filtered and low-pass filtered in-cylinder pressure are smooth without an additional process; while the profiles with the original pressure signal are full of spikes. The main reason is that differentiation in the calculation amplified the higher frequency components. Variations of combustion in each engine cycle are illustrated clearly. It is shown that variations of the combustion phase are especially large during a low load period. In general, the combustion phase is advanced with the advancing of spark timing during engine transients. As for the linear and zero-phase filtering cases, the noise is reduced by averaging but there are a number of ripples in the RoHR profiles, especially in the late combustion period. The noise of the low in-cylinder pressure was amplified through differentiation and erroneously incorporated as heat release. In short, the linear filter and zero-phase filter could reflect the primary cycle-by-cycle combustion performance, but the RoHR required further smoothing for proper visualization.

To compare the effect of different filters on combustion analysis specifically, two engine cycles during the load increase tests were picked for detailed comparison. The 50^{th} and 120^{th} cycles are selected, as the former is approximately in the middle of the load increase and the latter occurs close to the end of the load increase.

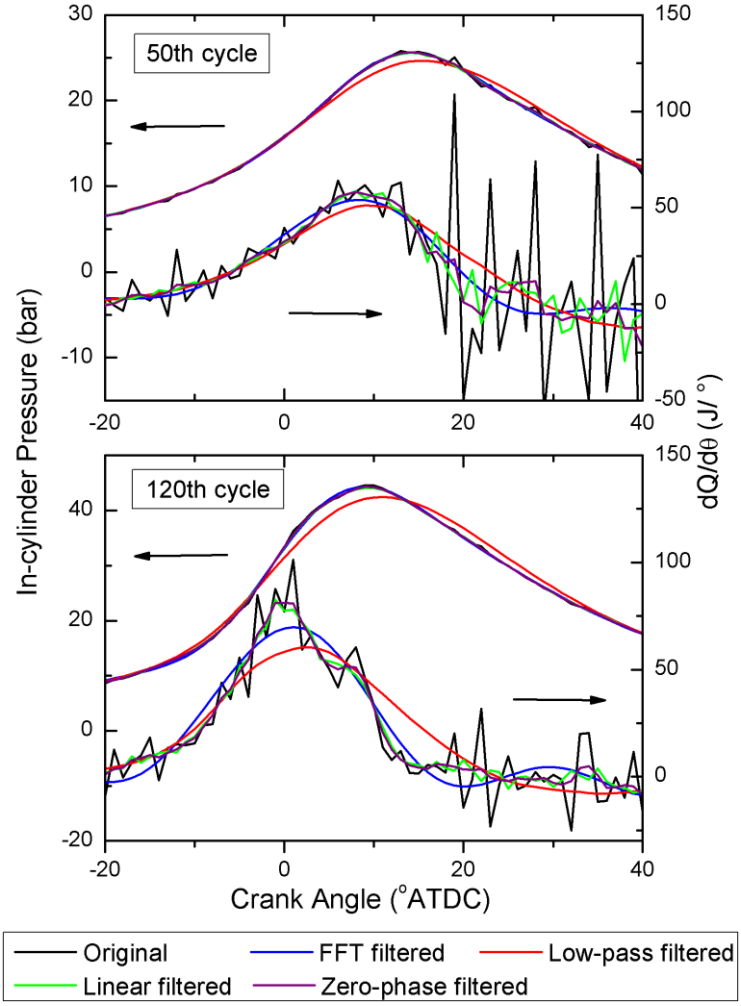

Figure 4-8 In-cylinder Pressure and RoHR Profiles of Two Representative Cycles with Different Filtering in the Gasoline Engine Test

In Figure 4-8, it is apparent that the low-pass filtered data has the most distortion both in amplitude and phase. The changes in important parameters like the peak cylinder pressure and peak pressure position by the low-pass filter render them improper for combustion analysis; while they could be easily used to illustrate the trends in experimental works. The processed data by either the linear filter or the zero-phase filter is very close to the in-cylinder pressure and RoHR profiles. It is interesting that in the 120th cycle, the original heat release rate has an obvious drop after the peak and the data from the linear filter and zero-phase filter keep this feature, while the FFT filter does not. Considering the engine heat

release pattern, this drop is probably due to the in-cylinder pressure oscillation rather than a sudden reduction of heat release. Thus, the profile from the FFT filtered data is closer to the real situation than the results from other filters. In the 50th cycle, the engine load is lower and the difference of RoHR obtained from the data filtered by different filters is tiny, except for the results from the low-pass filtered data.

It should be noted that the removal of high-frequency components from the in-cylinder pressure data can cause loss of some combustion characteristics. For instance, knock cannot be detected when the cut-off frequency is low in the application of FFT and low-pass filters. Meanwhile, the moving average filters, like the linear and zero-phase filtering, in this study are attenuating the fluctuation in essence. It is difficult to distinguish the small noise from instruments and combustion instability. In this gasoline engine case, FFT filtering was the best suited filter for investigation of transient engine combustion performance. Linear and zero-phase filtering are capable of roughly smoothing the profiles and retaining the main combustion information. The low-pass filtering is inappropriate to investigate the heat release analysis due to the series distortion.

Similarly, the RoHR profiles with different filtering of the diesel engine tests are presented in Figure 4-9. In the profile based on the original pressure data, although the figure has a small fluctuation, it can be seen that two spikes before the main combustion clearly show the influence of two pilot injections at the beginning of the transient operation and a small peak occurred after the main combustion, due to the post combustion. Also, the cycle-by-cycle RoHR profiles based on the FFT filtered and low-pass filtered in-cylinder pressure are smooth and show the main trend of the heat release during the transient operation.

However, the two spikes from the pilot injections are missing in those two profiles; this means the combustion information is incomplete. Higher cut-off frequencies are tested on the FFT and low-pass filters but the difference is very small. Those two filters are not able to retain the high-frequency components caused by combustion based on the current sampling frequency. Meanwhile, the linear and zero-phase filtering removed the most fluctuations and retained the main characteristics of the combustion.

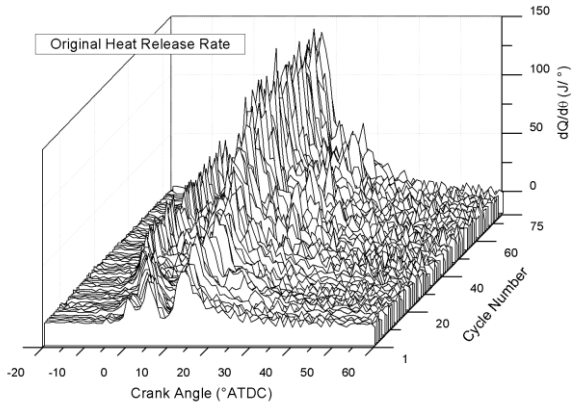

(a)

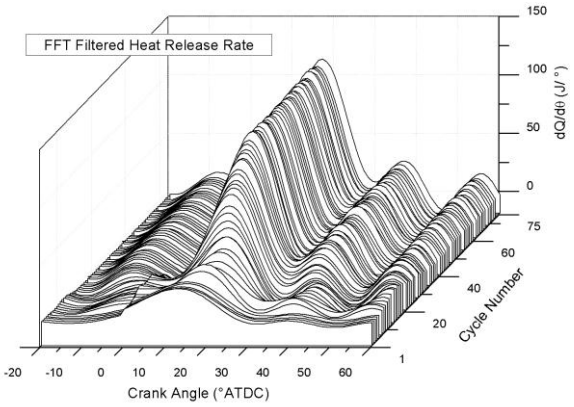

(b)

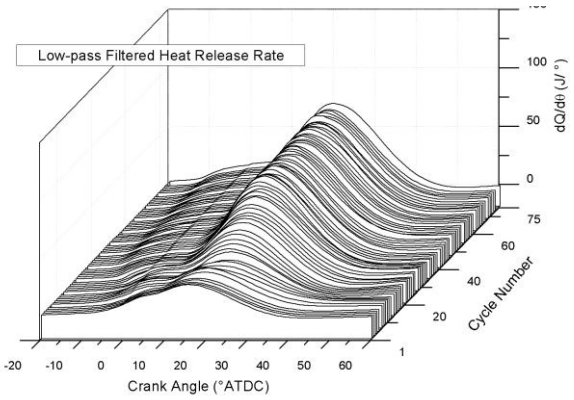

(c)

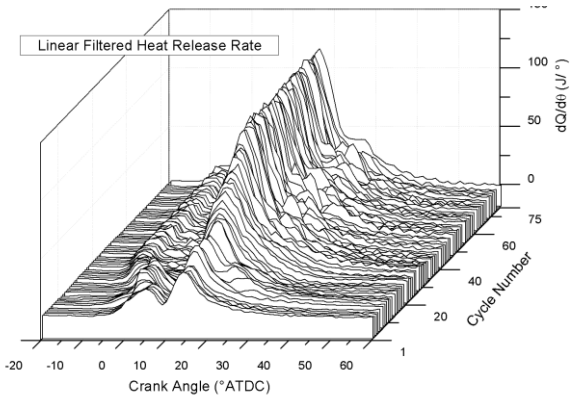

(d)

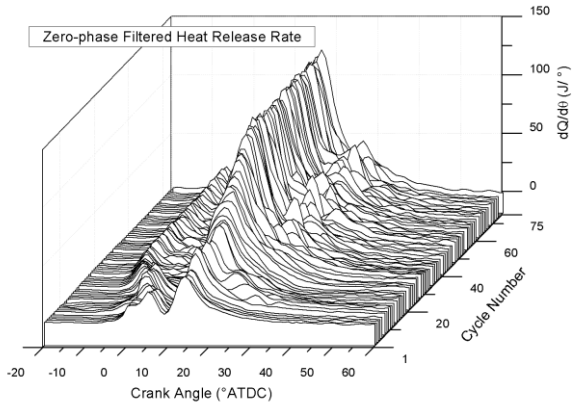

(e)

Figure 4-9 Calculated Cycle-by-cycle Heat Release Profiles in the Diesel Tests; (a) Based on Original Pressure Data; (b) FFT Filtered Pressure; (c) Low-pass Filtered Pressure; (d) Linear Filtered Pressure; (e) Zero-phase Filtered Pressure.

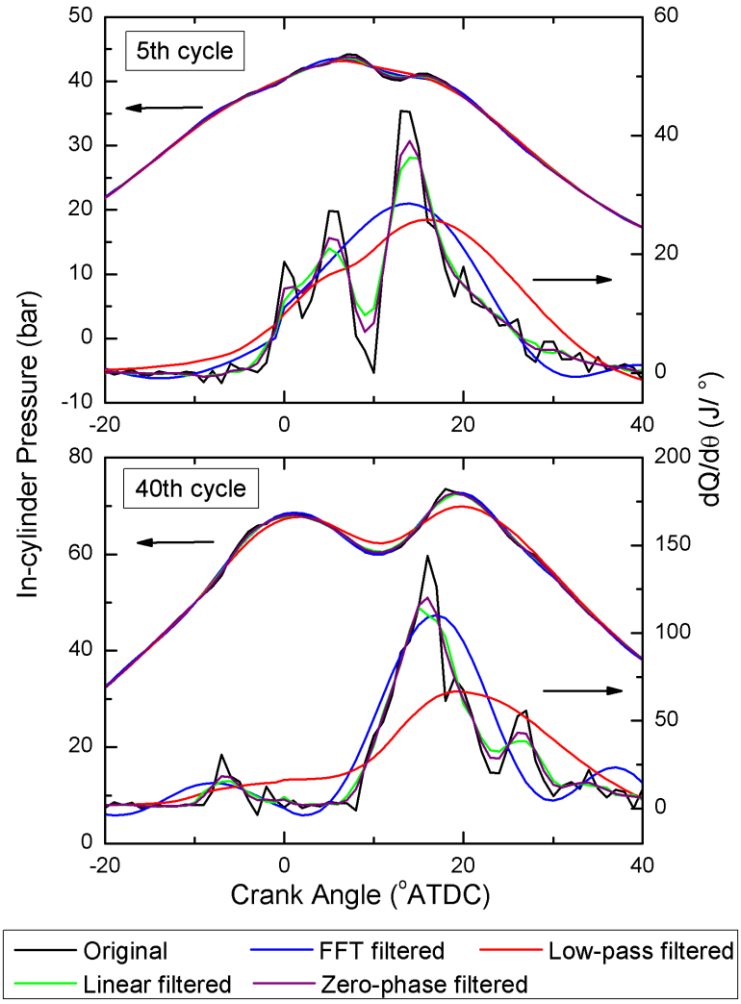

Figure 4-10 In-cylinder Pressure and RoHR Profiles of Two Representative Cycles with Different Filtering in the Diesel Engine Test

In the designed test sequences, two cycles, the 5th and 40th are chosen for detailed analysis to represent the changing process. At the 5th cycle, as mentioned above, it is observed that two pilot combustions occurred at 0 to 10 °ATDC. The differences of the filtered in-cylinder pressure profiles in this range are small, but the corresponding profiles of the heat release rate show interesting differences. Since the frequency components of the pilot combustion are close to the noise of the instrument, if either FFT or low-pass filters are applied, the pilot combustion information cannot be reconstructed, which is unacceptable. While the linear and zero-phase filters attenuate the noise and therefore retain more combustion information. At the 40th cycle, the retarded main injection timing resulted in two spikes in the in-cylinder pressure and there is one small peak in the RoHR due to the post injection and the low-pass filtered in-cylinder pressure being less accurate. The RoHR calculated from the low-pass filtered data almost misses all the important information. Besides, the RoHR profile of the FFT filtered pressure data tends to be in smooth arcs and does not correctly represent the main combustion profile, especially close to the post injection phase. Similarly to the 5th cycle, the linear and zero-phase filters simply smoothes the jagged edges and keeps the main shape of the RoHR.

As discussed above, in this diesel engine case, FFT and low-pass filters are not suitable to investigate the combustion characteristics. Based on the Nyquist–Shannon sampling theorem, the small combustions in the diesel engine require a much higher sampling frequency to recognize the noise and combustion instability and thereby visualize the combustion information correctly after filtering. The linear filtering is able to preserve the combustion phase but tends to excessively attenuate the peak of combustion. The zero-phase filtering is the most appropriate method on balance, considering its convenience of

examination and information preservation. All in all, the suitable filtering method for the cycle-based in-cylinder pressure is dependent on the objective and the specific case. For the single injection combustion, FFT filtering can easily smooth the curve of pressure and produce a presentable and reliable RoHR profile. For the multiple injection combustion, zero-phase filtering is the best option to batch process the original in-cylinder pressure in the current sampling frequency. In the case with the relatively low sampling frequency, it is required to maintain high-frequency components containing useful information; a moving average filter such as the zero-phase filter is best. In the case with the relatively high sampling frequency, the FFT filter is better due to its advantage on removing the unnecessary noise and keeping the phase.

4.3 Transient Emission Data Processing

Instantaneous emissions, including the NO, HC and particulate matter, were measured in the engine transient experiments. The CLD500 and HFR500 were used as the gaseous emission analysers; they had short response times of 2 ms and 0.7 ms $T_{10\text{-}90\%}$ respectively (Cambustion 2012) (Cambustion 2013). The fast response provides the possibility of measuring the cycle-by-cycle variation of emissions with high sampling frequencies. In these tests, the acquisition rates of NO and HC were chosen as 10 kHz. However, the data collected contained high-frequency noise and it was necessary to filter the data sets (Pickering and Brace 2007).

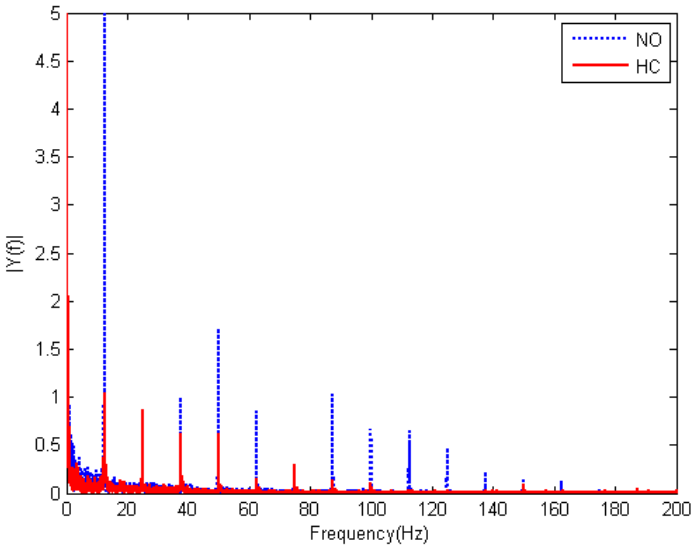

Figure 4-11 FFT Power Spectrum of Instantaneous NO and HC during the Load Increase Experiment

The FFT of a set of instantaneous NO and HC from diesel transient experiments was conducted before filtering. Figure 4-11 illustrates the high correlation of the engine speed and time-resolved emissions. NO is produced at high temperature combustion, thus the peak of NO corresponds to the cyclic firing frequency, 12.5 Hz. The frequency of HC Fourier components coincided with the firing frequency as well, but with lower cyclic oscillation than NO due to the variety of HC emission formations.

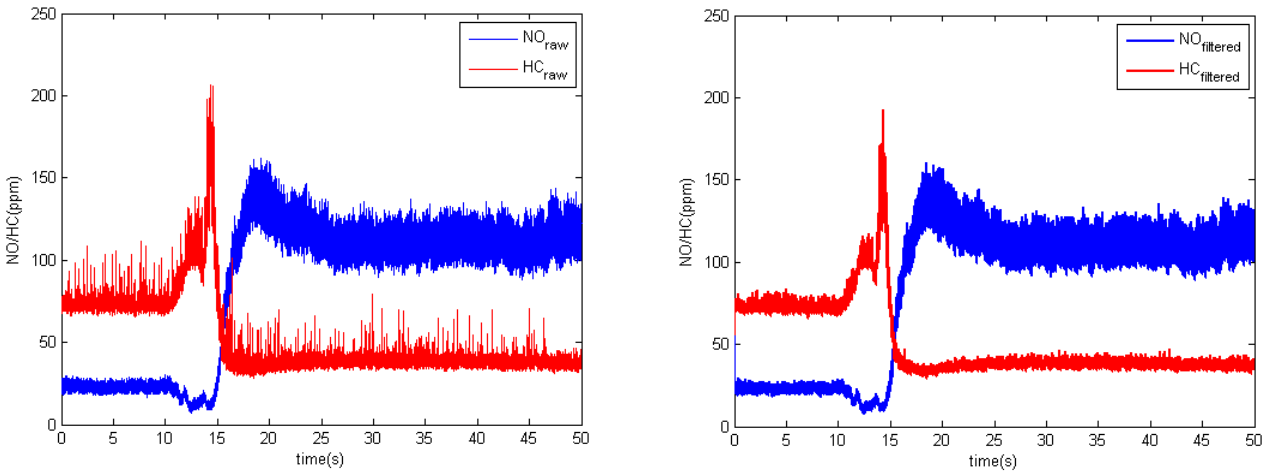

Figure 4-12 (a) Raw Data of Instantaneous NO and HC during the Load Increase Experiment; (b) FFT Filtered Data of Emissions

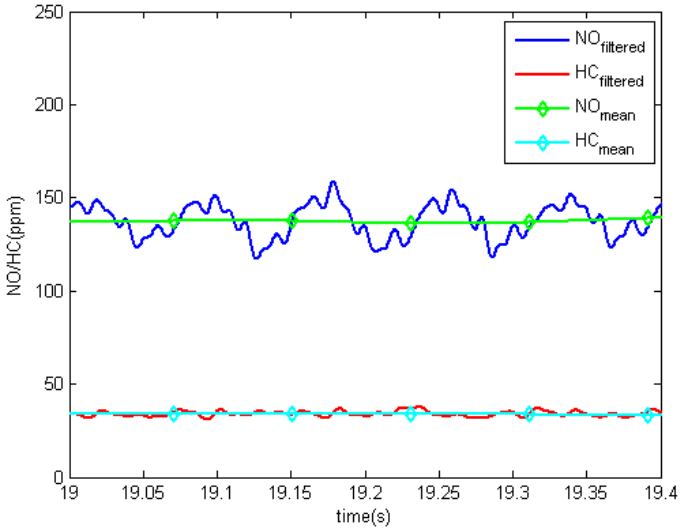

Figure 4-13 Mean Value Determination of Instantaneous Emission according to Engine Speed

In Figure 4-12, the raw and FFT filtered instantaneous NO and HC emissions are presented. Owing to the high acquisition frequency and intrinsic characteristics of the facility, a high level of noise exists in the emission data, especially for HC. After the data is filtered against high-frequency components, the breadth of data is still unsuitable for examination and analysis. The variation in the measured emissions is derived from the continuously varying combustion of each cycle and the changing exhaust flow due to the exhaust valve switching. The detailed variations in HC/NO emissions are depicted in Figure 4-13. Furthermore, the sample points of the emissions analysers were downstream of the exhaust manifold and samples included exhaust air from all six cylinders. As a result, the observed variations are meaningless for the emission analysis in this test.

Considering each cylinder fires every 720° CA and combustions occur every 120° CA for the six cylinder four-stroke engine, a linear mean value filter over each engine rotation was designed to fully adapt the process characteristics (Kessel 1999), as in the equation below:

$$Y(n) = \frac{1}{L}\sum_{i=0}^{(L-1)} y_{original}(nL - i) \qquad \textbf{Equation 4-4}$$

$$L = round(\frac{1}{f_{firing}} f_{acquisition}) \qquad \textbf{Equation 4-5}$$

Where L is the variable length of one combustion cycle; n is the number of engine cycles; f_{firing} and $f_{acquisition}$ represent the frequency of the engine combustion and signal acquisition respectively.

The filter provided a good compromise between the noise attenuation and response quality of the data. In general, the data is processed by cyclic calculation and became cycle based. Figure 4-14 shows linear mean value outputs of transient emissions. The data contained accurate information of every engine cycle and specific values could be determined versus time.

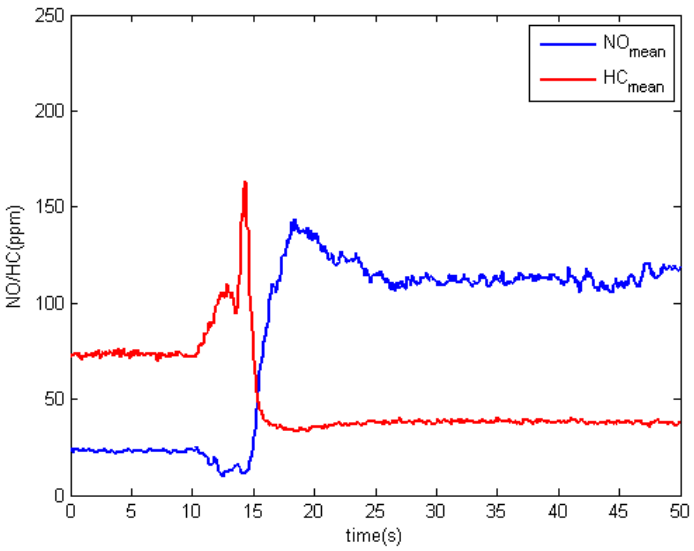

Figure 4-14 Linear Mean Values of Instantaneous Emissions

The particulate number and mass were measured by DMS with a frequency of 10 Hz. Due to the relatively low acquisition frequency and the included processing tool, it is not necessary to further filter the data.

4.4 Alignment of Transient Data

As discussed above, engine transient experiments usually involved more than one acquisition system with different acquisition rates. There is a need to combine all signals together before the detailed investigations. Accordingly, the data time alignment obtained from different acquisition systems is an important issue during data processing.

The following factors should be considered in the time alignment of transient data:

a) Discrepancy on the timeline of the data due to different starting time and sampling frequency.
b) Analyser's response time is determined by the internal sensors and related operation principles.
c) Transport time between readings of engine parameters and corresponding emissions; since time is needed for exhaust gas to travel from the engine to the exhaust sampling point.

For recording the data from Fast FID and Fast NOx, a LabVIEW code is applied, triggered by a signal from the engine operating system through Ethernet. The AVL AMA i60 is connected with the PUMA system and the gaseous emission data is recorded automatically. One analogue input of the torque signal from the operating system is connected to the DMS for

particulate emission alignment with the engine data; since the tests designed were load transient tests with a constant engine speed. Some basic combustion information, the crank angle based parameters such as IMEP and peak pressure, are transmitted to the PUMA from the combustion analyser Indicom. The engine control parameters from the ECU are transmitted to the PUMA through ASAP3. Based on the PUMA system, the data from most of the analysers are collected in the same timeline. Besides, through statistical comparison of torque signals, the discrepancy originating from other acquisition systems can be determined as well.

4.4.1 Analyser Dynamics Compensation

For the gaseous emission measurement, the AVL AMA i60 was employed in the transient experiment as well. Differing from Fast FID and Fast NOx discussed in the last section, the analysers of AVL AMA i60 have a far longer response time which cannot be neglected. The detailed information of the individual analysers is shown below.

Table 4-1 Technical Calibration Data of AVL AMA i60

	FID (THC)	**CLD (NO)**	**CLD (NOx)**	**CO2**
Rising time [s]: T_{10}-T_{90}	1.00	1.00	1.00	1.00
Falling time [s]: T_{90}-T_{10}	0.92	1.02	0.92	0.69

In the important emission data of THC and NOx, both have around a one second response time, which has a significant influence on the analysis of the results. Therefore, the dynamic characteristic of the analysers is required to be compensated accordingly.

The intrinsic response delay is reasonably assumed as a first order inertial element existing in the analyser. The transfer function can be expressed as below:

$$G(s) = \frac{1}{1 + s \cdot T} \qquad \textbf{Equation 4-6}$$

Where T is the time constant. In this study, T is calculated according to the definition of rising time T_{10}-T_{90} as shown in Figure 4-15(a). The rising time and falling time of FID and CLD are set as 1 second. Therefore, T in this function is 0.45.

To cancel the response delay, could be achieved by multiplying with its inverse function:

$$H(s) = \frac{1 + s \cdot T}{1} \qquad \textbf{Equation 4-7}$$

To meet the principle of causality, a realization pole has to be added into the function:

$$H(s) = \frac{1 + s \cdot T}{1 + s \cdot T_{new}} \qquad \textbf{Equation 4-8}$$

Where T_{new} is set as 0.1, a much lower value than T; which means the initial element has been compensated (Systems et al. 2005). The transfer function does not have a steady state error, the stability of the outputs is ensured.

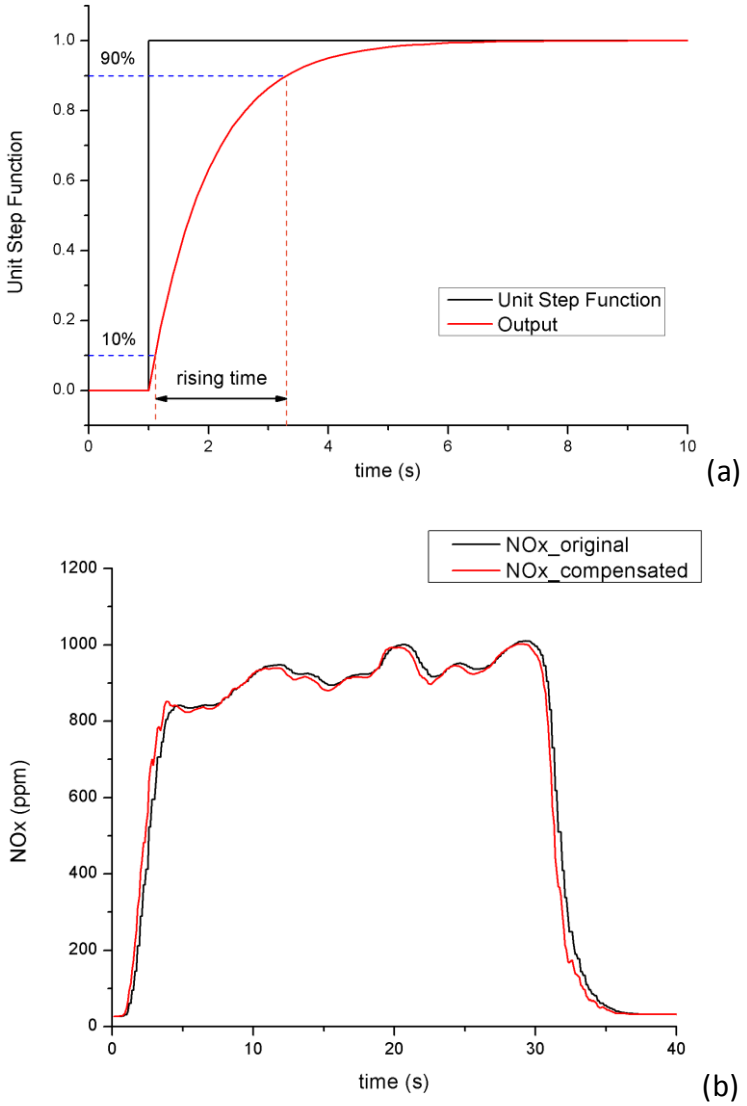

Figure 4-15 (a) The Output of Classical First Order Initial Element (T=1) with Unit Step Function; (b) Measurement and Compensation of NOx from i60 during the Transient Test

The difference between the original NOx data and the output after compensation is shown in Figure 4-15(b). It has illustrated that the response delay has been corrected during the sudden rising and falling process. It is worth noting that the dynamic correction includes a differential element which tends to increase fluctuation in the data. Therefore, T_{new} cannot be too small to avoid unacceptable noise.

4.4.2 Transport Delay Estimation

After the compensation for the analysers response delay, transport time is required to be estimated to align the time-series data properly. The common method of transient emission alignment is to focus on the starting moment of the engine's operation change. In Figure 4-16, diesel engine parameters and transient emissions during the load increase test are presented on the same timeline after time-alignment. The NO emissions change a little at the beginning of the load increase; while the air-fuel ratio decreased dramatically. This change could be used for time-alignment. In addition, the peak-to-trough method (I. Brahma and Chi 2011a) is employed to align the transient emission data. A trade-off between NO and EGR fraction exists in diesel engine operation. Thus, it can be deduced that the NO peak corresponds with EGR fraction minima during the transient tests. The correspondence is marked at 17.5 seconds as presented. Besides, the statistical method could be applied to determine the time delay as well. In Figure 4-16(a), the engine parameters and particle number during the load decreased test are presented. For the gasoline engine, the air-fuel ratio has a strong negative correlation with particulates. The period of the air-fuel ratio data was selected from the beginning of the spark timing change until the 10^{th} second when the engine almost reached its steady state. Meanwhile, a series of particle number data starting with different moment (±0.1s due to 10 Hz rate) was picked with the same length. Then, the negative correlation coefficients of data sets were compared and the highest value was chosen as the correct time-alignment.

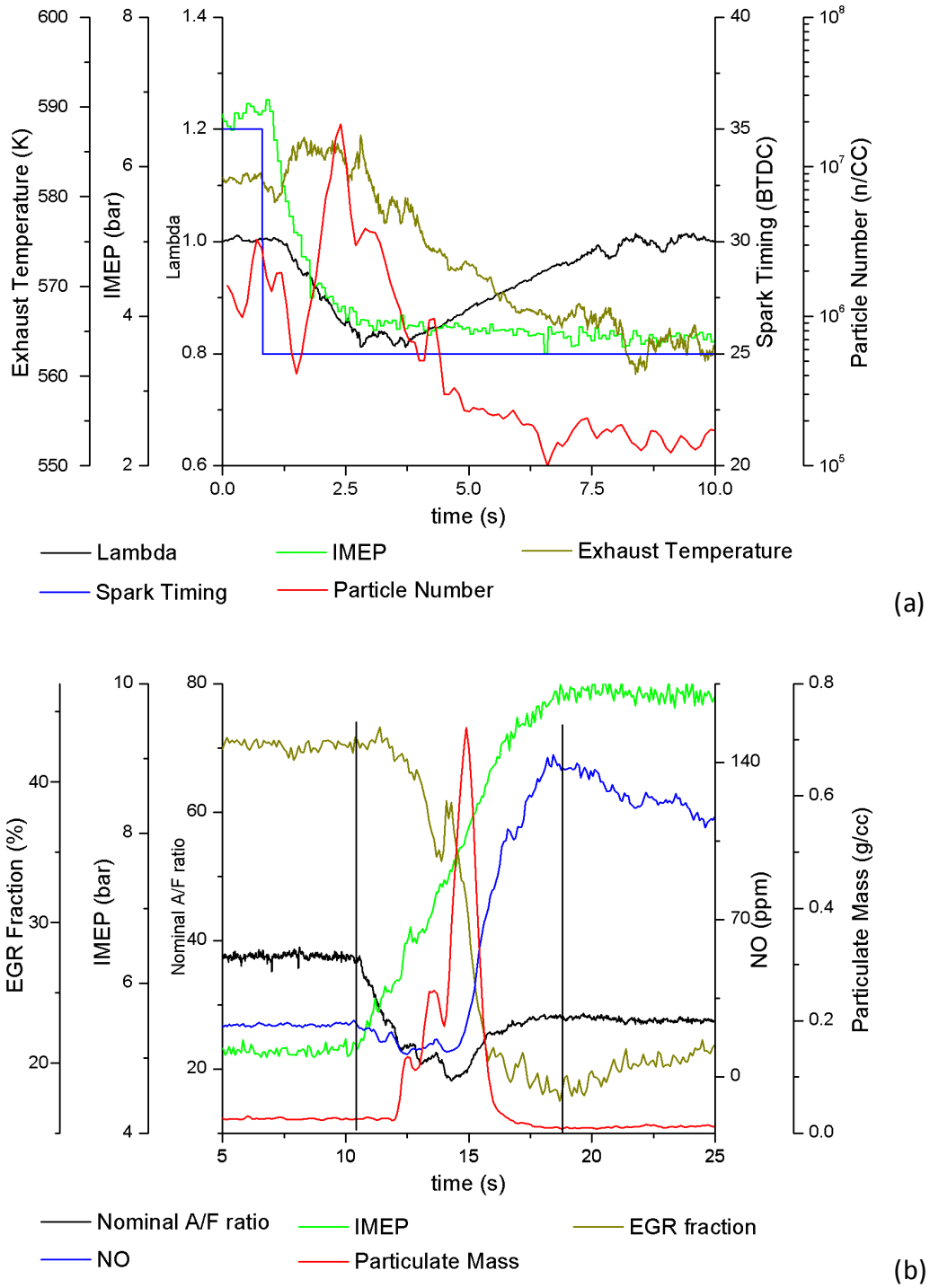

Figure 4-16 Engine Performance and Emission Behaviour during the Load Transient Test; (a) Gasoline Engine; (b) Diesel Engine

In summary, the time alignment was based on the identification of relationships between engine parameters and emissions during transient tests. The proper method was determined by the correct and accurate correspondence of the data.

4.5 Discussion on Transient Data Quality

Investigation often reveals that the reliability and accuracy of analysis and model generation is closely related to the quality of the data used (Beattie, Osborne, and Graupner 2013). For the engine transient operation tests, simply increasing the number of tests cannot improve the data quality due to the complicated process and dynamic characteristics, let alone the waste of testing time and instruments resources. Therefore, in order to ensure the data quality in this study, corrective measures are summarized and employed as shown in Table 4-2.

Table 4-2 Overview of Corrective Measures to Maintain Transient Data Quality

<table>
<tr><th></th><th>Human Errors</th><th>Environment Inconsistency</th><th>Equipment Issue</th><th>Post-processing</th></tr>
<tr><td rowspan="2">Corrective Measures</td><td rowspan="2">Automation Testing</td><td rowspan="2">Advanced Conditioning System</td><td rowspan="2">Calibration Before Tests</td><td>Noise Filtering</td></tr>
<tr><td>Dynamic Compensation</td></tr>
<tr><td>Warning System</td><td>Standardization</td><td>Proper Maintenance</td><td>Data Alignment</td></tr>
</table>

Also, in order to quantify the test data quality, the Coefficient of Variation (COV) is introduced and would be considered in the experimental study and results analysis. The expression is shown as below:

$$COV = \frac{Standard\ deviation}{Mean} \qquad \textbf{Equation 4-9}$$

The COVs of important parameters such as IMEP and emissions during the steady state of repeated tests are used to monitor the condition of the test facility. Although this study focuses on engine transient behaviour, the stable performance of steady state is the foundation of reliable transient data.

4.6 Summary

Measurements and processing methods of instantaneous data during engine transient tests are developed and discussed in this chapter. The methods are classified into combustion diagnostic data processing, transient emissions data processing and transient data time-alignment.

From the FFT power spectrum, low power higher harmonics and noise in the in-cylinder pressure data is detected mainly due to the electrical instrumentation and engine vibration. For transient tests, four methods are employed to filter cycle-by-cycle in-cylinder pressure signals. FFT filtering is the best suited method in gasoline engine tests. The filter designed eliminated most pressure fluctuation and provided smooth RoHR profiles for each cycle. The processed data outputs from the linear and zero-phase filters were close but small pressure fluctuations remained in the processed pressure signal resulting in relatively large fluctuations in the calculated RoHR curve. As for the low-pass filter, the distortion of amplitude and phase are much greater compared to other filters, making the low-pass filter the least acceptable option. In the diesel engine tests, the sampling frequency is relatively low due to the complicated characteristics of multiple injection combustion. A moving

average filter such as the zero-phase filter, presents the best performance on balance, considering its convenient examination and information preservation.

Also, a detailed method is developed to filter high-frequency instantaneous emission data. The FFT filter is used to remove data noise and then cycle based averaging is employed. The filtered emission data contains accurate information for each engine cycle and it is more suitable for data analysis of engine transient performances.

One approach to compensate for the analyser's long response time is developed and three methods for the time-alignment of transient data are summarized. The synchronization by the starting moment of the engine operation change is useful for emission data which is sensitive to changes of certain engine parameters. The peak-to-trough method is applied where clear one-to-one correspondence between two data occurred. When the trend of correlation between data was not apparent, the statistical method could be successfully applied for data alignment.

CHAPTER 5

ANALYSIS OF DIESEL ENGINE TRANSIENT OPERATION

In this chapter, the experimental study of a turbocharged diesel engine during transient operation is conducted. The specific change in the air system is investigated in test sequences at different engine speeds and different calibrations on EGR. The specific effects of gas exchange process on combustion performance and emission behaviour are discussed. Finally, an alternative fuel is used to study the sensitivity of fuel properties in effecting the dynamic performance during transient operation.

5.1 Introduction

Turbocharged diesel engines are becoming mainstream products in most countries' vehicle market. The utilization of the available exhaust gas energy through a turbocharger largely increases the efficiency of the diesel engine with the cooperation of EGR. However, the engine transient response deteriorates with the use of a turbocharger and the resulting response delay is called turbo-lag. The employment of a VGT has improved the turbo-lag to some extent, especially at low engine speed (Constantine D. Rakopoulos and Giakoumis 2009b). To study the dynamic performance on a turbocharged diesel engine during transient operation, experiments have been designed and conducted with an automated operation system.

In this study, the engine speed is maintained at a constant value with a step change of load from 20% to 45%; the reason to choose these operation modes is because they are frequently used in vehicles with the EGR valve changed from a high value to the minimum while the secondary turbo is not involved. The transition period is defined as the time from the beginning of the load step to next steady state. In addition, the EGR is set at different calibration maps to analyse and compare the effect of different control strategies on the engine air path. Since the detailed value in the EGR calibration map is confidential, the settings of the EGR are abbreviated as 'lowest', 'low', 'medium', 'high' and 'highest'. The detailed test conditions are listed in the table below.

Table 5-1 Test Conditions for Engine Transient Operation

Engine speed (rpm)	1000	1250	1500	1750	2000
Transition period (sec)	1			5	
EGR setting	Off	Lowest	Low	Medium	High	Highest
Fuel	Diesel		HVO30	HVO60	

5.2 Engine Speed Effects

Compared with the fuel injection system, the air path of a turbocharged engine has a slower response during transient operation, worsening the combustion and emission behaviour. For a turbocharged diesel engine, the air path change is complicated at different engine speeds. The parameters which can reflect the instantaneous trends of dynamic performance are designated to analyse the detailed effects in transient operation. Cycle-by-cycle in-

cylinder pressure data and heat release rate are presented to explore the combustion performance. Also, real-time emission behaviour is measured and discussed.

5.2.1 Gas Exchange Process

Boost Pressure

The boost pressure is dependent on the exhaust gas entropy drop and is controlled by a coupled VGT and EGR system in the modern turbocharged engine. The air supply is the most important influence in engine transient conditions and it is determined by the engine speed and inlet pressure. Therefore the boost pressure is the key factor in analysing these dynamic characteristics of an engine. Firstly, the EGR valve is fully closed (EGR off) to explore the VGT effect on the boost pressure during the engine load transients.

As shown in Figure 5-1, the boost pressure profile of each test has varied response times and characteristics at different engine speeds. The vane of the VGT is closed when the VGT position is equal to 0% and is fully open when it is 100%. In theory, the opening of the VGT would decrease the velocity of the exhaust gas into the turbocharger, thereby lowering the boost pressure. For this engine, the VGT control is in open loop mode when load is low and turns to a closed loop mode when load increases. This switch of control mode is shown clearly in the 5s load increase test. During the first three seconds, the VGT moves to around 22% in each case, as illustrated in Figure 5-1 (d). Then, it changes rapidly to achieve the desired boost pressure value in the closed loop control. It is noticed that there is a long response time, approximately 2 seconds for the VGT position to affect the boost pressure.

For example, in 5s load transients when the engine speed is 1750 rpm, the dramatic rise of VGT at the 3rd second contributes to the small drop of boost pressure at the 4th second. Also, it is observed that the boost pressure at low engine speed increases more slowly and with smaller amplitude compared with that at high speed during load increased transients, although the VGT position is lower and the load designated is the same. When the engine speed is 1000rpm, the VGT opens the vane position quickly to adapt to the expected larger gas flow. However, due to the initial low value of the intake air flow at a low engine speed, the exhaust gas energy is insufficient to boost the intake pressure quickly; meanwhile the opening of the VGT vane reduces the exhaust flow velocity, deteriorating the process. When the VGT turns to the closed loop control, the VGT position is reduced and the boost pressure rises immediately. Thus, the delay of reducing the VGT position in the original control strategy contributes to the poor dynamic performance of the air supply at low speed.

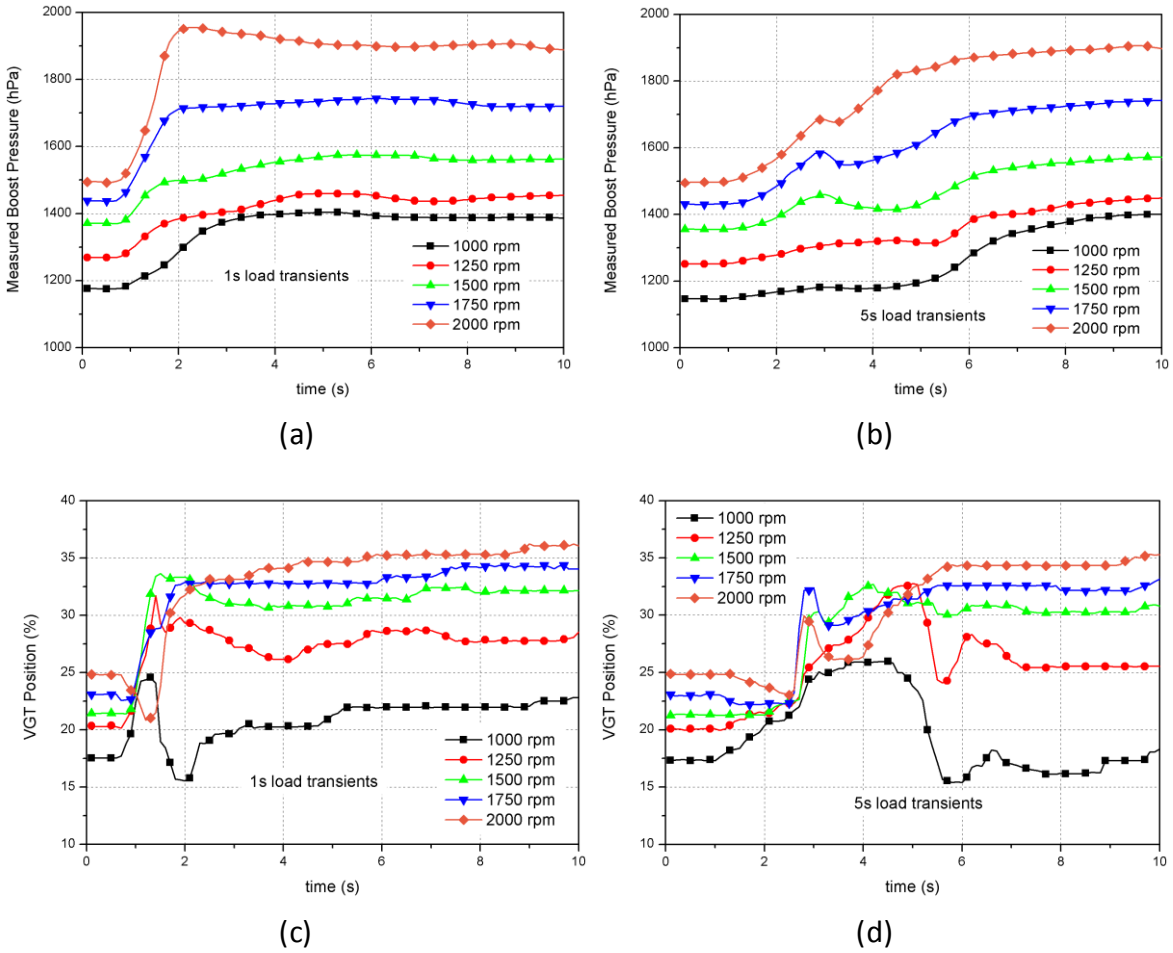

Figure 5-1 Boost Pressure Profile and VGT Position during Load Increase Test - When EGR is off at Different Engine Speeds and Different Load Increase Periods

In the 1s transient case of 1500rpm engine speed, the boost pressure rises to 1500hPa rapidly then slowly increases to almost 1600hPa. Compared with the low engine speed, the more exhaust energy from the larger intake air flow at a higher engine speed results in a faster response of the boost pressure. While the quick opening and the following overshoot of the VGT at the beginning of the transition leads to a delay of boost pressure in reaching the next steady state value. In the 2000 rpm cases, the small drop of VGT benefits the fast growth of boost pressure, which is shown as the boost pressure at around 1.5th second.

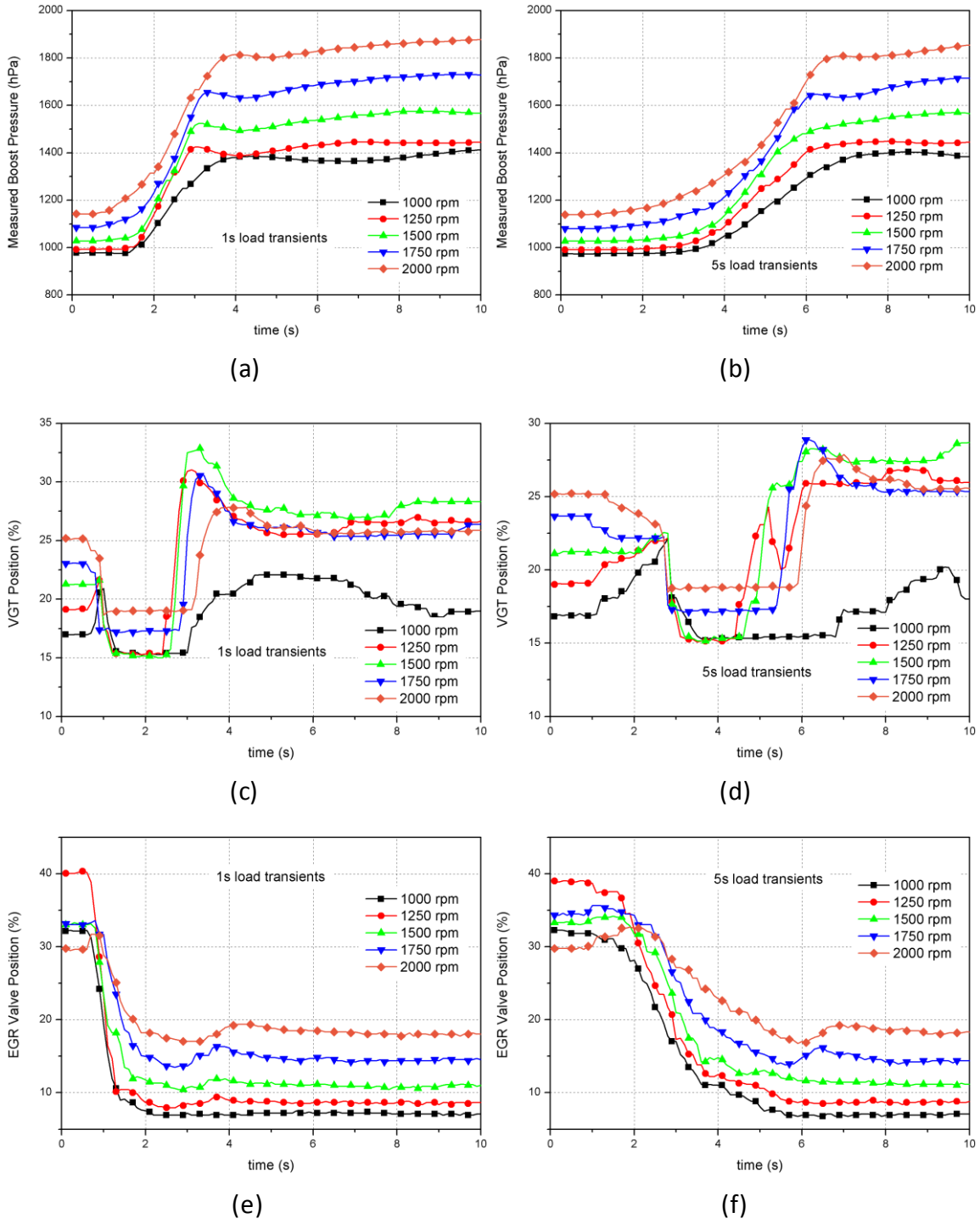

Figure 5-2 Boost Pressure Profile with VGT and EGR Valve Position during Load Increase Test when EGR is Involved

Figure 5-2 presents the boost pressure profiles when EGR control is involved as the original calibration. It is indicated that the boost pressure in light load mode is lower in the EGR valve open case compared with when the EGR is off. This can be easily explained by the

decline of exhaust gas energy for the turbocharger since part of exhaust gas flows back to the intake manifold. In the 1 second load transients, due to the involvement of EGR, the closed loop control of the VGT drops to a low value at around 1 to 3 seconds to promote the increase of boost pressure. As shown in the 1000 and 1250rpm cases, even though the EGR valve quickly closes and a higher proportion of exhaust gas flow through the turbocharger is expected, due to the dynamics of the exhaust flow, boost pressure has a longer response time to increase compared with that in the EGR off case. When the engine speed is higher, boost pressure begins to increase earlier but reaches the next steady level value more slowly; it is expected to be derived from different EGR ratio settings in varied engine speeds. Besides, in the 5 seconds load increase tests, boost pressure of each case reached the next steady state level slightly more slowly than that in the 1 second tests; however, the delay of boost pressure at each engine speed is still apparent.

Pressure Drop between Intake Manifold and Exhaust Manifold

The pressure difference between the intake manifold and the exhaust manifold largely determine the EGR mass flow. Due to the employment of a VGT and the replacement of the waste gate, the exhaust manifold pressure of this engine is higher than the intake manifold pressure in most situations. During the valve overlap period, higher pressure drop indicates that a large amount of residual gas would flow back to the cylinder or intake system, influencing the control of the EGR ratio and the efficiency of the discharging exhaust gas. More importantly, pumping loss would largely increase with excessively high pressure drop; thereby reducing the total engine efficiency and dynamic response during transient operation.

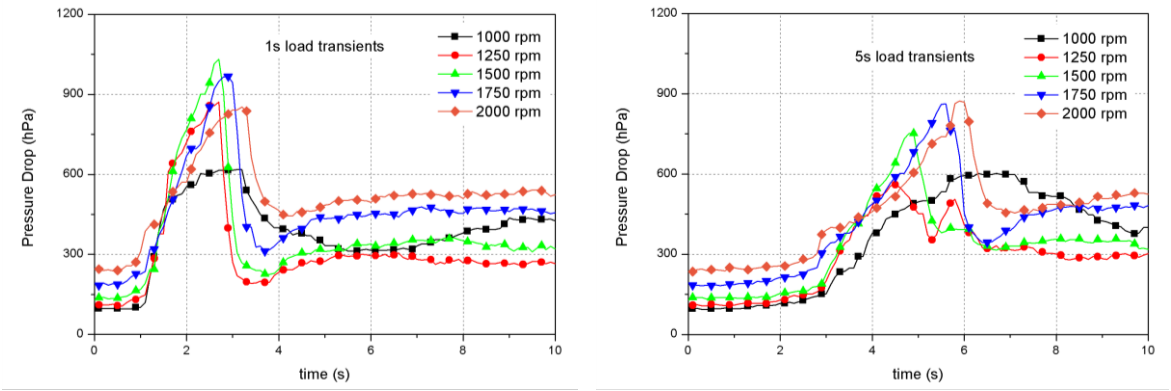

(a) (b)

Figure 5-3 Pressure Drop Profiles during Load Increase Transient Tests: (a) 1 Second Load Increase; (b) 5 Seconds Load Increase

Figure 5-3 presents the comparison of pressure drop profiles during load increase tests at different engine speeds with the original calibration of EGR. Obvious spikes of pressure drop are found at around 2nd second in the 1 second load increase tests. Based on Figure 5-2, during the period of spikes, the VGT keeps at a relatively low value to increase the gas flow velocity and boost pressure; meanwhile it obviously raises the back pressure rapidly. Specifically, in the cases of 1000, 1250 and 1500rpm, the VGT position is around 15% while the pressure drop of the 1500rpm case has the biggest spike. The energy from the turbocharger has a serious delay in boosting the intake pressure which leads to the spike of pressure drop and higher engine speed with higher pressure drop. For the 1750 and 2000rpm cases, since the VGT position is slightly higher than the low engine speed cases, the pressure drop has a lower peak value. In addition, in the case of the 5 seconds load transients, a lower peak pressure drop value is found mainly due to the smaller air mass flow when the VGT is at a low position. Thus, low VGT position contributes to the form of pressure drop peak and the trade-off exists between the fast increase of the boost pressure and low pressure drop during transients.

In-cylinder Pressure at IVC

Although one air mass flow sensor was installed in the engine, it is difficult to measure the instantaneous air flow rate entering the cylinder due to the dynamics of the intake system and intrinsic response characteristics of the flow meter. In this study, to explore the dynamic performance of the intake air to the cylinder, the cycle-by-cycle in-cylinder pressure at the intake valve close (IVC) position is compared; since the pressure basically reflects air input in the cylinder (Grahn and Tomas 2011). This is based on the ideal gas law and the neglect of cylinder-by-cylinder variation.

As shown in Figure 5-4 (a), there is an in-cylinder pressure drop for each case after the EGR valve reaches its lowest position, but this drop is most apparent for the 1000 rpm and least for the 2000 rpm tests. This indicates the air amount in the cylinder during this period is far lower than the required value for the 1000 rpm test. Since the EGR valve is almost shut after transition at 1000 rpm, the slowly increased boost pressure and dynamic of the intake system including the intercooler, intake pipe and manifold, result in a delay of compensating initial intake air and this drop is caused. For all the cases except for 1000 rpm, a small peak of in-cylinder pressure is found before it reaches the next steady value. This peak probably derives from the high pressure drop value resulting in suddenly increased exhaust gas back flow to the cylinder. Then, the pressure drop is reduced and the boost pressure is increased resulting in the in-cylinder pressure rising to the next steady level.

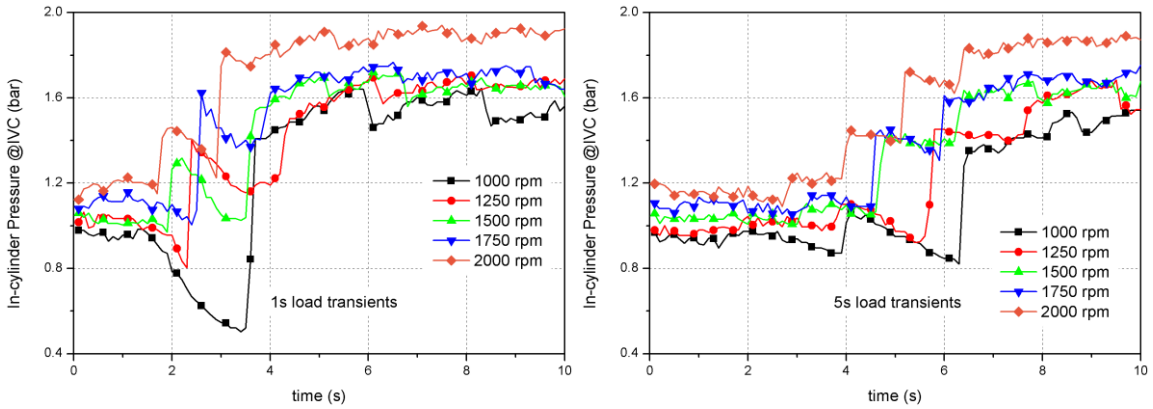

(a) (b)

Figure 5-4 Profiles of In-cylinder Pressure at IVC Position during Transient Operation

Oxygen Concentration and Air-fuel Ratio

In modern diesel engines, EGR is widely employed to reduce the NOx emissions and it becomes an important manipulated variable in the control strategy. Currently, EGR control relies on the simulated EGR ratio or intake mass air flow measured far away from the intake manifold. It is difficult to predict an instantaneous EGR ratio and the error always exists between the measured and predicted values. In addition, with the same EGR ratio, the oxygen concentration in the intake manifold can be different during transient operation due to the dynamic characteristics of the gas flow. Thus, in order to specifically investigate the combustion performance during engine transient operation, the oxygen concentrations in the intake manifold (O2_i) and in the exhaust manifold (O2_e) are measured and presented in the tests.

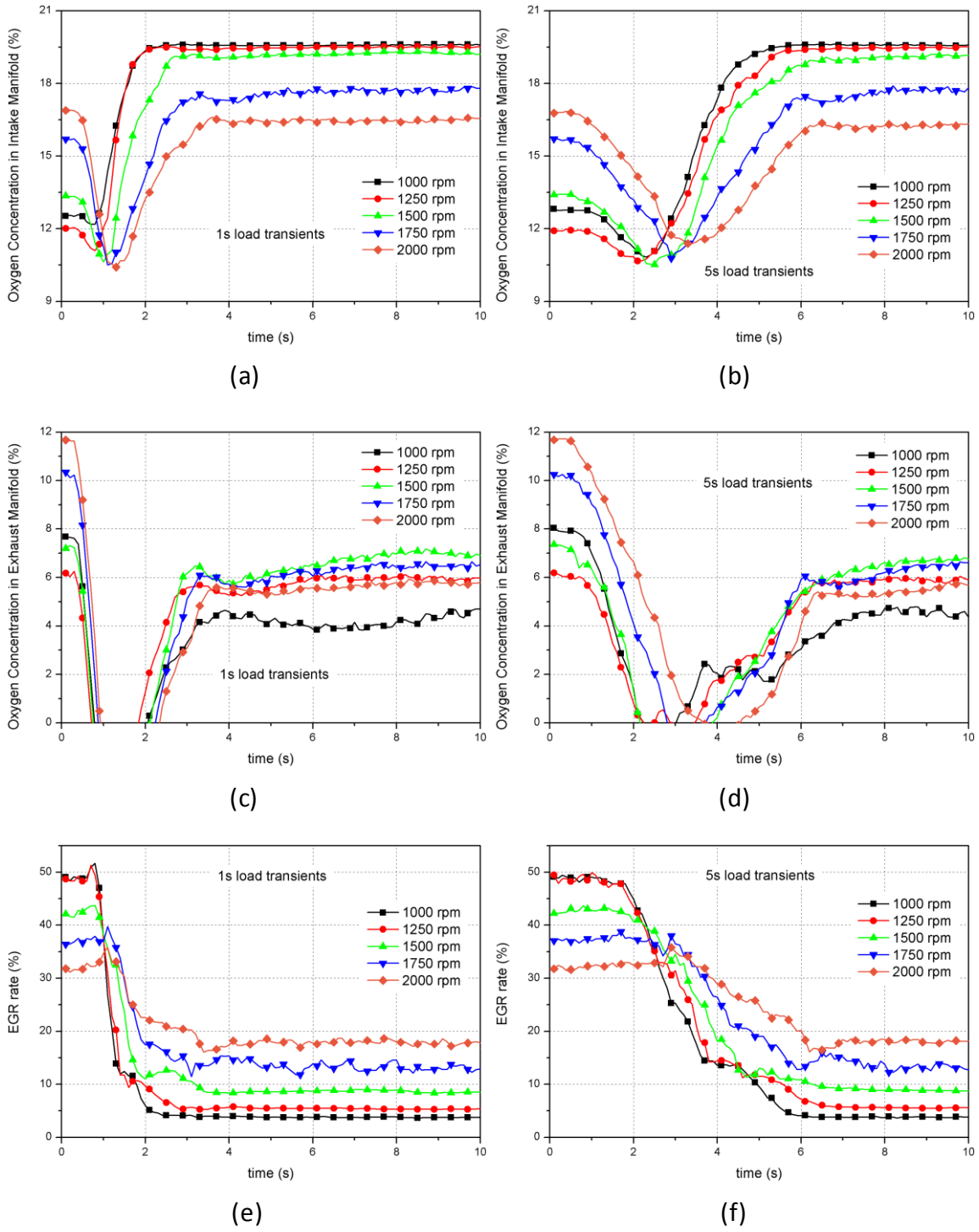

Figure 5-5 Comparison of Oxygen Concentration and EGR Ratio during Load Increase at Different Engine Speeds

In the 1 second load transient of the 1000rpm case, it is noticed that the oxygen concentration in the intake has a tiny drop before the rise to the next stage value. It can be explained by the excessively high EGR flow entering the intake manifold due to the high

pressure drop in the transient conditions. Similarly, in the 1 second cases at a high engine speed, the trend of the drop is found as well and becomes more obvious. As an obvious drop of oxygen concentration in the exhaust occurs at the beginning of each case, although the EGR ratio only has a small spike at a higher engine speed, it can be seen that the exhaust gas from the rich combustion during the transient periods facilitates the drop of oxygen concentration. In other words, the EGR flow does not reduce rapidly during the transient operation; meanwhile the faster response of the fuel injection leads to rich combustion, causing insufficient O2_i and worsening the combustion further. Compared with the 1 second cases, the longer period of transition does not largely improve the deficiency of oxygen in the intake manifold. The EGR valve closes gradually and the mismatch of the air-fuel ratio still exists, resulting in a low oxygen concentration in the intake manifold. Therefore, the rapidly changing oxygen concentration presents more information about the combustion during the transient periods compared with the EGR ratio obtained in this study.

The nominal air-fuel ratio is obtained and calculated from the ECU signal, mass air flow and injected fuel quantity. Although this value cannot reflect the local air-fuel mixture composition, it is able to reveal the global characteristics in the cylinder. The air-fuel-ratio normally has a drop during the acceleration period, which would affect the oxygen concentration in the exhaust gas (Wijetunge et al. 1999). In Figure 5-6 (a), it is shown that the nominal air-fuel ratio drops rapidly at the beginning of transition and settles at one steady value at around the 3rd second, nearly the same trend as with O2_ac. While in the 5 second load transient periods, the minimum value of the air-fuel ratio at each speed is higher than that in the 1 second transient period; showing that the longer period of transition does mitigate the mismatch between the intake air and fuel injection.

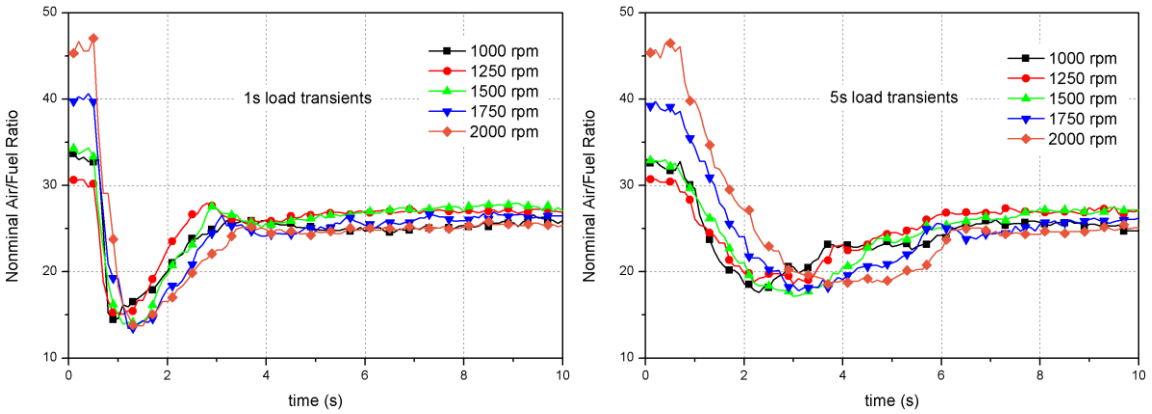

(a) (b)

Figure 5-6 Comparison of Nominal Air-fuel Ratio during Load Increase Tests

5.2.2 Combustion Characteristics

Based on the understanding of gas exchange process during engine transient tests, combustion characteristics are investigated by measuring the cycle-by-cycle in-cylinder pressure and analysis of the heat release rate. The methods used for the calculation of the heat release rate in this study have been introduced in the previous chapter. Detailed comparisons of combustion performance during transient tests are introduced.

Heat Release Rate Analysis

To illustrate the specific change of combustion characteristics, representative cycles were picked from the transient tests at different engine speeds. The EGR ratio, boost pressure and injection signals were obtained and are presented. It should be noticed that there is a tiny delay between injection signal and actual injection event in the tests (Zhang 2013).

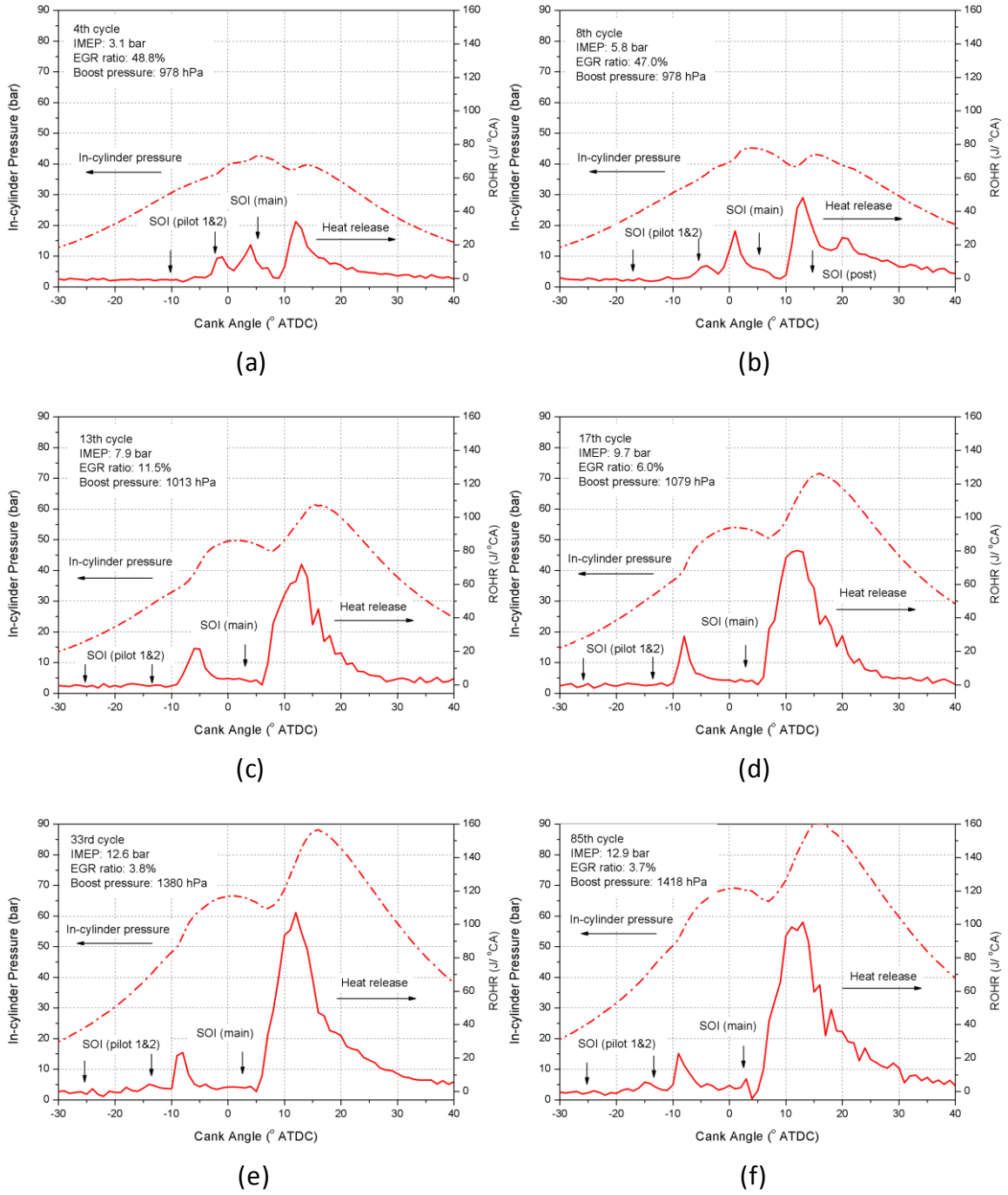

Figure 5-7 Heat Release Rate of Representative Cycles during Load Increase Test @1000rpm with Original Calibration

The profiles of the in-cylinder pressure and heat release rate during the transient test are plotted in Figure 5-7. At the 4th cycle, the engine is at low load and the change of operation mode does not start. Two heat release profiles by pilot injections are clearly shown with the

short ignition delay. At the 8th cycle, the amount of fuel injection increases and post injection strategy is employed. Since the boost pressure is unchanged compared with the 4th cycle, the fuel from the advanced pilot injection undergoes a longer ignition delay due to lower in-cylinder pressure during atomization and evaporation. Only a small amount of fuel from the first pilot injection actually burns before the start of the second pilot injection. From the 13th cycle to the 85th cycle, there is no post injection again and only one heat release occurrs before the main injection. In addition, it is observed that the ignition delay of the pilot injection becomes slightly shorter during this period. This derives from two factors: lower EGR ratio and higher in-cylinder temperature with higher load. The amount of fuel injection is the same at the 33rd and 85th cycles, but slowly increased intake air and less heat transfer to the warmer cylinder wall improves the efficiency with higher IMEP.

Figure 5-8 presents the heat release rate and in-cylinder pressure of the load increase test at 1500rpm. Similarly, the 4th cycle is chosen to show the combustion at the start stage. At the 9th cycle, the post injection begins and the heat release is clearly shown in the late stage of combustion. It is the same with the low speed case; the fuel from the first pilot injection cannot combust until it is combined with the second pilot injection and forms a small peak of heat release. At the 23rd cycle, the injected fuel amount reaches the maximum while the boost pressure is far lower than the required value with insufficient oxygen in the cylinder. As a result, the IMEP of the 23rd cycle is smaller than that of the 33rd cycle and the fuel from post injection barely burns.

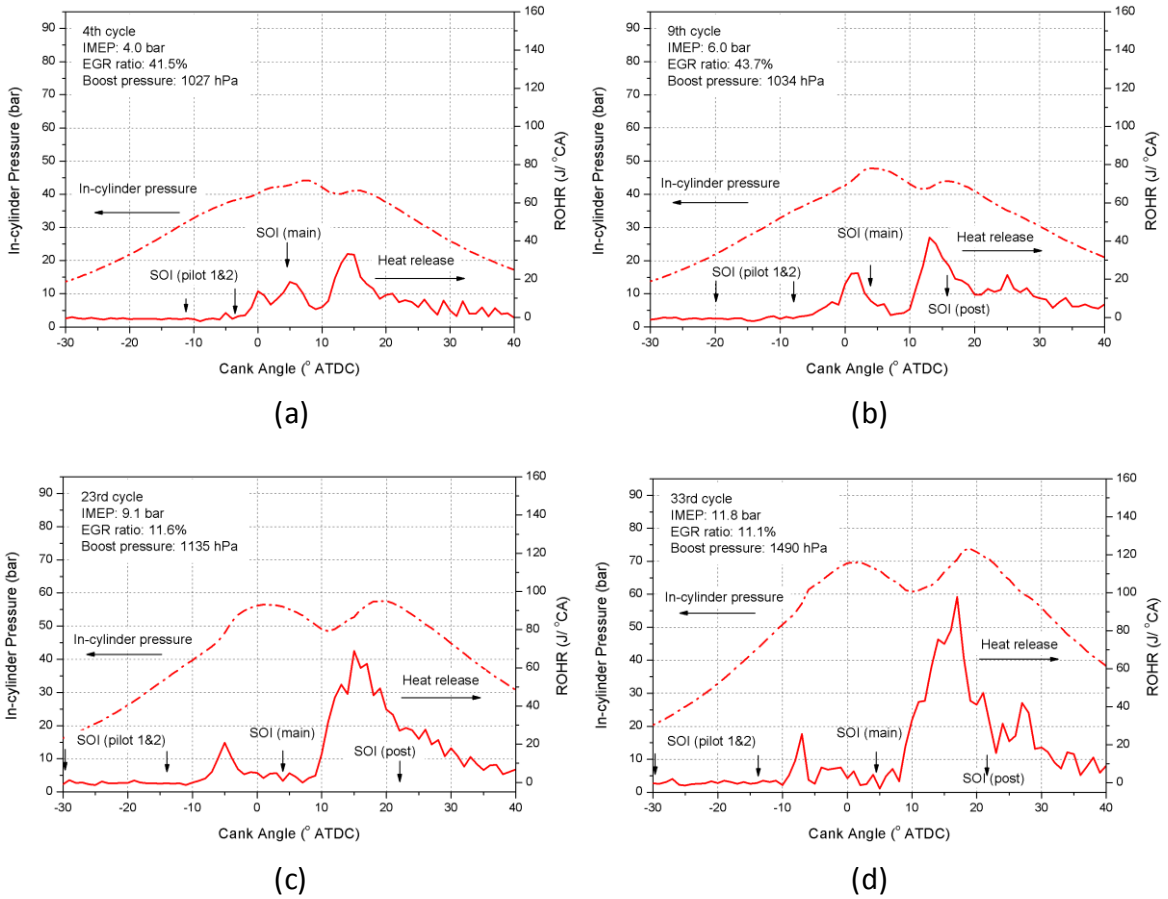

Figure 5-8 Heat Release Rate of Representative Cycles during Load Increase Test @1500rpm with Original Calibration

When the engine speed is 2000rpm, the periods between multiple injections are relatively shorter and ignition delays of the injections become longer in the crank angle. It is observed that with increased engine speed, RoHR associated with the two pilot injections is less pronounced. At 1000 and 1500 rpm, two separate peaks are clearly observed at the early stage of the transient period, corresponding to the two pilot injections. However, at 2000 rpm with higher in-cylinder pressures, the peaks of heat release are small and short. Since droplet vaporization rate is very sensitive to its environmental pressure, droplets of the two pilot injections' evaporation rates decrease with increasing in-cylinder pressure and consequently combustion rates and RoHR are reduced. The increased in-cylinder pressures are caused by the higher boost pressure required for high engine speed. It is noticed that

the pilot injections are advanced to compensate for the increased evaporation time. In addition, apparent fluctuations of RoHR are found at the late phase of combustion during high engine speed transient conditions. One possible factor is the poor atomization and evaporation of fuel in transient operation due to relatively colder cylinder temperature compared with steady state. The other factor is the high amount of exhaust gas in the cylinder deteriorating the local oxygen concentration, resulting in more fuel combusted irregularly in the late phase.

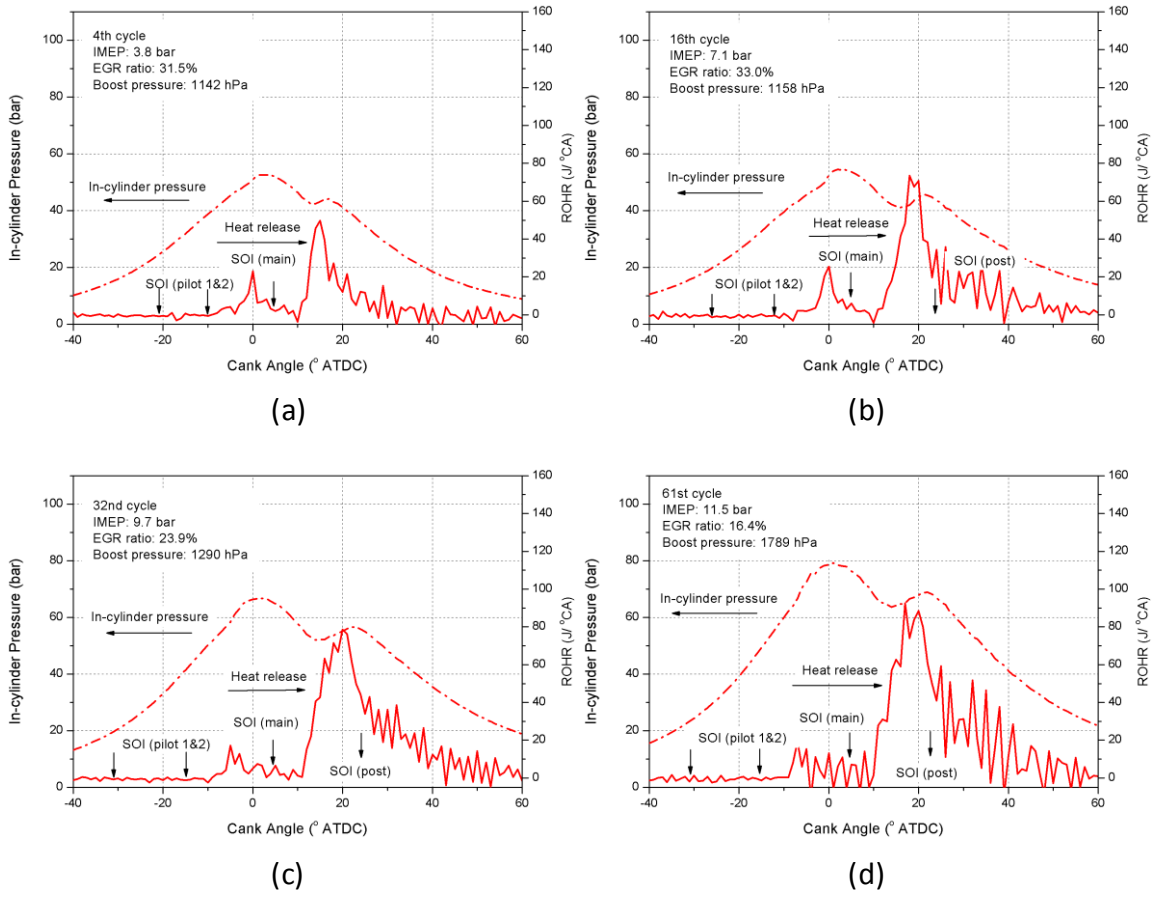

Figure 5-9 Heat Release Rate of Representative Cycles during Load Increase Test @2000rpm with Original Calibration

Combustion Performance

From the in-cylinder pressure and RoHR data, several combustion parameters can be obtained. In this section, the crank angle position, where 50% of cumulative heat release occurs (HR50) and the maximum heat release rate (HR_{max}), are used to explore the combustion performance during transient operation at different engine speeds, as presented in Figure 5-10. HR50 is an important parameter which shows the combustion phase and significantly affects the combustion efficiency. Additionally, HR50 is relatively independent of engine speed and load, which facilitates the study of combustion during transient operation.

Figure 5-10 (a) shows that there is a peak of HR50 at around 1 second of each load increase test; and is higher when the engine speed increases. For this phenomenon, one factor is the application of post injection in this period, as shown in last section. The other factor is that more fuel is injected to reach a higher load but the low oxygen concentration results in a lower proportion of the premixed combustion and incomplete combustion, retarding the combustion phase. In the high engine speed case, the phenomenon is more obvious due to the shorter period for air-fuel mixing before the main combustion. The value of HR_{max} reflects the intensity of combustion and it shows an interesting trend in Figure 5-10 (b). At low speed, HR_{max} increased steadily during the load increase test, which implies most of fuel burned completely. However, at high speed as in the 1750 and 2000 rpm cases, one drop of HR_{max} is observed at around 1 second before it rises to the value of the next steady state. Based on the RoHR in Figure 5-8 (b), the heat release of main combustion rises slowly and a lot of fuel burns at the late combustion phase, explaining the drop of HR_{max}. Also, the higher

EGR ratio with lower oxygen concentration at high engine speed contributed to the low HR_{max}.

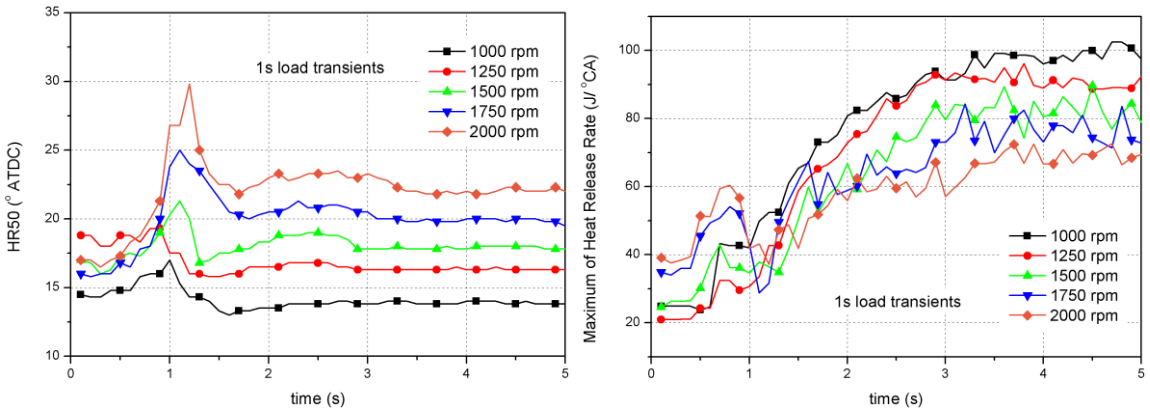

(a) (b)

Figure 5-10 Combustion Performance at Different Engine Speeds during Load Increase Test: (a) HR50; (b) Maximum of Heat Release Rate

5.2.3 Emission Behaviour

Four types of emissions: nitrogen oxide (NOx), hydrocarbon (HC), particulate number (PN) and particulate mass (PM) during the load increase tests at different engine speeds are presented. The instantaneous emission data shown has been processed to compensate for the transportation and analyser's delay by the methods introduced in Chapter 4.

Gaseous Emissions

In Figure 5-11, it is found that NOx increases steadily at low engine speed while a valley of NOx occurs at high engine speed. This can be explained by the oxygen concentration and EGR ratio in Figure 5-5. At low engine speed, the oxygen concentration increases rapidly

after a tiny drop due to the close of the EGR valve. The rapid increase of oxygen concentration results in high NOx emissions. In contrast, the EGR ratio is relatively higher in the high speed case; a big drop of oxygen concentration is found and it brings about the low NOx during the transition. Additionally, the combustion temperature increases and ignition delay is reduced; the NOx emissions increase accordingly. Compared with the 1 second transient periods, the long period of transition does not apparently change the trend of NOx emissions. One overshoot of NOx is noticed in the 1000 rpm test and it is highly likely derived from unstable boost pressure at low engine speed. Therefore, the crucial role of oxygen concentration in NOx emissions during transient operation is evident and the combustion temperature shows a strong correlation with the NOx emissions.

As for hydrocarbon emissions, the profile in each case shares the same trend, one sharp peak at the load increase test, a higher engine speed with higher peak value of HC. Low oxygen concentration during transient conditions at high engine speed is expected to be responsible for this phenomenon. Furthermore, post injection is used during the load increase. In the oxygen deficient condition, the fuel from post injection combusts incompletely, resulting in a great deal of HC. In Figure 5-9, there is a high proportion of combustion which happened at that last phase; this proves this interpretation. Interestingly, unlike the NOx emissions with a slow increase, the HC decreases from the peak value dramatically to the next steady state condition. The relatively slow change of combustion temperature has little effect on HC.

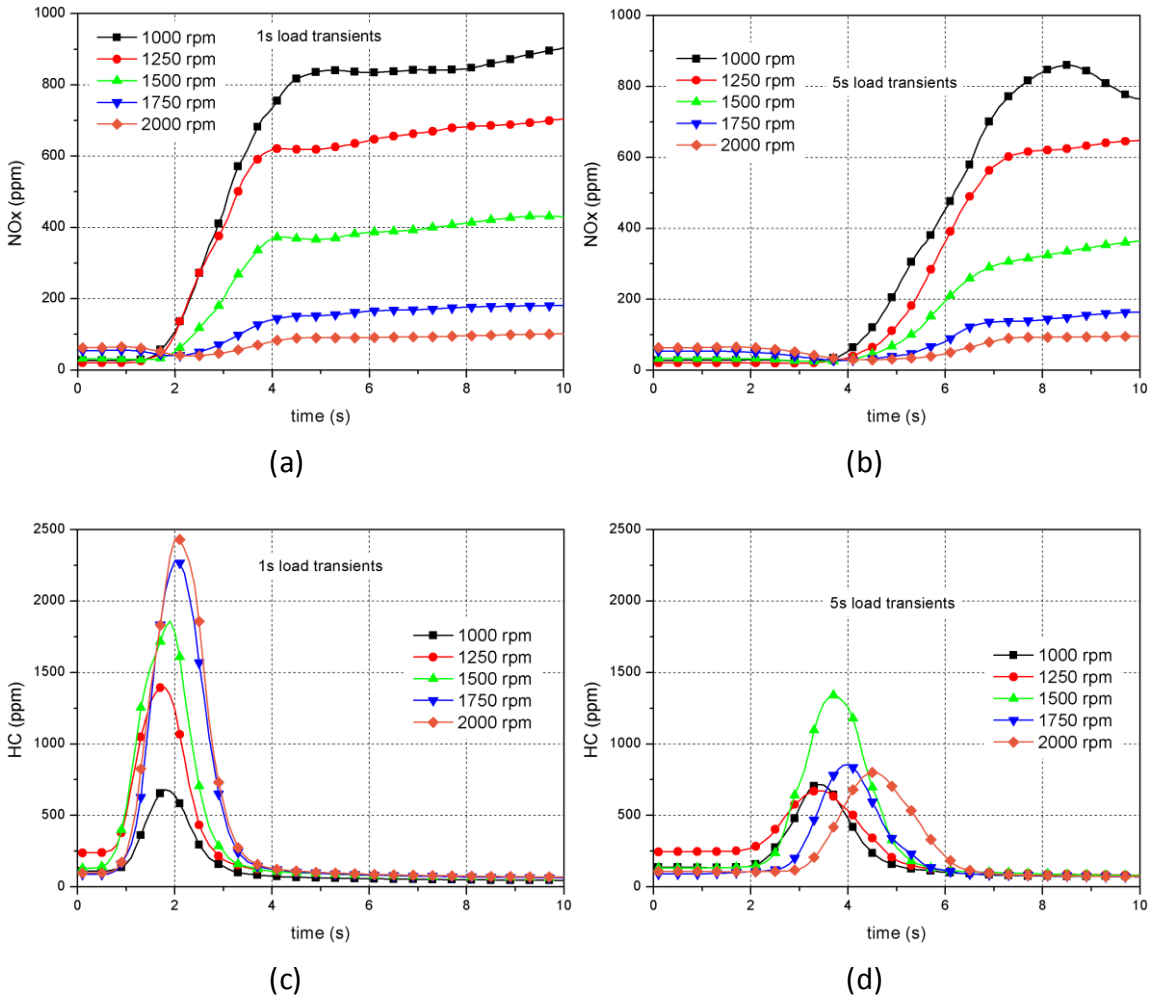

Figure 5-11 Gaseous Emission Behaviour during Load Increase Tests

In the 5 second transient periods, the overshoot of HC emissions at a high engine speed is largely reduced; while the value at 1000 rpm is close compared with that in the 1 second transients. Additionally, the HC emissions of 1500 rpm show the highest peak value, even though the air-fuel ratio of 1500 rpm is not lower than that at the higher engine speed. It is revealed from Figure 5-5, the oxygen concentration before combustion dominates the formation of HC during transients, since a large amount of incomplete combustion occurs in insufficient oxygen. Thus, the oxygen concentration is a good control objective to reduce the HC emissions during transient operation.

Particulate Matter

Regarding the particulate matter at different engine speeds, in general one obvious overshoot of PN and PM in each case occurs during the load change. Combining Figures 5-5 and 5-12, the oxygen concentration in the exhaust and air-fuel ratio correspond well with PN and PM both in 1 second and 5 second transient cases. It proves that particulate emissions heavily depended upon these two factors during the load transition (Hagena, Filipi, and Assanis 2010). Due to the turbocharger lag, there are more fuel-rich zones at the start of the transient operation as discussed earlier. In this oxygen-deficient atmosphere, thermal and oxidative pyrolysis of fuel molecules initiates the formation of particles (Suzuki et al. 2003).

In addition, it is found that particulate mass has a small drop at around 1.5 seconds in the 1750 and 2000 rpm tests. Connected with the delay of HR50 and drop of HR_{max} in Figure 5-9, it is expected that in a high engine speed condition, the low oxygen concentration and shorter period of air-fuel mixing largely postpone the combustion phase and decrease the temperature in the cylinder. As a result, mild combustion in the later stage reduced the soot formation at that time. However, with the increase of oxygen concentration and fuel amount, the rapid premixed combustion raises the temperature and favours the formation of particulates. In the comparison of two different transition periods, the peak value of PN at each engine speed in both cases is close; however, the PM varies almost by an order of magnitude, indicating that the average size of particles formed is smaller. In other words, the higher air-fuel ratio during the load increase abates the overshoot of particulate mass,

inhibiting the soot agglomerate process but a high amount of particles are still generated by insufficient oxygen concentration.

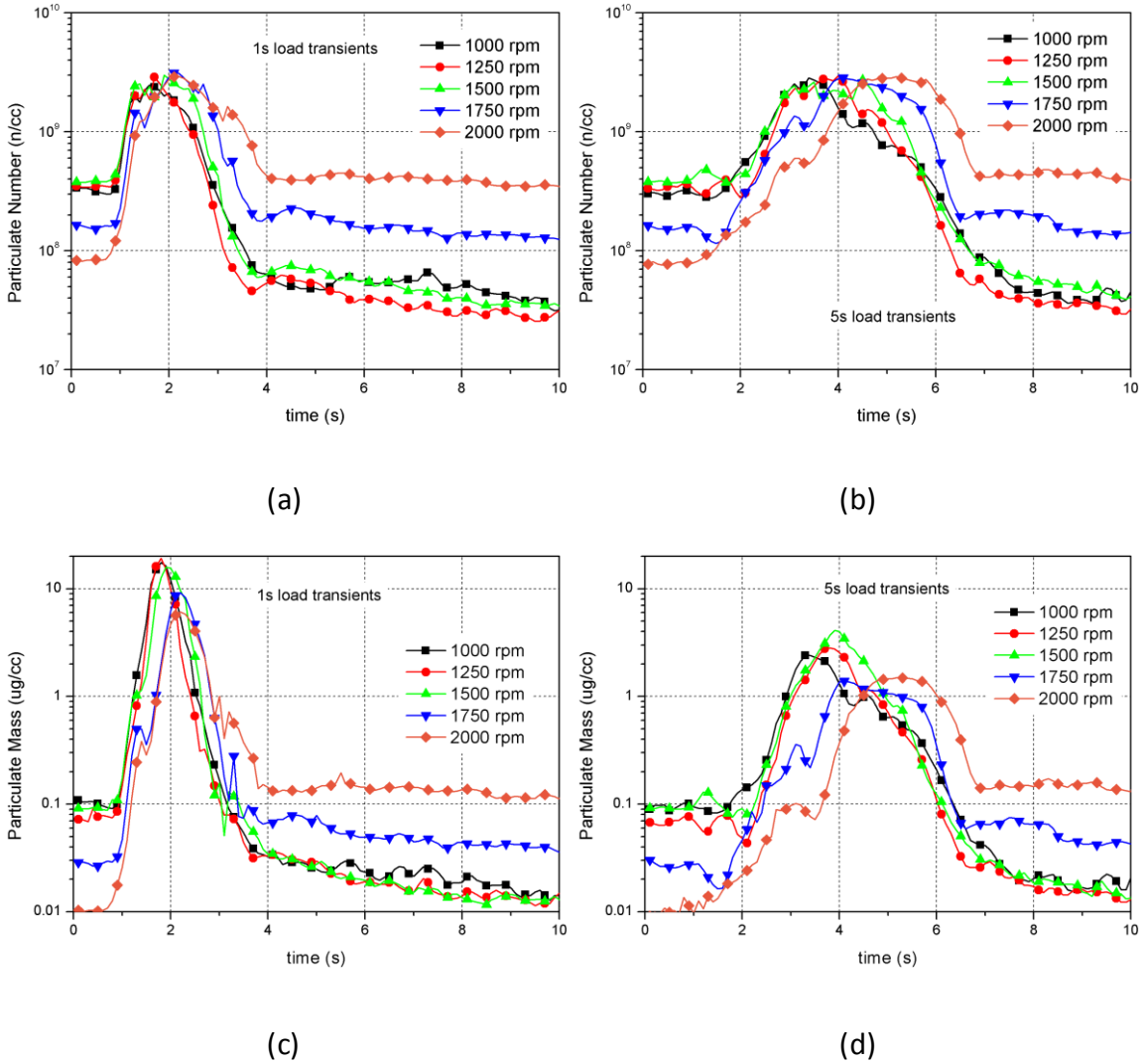

Figure 5-12 Particulate Matter of Load Increase Test at Different Engine Speeds

5.3 EGR Effects

In this section, the EGR calibration map is modified to achieve different EGR dynamic behaviour during the engine transient operation, as shown in Table 5-1. The EGR effects on

gas exchange process are discussed and meanwhile the combustion performance and emission behaviour are presented.

5.3.1 Gas Exchange Process

The boost pressure profiles and related valve position at different EGR settings are shown in Figure 5-13. With different EGR valve positions, the VGT position adjusts accordingly in the transient period. For the lowest EGR case, the boost pressure increases fastest and reaches a high value within one second, so that the VGT opened the vane earlier than in the other cases to compensate for the overshoot. This benefit comes from an almost closed EGR valve which causes most of exhaust gas to flow through the turbocharger at the beginning of the transient periods. Additionally, the boost pressure profile of each case shares a small drop since the VGT opens the vane for compensation. Interestingly, because of the open loop control mode, the VGT position stays exactly the same at the beginning of transition in each case, but the boost pressure presents different responses. The results state that the EGR valve has a strong effect on the rise of the boost pressure at the starting stage of acceleration. From the control perspective, EGR has a higher priority in affecting the boost pressure compared with the VGT in light of the delay of energy transition from exhaust gas entropy to intake air.

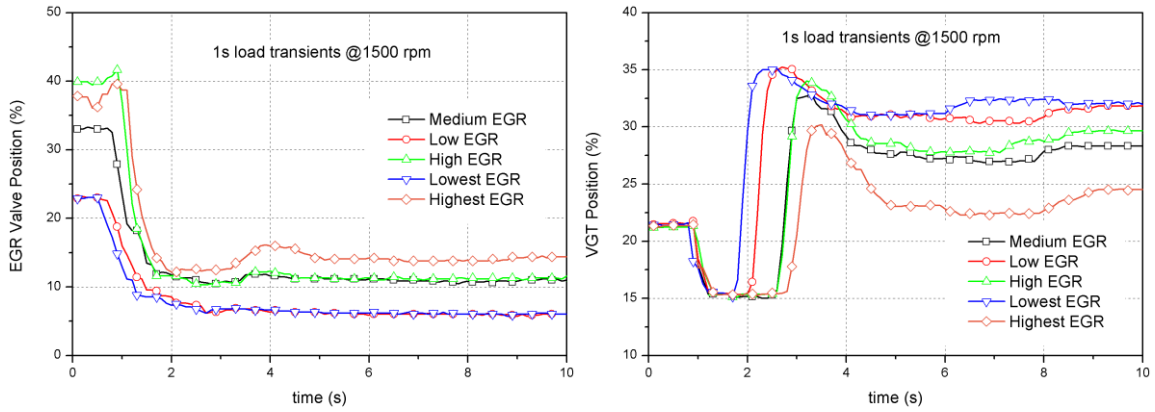

(a) (b)

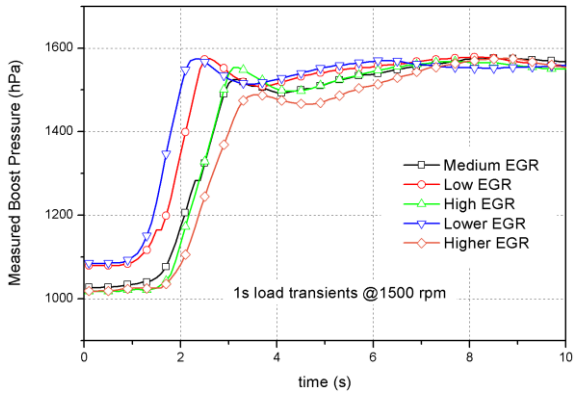

(c)

Figure 5-13 Comparison of Boost Pressure Profiles with Different EGR Settings during Load Increase Test: (a) EGR Valve Position; (b) VGT Position; (c) Boost Pressure

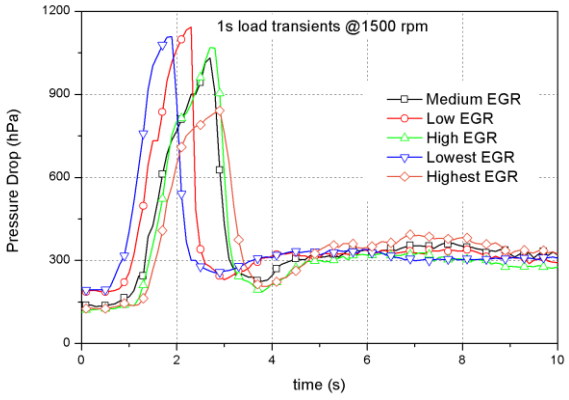

Figure 5-14 Comparison of Pressure Drop Profiles in 1 Second Load Increase Test with Different EGR Settings

As shown in Figure 5-14, the lowest EGR case results in an earlier rise of pressure drop since a larger value of exhaust gas flows through the turbocharger and the earlier opening of the VGT vane quickly decreases the pressure drop down to a low value. Apart from the response difference at the beginning of the transient periods, the pressure drop of each case has a close maximum value and ultimate steady value. Due to the closed-loop control of the VGT, the boost pressure is maintained well after the transition and the pressure drop keeps the same value with different EGR valve positions. Thus, the EGR ratio has an obvious effect on pressure drop response during transient conditions but the VGT plays a more important role determining the value of pressure drop after the stability of the boost pressure.

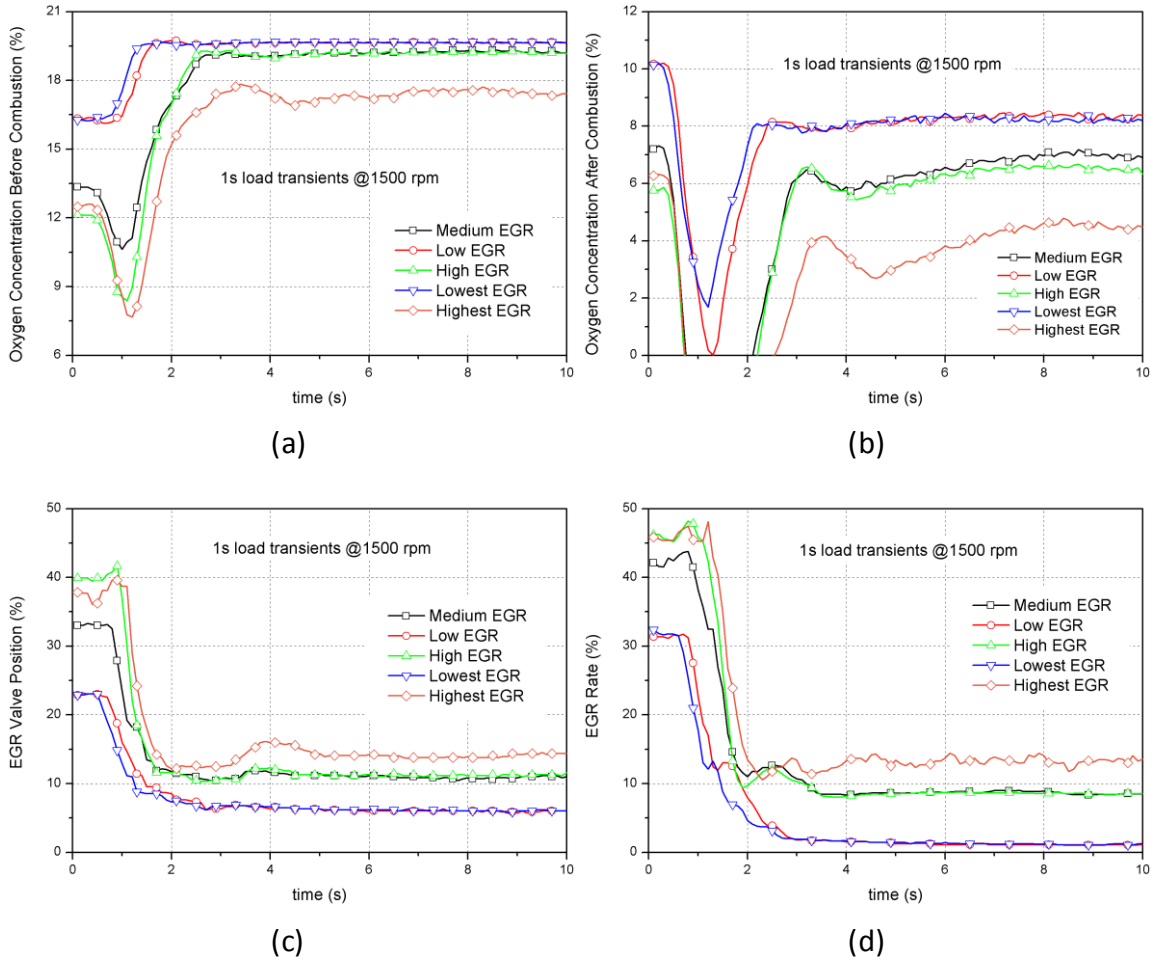

Figure 5-15 Comparison of Oxygen Concentration with Different EGR Settings during Load Transient Tests

With different EGR calibrations, the comparisons of oxygen concentration in the intake and exhaust are shown in Figure 5-15. In the low and lowest EGR cases, the EGR valve starts at a low position and fully closes during the transient periods, which leaves the EGR ratio at almost zero. As a result, no drop of oxygen concentration before combustion occurs in these two cases; but the serious reduction of oxygen concentration in the exhaust seems inevitable in each case. In the case of the highest EGR, the high EGR ratio at the beginning of the transition results in an obvious reduction of O2_i due to the intake of exhaust air with deficient oxygen. Then severe over-rich combustion forms, as shown from the oxygen concentration after combustion. Thus, a high initial EGR valve position leads to insufficient oxygen in the intake air during the transient operation and deteriorates the combustion with an unacceptable air-fuel ratio.

5.3.2 Combustion Characteristics

Due to the multiple injection strategy, it is difficult to obtain the traditional combustion parameters such as ignition delay and combustion duration accurately, especially in transient operation. Accordingly, some alternative cycle-based parameters are presented and discussed, namely, HR50, peak in-cylinder pressure and peak in-cylinder temperature.

Combustion Performance

Figure 5-16 (a) shows the profile of HR50 during the load increase tests at 1500 rpm. At the steady state condition before the transition, it is clearly shown that when the injection timing remains the same, the increase of EGR ratio delays the HR50, with the expected

longer ignition delay of the main injection and lower temperature. When the load increases, HR50 of each case is postponed at the beginning stage. As discussed in the previous section, insufficient oxygen concentration and post injection contribute to this phenomenon. It is noticed that except in the low and lowest EGR cases, one obvious advance of HR50 occurs in the original and high EGR cases. Since the main injection timing is around 5 ATDC in the test shown in Figure 5-8, when HR50 is advanced to almost 10 ATDC, it is highly possible that a large amount of fuel from the main injection does not burn in these cycles due to a low oxygen concentration and temperature from the high EGR ratio. Besides, the heat release from the main injection and post injection is expected to be low in the meantime. Thus, combined with the profiles of oxygen concentration in the intake, during the transient operation, a higher EGR ratio caused a slower response of boost pressure and intake air; meanwhile, more EGR mass itself aggravated the insufficient oxygen concentration, which largely deteriorated the combustion. In contrast, a low EGR case could cause the misfire of the pilot injection and maintain a relatively steady HR50, which improves the total combustion efficiency.

From the profiles of peak in-cylinder pressure, a sudden increase in the high and highest EGR cases is found. This further proves the interpretation that the fuel of the pilot injection burns at a late phase, close to TDC. Apart from that, it is observed that the lower the EGR ratio setting, the faster the peak pressure increases to the next steady level. This can be explained by the boost pressure change. Since the response of the boost pressure in a low EGR setting is preferable, as discussed in the previous section, the fuel injection amount which is limited by boost pressure is capable of increasing faster.

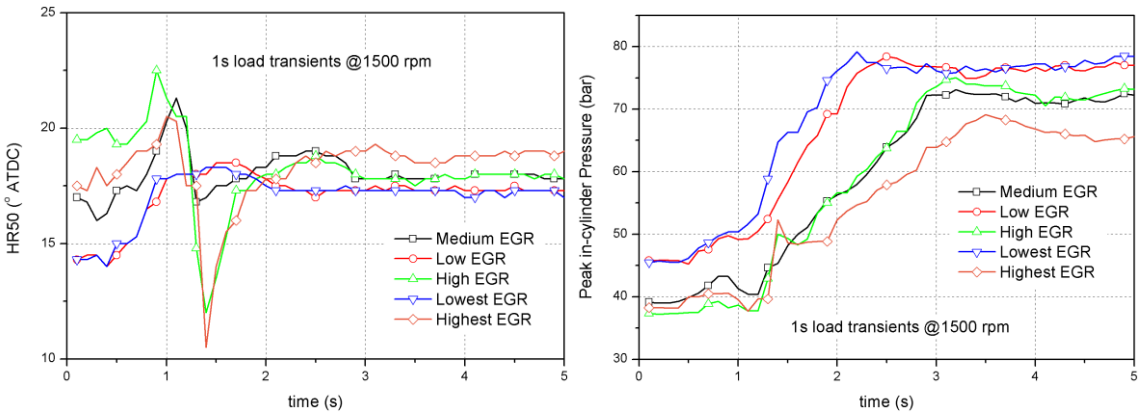

(a) (b)

Figure 5-16 Comparison of Combustion Performance with Different EGR Settings during Load Increase Test: (a) HR50; (b) Peak In-cylinder Pressure

The in-cylinder temperature is calculated from the in-cylinder pressure and instantaneous volume by the ideal gas law based on the assumption that the mass in the cylinder is constant after IVC; the peak value of each cycle during the transient periods was picked and presented in Figure 5-17. Even though this method neglected the fuel-air mixing process, the global trend in the transient period can be illustrated. It is shown that the peak in-cylinder temperature rises rapidly and has an overshoot in low and lowest EGR cases. While in the cases of high EGR, the temperature has one drop, corresponding to the explanation about HR50.

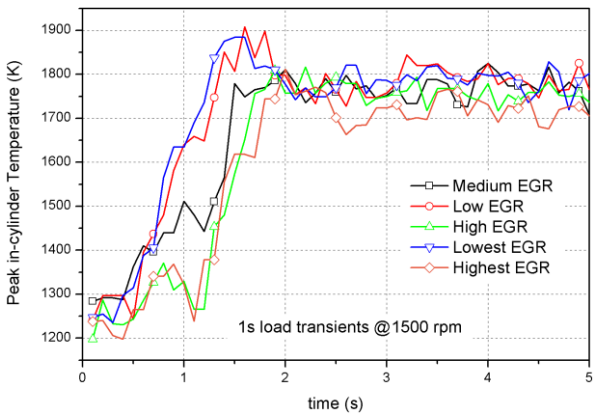

Figure 5-17 Comparison of Peak In-cylinder Temperature with Different EGR Settings during Load Increase Tests

Dynamics and Stability

For transient operation, dynamic behaviour with different EGR settings is compared. Figure 5-18 shows the profiles of IMEP and BMEP with the instantaneous fuel injection quantity. The BMEP is calculated based on measured torque and engine displacement. There is one assumption in this comparison; the cylinder by cylinder variation is neglected. It is shown that the fuel injection amount increases earlier in a low EGR case compared with the other cases. This is due to the fuelling limitation by the boost pressure and the better response of boost pressure in the low EGR case resulting in a faster increase of fuel injection. Accordingly, IMEP and BMEP rise more rapidly than in other cases. Besides, a drop of IMEP is found both in the high EGR and in the original case, even though the fuel injection increased at that time. It indicates that the combustion phase delay mentioned in Figure 5-16 derives from incomplete combustion. Therefore, during a load increase event, slow response of intake air and high EGR would lead to poor combustion and power loss, which should be avoided.

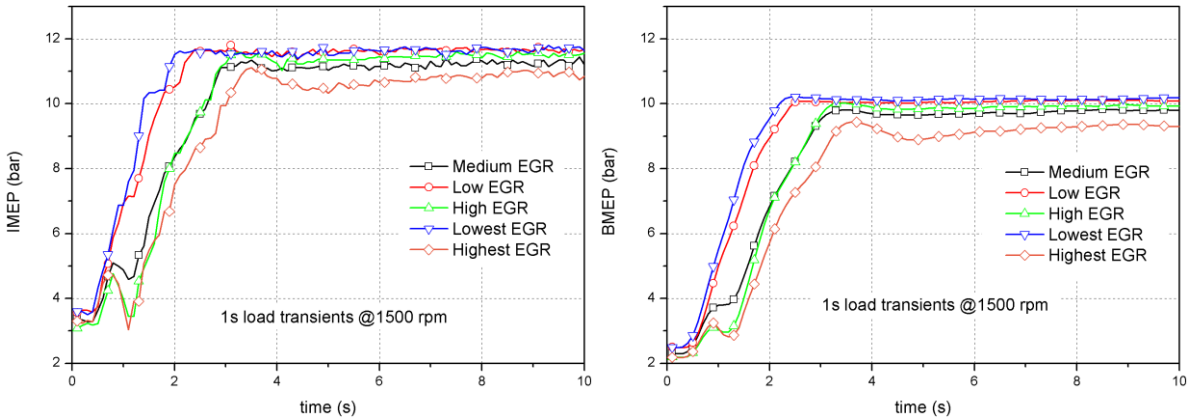

(a) (b)

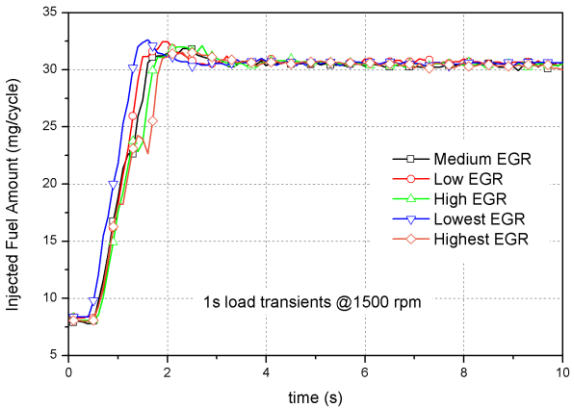

(c)

Figure 5-18 Comparison of Dynamic Behaviour during Transient Tests: (a) IMEP; (b) BMEP; (c) Injected Fuel Amount

After the transient process, the stability of the engine is compared with different EGR settings in this study. To analyse it quantitatively, the COV of IMEP in the transient operation as one important measure of cyclic variability is used. The value is calculated by the standard deviation in IMEP divided by the mean IMEP of the last 20 cycles.

$$COV_{transient} = \frac{\sigma_{IMEP}}{IMEP} \times 100 \qquad \textbf{Equation 5-1}$$

As shown in Figure 5-19, the maximum and average COV presents the same trend. In the cases of low EGR and lowest EGR, the COV is lower compared with the other cases; mainly because the relatively stable and higher oxygen concentration assures complete combustion during transient operation. When the EGR ratio increases, the COV appears as a larger value. The drop of IMEP presented in Figure 5-18 is able to show the instability of the combustion and reflects it clearly in the COV. Interestingly, it is found that the highest EGR case had a smaller COV than the original EGR case. This meant that an excessively high EGR ratio largely deteriorated the combustion efficiency and reached a status of steady poor combustion.

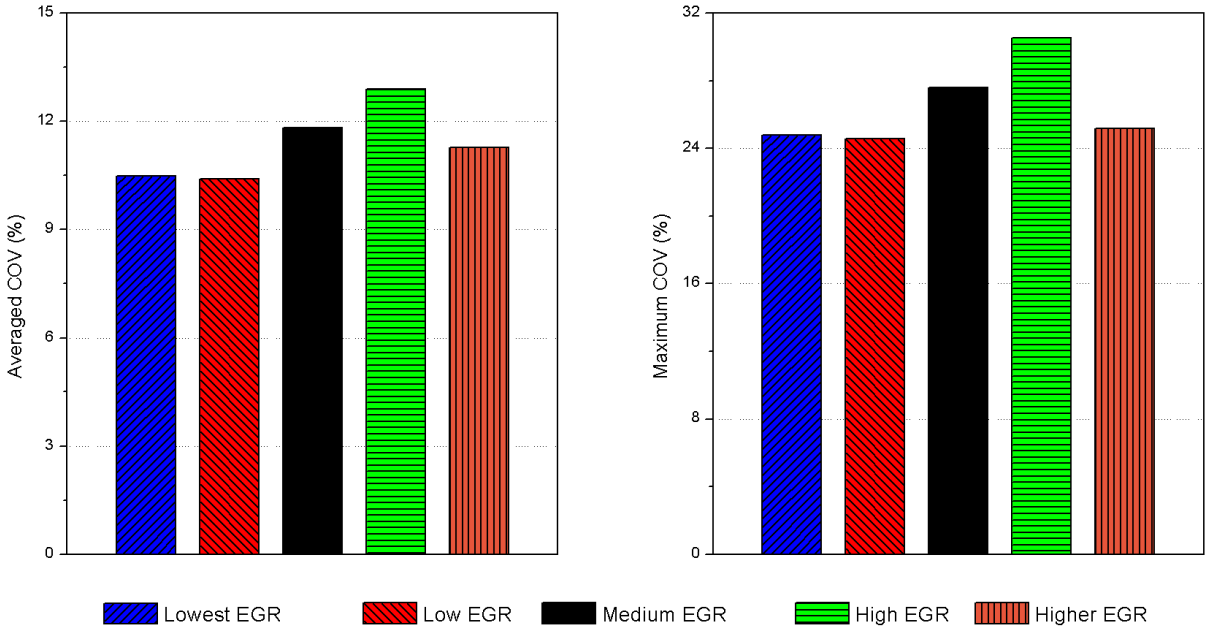

Figure 5-19 Comparison of Stability with Different EGR Settings during Load Increase Tests

5.3.3 Emission Behaviour

Gaseous Emissions

Figure 5-20 (a) presents the instantaneous NOx emission profiles of different EGR settings during load increase tests. As expected, higher NOx emissions are found when the EGR ratio is lower in general. It is observed that when the EGR ratio is low, NOx increases faster; while in the case of high EGR, a longer delay of increase occurs. In the first two seconds, NOx remains a low value even though the fuel injection amount and IMEP increases in the original and high EGR cases; this is caused by the serious drop of oxygen concentration before combustion, as previously mentioned. Besides, it is noticed that NOx increased slowly after the transition in each case; which shows the thermal lag in transient periods and the effect of cylinder temperature on NOx emissions.

In low and lowest EGR cases, HC emissions are much lower compared with the other cases. Although the fuel injection amount increases earlier and O2_e is rapidly reduced at the beginning of the transient period, as shown in Figure 5-15, the HC emissions do not dramatically increase as in the high EGR case. Thus, with a low EGR rate, the peak of HC during transients can be avoided when the oxygen concentration is sufficient and the glo bal air-fuel ratio is not low enough to cause incomplete combustion, showing O2_e as positive. In addition, a slow decrease of HC after transition is observed. The better atomization of the fuel with the increased in-cylinder temperature during transients is expected to be responsible for this phenomenon.

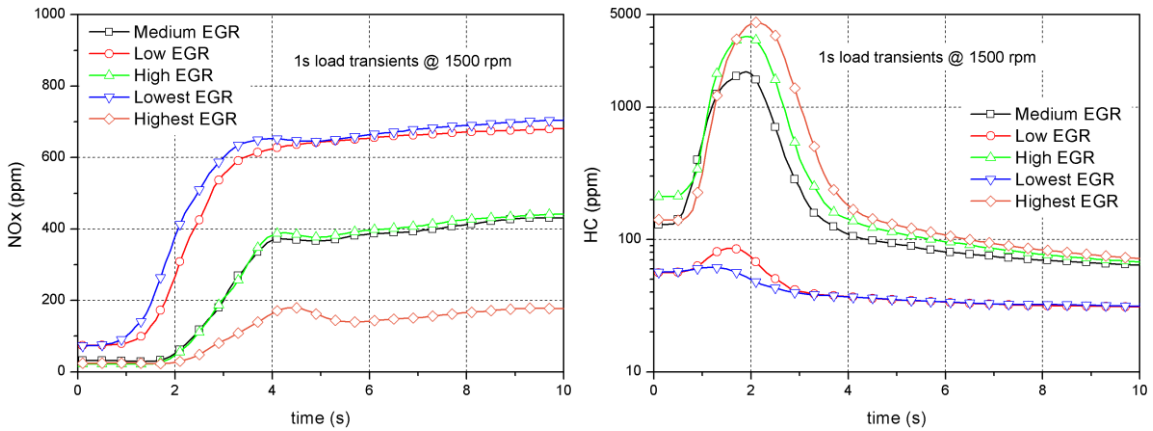

(a) (b)

Figure 5-20 Gaseous Emission Behaviour in Load Increase Tests with Different EGR Calibrations: (a) NOx; (b) HC

Particulate Matter

As for the particulate matter, it is shown that EGR has an obvious effect as well. Unlike the trend of HC, one apparent peak of particulate number and mass is observed in low and

lowest EGR cases. During the load increase, particulate number rises rapidly with the increased fuel amount. The time of the peak value corresponded with the drop of oxygen concentration in the exhaust as well. It proves that the air-fuel ratio, oxygen-fuel ratio more specifically, has a strong correlation with particulate emissions during transients. According to the discussion about HR50, lower cylinder temperature is expected in the initial transient operation. This would enhance the accumulating process of soot. On the other hand, due to the longer ignition delay during the transient operation, the remaining time after combustion decreases, this deteriorates the soot oxidation.

Moreover, it is found that the peak value of particulate number in each EGR case is close while the peak value of particulate mass varied, with a higher value with a higher EGR setting. This means that the average size of particulates formed in a higher EGR setting is bigger than that in the lowest EGR tests. Due to the EGR, some soot in the exhaust is returned back into the cylinder, aggravating the formation of soot in the oxygen-deficient condition during the transient operation and small particles were easily adhered to the soot from the exhaust gas. Hence, in view of both the load response performance and particulate emissions, EGR should be lower in transient operation than the steady state calibration value to reduce the particulate emissions.

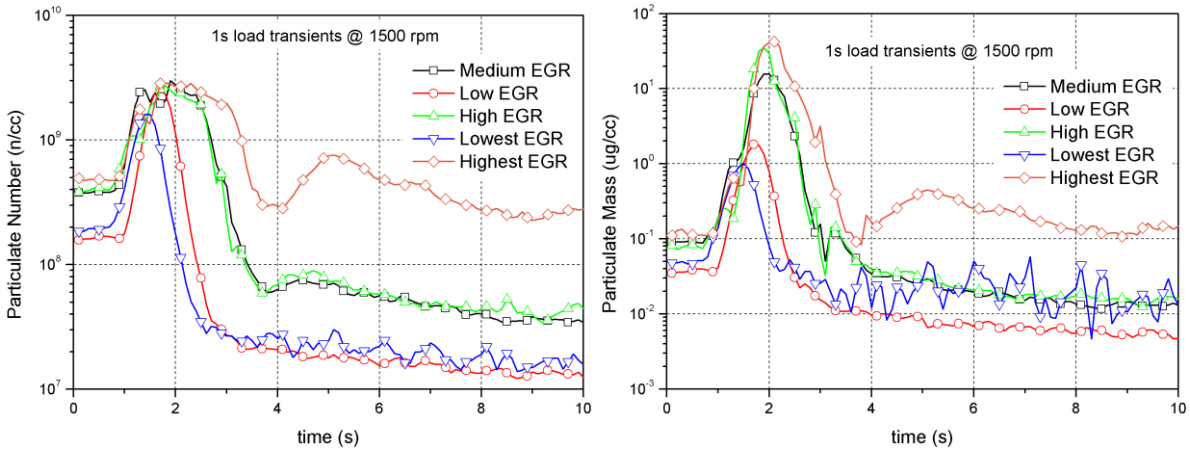

(a) (b)

Figure 5-21 Comparison of Particulate Matter in Load Increase Tests with Different EGR Calibrations: (a) Particulate Number; (b) Particulate Mass

NOx-PM Trade-off

After the EGR calibration map is modified, the emission characteristics vary accordingly. In order to compare and illustrate the emission behaviour quantitatively, it is necessary to normalize the transient emissions by considering engine power outputs. The data analysed for each test is selected only for the load transient period and the steady operation data are omitted; i.e. only data of the first 5 seconds for the load step tests is used. In this way, only the transient data are compared and the influence of steady operation is cut off.

The emission analysers NOx concentration output data are in parts per million (ppm) which are converted to brake specific NOx (BSNOx) in g/kWh from accumulated NOx (g) and output power (kWh) using the following equations (Constantine D. Rakopoulos et al. 2010):

$$NOx(g) = \int_{t=5}^{t=t_n} \frac{ppm_{NOx}}{10^6} \cdot \frac{MW_{NOx}}{MW_{Exhaust}} \cdot (\dot{m}_{air} + \dot{m}_{fuel})dt \qquad \textbf{Equation 5-2}$$

$$W_{output}(kWh) = \int_{t=5}^{t=t_n} \frac{T_{tq} \cdot n}{9550} dt$$ **Equation 5-3**

Where MW_{NOx} and $MW_{Exhaust}$ stand for the molar mass of NOx and exhaust air; $\dot{m}_{air}$ and $\dot{m}_{fuel}$ are the fuel and air mass flow rate; n stands for engine speed.

Also, PN output data is converted to numbers using the following equations:

$$PN = \int_{t=5}^{t=t_n} N / cc_{PN} \cdot 10^3 \cdot \frac{22.7}{MW_{Exhaust}} \cdot (\dot{m}_{air} + \dot{m}_{fuel}) dt$$ **Equation 5-4**

In the above equation, the 22.7 is litres per mole, since the DMS500 calculates particle concentrations at 0 °C and 100 kPa.

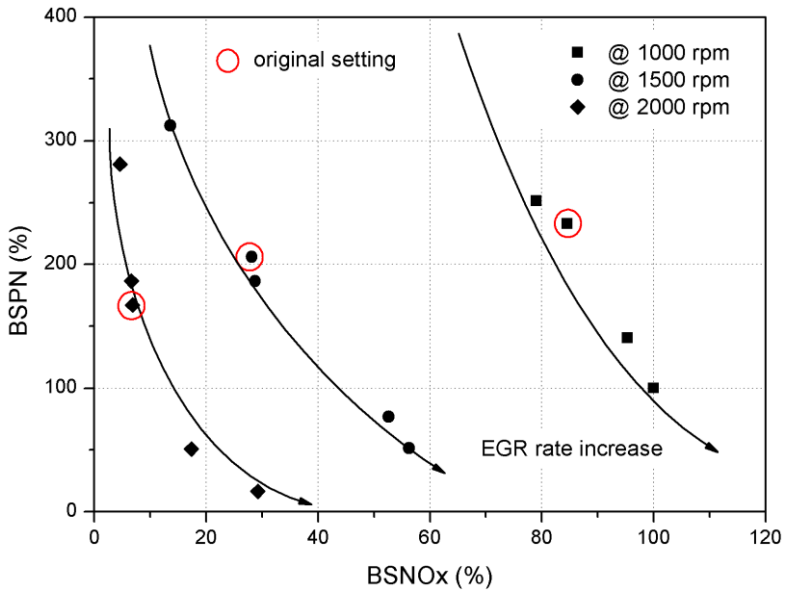

Figure 5-22 Trade-off between NOx and PM during Load Increase Tests

Figure 5-22 presents the trade-off between NOx and PM in the transient tests after the normalization, using the original brake specific emission results at 1000 rpm as the reference data. It shows that when the total EGR rate is increased through the change of the

EGR calibration map, the number of the particulate matter in the transient tests would drop dramatically at each engine speed. However, it comes with the penalty of the augmenting of the NOx emissions. Adjusting the EGR map setting can move along the NOx-PM trade-off curve, but it is difficult to minimize both target values. Thus, an optimal control strategy of EGR and the VGT is necessary.

5.4 Sensitivity of Alternative Fuel

To determine the sensitivity of alternative fuel on engine performance and emissions during transient operation, HVO blends are used as test fuels for the investigation and comparison purposes. The test sequences are load increase with a constant engine speed. The torque and speed settings are kept the same for each fuel in each transient sequence.

5.4.1 Fuel Properties

HVO is a remarkable alternative diesel fuel, made by a refinery-based process that converts vegetable oils and animal fat into paraffinic hydrocarbons. In this study, the HVO blends are all supplied by Shell Global Solutions UK. HVO30 and HVO60 stand for the 30% and 60% blend ratio of HVO with the conventional diesel by mass. The properties of the test fuels are listed in Table 5-2.

Table 5-2 Properties of Diesel and Two Fuel Blends

Property	Diesel	HVO30	HVO60
Carbon Content (% wt)	85.9	85.5	85.1
Hydrogen (% wt)	13.6	14	14.4
Cetane Number	56.7	58.8	64.3
Aromatics (% wt)	24.87	17.78	10.37
Lower Heating Value (MJ/kg)	42.72	42.76	43.66
Viscosity (10^{-3} Pa·s)	3.6	3.49	3.43
Density (kg/m^3)	832.7	815.5	798.7
Oxidation Stability (Hrs)	18.6	40+	40+

The cetane numbers of HVO blends are higher than those of diesel. This means HVO blends have a shorter ignition delay and better cold start performance. This property affects the emission behaviour in both steady state and transient operation. In addition, since HVO is a mixture of paraffinic hydrocarbons and it is free of aromatics which play an important role in soot formation (Aatola et al. 2008), it has a lower particulate matter emission. Although

DPF are common equipment in modern diesel vehicles, it is an advantage to have low PM emissions to face the increasing stringent emission standards.

Compared with traditional biodiesel such as rapeseed methyl ester (RME) or soy methyl ester (SME), HVO has a better oxidation stability and lower viscosity. Oxidation stability is important for vehicle fuel systems. Poor oxidation stability limits the concentration of biodiesel blends and also high viscosity has an adverse influence on the injection system (Sugiyama et al. 2011).

5.4.2 Combustion Characteristics

Figure 5-23 shows the maximum cylinder pressure during the 5 seconds load transient period fuelled with HVO30, HVO60 and diesel. All types of fuels show similar cylinder pressure trends and values. Based on this observation and since their energy density is very close, it is expected that they have comparable emissions. Previous research also proves that HVO does not result in lower torque at the same indicated value of injection duration as diesel (Sugiyama et al. 2011). Thus, although the engine is not calibrated for HVO blends, its transient responses are highly consistent as those of diesel.

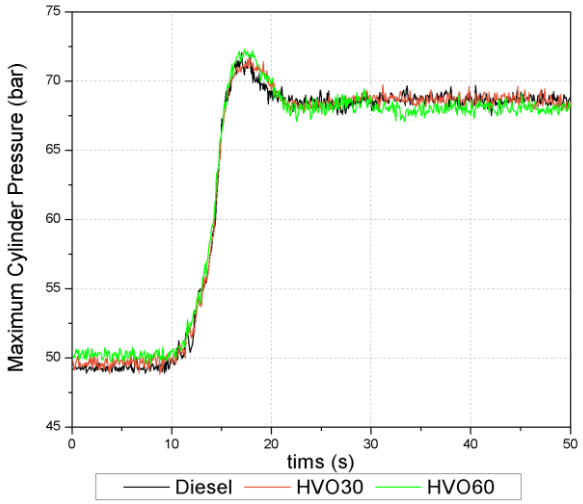

Figure 5-23 Cylinder Pressure Comparison of HVO Blends and Diesel for Load Transient Tests @ 1500 rpm

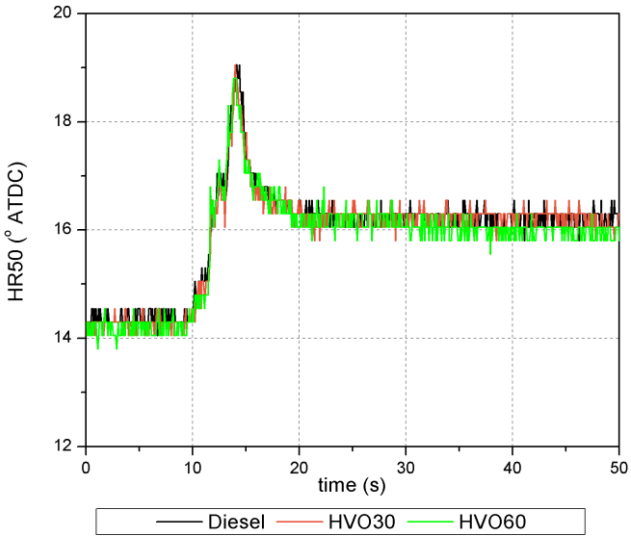

Figure 5-24 Comparison of HR50 of Alternative Fuels during Load Increase Tests

The HR50 of all the fuels during the load transient events is presented in Figure 5-24. Despite HVO's higher cetane number, the main combustion progress of HVO blends are not advanced compared with diesel in this engine during both the steady state and transient operation. This phenomenon can be explained by the following factors:

1. The engine was equipped with a common-rail system in which the physical properties of the fuels had little influence on the injection timing.
2. The injection strategy is two pilot injections before the main injection, which decreases the effect of biodiesel's higher cetane number on reducing the ignition delay.
3. The fluidity of HVO blends is close to diesel (Table 5-2) resulting in little difference in the injection properties.

From Figure 5-25, it is evident that HVO blends have a shorter ignition delay and higher heat release in the first pilot injection due to their higher cetane number; resulting in a higher internal gas temperature and a longer high-temperature period before the main injection. As for the main injection and post injection, the difference between diesel and HVO blends is tiny.

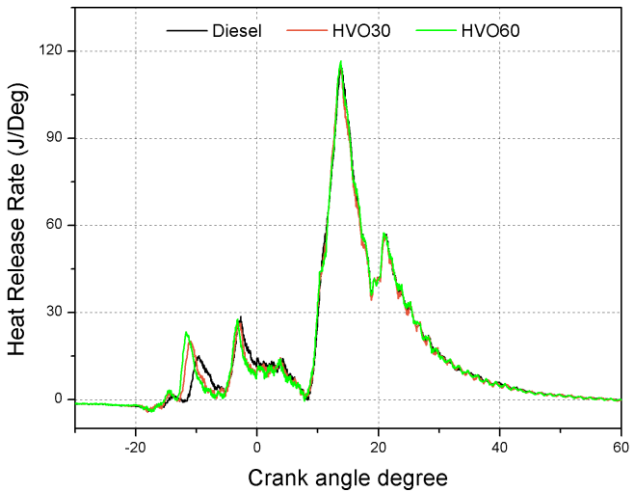

Figure 5-25 Average Rate of Heat Release during Load Transient Tests

5.4.3 Emission Behaviour of Alternative Fuel

The time-resolved NO emissions of each fuel tested are shown in Figure 5-26 (a). Obvious drops are found in each case before the NO emissions increase to new steady state levels. This observation can be explained by a higher EGR ratio and low oxygen concentration as discussed previously. The NO emissions of HVO blends have the same trend as diesel but they are slightly higher in levels for transient operation. In order to compare the emissions of different fuels, the BSNO of each fuel type is calculated, as in Figure 5-27. About 14% higher NO emissions are found for HVO30 and about 30% for HVO60 in the transient tests. Previous research has shown that HVO blends have lower NO emissions comparable to diesel (Pflaum et al. 2010). One reason for this discrepancy is the two pilot injections used in the test engine while other researchers operated with either a single injection or two injections strategies. Based on Figure 5-25, it is evident that HVO blends have a shorter ignition delay and higher heat release in the first pilot injection resulting in a higher internal gas temperature and longer high-temperature period before the main injection. It is reported that the critical time period for NO formation is between the start of combustion and shortly after the occurrence of peak cylinder pressure (Heywood 1988). Thus, more NO emissions are generated after the pilot injection for the HVO blends.

Regarding the HC emissions, a sharp spike of HC concentration appears after a small hump during the 5 seconds load increase period as shown in Figure 5-25 (b). It is clear that HVO blends have lower HC emissions than diesel in transient operation, because the main composition of HVO is paraffin which reacts more easily than aromatics. Thus, HVO blends have higher combustion efficiency at high fuel-air equivalence ratio and lower temperature

during load transient operation. Also, HVO blends have shorter recovery periods for the HC concentration to be reduced to the steady state value. When load increases to the required value, the HC emission of the HVO blends rapidly reaches a very low concentration but diesel has a small delay for the reduction of HC. This is also attributed to the lower concentration of aromatic compounds for HVO blends. When the internal gas and wall temperature was lower than the steady state value because of the thermal inertia, aromatic compounds were hard to combust.

In Figure 5-26, 20% and almost 30% lower HC emissions were produced by HVO30 and HVO60 respectively, compared to diesel. The difference between HVO30 and HVO60 is very small; this is because the branched paraffin, the main composition of HVO, is not easy to break down in low combustion compared to liner paraffin and naphthenic. With less aromatic compounds, a higher ratio of HVO blends does not have the advantage of fewer HC emissions during the load transients.

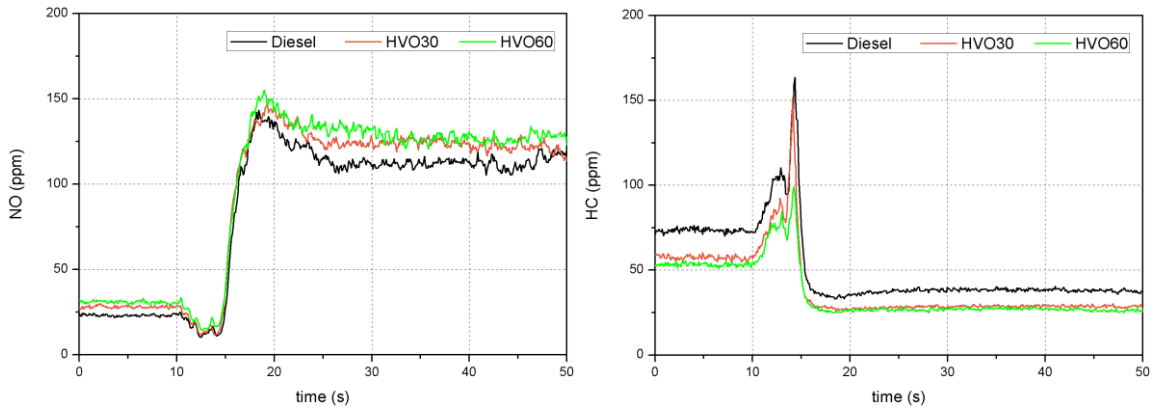

(a) (b)

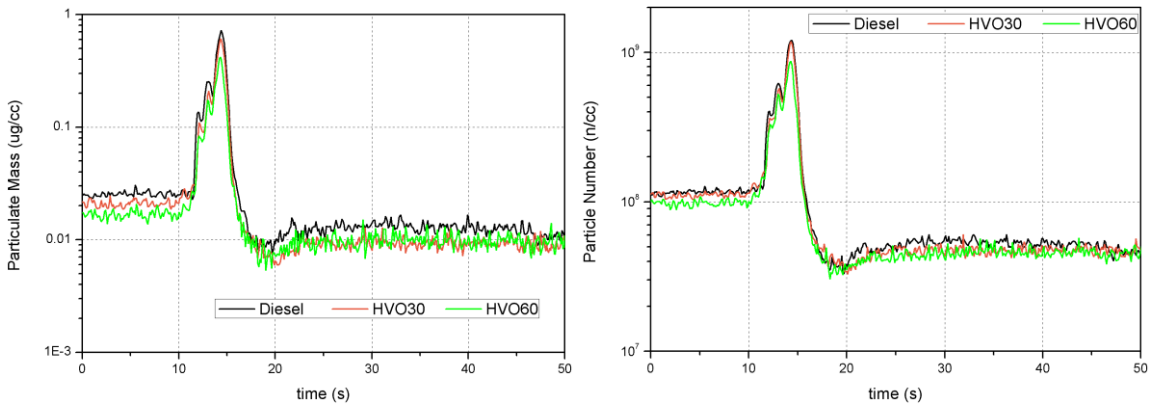

(c) (d)

Figure 5-26 Real-time Emission Behaviours of Engine Load Increase Tests: (a) NO; (b) HC; (c) Particulate Mass; (d) Particle Number

In Figures 5-26 (c) and (d), the time-resolved particle number and particulate mass of HVO blends and diesel are presented. There is a small hump before the large spike in the particulate matter because of the post injection, the same as for the HC emissions. As for the comparison of fuel type, the HVO blends have lower PN and PM than diesel. With the HVO ratio increased, both the peak values of particle number and particulate mass are reduced. Meanwhile, the peak periods of the HVO blends are shorter than those of diesel, which is similar to the HC emissions. Unlike traditional biodiesel which contains oxygen, HVO is composed of paraffin only and no aromatic compounds, which play an important role in soot formation (Kopperoinen, Kytö, and Mikkonen 2011).

Also, it is found that the particulate mass of HVO60 in three load transient operation is just 60% of that of diesel; while reduce of particle number is 20%. HVO30 has a very close particle number to diesel and lower particulate mass relatively.

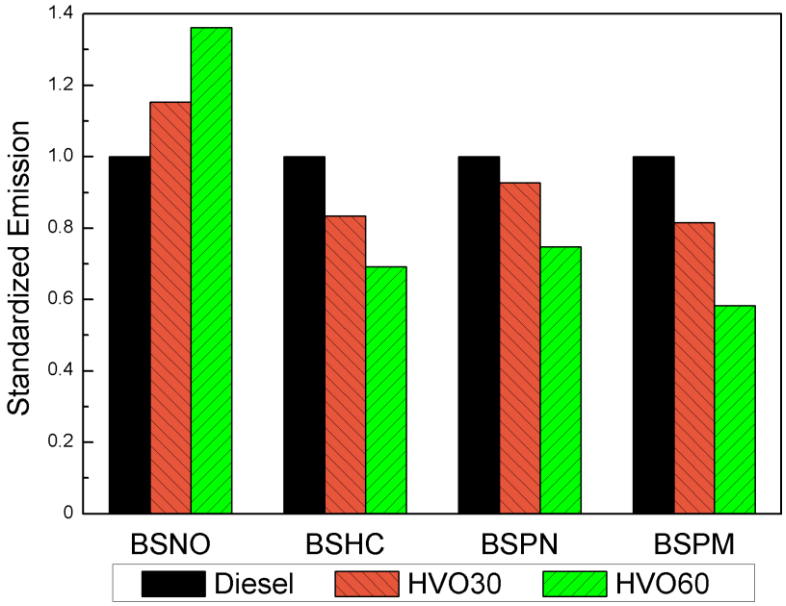

Figure 5-27 Standardized Emission Behaviour of Alternative Fuels during Load Transient Tests

To analyse the problem, particle size distribution for all the fuel types during transient operation are presented in Figure 5-28. It is clearly shown that the number of accumulation mode particles decreases and the mean diameters are reduced with a longer acceleration period for all the tested fuels. Meanwhile, nucleation mode particles change a little in the different tests.

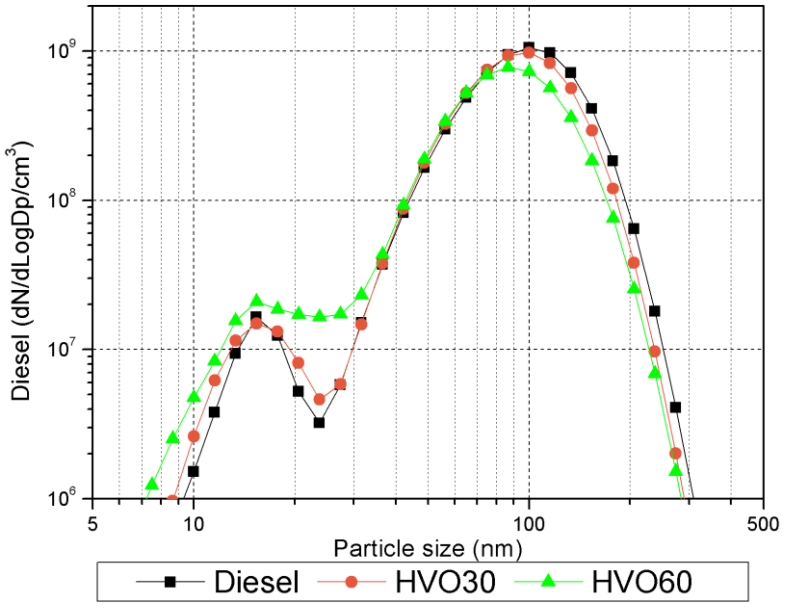

Figure 5-28 Particle Size Distribution of Alternative Fuels during Load Increase Period

In the nudeation mode, the HVO blends produce more particles during the load transient operation; while the mean diameters are similar to diesel. Small particles (5 to 10 nm) are produced by the HVO blends; whereas diesel has no partides in this size range. In previous studies, increased fuel injection pressure is associated with the increased concentration of particles at small sizes for biodiesel (Chuepeng et al. 2011). However, the same fuel injection pressure is applied to all the tested fuels (with close viscosity and energy density of HVO) in this study. Since oxidation and pyrolysis products of fuel molecules have typically included acetylene with its higher analogues and also polycyclic aromatic hydrocarbons (PAH) (Heywood 1988), HVO blends produced less PAHs and smaller particulate by containing fewer aromatics.

In the accumulation mode, the HVO blends have lower particle numbers and smaller particle sizes. Interestingly, in 30 to 60 nm diameter range, the HVO blends are highly consistent with diesel. However, in the larger sizes, HVO blends produce less particulate matter due to having fewer aromatics, as discussed previously. Due to the greater mass of larger particles and the relatively negligible mass of small particles, HVO blends have a lower total of PM than diesel in all the tests.

5.5 Summary

During transient operation, the gas exchange process plays an essential role in engine combustion performance and emission behaviour. The experimental study on a turbocharged diesel engine is presented. Specifically, the effects of engine speed and EGR

are discussed and analysed. Also, the sensitivity of fuel properties on the effects of engine dynamic performance during transient operation is tested using alternative fuels. The major findings are summarized:

Engine Speed Effects

1. The boost pressure at low engine speed increases more slowly with smaller amplitude during load increase tests, compared with the pressure at high engine speed. It is mainly due to the initial low value of the intake air flow at low engine speed and the exhaust gas energy is insufficient to boost the intake pressure. As a result, the VGT position has a more significant influence on boost pressure at a relatively high engine speed.
2. At high engine speed, obvious spikes of pressure drop are found in the transition of the load increase tests. This derives from the delay of the energy at the turbocharger to boost the intake pressure. Also, the low value of the VGT position contributes to the form of the pressure drop peak.
3. One apparent drop of oxygen concentration in the intake manifold is observed at high engine speed during transient operation. The EGR flow does not reduce rapidly due to the transport delay; meanwhile the faster response of the fuel injection leads to rich combustion, intensifying the deficiency of oxygen. Accordingly, incomplete combustion and excessive HC and PM emissions occur, up to 10 times the steady state value within this period.
4. The delays of the combustion phase, from 3 to 15 crank angle degrees, occur at the transition and are larger when the engine speed increases. Employment of a post

injection strategy, less proportion of premixed combustion and incomplete combustion contribute to the delays.

EGR Effects

5. The low EGR valve position facilitates the faster rise of the boost pressure during load increase tests when the VGT keeps constant. Meanwhile, earlier peaks of pressure drop are also observed.
6. The drop of oxygen concentration in the intake during transients is eliminated when the EGR rate is down to 30%; while a higher EGR rate leads to the insufficient oxygen and deterioration of the combustion with an unacceptable air-fuel ratio.
7. In general, lower NOx emissions and higher HC and particulate emissions are observed with a higher EGR ratio case. Within the transient period, only adjusting the EGR map setting can move along the NOx-PM trade-off curve, but it is difficult to minimize both values. An optimal control strategy of the EGR and VGT is necessary.

Sensitivity of Alternative Fuel

8. With the increase of the HVO ratio, from 0 to 60%, the HVO blends produce more NO emissions than diesel due to a shorter ignition delay in the pilot injections and they have lower HC emissions and a shorter recovery period under each condition, due to fewer aromatic compounds.
9. The total PN and PM of the HVO blends are less than for diesel, up to 40% lower. In the nucleation mode, the HVO blends have higher particulate concentrations with a similar mean diameter; in the accumulation mode, HVO blends produce fewer particles and smaller particulate than diesel.

CHAPTER 6

REAL-TIME DIESEL ENGINE MODELLING

In this chapter, the detailed description of control-oriented engine modelling is introduced. The objective of the modelling is to build a model with basic physical insight and a simple structure for real-time control of EGR valve and VGT position. Also, nonlinear dynamic emission models of NOx and particulate matter are introduced. The engine model integrated with the emission models is able to act as a complete model plant for model-based control. Lastly, the results and discussion are presented.

6.1 Introduction

Based on the discussion and analysis in the previous chapter, gas exchange process during transient operation plays an important role in engine combustion and emission characteristics. There is a need to develop a novel control strategy to optimize the control of the air-related actuators. Building an engine model plant is an essential step in order to reduce the cost of experimental work and avoid unnecessary damage to the engine. Since the application of the air system model is a relatively slow process and requires low computational complexity, mean-value models are chosen in this study. After limited fitting on some key parameters, the engine model can be easily applied to an individual engine. Considering the high complexity and difficulty in emission prediction, nonlinear dynamic

models through a system identification approach were constructed. Unlike the conventional data driven emission models, basic physical principles are considered and the parameters closely related to combustion characteristics are chosen and processed as the inputs of these models. With a small quantity of experimental results, the emission models can be quickly developed with reasonable accuracy in a wide range.

6.2 Control-oriented Engine Model

The detailed methodology of engine model development is introduced and presented in this section. The assumption and suitability of models are discussed as well.

6.2.1 Model Outline

The control-oriented engine model was developed using Simulink with a fixed simulation step. The sample time was set as 0.1 seconds in light of most parameters in the tests were acquired in 10 Hz, which kept the simulation and experiment data in accord. The model is capable of simulating both steady state and transient operation of an engine performance in a certain range. The EGR valve position, VGT position, engine speed and fuel injection amount are designated as variables in the model. The model consists of three major parts: the air system model, engine combustion model and dynamic emission models. The main outputs of the model include the EGR rate, oxygen concentration, IMEP, NOx and particulate matter.

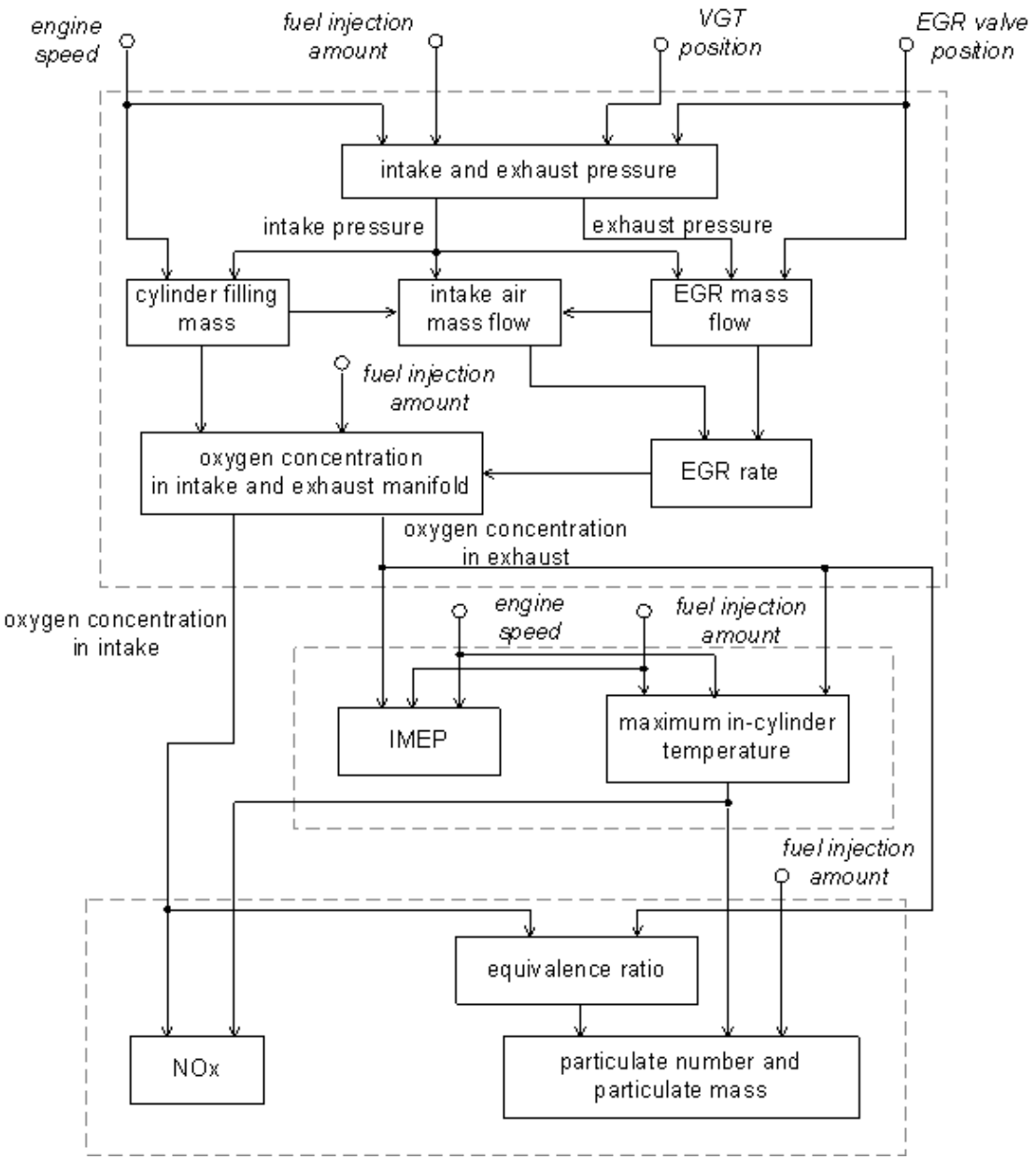

Figure 6-1 Qualitative Input-output Relation of the Control-oriented Engine Model

The structure of the whole control-oriented engine model showing the relationship between the engine parameters and modules is given in Figure 6-1. As shown, the whole modelling is based on four variables listed in the first row. These variables are chosen because they can be manipulated easily in a real engine and act as the fundamental variables in engine calibration. In order to simulate the engine transient operation, dynamic behaviour is considered in modelling when parameters with a slow response are involved

such as air flow rate, intake pressure and emission behaviour. Additionally, since many parameters are mutually coupled and obtained by deduction, limited errors and fluctuations in parameters are inevitable in a few operation modes. Detailed discussion and results of this issue will be presented later. The working range of the variables in the engine model is listed in Table 6-1.

Table 6-1 Adjustable Range of Variables in the Engine Model

	Engine Speed (rpm)	Fuel Injection Amount (mg/hub)	EGR Valve Position (%)	VGT Position (%)
Min	1000	5	5	10
Max	2000	40	80	40

Detailed descriptions of each module in each part of the model are given in the following section.

6.2.2 The Air System Model

As mentioned previously, for a turbocharged diesel engine, one of the main problems is the delay in the air system during transients. Therefore, it is important to develop the air system model with proper dynamic characteristics. In this study, the main parts in the air system included the turbocharger, intake manifold, engine cylinder, exhaust manifold, EGR valve and VGT. The structure of the system is shown in Figure 6-2.

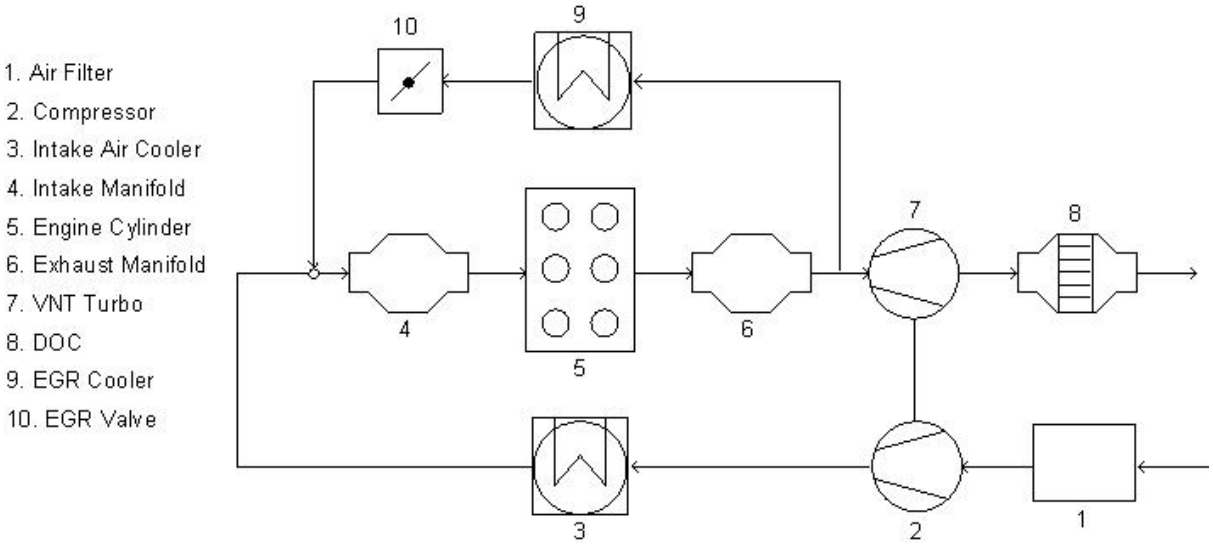

Figure 6-2 Schematic of Air Path of Turbocharged Diesel Engine

As presented in Figure 6-2, the air system is a highly inter-coupled system. For instance, the EGR mass flow is determined by the EGR valve position, upstream pressure and downstream pressure of the EGR valve. Meanwhile, the pressure in the exhaust manifold largely determines the upstream pressure of the EGR and the exhaust air through the turbo, having an influence on intake pressure which can be assumed as downstream pressure of the EGR valve. Besides, the intake pressure plays an important role in engine combustion, thereby having a close relationship with exhaust pressure. In order to start the simulation from the chosen four variables, two parameters, intake pressure and exhaust pressure, are directly calculated through a neural network, similar to the look-up table method. The main advantages of using a neural network and not an equation with physical insight in these two parameters are the reasonable accuracy and stability during transients with low computation cost. Due to the mutually coupled characteristics, if all the parameters are obtained through deduction, one tiny error would result in unacceptable inaccuracy in some operation modes, especially in the transient cases. More importantly, the turbocharger modelling involves complicated efficiency maps which require a large amount of

experimental data. In real application, the pressure signal can be easily measured by a pressure transducer with preciseness and quick response. The simulation of pressure is only for the engine modelling work before being applied in real engine control.

The neural network of the intake and exhaust pressure was trained by 270 groups of steady state experimental data. A two-layer feed-forward network was employed and the network was trained with the Levenberg-Marquardt back propagation algorithm. Since the VGT and EGR valves are pneumatically actuated, rate limits of opening and closing were added into the model. In order to reflect dynamic characteristics, transport delay was considered and the model was tuned based on transient experimental data. Also, the effect of a reservoir in the intake system was noticed so that a FIR filter was added and tuned to simulate the dynamic characteristics. The detailed results will be presented in the following subsection. The engine intake and exhaust pressure model is given in Figure 6-3.

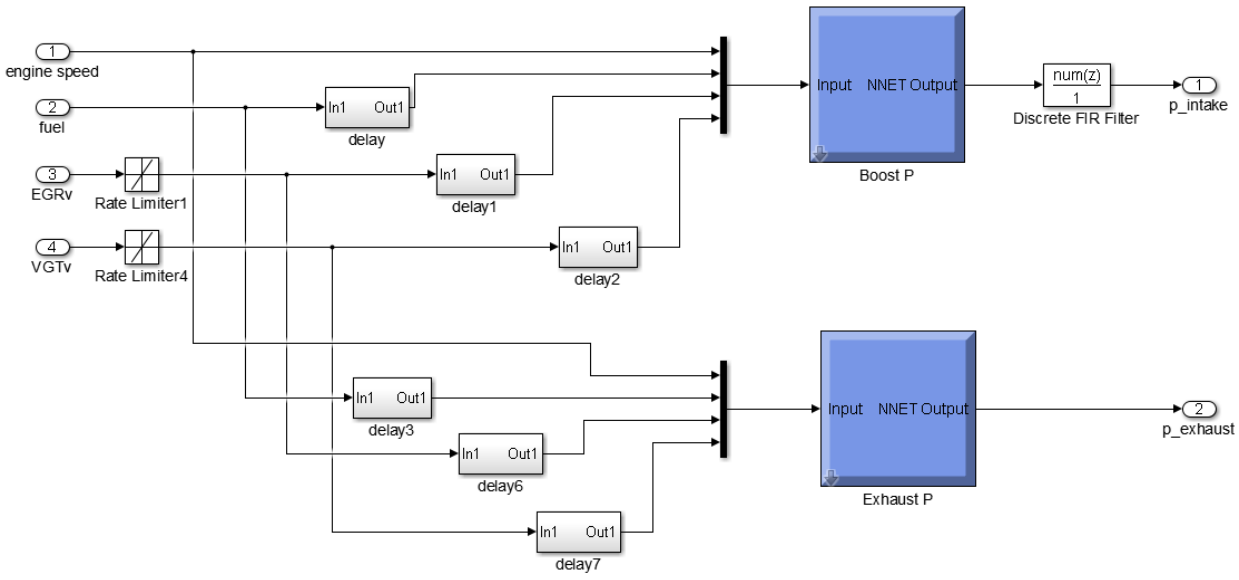

Figure 6-3 Intake and Exhaust Pressure Model

Dynamics of the Boost System

From Figure 6-2, it is found that the air path starts from the intake air. The fresh air after the air filter goes through the compressor and intake air cooler, namely the boost system. The boost system was assumed as one receiver with a fixed volume. The reservoir effect was considered through adding one item based on change of intake pressure. The mass flow through the compressor and intercooler was determined by the equation:

$$\dot{m}_{air\_\mathrm{int}} = \dot{m}_{air\_bc} - \frac{V_{boost}}{R \cdot T_{cooler}} \cdot \dot{p}_{\mathrm{int}} \qquad \textbf{Equation 6-1}$$

Where $\dot{m}_{air\_\mathrm{int}}$ is the air mass flow after the intake air cooler; $\dot{m}_{air\_bc}$ is the air mass flow before the compressor; V_{boost} is the volume of the boost system; R is the specific gas constant, given by the molar gas constant divided by the molar mass of the gas, 0.287 J/(g·K); T_{cooler} is the temperature of air in the cooler, set as 300 K according to the test data and $\dot{p}_{\mathrm{int}}$ is the derivative of the intake pressure. The $\dot{m}_{air\_bc}$ can be validated by a measurement value through the air flow meter and the data signal obtained in the ECU. The model of the dynamics of the boost system is given in Figure 6-4.

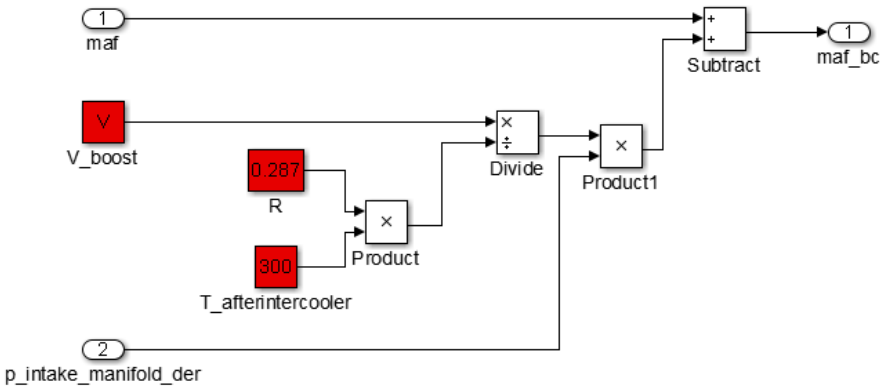

Figure 6-4 Model of the Dynamics of the Boost System

EGR Mass Flow

The simulation of mass flow through the EGR valve is one of the cores of the whole model since EGR has a strong influence on engine combustion and emission behaviour. The EGR mass flow was modelled as a simplification of the compressible flow restriction with variable area (Heywood 1988). In this study, the pressure difference between the EGR valve upstream and the exhaust manifold was ignored to avoid unnecessary complexity of the model. Also, the temperature of the EGR gas after the EGR cooler was assumed as a constant due to the minor effect on model accuracy (Wahlstrom and Eriksson 2011). The EGR mass flow $\dot{m}_{EGR}$ is given by the equation (Guzzella 2010):

$$\dot{m}_{EGR} = C_{D(EGRv)} \cdot A_{EGRv}(\phi) \cdot \frac{p_{EGRvus}}{\sqrt{R \cdot T_{EGRvus}}} \cdot \psi\left(\frac{p_{EGRvds}}{p_{EGRvus}}\right) \qquad \textbf{Equation 6-2}$$

Where $C_{D(EGRv)}$ is the discharge coefficient of the EGR valve; $A_{EGRv}(\phi)$ is the open area of the valve, which is a function of the EGR valve position ϕ; R is the specific gas constant, 0.287 J/(g·K); p_{EGRvus} and T_{EGRvus} represent the valve upstream pressure and temperature; p_{EGRvds} is the valve downstream pressure. Also, the flow function $\psi(\cdot)$ is defined by:

$$\psi\left(\frac{p_{EGRvds}}{p_{EGRvus}}\right) = \begin{cases} \sqrt{\gamma \cdot \left(\frac{2}{\gamma+1}\right)^{\frac{\gamma+1}{\gamma-1}}} & for \quad p_{EGRvds} < p_{cr} \\ \left(\frac{p_{EGRvds}}{p_{EGRvus}}\right)^{\frac{1}{\gamma}} \cdot \sqrt{\frac{2\gamma}{\gamma-1} \cdot \left[1 - \left(\frac{p_{EGRvds}}{p_{EGRvus}}\right)^{\frac{\gamma-1}{\gamma}}\right]} & for \quad p_{EGRvds} \geq p_{cr} \end{cases}$$

Equation 6-3

$$p_{cr} = \left(\frac{2}{\gamma + 1} \right)^{\frac{\gamma}{\gamma - 1}} \cdot p_{EGRvus} \qquad \textbf{Equation 6-4}$$

Where γ is the specific heat ratio, set as 1.3 and p_{cr} is the critical pressure where the flow achieves a sonic condition in the narrowest part. The model of the EGR mass flow and flow function is developed in Simulink and given in Figure 6-5 and Figure 6-6.

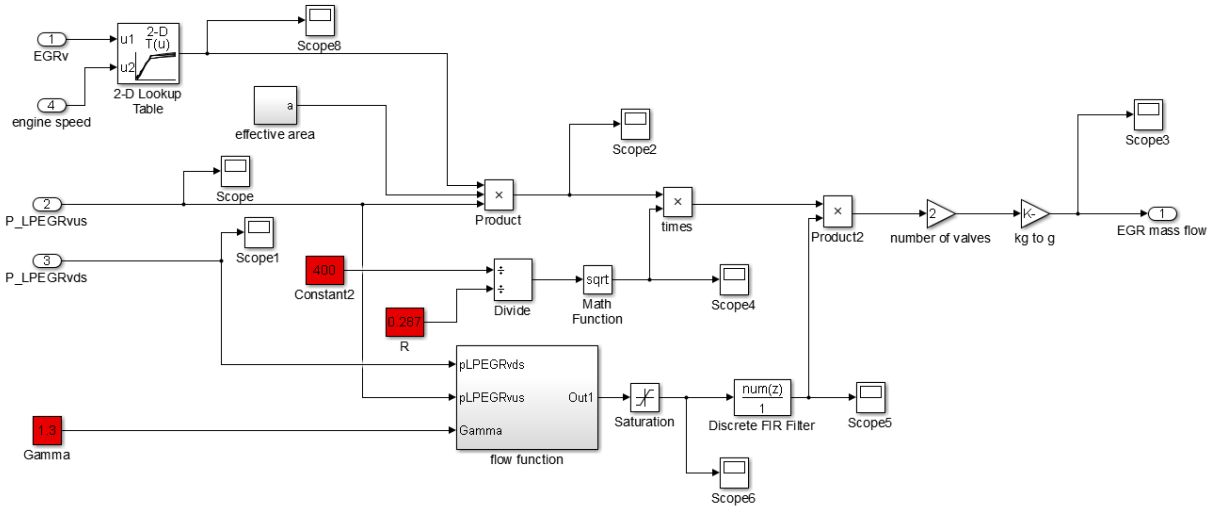

Figure 6-5 EGR Mass Flow Model

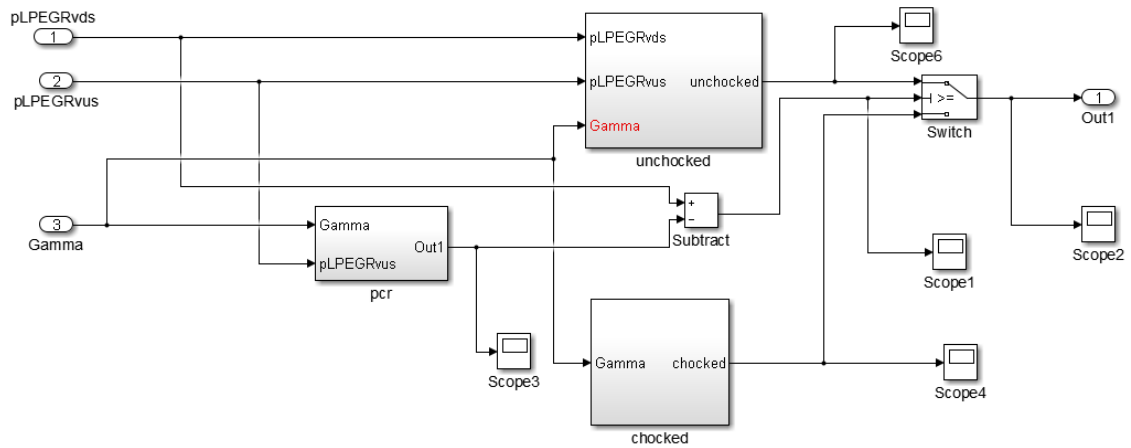

Figure 6-6 Flow Function in the EGR Mass Flow Model

Cylinder Charge

The air mass flow through the engine cylinder was simulated based on the ideal gas law. When the intake valve is closed (at IVC), the current intake pressure was assumed as the in-cylinder pressure and the cylinder volume at IVC can be calculated using the equation (Stone 1999):

$$V = V_d + V_c = \frac{\pi B^2}{4} \cdot \left[R \cdot (1 - \cos\theta) + L \cdot \left(1 - \sqrt{1 - \left(\frac{R \sin\theta}{L} \right)^2} \right) \right] + \frac{\pi B^2 R}{2(r_c - 1)}$$

Equation 6-5

Where V_d is the cylinder displacement volume; V_c is the clearance volume; θ is the current crank angle (CAD); B is the bore diameter; R is the crank radius; L is the length of rod and r_c is the compression ratio. The crank angle in this case is IVC, 160° BTDC.

The equation of cylinder air mass is given below:

$$m_{filling} = \frac{p_{IVC} \cdot V_{IVC}}{R T_{IVC}}$$

Equation 6-6

Where $m_{filling}$ is the air mass in each cylinder volume; p_{IVC} and V_{IVC} represent in-cylinder pressure and cylinder volume at IVC; R is the specific gas constant, 0.287 J/(g·K) and T_{IVC} is the temperature of the in-cylinder air. In this study, p_{IVC} was assumed as the intake pressure. Although the temperature of the air and EGR gas mixture varied in different operation modes, the temperature in this case was assumed as a constant, 300K. As shown in the equation, the reasonable range change of gas temperature has little influence in the

calculation and the temperature cannot be measured and validated. Lastly, the cylinder charge flow rate can be obtained by multiplying the engine speed and number of cylinders. The cylinder-by-cylinder variation was also ignored to reduce the cost of computation. Compared with the experimental steady state data, the correlation coefficient of the cylinder air mass flow is 0.95, which indicated the assumption is reliable. The model of the cylinder charge is given in Figure 6-7.

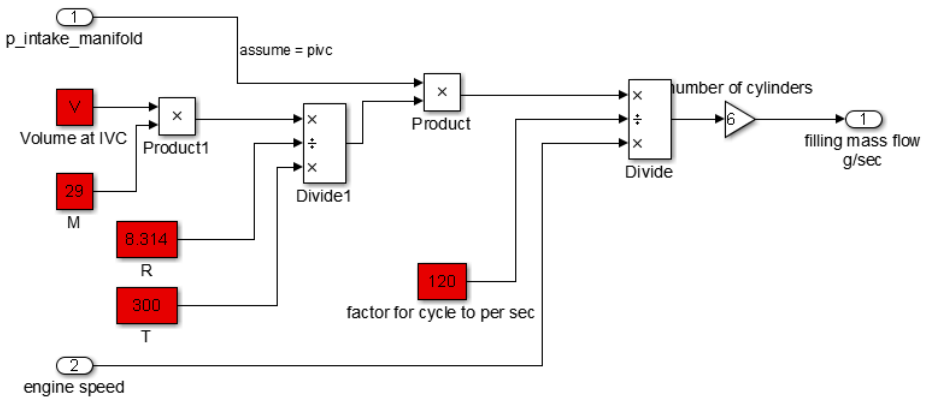

Figure 6-7 Model of the Cylinder Charge

Dynamics of the Intake Manifold

The intake manifold is assumed as a receiver, similar to the boost system. As shown in Figure 6-2, the inputs are the air mass flow from the boost system and the EGR mass flow; while the output is the air mixture flow into the cylinder. Dynamic behaviour was reflected by considering the reservoir effect of the air flow. The equation is shown below:

$$\dot{m}_{air\_\mathrm{int}} + \dot{m}_{EGR} - \dot{m}_{filling} = \frac{\dot{p}_{\mathrm{int}} \cdot V_{\mathrm{int}}}{R \cdot T_{\mathrm{int}}} \qquad \textbf{Equation 6-7}$$

Where $\dot{m}_{air\_\mathrm{int}}$ is the air mass flow after the intake air cooler; $\dot{m}_{EGR}$ is the mass flow through the EGR valve; $\dot{m}_{filling}$ is the air mass flow rate through the engine cylinders; R is the specific gas constant, 0.287 J/(g·K); T_{int} is the temperature of the air in the intake manifold, assumed to be a constant 300 K; V_{int} is the volume of the intake manifold and $\dot{p}_{\mathrm{int}}$ is the derivate of the intake pressure. The model of the intake manifold is given in Figure 6-8.

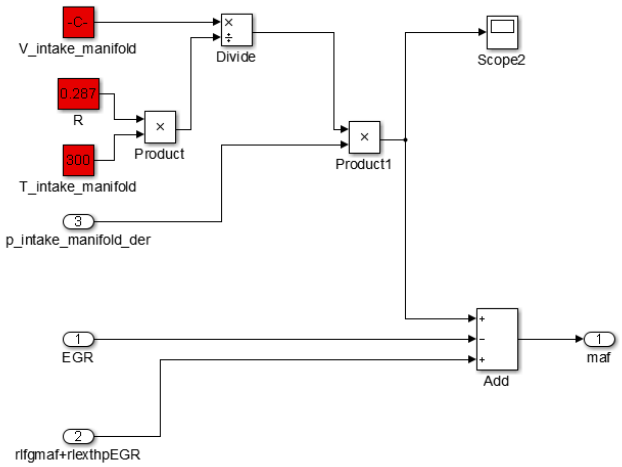

Figure 6-8 Model of the Intake Manifold

EGR ratio

In this study, the EGR ratio is defined as:

$$r_{EGR} = \frac{\dot{m}_{EGR}}{\dot{m}_{air\_\mathrm{int}} + \dot{m}_{EGR}} \qquad \textbf{Equation 6-8}$$

Where $\dot{m}_{air\_\mathrm{int}}$ is the air mass flow after the intake air cooler and $\dot{m}_{EGR}$ is the mass flow through the EGR valve. For this engine, the EGR flow joined into the intake manifold through

a Venturi tube and the transport delay of the EGR mass flow from the EGR valve to the intake manifold is ignored.

Oxygen Concentration Model

The oxygen concentration was not measured and taken into consideration in most research. However, as mentioned in the previous chapter, the oxygen concentration is able to reflect air dynamic characteristics during engine transient operation and has a significant influence on engine combustion and emission behaviour. Therefore, it is essential to simulate the oxygen concentration in the intake and exhaust in order to develop a dynamic model which is closer to the real-life situation. The relationship of the oxygen concentration with the mass flow and EGR rate is given as follows:

$$\dot{m}_{total} \cdot O_{2\_bc} = \dot{m}_{fresh} \cdot X_{o2} + \dot{m}_{EGR} \cdot O_{2\_ac} \qquad \textbf{Equation 6-9}$$

$$\dot{m}_{EGR} = \dot{m}_{total} \cdot EGR_{rate}$$

$$\dot{m}_{total} = \dot{m}_{fresh} + \dot{m}_{EGR}$$

$$\dot{m}_{EGR} = \dot{m}_{fresh} \frac{EGR_{rate}}{1 - EGR_{rate}}$$

$$\Rightarrow \qquad EGR_{rate} = \frac{X_{o2} - O_{2\_bc}}{X_{o2} - O_{2\_ac}} \qquad \textbf{Equation 6-10}$$

$$\dot{m}_{filling} \cdot O_{2\_bc} - \dot{m}_{fuel} \cdot \alpha \cdot AFR_{stoich} = \dot{m}_{filling} \cdot O_{2\_ac} \qquad \textbf{Equation 6-11}$$

Where $\dot{m}_{total}$, $\dot{m}_{fresh}$ and $\dot{m}_{EGR}$ represent the mass flow rate of the total mixture, fresh air after the compressor and EGR; O_{2_bc} and O_{2_ac} are defined as the oxygen concentration in

the intake manifold (before combustion) and in the exhaust manifold (after combustion); X_{o2} is the oxygen concentration of the atmosphere, set as 20.9% in this case; $\dot{m}_{filling}$ is the air mass flow rate through the engine cylinders; $\dot{m}_{fuel}$ is the fuel injected amount, it is to be noted that the unit is converted to grams per second to keep the calculation correct; AFR_{stoich} is the stoichiometric air-fuel ratio for diesel fuel and α is a factor to compensate the efficiency of fuel combustion at different operation modes. The oxygen concentration model is given in Figure 6-9.

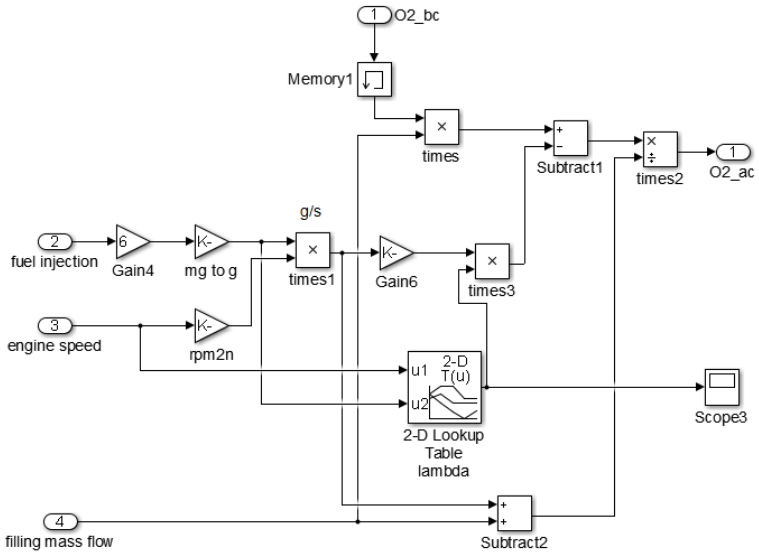

Figure 6-9 Oxygen Concentration Model

In general, the air system model is developed in Simulink and the model size is 270 KB, small enough to be embedded into the engine ECU. More importantly, the model is capable of operating in real time. The wiring diagram of the air system model is shown in Figure 6-10.

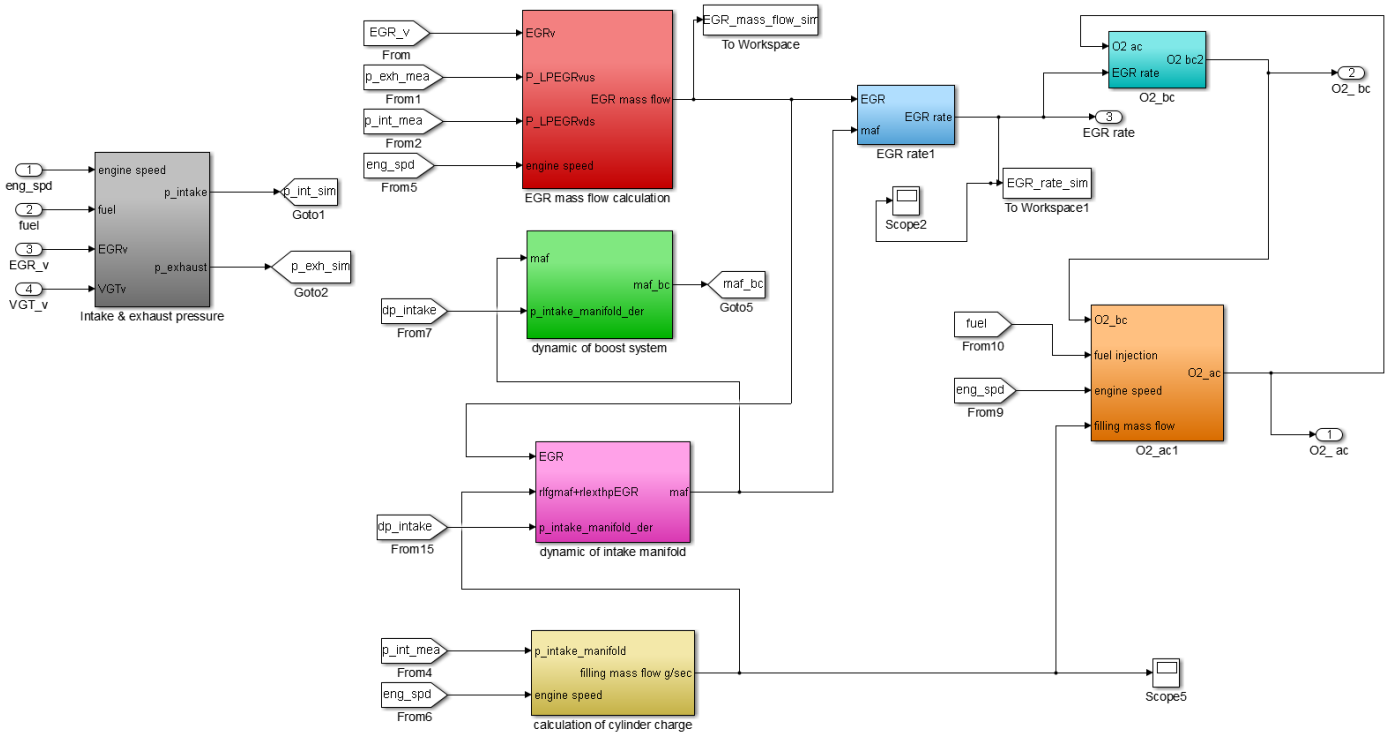

Figure 6-10 Wiring Diagram of the Air System Simulink Model

6.2.3 Engine Combustion Model

As the model is for the purpose of real-time control, a detailed thermodynamic mechanism is not involved in the engine combustion modelling, considering the great amount of computation time necessary. Combustion is often assumed as quasi-static since it has much faster dynamic characteristics compared with the air path (Benz, Onder, and Guzzella 2010). In this study, IMEP and the maximum in-cylinder temperature were chosen as the outputs of the combustion model. IMEP is an important evaluation of engine combustion, directly reflecting the efficiency and it can be used as the reference for emission control. As discussed in Chapter 5, the maximum in-cylinder temperature was obtained from the in-cylinder pressure data. The value is suitable to show the trends of combustion in transient operation and plays an essential role in NOx emission modelling. In the simulation of both

parameters, the approach employs physical insight to separate the influence of related variables and then simplification into a low-dimensional model.

IMEP

In this study, the IMEP model is a nonlinear function of related variables. At first, fuel mean effective pressure is defined (Guzzella and Onder 2010):

$$p_{m\varphi} = \frac{H_l \cdot m_\varphi}{V_d} \qquad \textbf{Equation 6-12}$$

Where $p_{m\varphi}$ is the fuel mean effective pressure; H_l is the lower heating value of diesel, set as 42.6 Mj/kg; m_φ is the fuel injected amount per combustion cycle and V_d is the cylinder displaced volume.

Based on the $p_{m\varphi}$, the equation of IMEP can be expressed as below:

$$IMEP = \eta_e(\omega_e, m_\varphi, O_{2\_e}) \cdot p_{m\varphi} \qquad \textbf{Equation 6-13}$$

Where η_e is the combustion efficiency; ω_e is the engine speed; m_φ is the fuel injected amount per combustion cycle and O_{2_e} is the oxygen concentration in the exhaust. Normally, the combustion efficiency can involve many variables such as air-fuel ratio, EGR rate, injection timing. However, the model with more variables requires a vast number of experimental results and unnecessary over-fitting, since some variables are mutually related. In this case, the focus of the modelling is on the air path control so the fuel injection related variables like injection timing and rail pressure are ignored. Besides, the oxygen

concentration in the exhaust is capable of reflecting the change of air-fuel ratio and EGR rate and the correlation coefficients of the simulation results both in steady state and transient operation are acceptable.

Maximum In-cylinder Temperature

Essentially, the rise of the in-cylinder temperature is due to combustion and volume change. Considering the stationary regulation of volume change, the modelling of in-cylinder temperature is based on the fuel burning process. For the compromise of performance between accuracy and complexity, a similar equation to the IMEP is given:

$$T_{\max} = f(\omega_e, m_\varphi, O_{2\_e}) \cdot m_\varphi \cdot H_l \qquad \textbf{Equation 6-14}$$

Where $T_{\max}$ is the maximum in-cylinder temperature per cycle; f is the factor to convert ideal combustion energy to in-cylinder temperature; ω_e is the engine speed; m_φ is the fuel injected amount per combustion cycle; O_{2_e} is the oxygen concentration in the exhaust and H_l is the lower heating value of diesel. The engine combustion model is given in Figure 6-11.

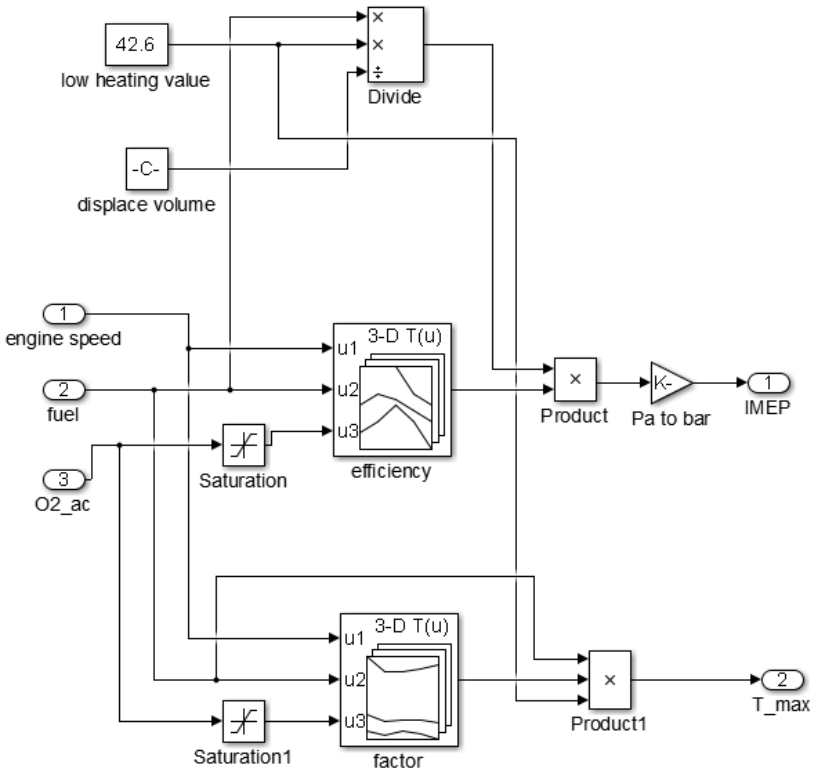

Figure 6-11 Engine Combustion Model

6.2.4 Nonlinear Dynamic Emission Models

Emission control is an important target for the automotive industry and is driven by more and more stringent legal requirements. Due to the difficulty and high cost of installing an on-board emission measurement analyser in a vehicle, many efforts have been made to predict the emissions and design the virtual sensors. However, it is difficult to predict engine emissions either theoretically or by numerical simulation. Many approaches such as quasi-steady models, multi-zone models and neural networks have been investigated as introduced in Chapter 2. After the comparison and compromise between accuracy and complexity, the nonlinear autoregressive model with exogenous inputs (NARARX) is employed in this study to develop the control-oriented emission models.

The nonlinear ARX model is an extension of a linear model. The linear ARX model can be represented as (Ljung 1999):

$$y(t)+a_1y(t-1)+a_2y(t-2)+\ldots+a_{na}y(t-na)= b_1u(t)+b_2u(t-1)+\ldots+b_{nb}u(t-nb+1)+e(t)$$

Equation 6-15

Where y(t) is the output; u(t) is the input and e(t) is the noise; na and nb are the maximum lags for the system input and output.

The output y(t) can be considered as a weighted sum of past output values and current and past input values. Therefore, the equation is rewritten as a product:

$$y(t)=[-a_1,-a_2,\ldots,-a_{na},b_1,b_2,\ldots,b_{nb}]* [y(t-1),y(t-2),\ldots,y(t-na),u(t),u(t-1),\ldots,u(t-nb-1)]^T$$

Equation 6-16

Where $y(t-1),y(t-2),\ldots,y(t-na),u(t),u(t-1),\ldots,u(t-nb-1)$ are delayed input and output variables, called regressors. The linear ARX model predicts the output y(t) as a weighted sum of its regressors.

To create a nonlinear ARX model, the structure is extended as:

$$y(t)=f(y(t-1),y(t-2),\ldots,y(t-na),u(t),u(t-1),\ldots,u(t-nb-1))$$

Equation 6-17

Where $f(\cdot)$ is a nonlinear function; inputs to $f(\cdot)$ are model regressors. The nonlinear mapping function used in this study is wavelet network.

In a simulation scenario, the nonlinear ARX model included both nonlinear and linear functions. The block diagram representing the structure is given in Figure 6-12.

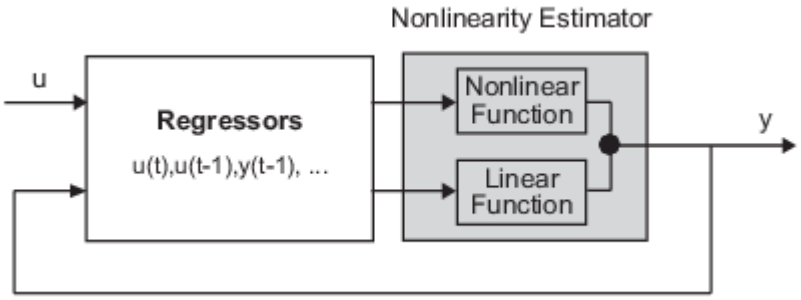

Figure 6-12 Structure of Normal Nonlinear ARX model

The nonlinearity estimator block can be expressed as (Mathworks 2014):

$$F(x) = L^T(x-r) + d + g(Q(x-r)) \qquad \textbf{Equation 6-18}$$

Where x is a vector of the regressors; $L^T(x-r)$ is the output of the linear function block; $g(Q(x-r)$ is the output of the nonlinear function block; r is the mean of the regressors; d is a scalar offset; Q is a projection matrix which makes the calculations well conditioned.

In order to identify the dynamic characteristic of emission formation, the order and delay of model inputs and outputs are tuned based on transient emission data from experimental results. Unlike the pure theoretical modelling or traditional statistic model, the method of nonlinear ARX model involves some physical insights through system identification in the linear function and achieves reasonable accuracy with low computation cost by the setting of the nonlinear function. Most importantly, these models can be generated in Simulink so it is compatible in a Matlab environment. The detailed approaches of dynamic emission models, namely, NOx, particulate number and particulate mass are introduced as in the following subsections.

NOx Model

NOx is one of the major emissions from internal combustion engines, especially diesel engines due to their fuel-lean combustion strategy. The NOx formation can be categorized as a prompt formation process, a fuel formation process and the thermal formation process (Fernando, Hall, and Jha 2006). As the prompt formation occurs when hydrocarbon fragments react with nitrogen, which is only common in fuel-rich combustion and the fuel formation process requires that nitrogen is chemically bound in the fuel, while standard diesel fuel does not contain nitrogen inherently, only the NOx thermal formation process is considered (Tesfa et al. 2014). Since NOx emissions are mainly composed of nitric oxide (NO) and nitrogen dioxide (NO_2) and NO is the predominant product, the well-known extended Zeldovich mechanism was used as the fundamental of the modelling (Heywood 1988). The equation is given as below:

$$\frac{d[NO]}{dt} = \frac{6\times10^{16}}{T^{1/2}}\exp(\frac{-69090}{T})[O_2]_e^{1/2}[N_2]_e \qquad \textbf{Equation 6-19}$$

Where $[NO]$ represents the species concentration of NO; $[O_2]_e$ and $[N_2]_e$ denote the equilibrium concentration of oxygen and nitrogen; T is the instantaneous in-cylinder temperature. It should be noted that the in-cylinder temperature varies within each combustion cycle and the equilibrium concentration is not homogenous. The accurate thermodynamic simulation requires many parameters which are difficult to obtain in a real experiment. Therefore, for the control-oriented model, proper simplification is made in this study. The parameters designated for this model are oxygen concentration in the intake and maximum in-cylinder temperature. These two parameters can be measured or calculated based on experimental results and simulated in the model introduced in the previous

section. The lambda sensor and in-cylinder pressure transducer can be installed in the vehicle for further application in the future. In order to utilize the known thermodynamic regulation and reduce the dimensions of the model, the equation above is converted to the structure shown as:

$$\log([NOx]) = f[T_{\max}, \quad [O_{2\_i}]] \qquad \textbf{Equation 6-20}$$

Where $[NOx]$ and $[O_{2\_i}]$ are the concentration of NOx and oxygen in the intake; while $T_{\max}$ is the maximum in-cylinder temperature. Although the formation of NOx is affected by other factors such as swirl intensity and fuel injection characteristics, which are not included in this model, these factors are assumed to be largely compensated through the nonlinear identification. The NOx model is given in Figure 6-13.

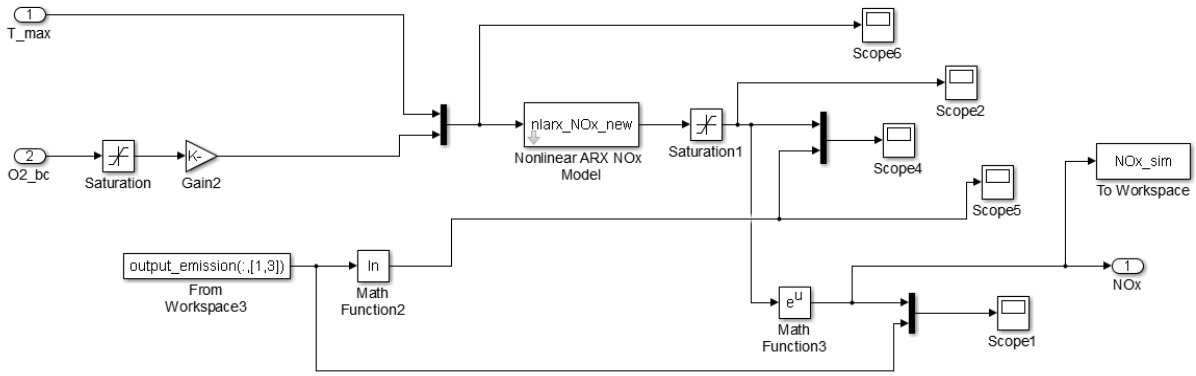

Figure 6-13 Model of NOx Emissions

Particulate Matter Model

The prediction of particulate matter is far more complicated than NOx. The level of particulate matter is influenced by two mechanisms, soot formation and soot oxidation simultaneously. In general, the formation of soot is mainly dependent on the fuel-air

equivalence ratio. A large amount of soot is formed when combustion occurs at high fuel-air equivalence ratios; while the oxidation of soot is mainly dependent on the temperature and the availability of oxygen in the late combustion phase (Heywood 1988). Due to the complexity of its mechanism, a detailed physical-based model of particles is not suitable for real-time modelling. Similar to the NOx model, the method of the nonlinear ARX model was used to identify the regulation and develop the dynamic model. Also, particulate matter have been found to correlate better with exponentials of input signals (Indranil Brahma, Sharp, and Frazier 2010). In this model, three parameters are chosen: maximum in-cylinder temperature, fuel injection amount and corrected equivalence ratio. The selection of in-cylinder temperature is due to its influence on soot oxidation and the fuel injection amount determines the operation mode, which is critical in prediction. The corrected equivalence ratio is defined by mass of oxygen to fuel amount. The reason not to use the traditional equivalence ratio lies in its neglect of oxygen concentration difference in the intake air and the corrected ratio ϕ_c can be expressed as:

$$\phi_c = \frac{\dot{m}_{fuel}}{m_{O_2}} = \frac{\dot{m}_{fuel}}{\dot{m}_{total} \cdot O_{2\_i}} \qquad \textbf{Equation 6-21}$$

$$\dot{m}_{total} \cdot O_{2\_i} - (\dot{m}_{total} + \dot{m}_{fuel}) \cdot O_{2\_e} = \dot{m}_{fuel} \cdot \lambda_{stoic} \qquad \textbf{Equation 6-22}$$

$$\Rightarrow \qquad \phi_c = \frac{1 - \frac{O_{2\_e}}{O_{2\_i}}}{AFR_{stoic}} \qquad \textbf{Equation 6-23}$$

Where $\dot{m}_{total}$ and $\dot{m}_{fuel}$ denote the total intake air flow and fuel injected amount per unit of time; O_{2_i} and O_{2_e} are the oxygen concentration in the intake and exhaust manifold; AFR_{stoic} is the stoichiometric air-fuel ratio of diesel fuel. Owing to the increasing interest in

PM size and concentration levels, the particulate number and particulate mass are designated as the outputs of the emission model. Therefore, the particulate number can be represented as:

$$\log([PN]) = f[\phi_c, \quad T_{\max}, \quad m_{fuel}] \qquad \textbf{Equation 6-24}$$

Where [PN] is the concentration of particulate number in units of n/cc. The structure of particulate mass modelling is the same. The PN and PM emission model is shown in Figure 6-14.

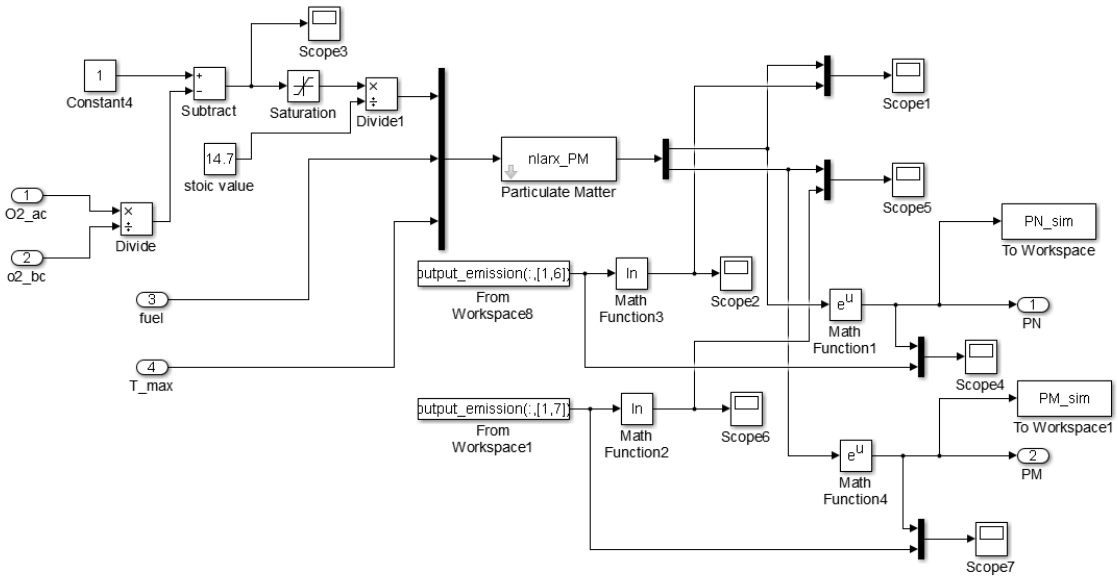

Figure 6-14 Model of PN and PM

6.3 Validation of the Model

In this section, the results of the models including the air path, combustion and emissions will be presented and discussed. The model is obtained from three groups of the experimental data from engine transient tests introduced in the previous chapter and

validated by the rest of the two groups of data. The simulation results of the model with the proposed method show a good correlation with the measurement data.

6.3.1 EGR Mass Flow and Oxygen Concentration

The EGR mass flow rate is mainly controlled by the EGR valve and it is widely used as the control reference of the valve position. Since there is no direct measurement equipment of EGR mass flow rate in the test bench, the measured value shown in this study was calculated based on the intake air flow rate and oxygen concentration. The oxygen concentration in the intake and exhaust were measured by a lambda sensor and compensated with pressure. Figure 6-15 and Figure 6-16 show the comparison of measured data and simulation of EGR mass flow rate and oxygen concentration in engine tests of load step with constant engine speed and speed change with constant load. Also, dynamic relative errors were calculated to illustrate the deviation. The dynamic error between a measured parameter y_{meas} and a modelled parameter y_{mod} was calculated as:

$$y_{error}(i) = \frac{y_{meas}(i) - y_{\mathrm{mod}}(i)}{1/N \sum_{i=1}^{N} y_{meas}(i)} \qquad \textbf{Equation 6-25}$$

In Figures 6-15 and 6-16, it is observed that EGR mass flow and oxygen concentration in the intake show good prediction at steady state, up to 6% error. Meanwhile the oxygen concentration in the exhaust presents slightly larger errors; this is mainly due to the complexity of combustion in the cylinder. The cycle-by-cycle variation and detailed combustion mechanism are not included in this modelling so that the simulation of exact oxygen consumption in each combustion cycle has a small deviation. In transient operation,

it is indicated that the simulation results have an apparent error during some operation mode changes. The maximum errors of the EGR mass flow rate and oxygen concentration in the intake and exhaust are 44.6%, 27.4% and 58.8%, respectively. For this phenomenon, one factor is that the EGR valve and VGT have a clear overshoot at the transition and the simulation based on these variables tends to excessively magnify this influence, resulting in the main discrepancy between simulation and measured value. Another factor is that it is difficult to match each transport delay in different load change steps due to the complicated air path characteristics and simplification of the model. The deviations of oxygen concentration in the intake and EGR mass flow during transients are smaller than those of the oxygen concentration in the exhaust, due to the same reasons introduced previously. In general, the simulation shows a fair agreement with the experimental data and most importantly, the model is capable of capturing most peaks and troughs of air path parameters during transients, reflecting the air path characteristics properly.

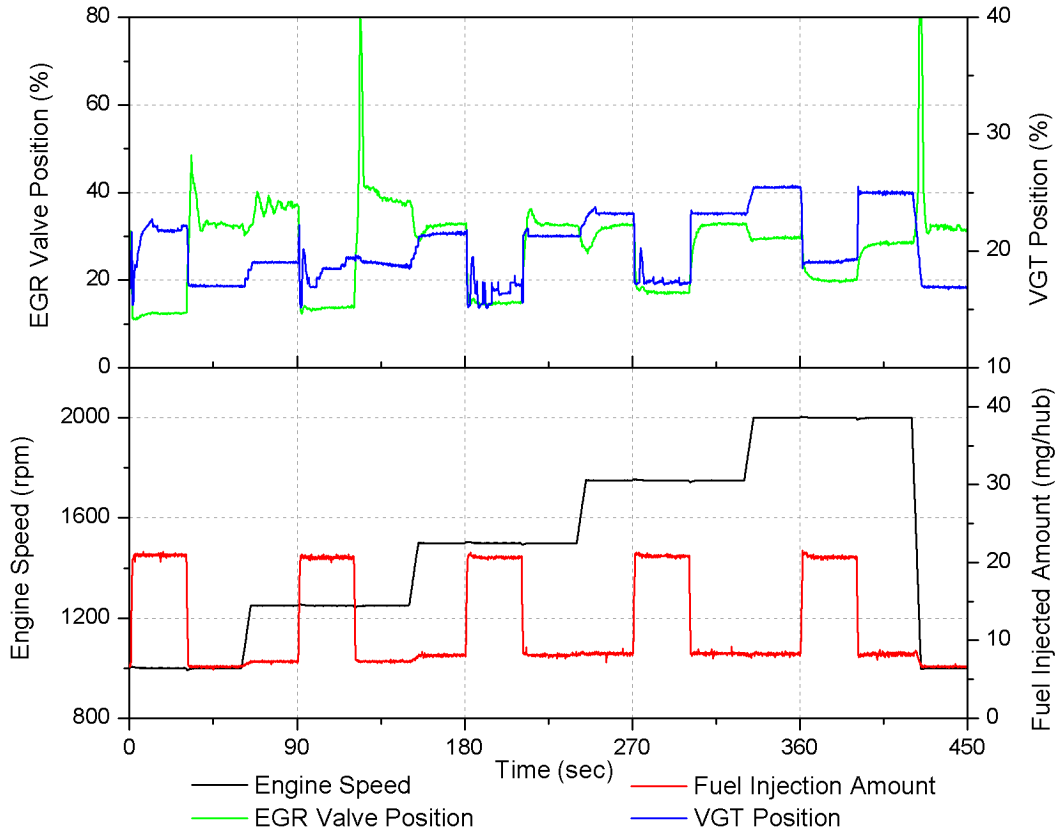
EGR Valve Position (%)
VGT Position (%)
Engine Speed (rpm)
Fuel Injected Amount (mg/hub)
Time (sec)
Engine Speed
EGR Valve Position
Fuel Injection Amount
VGT Position

(a)

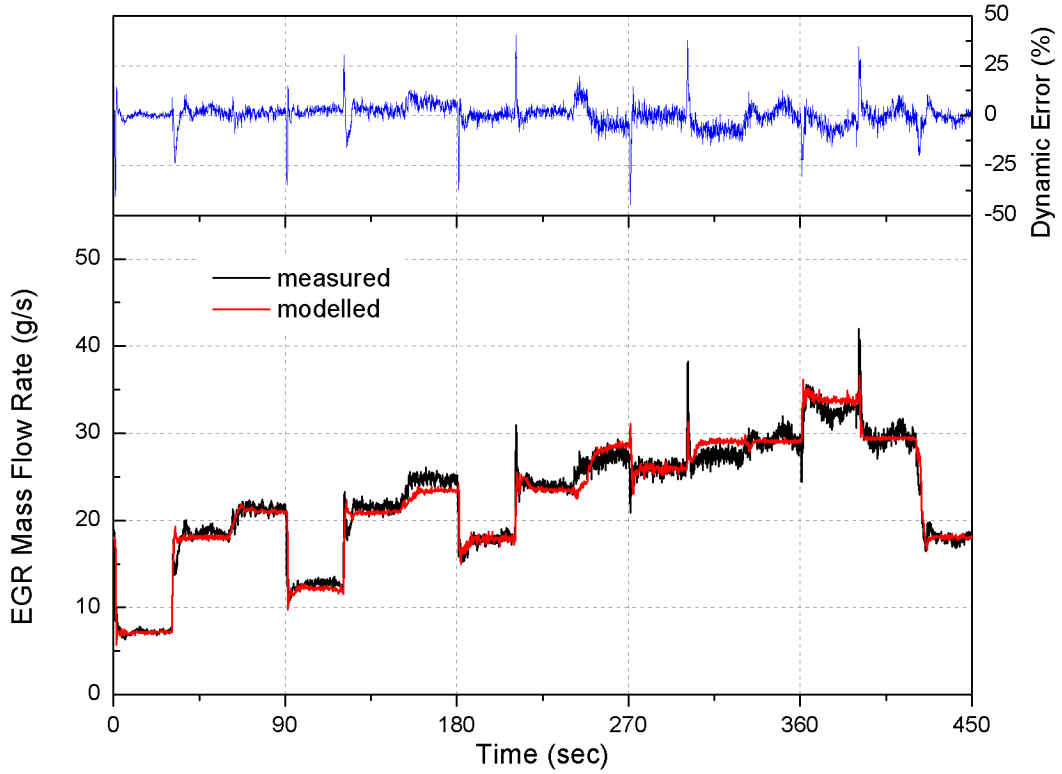
Dynamic Error (%)
EGR Mass Flow Rate (g/s)
measured
modelled
Time (sec)

(b)

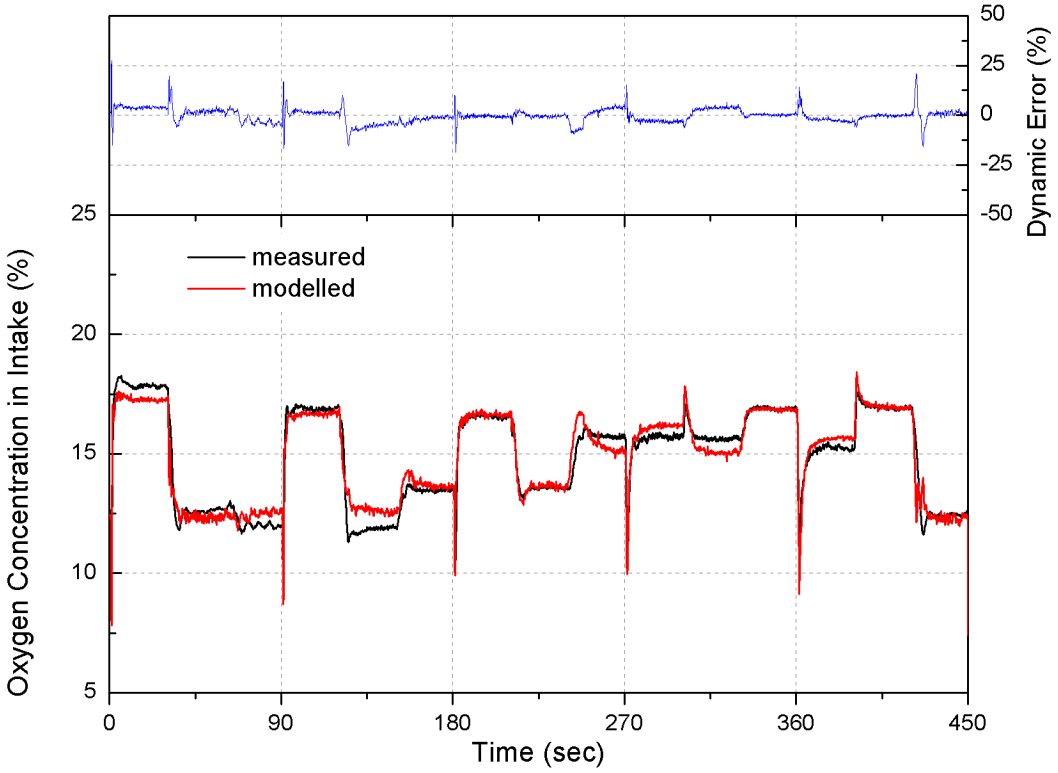

(c)

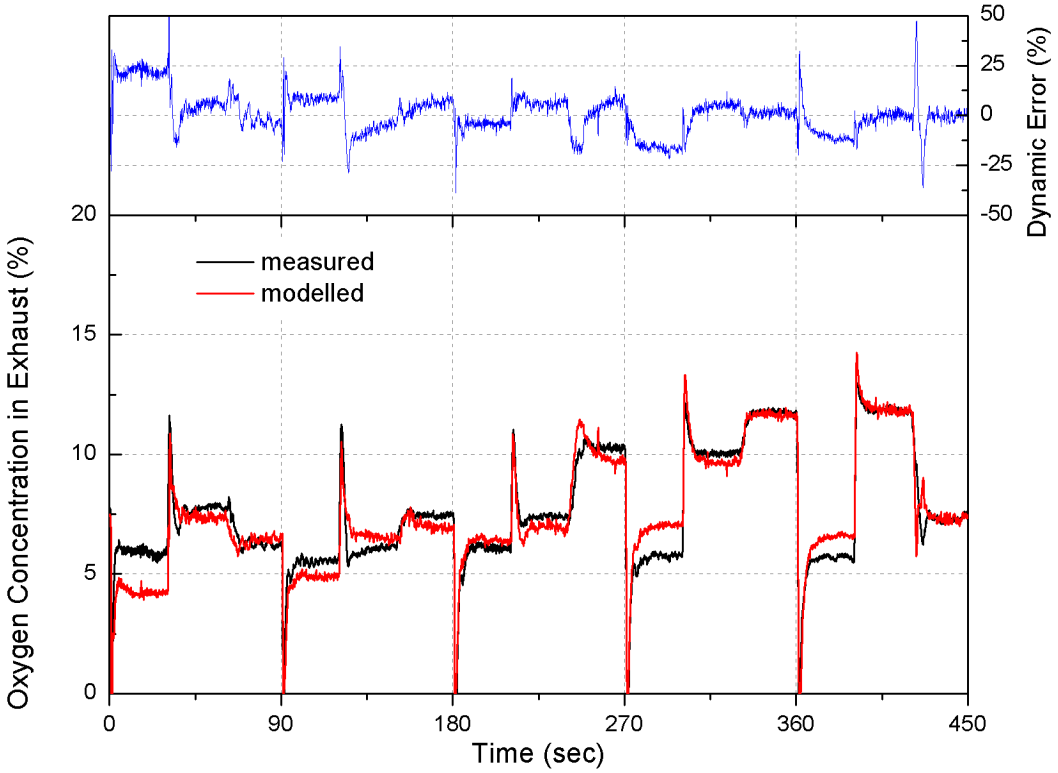

(d)

Figure 6-15 Comparison of Simulation Results and Measurement Data during Load Change between 20% and 35%; (a) Model Inputs; (b) EGR Mass Flow; (c) Oxygen Concentration in Intake; (d) Oxygen Concentration in Exhaust

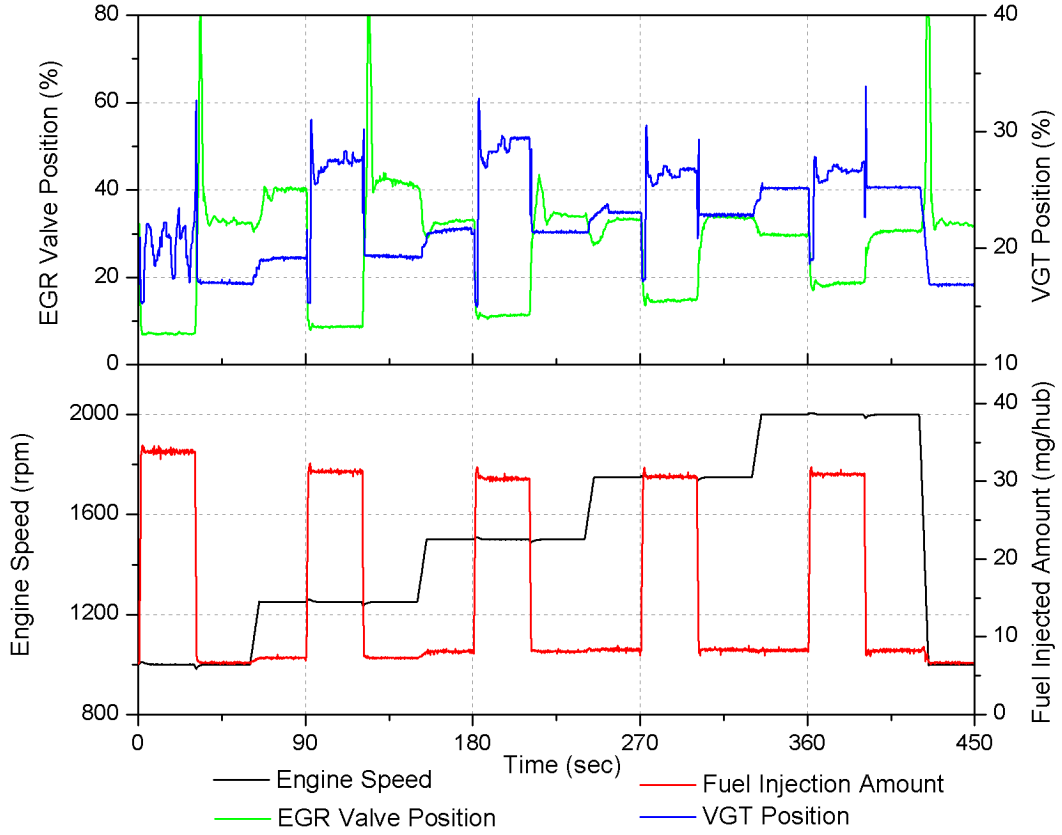
EGR Valve Position (%)
VGT Position (%)
Engine Speed (rpm)
Fuel Injected Amount (mg/hub)
Time (sec)
Engine Speed
EGR Valve Position
Fuel Injection Amount
VGT Position

(a)

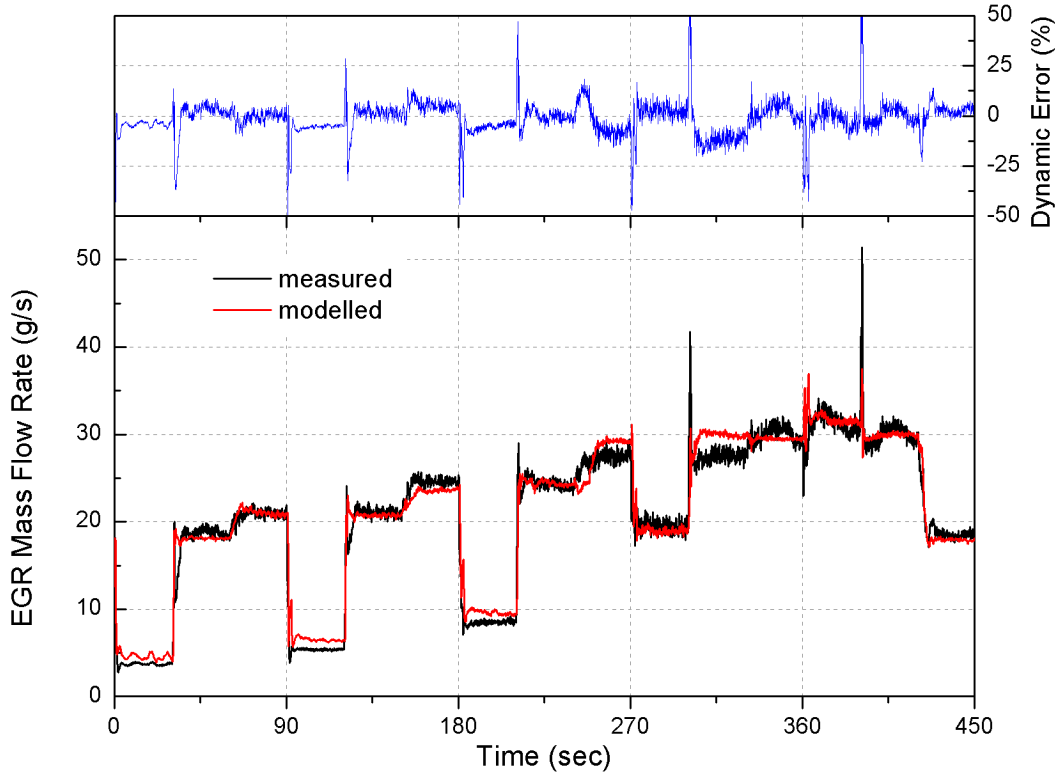
Dynamic Error (%)
EGR Mass Flow Rate (g/s)
measured
modelled
Time (sec)

(b)

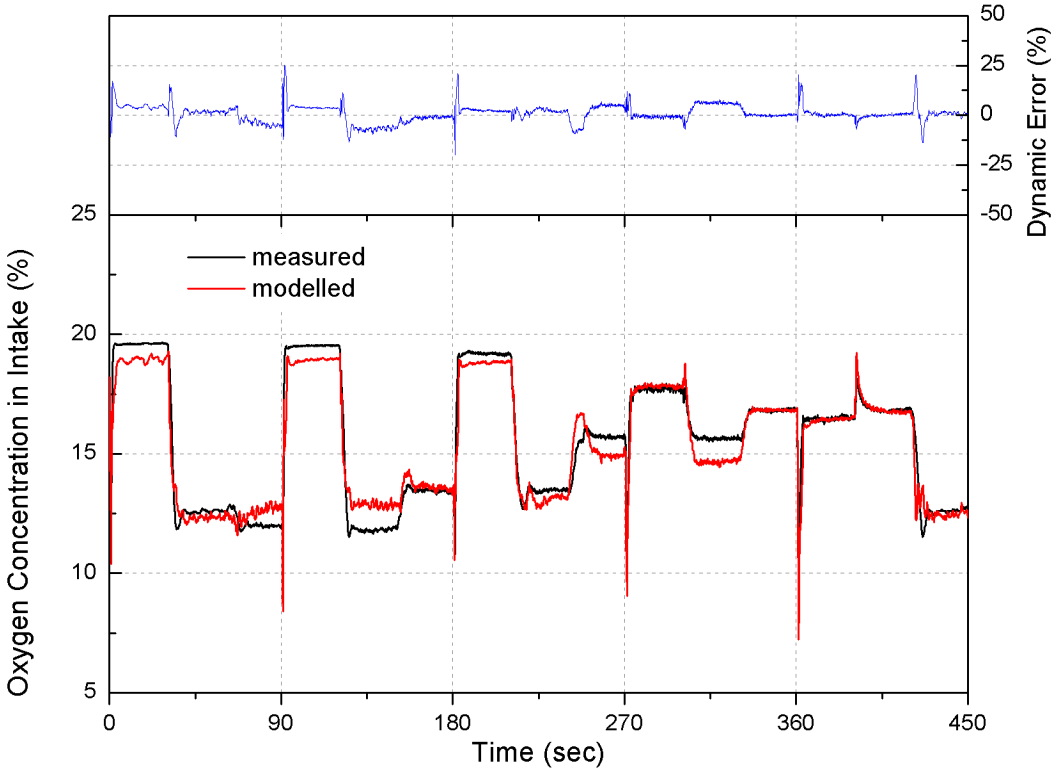

(c)

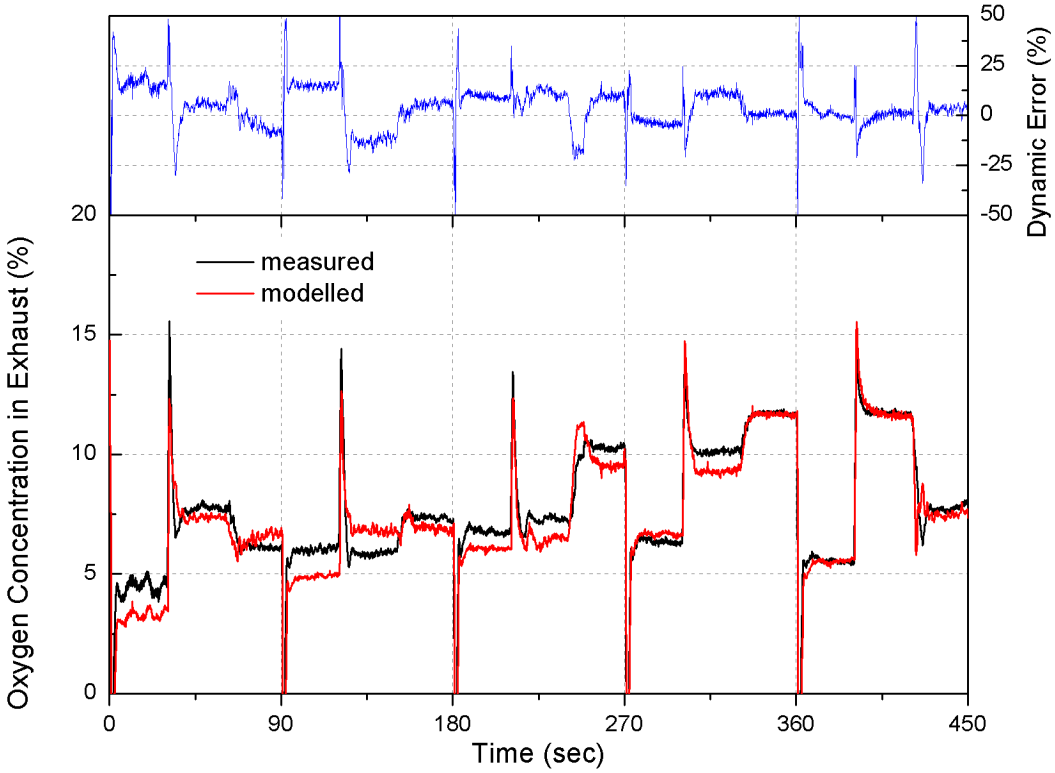

(d)

Figure 6-16 Comparison of Simulation Results and Measurement Data during Load Change between 20% and 45%; (a) Model Inputs; (b) EGR Mass Flow; (c) Oxygen Concentration in Intake; (d) Oxygen Concentration in Exhaust

In order to evaluate the dynamic simulation results more quantitatively, the model fit is defined as (Mathworks 2014):

$$fit = \left[1 - \frac{\|y - \hat{y}\|}{\|y - \bar{y}\|}\right] \times 100 \qquad \textbf{Equation 6-26}$$

Where y is the measured output; $\hat{y}$ is the simulated model output; $\bar{y}$ is the mean of the measured data sequence and '$\| \ \|$' represents the Euclidean distance.

Table 6-2 Model Fit of EGR Mass Flow Rate and Oxygen Concentration

	EGR mass flow rate	O_2 concentration in intake	O_2 concentration in exhaust
Load 20% - 35%	80.5	72.7	67.9
Load 20% - 45%	79.4	74.1	66.3

As shown in Table 6-2, the simulation is more accurate at tests of load between 20% and 45%. Since the intake air flow is larger at higher load, the influence of error from the EGR valve at a low position, as mentioned above, is reduced.

6.3.2 IMEP and Maximum In-cylinder Temperature

Compared with the air path, engine combustion has much a faster response in transient conditions and is mainly determined by the fuel injection amount. As a result, it is easier to simulate the related parameters such as IMEP and in-cylinder temperature. The comparison of measurement and simulation is presented in Figure 6-17. It is clearly shown that the simulation value of the IMEP has a good correlation with the measured data in most cases. The model fit of the IMEP is 92.96. As for the in-cylinder temperature, due to the intrinsic

combustion instability, the measured data has apparent fluctuation both in transient and steady state which cannot be reflected in simulation. However for the control purpose, the quasi-static model has the capability to follow the trend and shows reasonable accuracy.

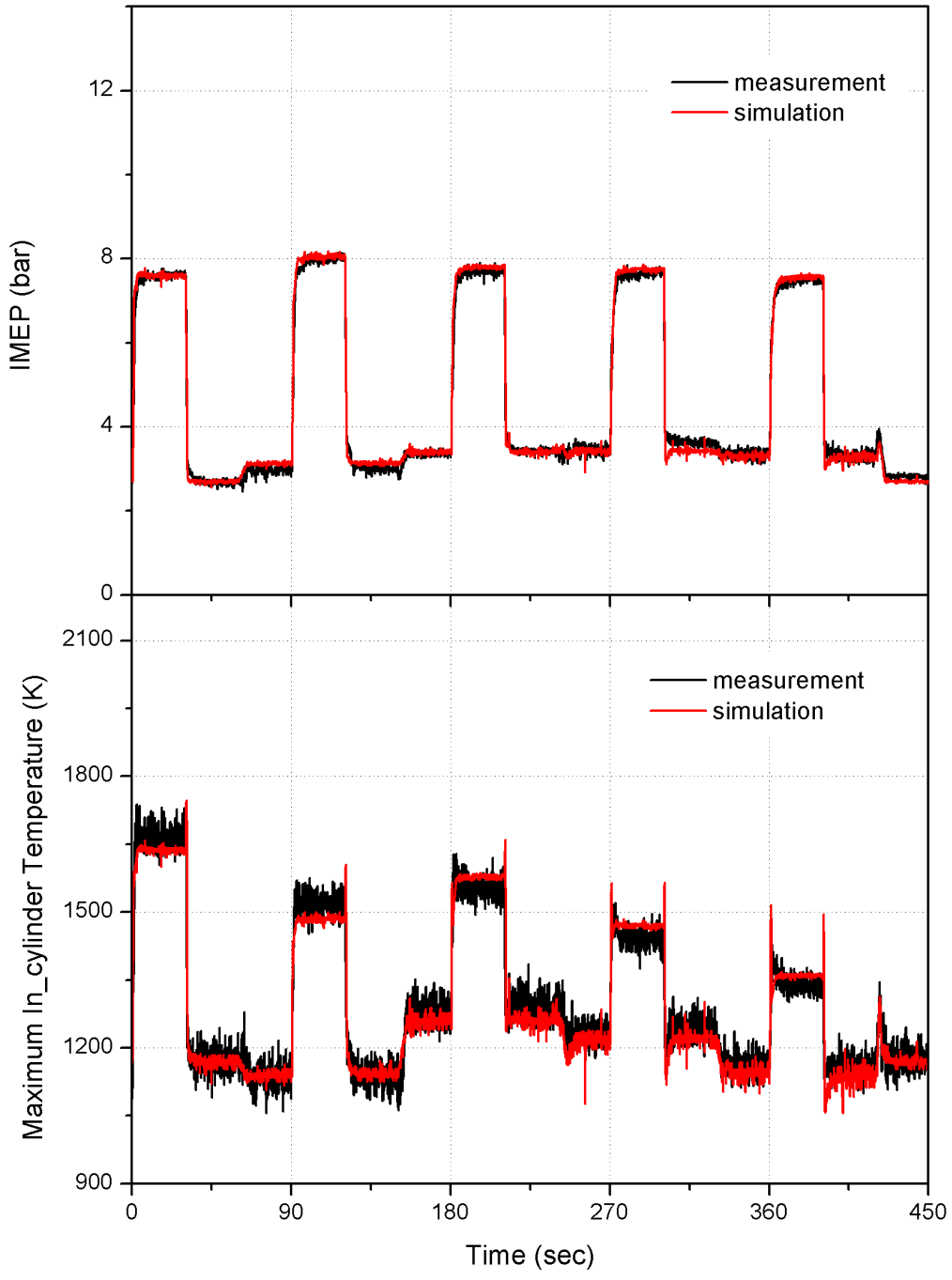

(a)

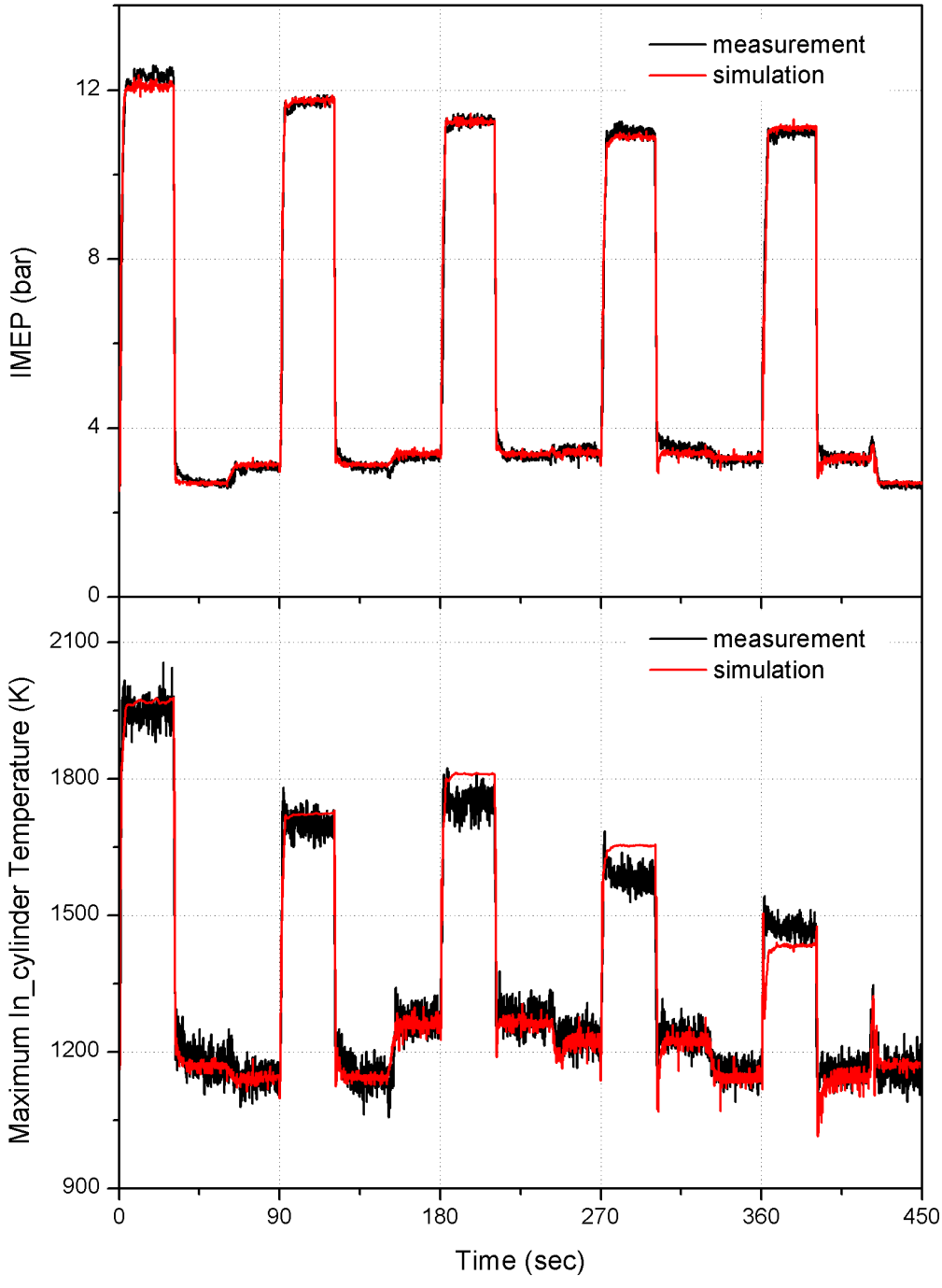

Figure 6-17 Comparison of Simulation and Experimental Data of the IMEP and Maximum in-cylinder Temperature; (a) Load Step between 20% and 35%; (b) Load Step between 20% and 45%

6.3.3 NOx and Particulate Matter

As introduced in Chapter 2, it is rather difficult to predict the emissions of an internal combustion engine, especially in transient operation. Deviation of simulation is always caused by many factors or detailed mechanisms which are not included in models. In this study, the objective is to develop a dynamic model with a mixed physics and statistics approach as a means to predict the relative influence of controllable variables such as an EGR valve and the VGT position. The simulation is based on the assumption that the emission formation depends, in a deterministic way, on the designated inputs such as in-cylinder temperature, oxygen concentration and equivalence ratio. Therefore, the trend change of the emissions is more important than the average value of the estimation in this modelling.

It should be noted that the functional structure of the emission model is derived with a nonlinear ARX approach. The data collected from different engine map settings is used for validation. Figures 6-18, 6-19 and 6-20 show the comparison between simulation results and measured data during load increase steps at different engine speeds. It is presented that the nonlinear ARX model approach can predict the NOx satisfactorily, based on the inputs of the experimental data. When the validated engine setting is changed, the simulation of NOx is capable of reflecting the basic trend during transients. However when the emission model is integrated with the combustion model, the deviation of NOx becomes larger. This is mainly due to the sensitivity of the NOx model to the oxygen concentration. One tiny error or delay of the oxygen concentration would have a huge impact on the prediction results of NOx. As for particulate number and particulate mass prediction, the model fit is slightly worse in the

simulation with the inputs of the measured data. As shown in Figure 6-17 (a), the small trough of the particulate number after the peak is not identified well in the nonlinear model. Accordingly, in the validation, the similar trend is not reflected in the particulate number prediction. However, it is observed that the results of the particulate matter simulation integrated with the combustion model are much better than those of NOx. In Figure 6-18 (b) and Figure 6-19 (b), the difference of the particulate number prediction between the engine model case and the measured inputs case is acceptable. It is highly possible that the PM model is identified with no detailed physical equation and the parameters are more nonlinearly constructed. Besides, the error from the emission model inputs such as oxygen concentration and in-cylinder temperature, which is simulated by the engine model, would inevitably increase the error of the emission prediction.

All in all, there shows a small deviation between the measured value and the prediction of the emissions with limited parameters and simple structure. However the main trends of the emission behaviour with a change of engine parameters can be reflected. The emission model is meaningful to act as a reference for actuator control and development of a control strategy.

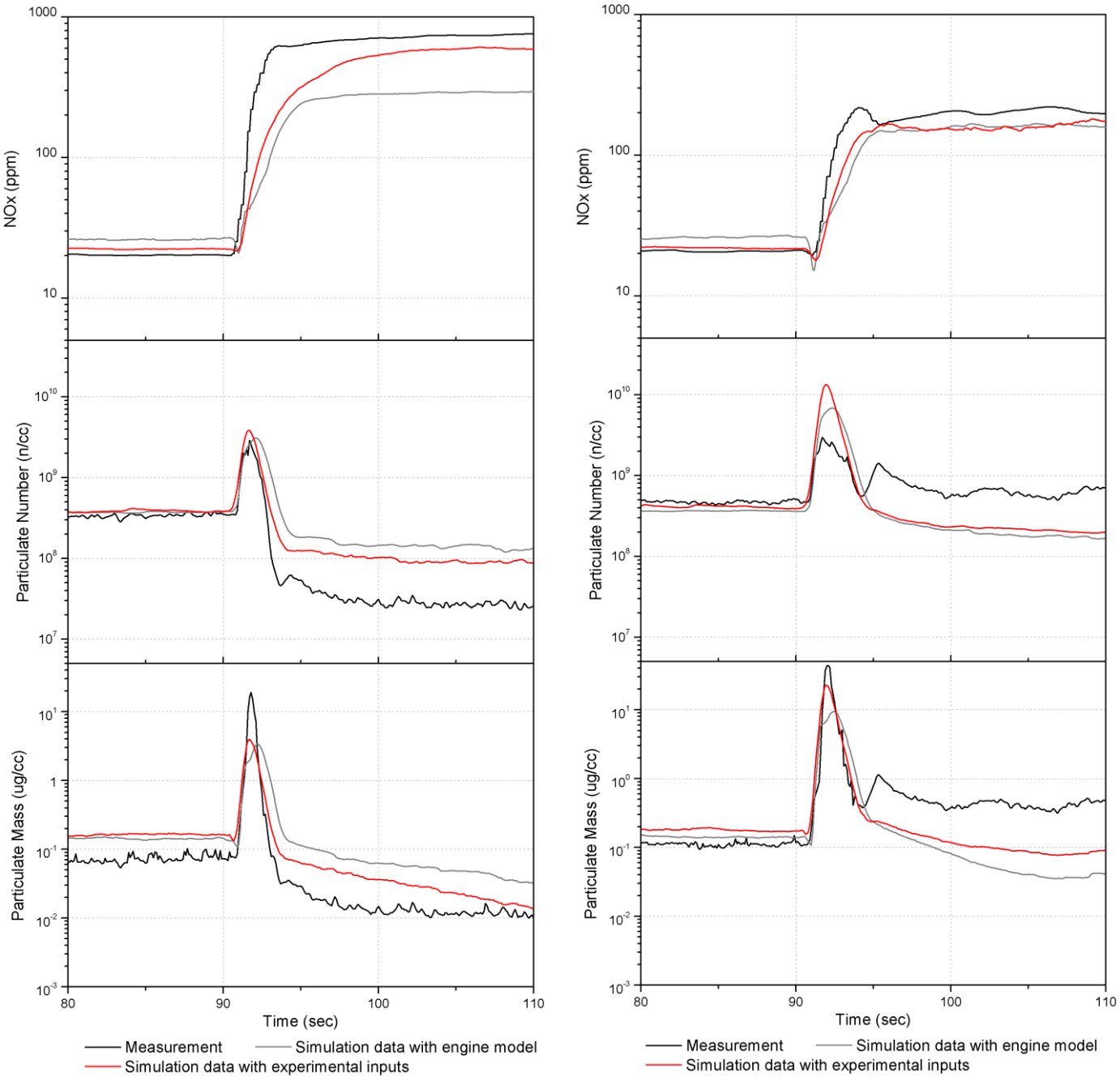

Figure 6-18 Comparison of Simulation and Experimental Data of NOx and Particulate Matter during a Load Increase from 25% to 45% at 1250 rpm; (a) Simulation based on Identification Data; (b) Validation

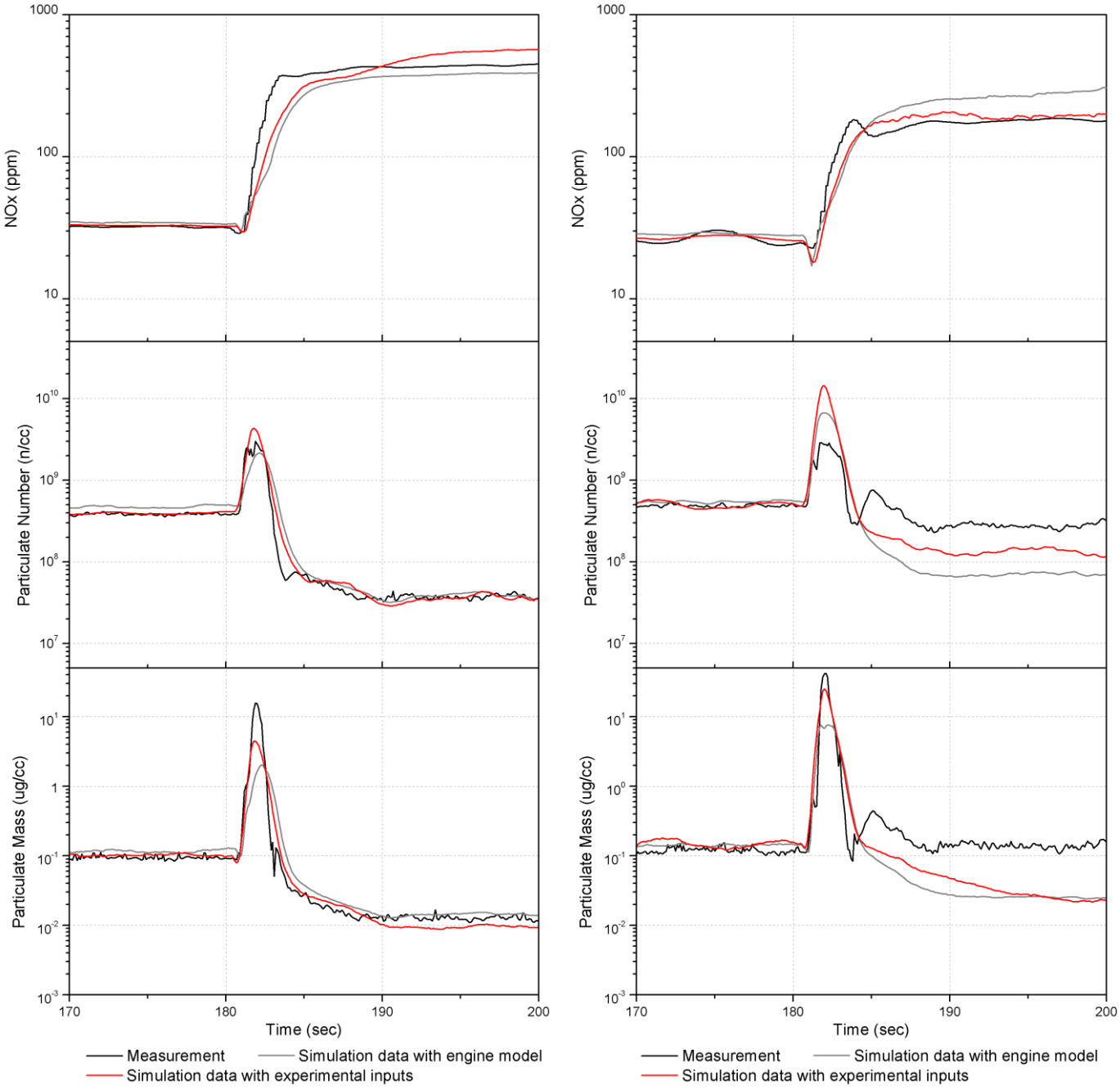

Figure 6-19 Comparison of Simulation and Experimental Data of NOx and Particulate Matter during a Load Increase from 25% to 45% at 1500 rpm; (a) Simulation based on Identification Data; (b) Validation

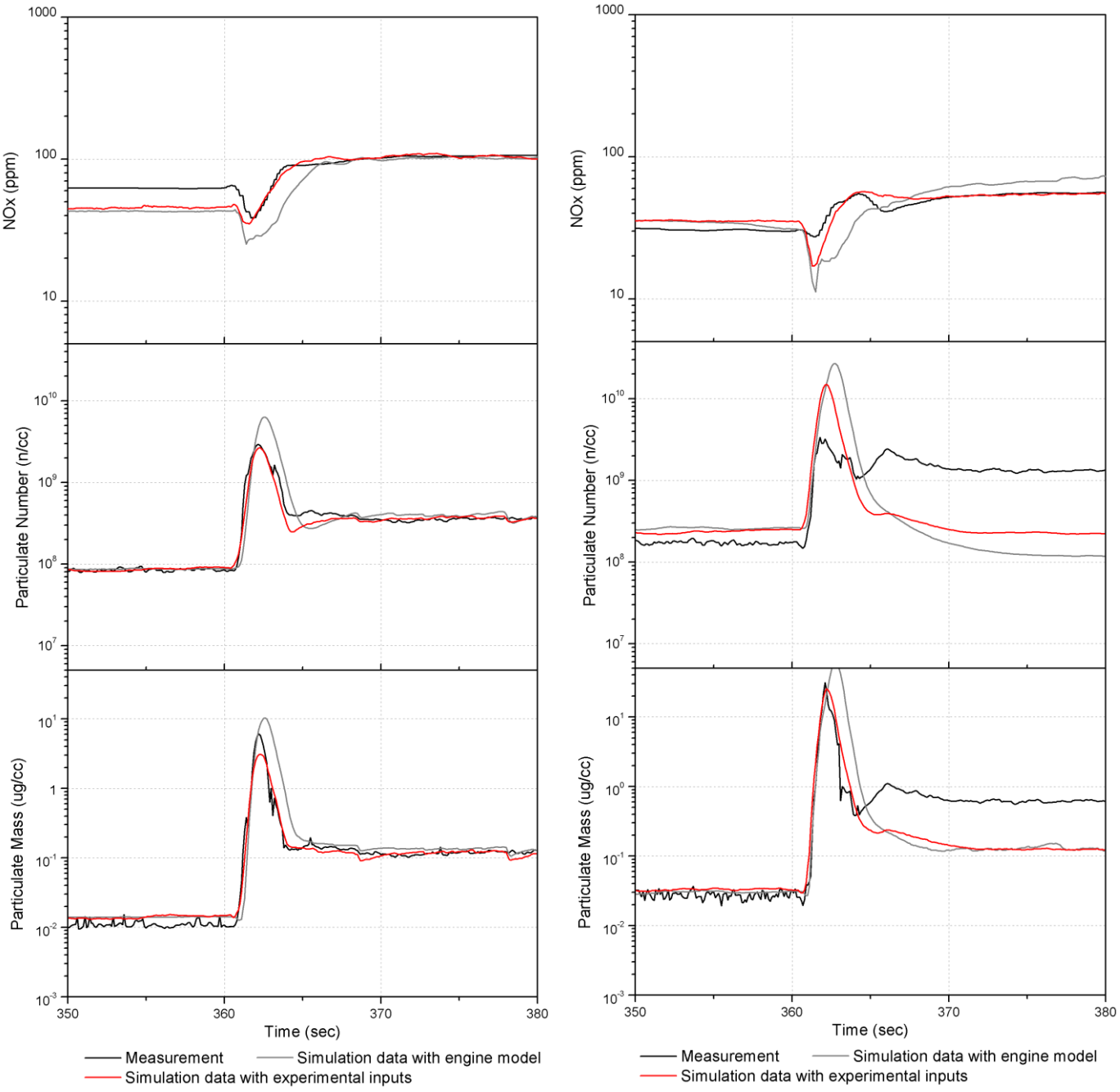

Figure 6-20 Comparison of Simulation and Experimental Data of NOx and Particulate Matter during a Load Increase from 25% to 45% at 2000 rpm; (a) Simulation based on Identification Data; (b) Validation

6.4 Summary

In order to implement the engine model-based control, it is necessary to develop a reliable and efficient model plant. In this chapter, the detailed modelling approaches for the air path, combustion and emission behaviour of a turbocharged diesel engine are introduced. The validation results of the engine modelling are also presented.

The developed model can simulate the main engine parameters such as the oxygen concentration, EGR mass flow, intake air mass flow, maximum in-cylinder temperature and IMEP. In addition, two important emissions of a diesel engine, NOx and particulate matter can be predicted with reasonable accuracy. In general, the model is capable of working as a simulator of an engine in both steady state and transient operation, reducing the experimental time and cost on real testing. Based on limited experimental data, the model can easily match different engines by updating the parameters and training the networks. Since the structure of the model follows the law of physics, the model can be implemented in the ECU for vehicle application.

The simulation results of engine parameters show a fair agreement with the experimental data. The fit of the EGR mass flow and oxygen concentration in the intake and in the exhaust during transient operation are 80%, 73% and 67% respectively. Also, the model is capable of capturing most peaks and troughs of the air path parameters during transients, reflecting the air dynamic characteristics properly. As for the dynamic emission model, the NOx and PM predictions present an acceptable accuracy. The main trends of the emission behaviour

following the change of engine parameters can be predicted. The emission model is capable of acting as a reference for the actuators' control strategy development.

CHAPTER 7

MODEL-BASED FAST PREDICTIVE CONTROL

This chapter presents an advanced fast predictive control approach applied on the air system of a turbocharged diesel engine. Oxygen concentration control on the EGR valve and VGT position, rather than conventional fresh air mass or EGR rate oriented control, is proposed and designed with the model predictive control approach. Also, a comparison of the MPC and conventional PID control strategies is conducted. Lastly, a new HIL simulation platform is described for testing and validating of the real-time engine model and MPC control strategy.

7.1 Introduction

Due to the highly nonlinear behaviour of a diesel engine air path and inter-coupled control parameters, conventional control strategies such as PID have difficulty to achieve precise control of the air management process. New control strategies such as predictive, neural and fuzzy control have been proposed concerning the issue (Arnold et al. 2006) (Langthaler & Re 2008) (Catania et al. 2011). However, there are still some limitations shown in the previous research such as poor robustness guarantees and a high requirement of parameters needing tuning, as mentioned in Chapter 2. Moreover, the traditional set-point variables used such as fresh air flow and EGR rate are subject to disturbances and uncertainty in light of their intrinsic measurement. In this study, an advanced model-based

predictive control approach based on oxygen concentration was developed and it was integrated with the dynamic engine model. The engine model was validated in Chapter 6 and it was able to reflect the nonlinear behaviour of dead zones, hysteresis and delays in a diesel engine air system. The reason for using MPC as the control strategy was its ease of input and output constraints treatment and its intrinsic suitability to cope with multivariable systems (Maciejowski 2001). In order to incorporate the MPC controller, local linear models were identified from the data generated by the dynamic nonlinear engine model. It was proved that a number of linear models were able to cover the whole operating range of the nonlinear system (Ortner et al. 2006). The block diagram of the model-based predictive control strategy is presented in Figure 7-1.

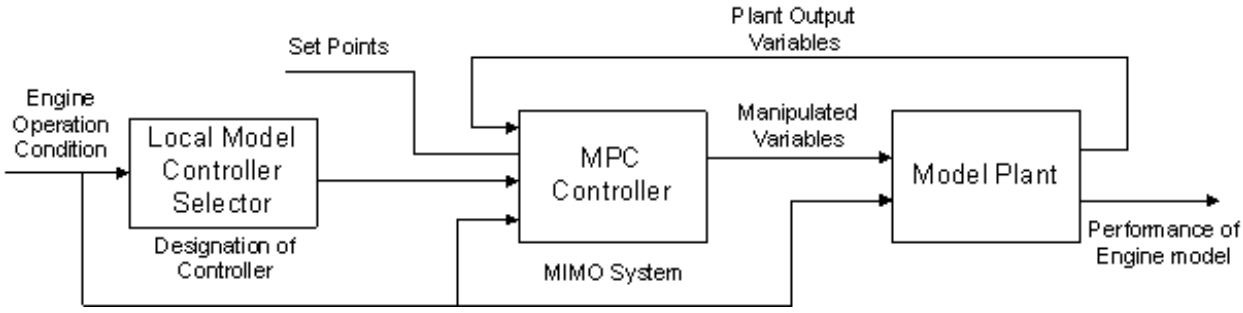

Figure 7-1 The Block Diagram of the Engine Model-based Predictive Control Strategy

As shown in Figure 7-1, the engine operation condition determines the local linear model and designed controller. The MPC controller is a Multi-Input Multi-Output (MIMO) system, which processes the reference values and plant output variables then produces the manipulated variables. The reference values are set points of the target parameters required for the control strategy. The model plant is the engine model and integrated dynamic emission model for estimating the performance. The whole control system could

be operated in real time with a microprocessor on a HIL simulation platform. Details of the control strategy implementation and control results are presented in the following sections.

7.2 Model-based Control Design

The model plant linearization and implementation of the control strategy on a diesel engine are presented in this section.

7.2.1 Model Plant Linearization

The air path of a turbocharged diesel engine is a highly nonlinear system and the engine model developed with physical insight is far too complicated to operate and be embedded online for predictive control schemes. It is essential to acquire simplified mathematical models which can provide acceptable accuracy and reduce the computational efforts in order to process systems with fast dynamics. Since the MPC relies on linear models as the model plant, the approach of multiple local linear models has been used. The idea is based on using a set of local linear models to accommodate local operating regimes (Camacho and Bordons 2005). This method was proved capable of reproducing the main dynamics of nonlinear plant from experiments (Garcia-Ortiz, Langthaler, and Del Re 2006). In this study, different regimes of the engine operating conditions are defined based on the engine speed and fuel injection; for each regime a local linear state-space model was developed. The engine speed and amount of fuel injection are two parameters widely used in engine calibration for the inputs of the look-up table to define the operation mode. Also, the

output constraint in the controller can be easily referred according to the setting of the previous calibration for each operation point; since the state-of-the-art calibration in a steady state can provide fine set-points on a manipulated variable. The representative operation points for defining each local linear model are listed in Table 7-1.

Table 7-1 Representative Operation Points for Local Linear Models

Point	Engine Speed (rpm)	Fuel Injection Amount (mg/hub)
1	1000	6.5
2	1000	21
3	1250	7.5
4	1250	20
5	1500	8
6	1500	20
7	1500	30
8	1750	8
9	1750	20
10	1750	30
11	2000	20
12	2000	31

In order to generate the data for local linear models, the air system model introduced in Chapter 6 was employed. Compared with the conventional method in which the linear identification is based on measured experimental data, linearizing the nonlinear engine model plant locally provides more flexibility, reduces the risk of damaging the engine and lowers the experimental costs. The process of system identification would cause a small deviation by its very nature, but the designed closed-loop control can eliminate the error. Accordingly, the small deviation of the simulated value from the model plant and the

experimental data is acceptable; this will be presented and explained in the following sections. The input spaces of the state-space model are u and w and the output is y, as shown below:

$$u = [u_{EGR} \quad u_{VGT}]^T \qquad w = [\omega_e \quad m_\varphi]^T$$

$$y = [O_{2i} \quad p_i]^T \qquad \textbf{Equation 7-1}$$

Where u represents the manipulated variables; u_{EGR} and u_{VGT} are defined as EGR valve position and VGT position in %; while w indicates the measured disturbance where ω_e and m_φ are defined as the engine speed and fuel injected amount; O_{2i} and p_i represent oxygen concentration in the intake manifold and intake pressure respectively. As discussed in Chapter 6, the EGR valve and VGT valve positions were the essential control variables in the air path of the diesel engine. Due to the direct and significant influence on engine combustion and emission characteristics, oxygen concentration was used as one of the outputs which could be measured locally and accurately during engine transients, compared to the conventional parameter, EGR ratio or fresh air mass.

The structure of the model plant is shown in Figure 7-2. The engine speed and fuel injection quantity are set as constant, added to some small normally distributed random numbers, determining the operation point. To simulate the step change of the valve positions, random noise is added into inputs which have a reasonable range based on the experimental data. It should be noted that although the engine model is developed considering the intrinsic dynamic characteristics of the actuators, there are differences between the actual position and the desired value which derive from the band-limited white

noise component. In order to make the linear model more realistic, inputs such as EGR valve position and VGT position are processed by a rate limiter to reflect the actual positions relative to time, which are physically achievable by the valves; they were obtained from the experimental data.

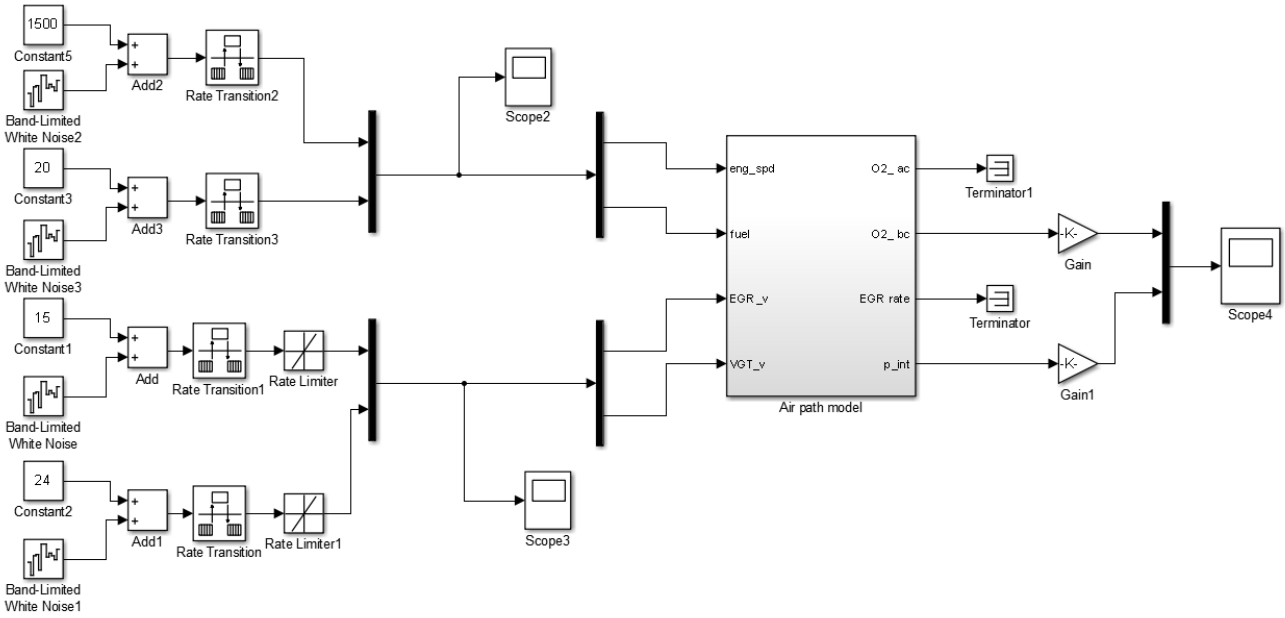

Figure 7-2 Structure of Model Plant for Identification of Local Linear Models

The linear models are obtained by system identification with prediction error minimization (PEM) method (Ljung 1999). The identified model is a discrete-time state-space model with the form:

$$x(t+Ts) = Ax(t) + Bu(t) + Kw(t)$$

$$y(t) = Cx(t) \qquad \textbf{Equation 7-2}$$

Where $x(t)$ is the state identified for the model plant; Ts is the sample time; A, B, K and C are the matrix estimated. In this study, the sample time is set as 0.1 second considering the data frequency of model plant. The order of each state-space model is picked from the

required accuracy in the range of 1 to 10 in each case after estimation. Considering the large time constant of the engine air path system, forward and backward prediction horizons are tuned in order to capture the main dynamic characteristics and maintain stability during steady state (Ljung 2014).

As shown in Figure 7-3, the state-space model identified is able to reflect the main trend of outputs with a maximum deviation of 6.2% after step change; as a result, the state-space model can be used as prediction model for the model-based control.

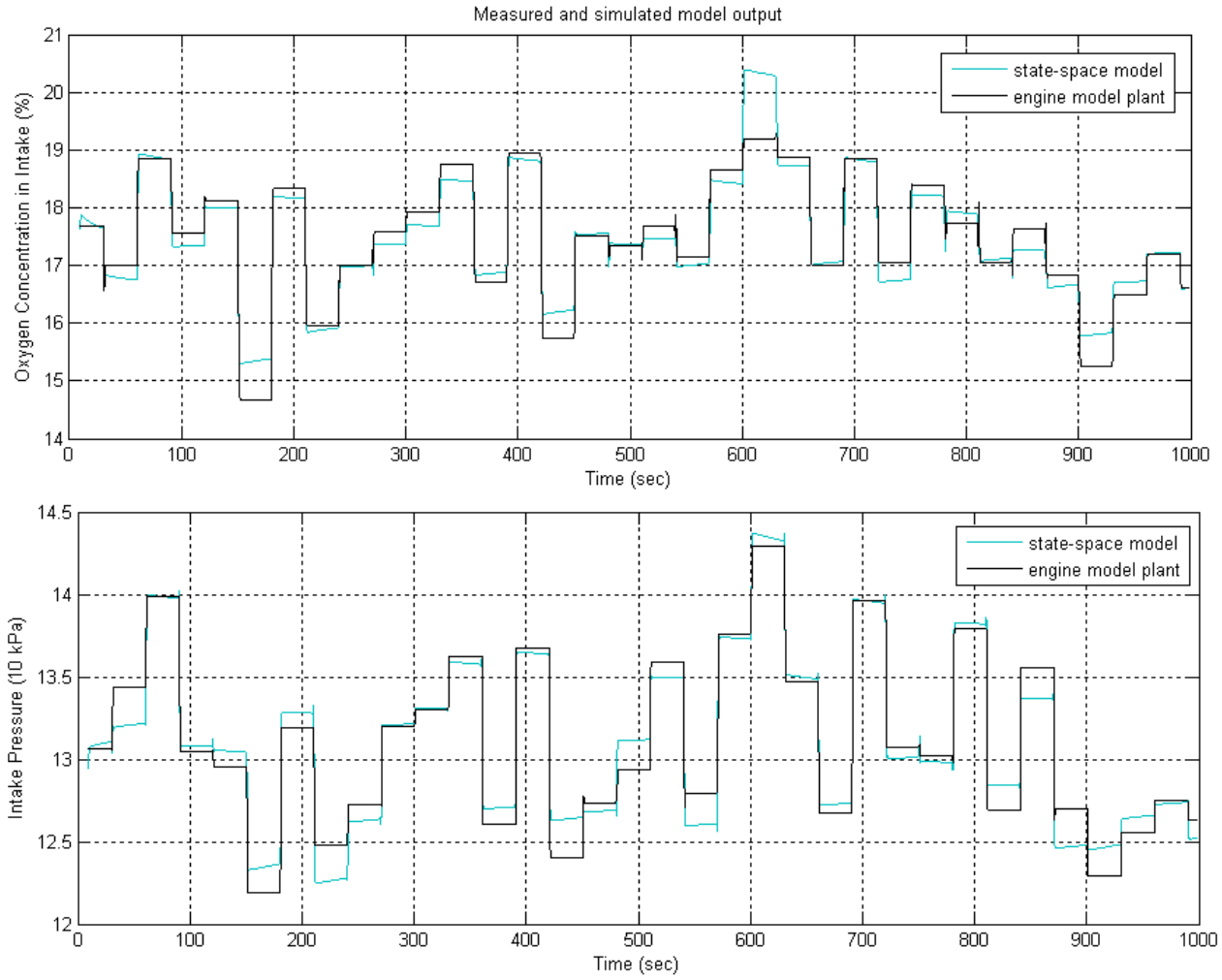

Figure 7-3 Validation of State-space Model

7.2.2 Implementation on a Diesel Engine Air System

MPC is employed in this study to optimize the control of engine transient behaviour due to its advantage in dealing with MIMO control; especially when the system has a large time constant. Basically, MPC solves an optimization problem through using a specific model to predict the future response of the process and determining the manipulated variables at each control interval. To clarify, the principle of MPC is illustrated for an SISO system in Figure 7-4. Three steps are summarized for this process:

1. **Formulation of reference trajectory**

   In order to allow an attenuation of the error, a reference trajectory y_{ref} is calculated based on measured output and set point y_{sp}. The y_{ref} is formed as a first-order exponential trajectory by default.

2. **Calculation of prediction trajectory**

   The output prediction y_p on a horizon T_p is obtained from inputs and measured outputs based on the model in the controller.

3. **Setting of input trajectory**

   The input trajectory on a horizon T_c is set using optimization calculation to achieve as close a match as possible between the reference and output prediction. The first element of the input trajectory is applied in the next control interval.

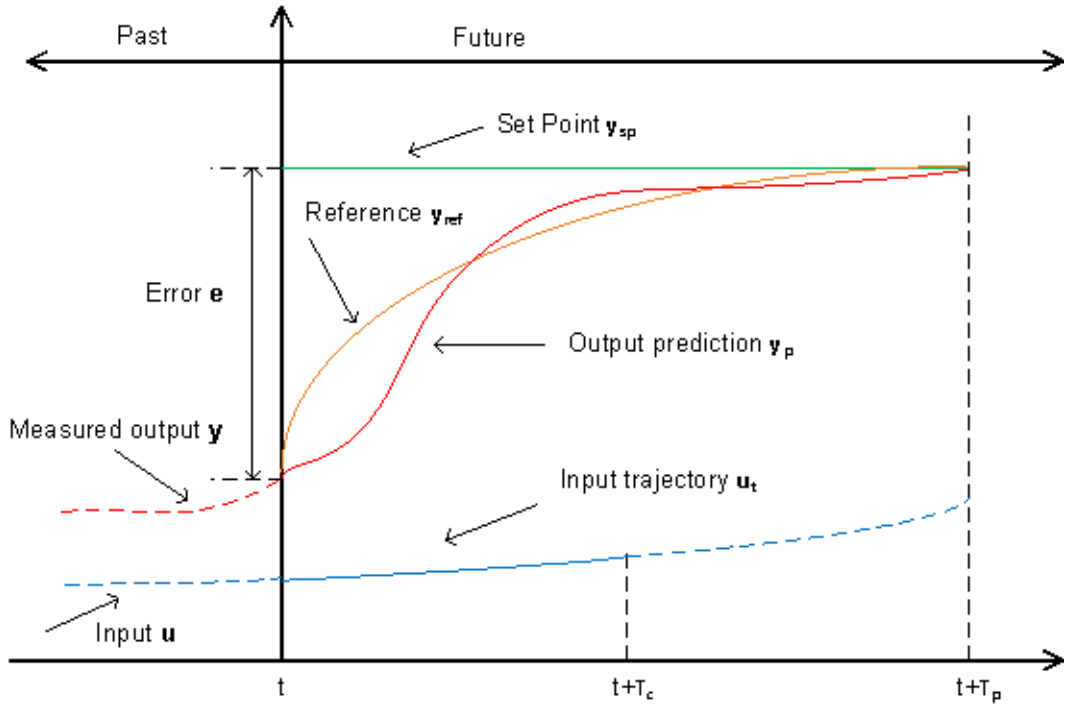

Figure 7-4 Principle of MPC

The objective of an optimization problem is usually represented as a cost function: (Bemporad, Morari, and Ricker 2014)

$$J(z_k) = J_y(z_k) + J_u(z_k) + J_{\Delta u}(z_k) + J_\varepsilon(z_k) \qquad \textbf{Equation 7-3}$$

Where z_k is the optimization problem decision, given by:

$$z_k^T = [u(k|k)^T \quad u(k+1|k)^T \quad \cdots \quad u(k+p-1|k)^T \quad \varepsilon_k] \qquad \textbf{Equation 7-4}$$

The denotation of each term in $J(z_k)$ is listed below, respectively.

$J_y(\cdot)$ is the cost function for output reference tracking:

$$J_y(z_k) = \sum_{j=1}^{n_y} \sum_{i=1}^{p} \left\{ \frac{w_{i,j}^y}{s_j^y} \left[r_j(k+i|k) - y_j(k+i|k) \right] \right\}^2 \qquad \textbf{Equation 7-5}$$

Where k is the current control interval; p is the prediction horizon; n_y is the number of plant output variables; $y_j(k+i|k)$ and $r_j(k+i|k)$ denote the predicted value and reference value of j th plant output at i th prediction horizon step; s_j^y is the scale factor for j th plant output and $w_{i,j}^y$ is the tuning weight for j th plant output at i th prediction horizon step.

$J_u(\cdot)$ is the cost function for manipulated variable tracking:

$$J_u(z_k) = \sum_{j=1}^{n_u} \sum_{i=1}^{p-1} \left\{ \frac{w_{i,j}^u}{s_j^u} \left[u_j(k+i|k) - u_{j,\ target}(k+i|k) \right] \right\}^2 \qquad \textbf{Equation 7-6}$$

Where n_u is the number of manipulated variables; $u_{j,\ target}(k+i|k)$ is the target value for j th manipulated variables at i th prediction horizon step. In some applications, the controller is ordered to keep selected manipulated variables near specified target values.

$J_{\Delta u}(\cdot)$ is the cost function for manipulated variable move suppression:

$$J_{\Delta u}(z_k) = \sum_{j=1}^{n_u} \sum_{i=1}^{p-1} \left\{ \frac{w_{i,j}^{\Delta u}}{s_j^u} \left[u_j(k+i|k) - u_j(k+i-1|k) \right] \right\}^2 \qquad \textbf{Equation 7-7}$$

This function is to measure the performance of manipulated variable moves so that small variable adjustments can be achieved.

$J_\varepsilon(\cdot)$ is the cost function for constraint violation:

$$J_\varepsilon(z_k) = \rho_\varepsilon \varepsilon_k^2 \qquad \textbf{Equation 7-8}$$

Where ε_k denotes a slack variable, defined as quantifying the worst case constraint violation, at control interval k; ρ_ε is the constraint violation penalty weight. Constraint violations occur in some application. $J_\varepsilon(\cdot)$ is employed to measure the corresponding performance.

The model used for prediction in MPC is a state-space model and it is assumed that the state $x(t)$ is available at the current time t. The optimization generates an optimal control sequence and the value in this sequence is applied to the process. In order to solve the optimization problem, the cost function equation above is converted to the form: (Rawlings 1999)

$$\min_{U=\{u_1,\cdots u_{1+N_u-1}\}} \{J(U,x(t)) = x'_{t+n_y|t} Px_{t+n_y|t} + \sum_{k=0}^{N_y-1}[x'_{t+k|t} Qx_{t+k|t} + u'_{t+k|t} Ru_{t+k|t}]\}$$

Equation 7-9

$$\begin{aligned}
& u_{\min} \le u_{t+k} \le u_{\max}, && k = 0,\ldots,N_u - 1 \\
& x_{t|t} = x(t), && \\
\text{s.t.} \quad & x_{t+k+1|k} = Ax_{t+k|t} + Bu_{t+k} + K\omega_{t+k}, && k \ge 0, \\
& y_{t+k+1|k} = Cx_{t+k|t}, && k \ge 0, \\
& u_{t+k} = L(x_{t+k|t}), && n_u \le k \le n_y,
\end{aligned}$$

Where the column vector $U \overset{\Delta}{=} \left[u'_t,\ldots u'_{t+N_u-1}\right]$; $x_{t+k|t}$ represents the predicted state vector at time t+k, obtained by applying the input space $u_t,\ldots u_{t+k-1}$ to the model; N_u and N_y are the control and prediction horizon, respectively; the matrixes Q and R denote the weighting on state and input; P and L are the terminal constraint and the control function.

In this study, the manipulated variables are the EGR and the VGT position; while the measured disturbances are engine speed and fuel injected amount. As introduced above, these four parameters compose the inputs of the prediction model in MPC. The set points for the controller are oxygen concentration and intake pressure. The specific structure of the MPC controller is illustrated in Figure 7-5.

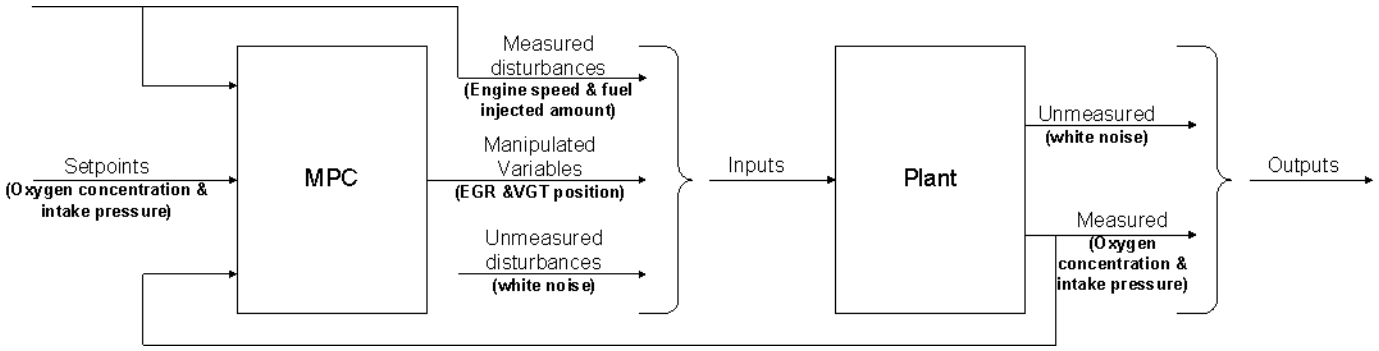

Figure 7-5 Structure of MPC Controller for Diesel Engine Air Path

The control interval is set as 0.1 seconds according to the model plant. The major tuneable parameters in this case are the prediction horizon, control horizon and output weights. In each operation mode, these parameters require cooperated tuning based on the local model and constraints. It should be noted that although increasing the weight of an output can achieve a faster response of the output tracking, an excessively large weight would result in instability and fluctuation due to the dynamic characteristics of the model. Fine tuning of the controllers is applied to the engine model plant in order to obtain a fast response of the outputs with little overshoot, avoiding unstable behaviour because of the nonlinear nature of the system.

7.3 Comparison of Control Strategies

The detailed results and discussion of model-based control application on the air path of a diesel engine are presented in this section. For comparison, conventional gain-scheduled PID control is employed as reference. Also, EGR rate oriented control is presented and compared with novel oxygen concentration oriented control.

7.3.1 Comparison between MPC and PID Control

In order to compare the performance of the novel MPC control strategy and conventional PID control, the results of representative cases are presented below. For PID control, two separate controllers are used to feedback the control oxygen concentration and intake pressure individually. For fair comparison, in each case, the PID controllers are well tuned to minimize the response time with little fluctuation. The system control tuner in MATLAB/Simulink was used for the tuning and the anti-windup method is employed to improve the stability.

In Figure 7-6, the performance of two control strategies is compared in a change of oxygen concentration where the intake pressure is fixed at the operation point of engine speed as 1500 rpm and fuel injected amount as 20 mg/hub. To evaluate the two control strategies, three key parameters, overshoot, response time and settling time are used and listed in Table 7-2. It is observed that for the MPC case, the value of oxygen concentration changes rapidly to follow the reference; the response time is 0.5 seconds. In comparison, the PID control makes a little overshoot but the response time is 1.3 seconds, far slower than that in

the MPC. Additionally, the overshoot for the MPC case is 9.4%, which is bigger compared with the PID but it is acceptable considering the emission results. As for the settling time, these two control strategies show little difference. Accordingly, the MPC presents better behaviour of tracking the set points of the oxygen concentration compared with the PID control.

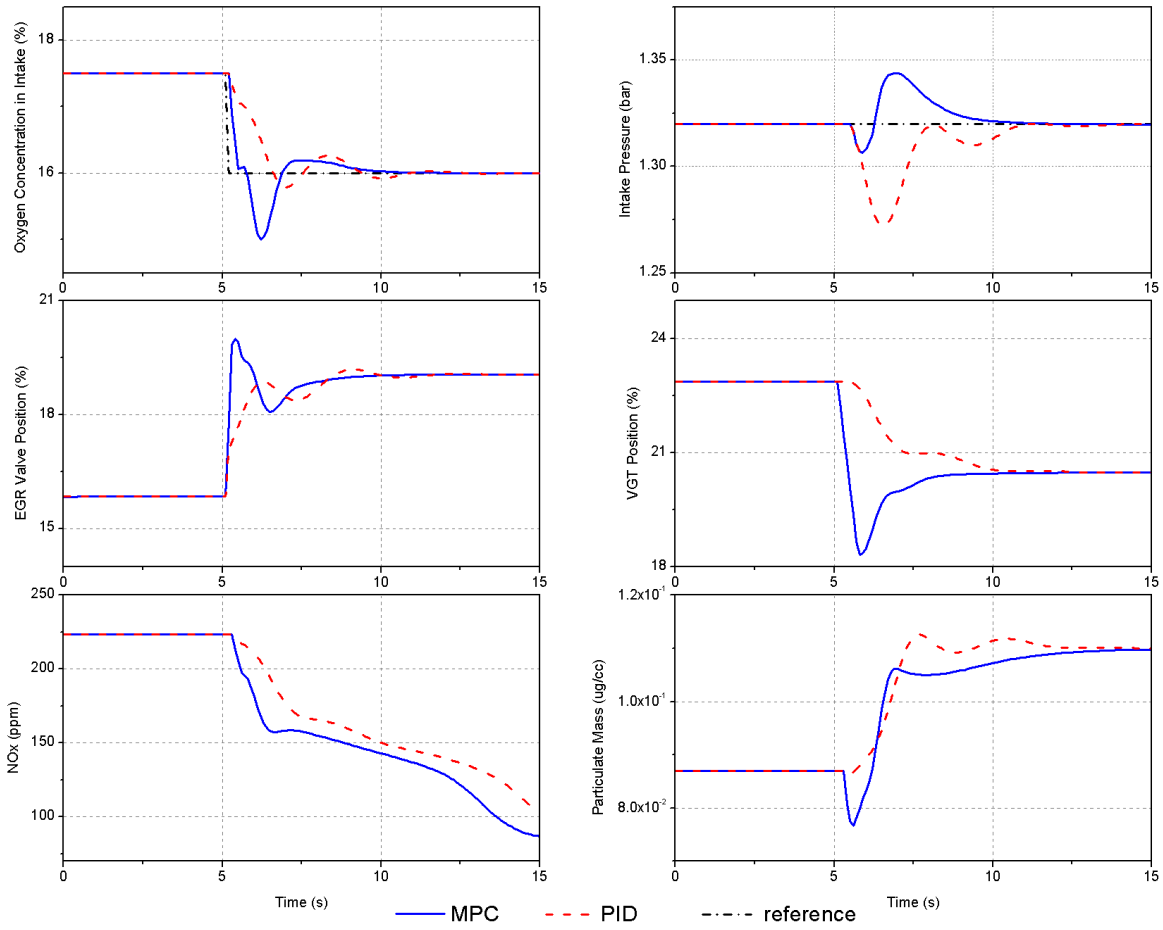

Figure 7-6 Comparison of MPC and PID - Step in Oxygen Concentration and Constant Intake Pressure @1500 rpm, 20 mg/hub

Table 7-2 Optimum Achievable Control Characteristics by Different Control Strategies for a Step Change in Oxygen Concentration

	MPC O2	PID O2	MPC p	PID p
Overshoot (%)	9.4	1.3	1.8	3.6
Response time (s)	0.5	1.6	1.3	3.1
Settling time (s)	4.1	4.9	4.4	5.5

Furthermore, as shown in the actuator's profiles (EGR valve position and VGT position), the EGR valve in the MPC closes steadily at the step change while in PID control, it has a softer change. More importantly, for the MPC, the VGT position adjusts immediately when the reference value changes while the position in PID control has an obvious delay. The difference largely determines the performance of the intake pressure, which shows an opposite change. This can be explained by the intrinsic nature of the two control strategies. Due to the model in the controller, the MPC is able to adjust the coupling parameters and compensate for the oxygen concentration demand through both the EGR valve and VGT position. However, the VGT position is close-loop controlled by the intake pressure individually in PID control. As a result, the move of VGT lags behind the variation of the EGR valve, maintaining the intake pressure. The emission characteristics, NOx and particulate mass are simulated based on the dynamic emission model introduced in the previous chapter. It is observed that both NOx and PM have a lower value in the MPC case compared with the PID. The faster decrease of oxygen concentration before combustion contributes to the lower value of NOx. Similarly, the PM emissions in the MPC benefit from the stable intake pressure and the corresponding larger intake air amount.

The profiles of two control strategies at a constant oxygen concentration and step in the intake pressure at an operation point of engine speed as 1250 rpm and fuel injected amount as 20 mg/hub are presented in Figure 7-7. It is shown that the response time of the intake pressure in the MPC is apparently shorter than that in the PID in this case. Meanwhile, the apparent overshoot of oxygen concentration is observed. Similar to the last case, the overshoot of oxygen concentration in the MPC is larger than that in the PID, of up to 5.2%. This is mainly caused by the aggressive behaviour of the VGT position as shown. Also, the opposite trend of the oxygen concentration is observed due to a similar reason as explained in the previous case. Interestingly, it can be noticed that the NOx and PM emissions in the MPC are largely decreased compared with the PID control; this is mainly derived from the fast response of the intake pressure. Although the emission data is obtained from the dynamic emission model, it shows great potential for solving the trade-off between NOx and PM during engine transient operation by applying MPC.

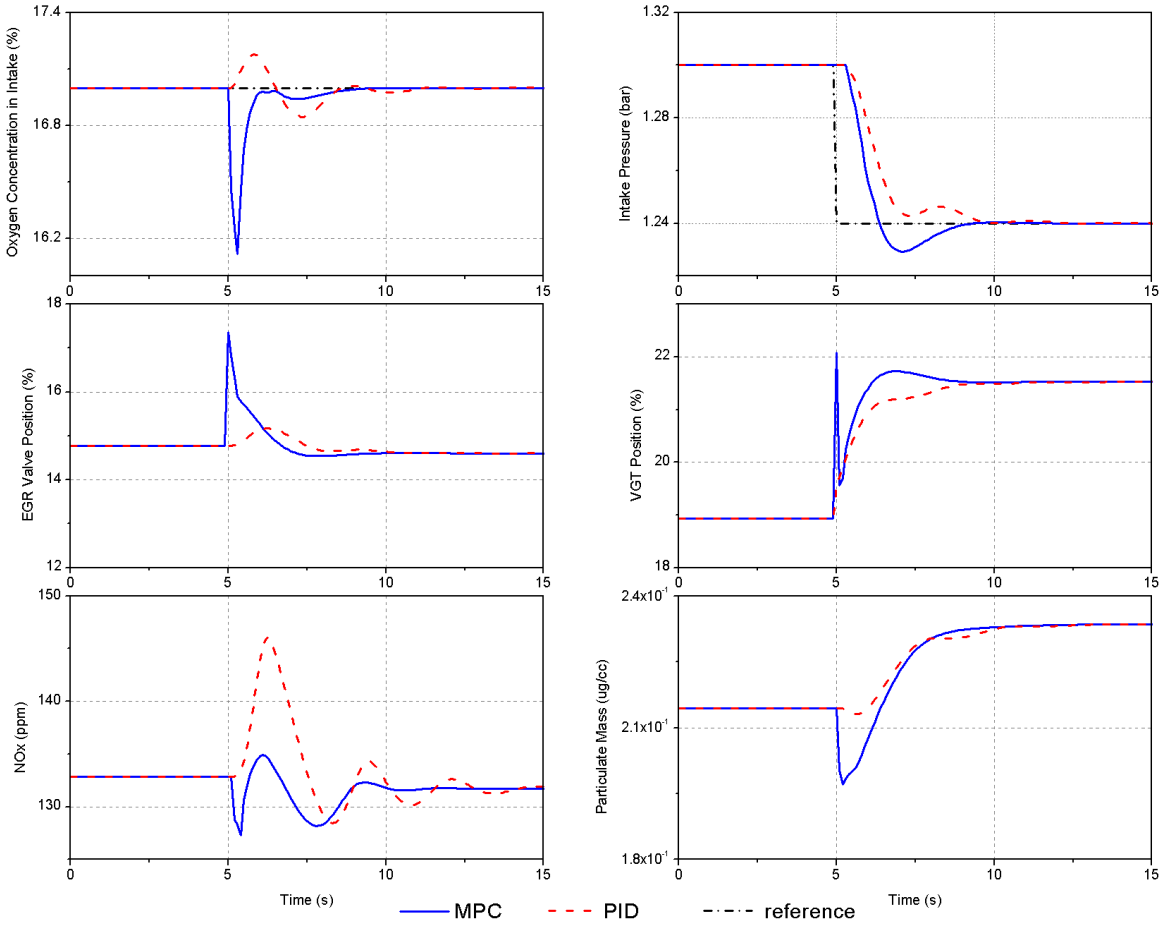

Figure 7-7 Comparison of MPC and PID - Step in Intake Pressure and Constant Oxygen Concentration @1250 rpm, 20 mg/hub

Table 7-3 Optimum Achievable Control Characteristics by Different Control Strategies for a Step Change in Intake Pressure

	MPC O2	PID O2	MPC p	PID p
Overshoot (%)	5.2	1.1	0.9	0
Response time (s)	1.1	1.5	1.4	4.6
Settling time (s)	1.0	3.8	3.6	4.2

The simultaneous step of oxygen concentration and intake pressure is tested in both control strategies and shown in Figure 7-8. For the oxygen concentration tracking, the MPC shows a

faster response, 0.3 seconds, with little overshoot compared with PID control. Meanwhile, the intake pressure value has a small difference between the two control strategies. The relatively slow response of the MPC in the intake pressure derives from the higher output weight of oxygen concentration tuned in the controller. In order to achieve a fast response of oxygen concentration and avoid high NOx emissions, the VGT position in the MPC has a small drop in the beginning to boost the EGR mass flow growth.

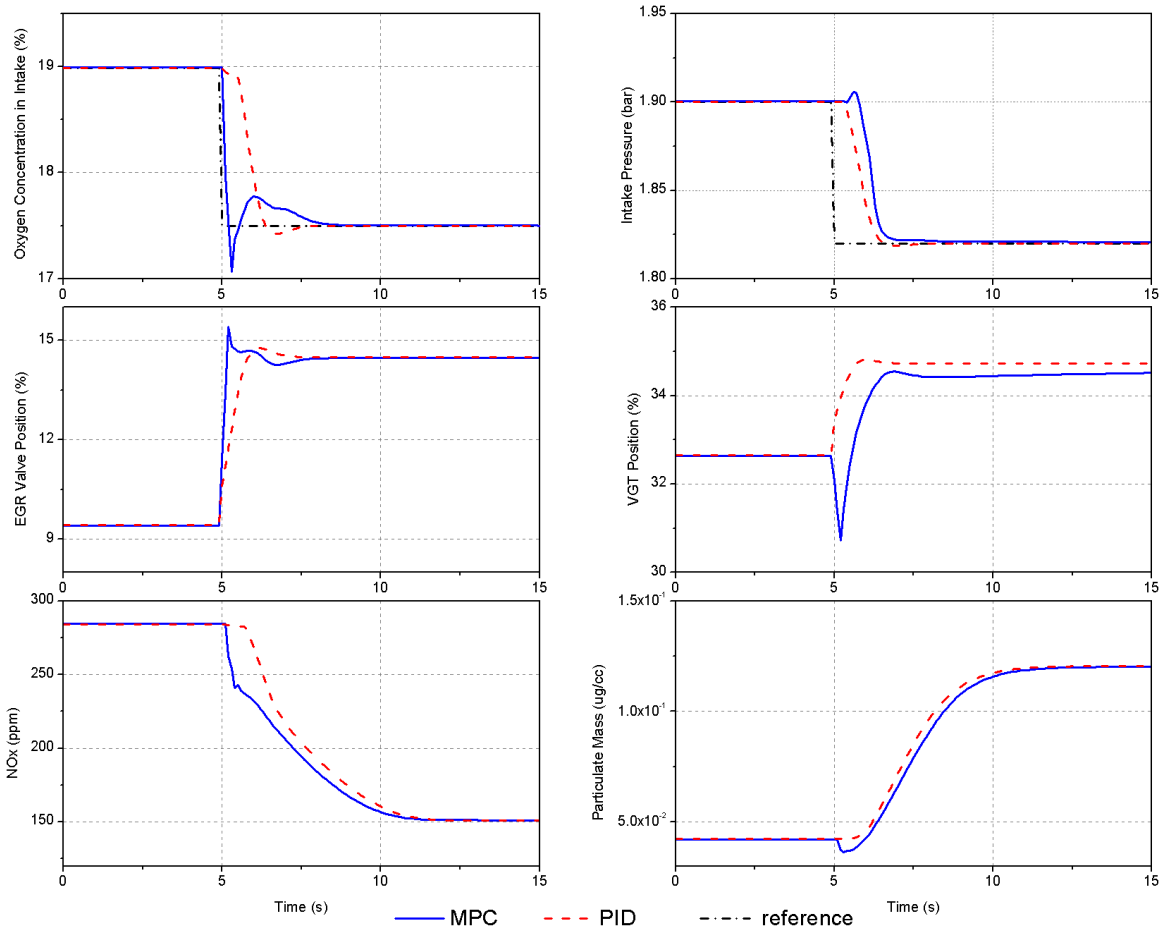

Figure 7-8 Comparison of MPC and PID - Step in Oxygen Concentration and Intake Pressure @2000 rpm, 31 mg/hub

Table 7-4 Optimum Achievable Control Characteristics by Different Control Strategies for a Step Change in Oxygen Concentration and Intake Pressure

	MPC O2	PID O2	MPC p	PID p
Overshoot (%)	2.5	0.4	0	0.1
Response time (s)	0.3	1.4	1.8	1.6
Settling time (s)	2.8	1.8	1.6	1.4

In general, MPC shows a better performance in dealing with the air path of a diesel engine compared with PID control. It could be found that the response time of the PID control is longer and fluctuation occurs when the tuning of the controller is marginally aggressive, as shown in Figure 7-8. In contrast, MPC is able to achieve and settle at the reference value faster at the expense of little overshoot. Also, the potential of MPC on emission control during transient conditions is found.

7.3.2 Comparison between Oxygen Concentration and EGR Rate Oriented Control

As discussed in Chapter 5, EGR rate and oxygen concentration have significant influence on transient engine performance. In theory, these two parameters are inter-related and both are able to control EGR valves. However, since the oxygen concentration can be measured accurately and locally by a lambda sensor with a short response time, it provides more information and has higher reliability during the transients. For the original setting, a gain-scheduled PID controller with the EGR rate as the feedback parameter is employed in this engine. The disadvantage of this strategy lies in that the value of the EGR rate is calculated,

which is not sufficiently accurate during transients and the PID controllers require tuning on a large number of parameters. In this study, one EGR rate oriented MPC strategy is implemented on a model plant and compared with the proposed oxygen concentration control strategy.

As mentioned in the previous section, oxygen concentration oriented MPC uses oxygen concentration and intake pressure as the reference values. For the EGR rate oriented MPC, the tracking parameters are the EGR rate and intake pressure instead. The set points of the EGR rate and oxygen concentration are set as the same in both strategies for clear comparison. The prediction horizon and control horizon are set as 20 and 2 in each case. In Figure 7-9, the profiles of the air path parameters during the step change are presented. It is revealed that different control strategies result in diverse profiles. For oxygen concentration tracking, MPC O2 shows a short response time with small overshoot; while the MPC EGR rate has a slow response. However, both control strategies can settle at a steady value within 5 seconds. Relatively, since EGR rate tracking is not considered in the MPC O2 controller, the overshoot of the EGR rate is apparent and the settle time is close to that in the MPC EGR rate, the same as the oxygen concentration. As for intake pressure, the MPC EGR rate has a better tracking performance in most cases. This indicates the trade-off between oxygen concentration and intake pressure tracking during the step. When the controller has a shorter response in the oxygen concentration, the other control target of the intake pressure is compromised. The trade-off can be adjusted through tuning the output weights in the design of the MPC.

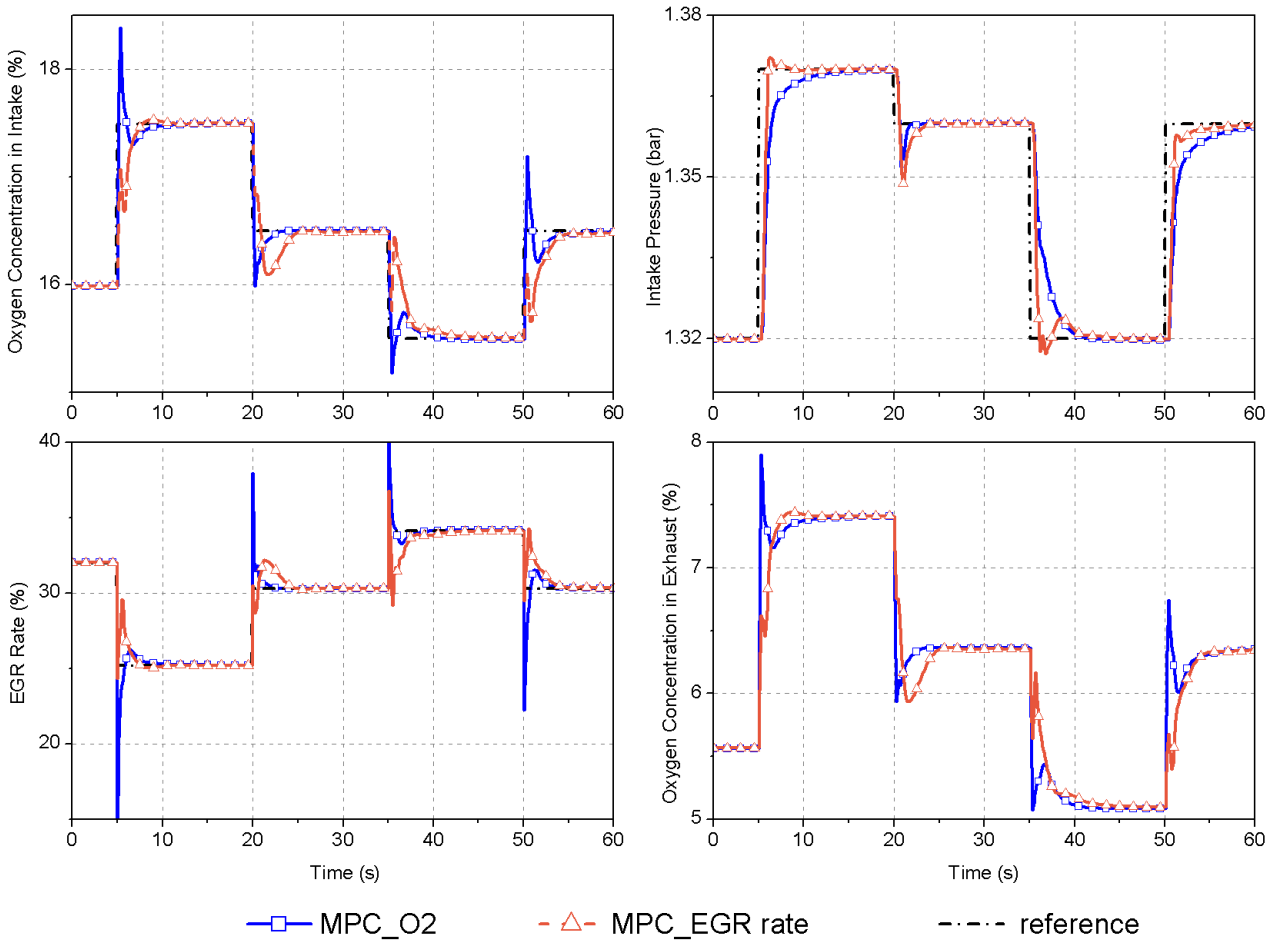

Figure 7-9 Comparison of O2 Oriented and EGR rate Oriented Control Strategy

The corresponding EGR valve and VGT position profiles are illustrated in Figure 7-10. The MPC EGR rate shows a slightly slower reaction in the EGR valve positioning. Meanwhile, the VGT in the two control strategies presents different trends during the step change. This can explain the main difference of the intake pressure performance in Figure 7-9. For instance, the sharp drop at around 5 seconds in the MPC EGR rate contributes to the fast rise of the intake pressure; while the small peak in the MPC O2 delays the increase of the intake pressure and facilitates the tracking of the oxygen concentration.

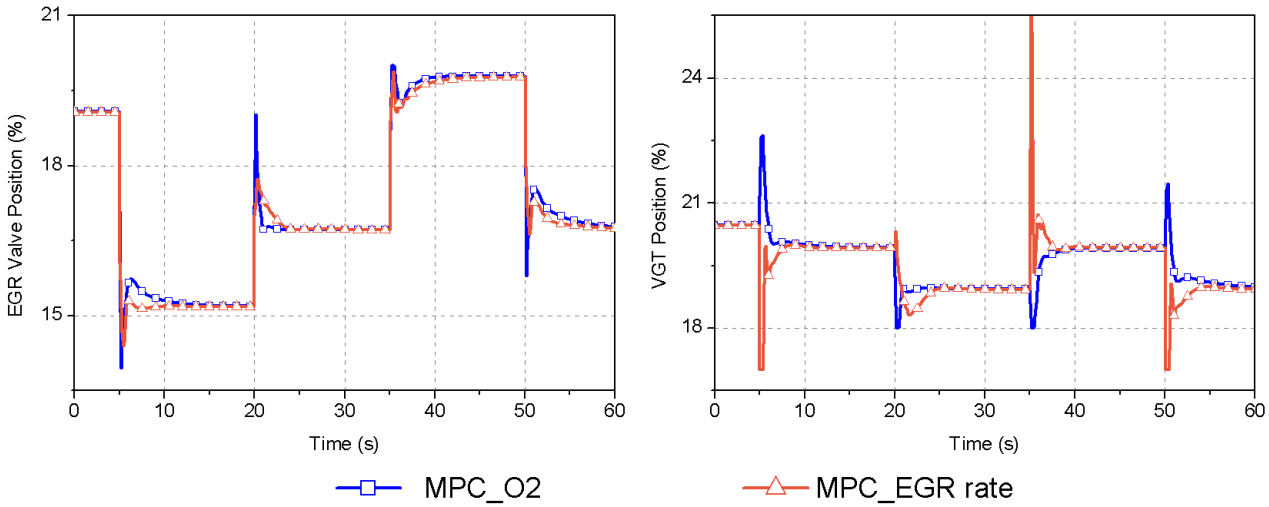

Figure 7-10 Profiles of Actuators during Transient Operation

The emission behaviours of the two control strategies shown in Figure 7-11 have small differences. The main difference lies in particulate mass. In light of the faster response of the oxygen concentration, PM in the MPC O2 has a lower value, especially during the fall step.

In general, both control strategies are able to follow the reference value without large errors and reach steady state within an acceptable period. It should be noted that the oxygen concentration and EGR rate in this case are both simulated in the same model; the issue of instantaneous EGR rate measurement has not been reflected. Therefore, considering the advantage of the direct measurement of the oxygen concentration by a lambda sensor, the oxygen oriented control strategy is feasible and promising for real application in turbocharged diesel engines.

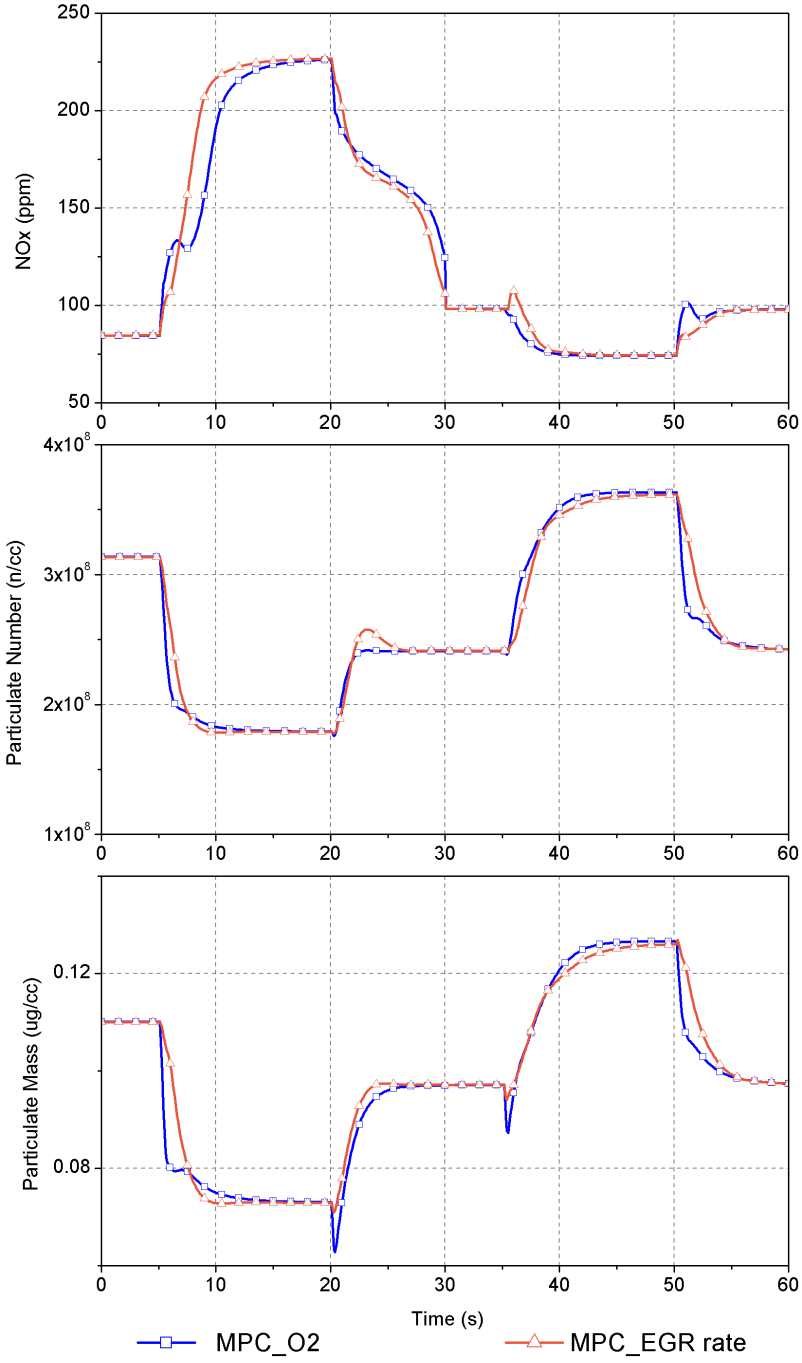

Figure 7-11 Comparison of Emission Characteristics between O2 Oriented and EGR rate Oriented Control Strategy

7.4 Validation on a Real-time Hardware-in-the-Loop Simulation Platform

The setup and configuration of a hardware-in-the-loop platform is introduced in this section. The model-based control strategy proposed is validated on the simulation platform in real time. The results of the simulation are presented and discussed in the last part of the section.

7.4.1 Setup of the HIL Platform

A HIL simulation is a rapid, low-cost prototyping test method for digital controller design. In this study, the HIL simulation replaces the simulated control system including the proposed control strategy with a real hardware controller, which interacts with the rest of the model on the simulator in real time. The purpose of a HIL system is to provide all of the electrical stimuli required and test the control strategy in a real ECU. Since the mathematical models used in the simulator present a reasonably accurate representation of the real process, the controller parameters can be tuned and tested in the platform directly. Besides, testing with HIL can largely reduce the time on experimental test but provide high flexibility and perfect repeatability (Zwaanenbug 2008). Therefore, it is essential to test a controller function with a simulated process before the controller is applied to the real process.

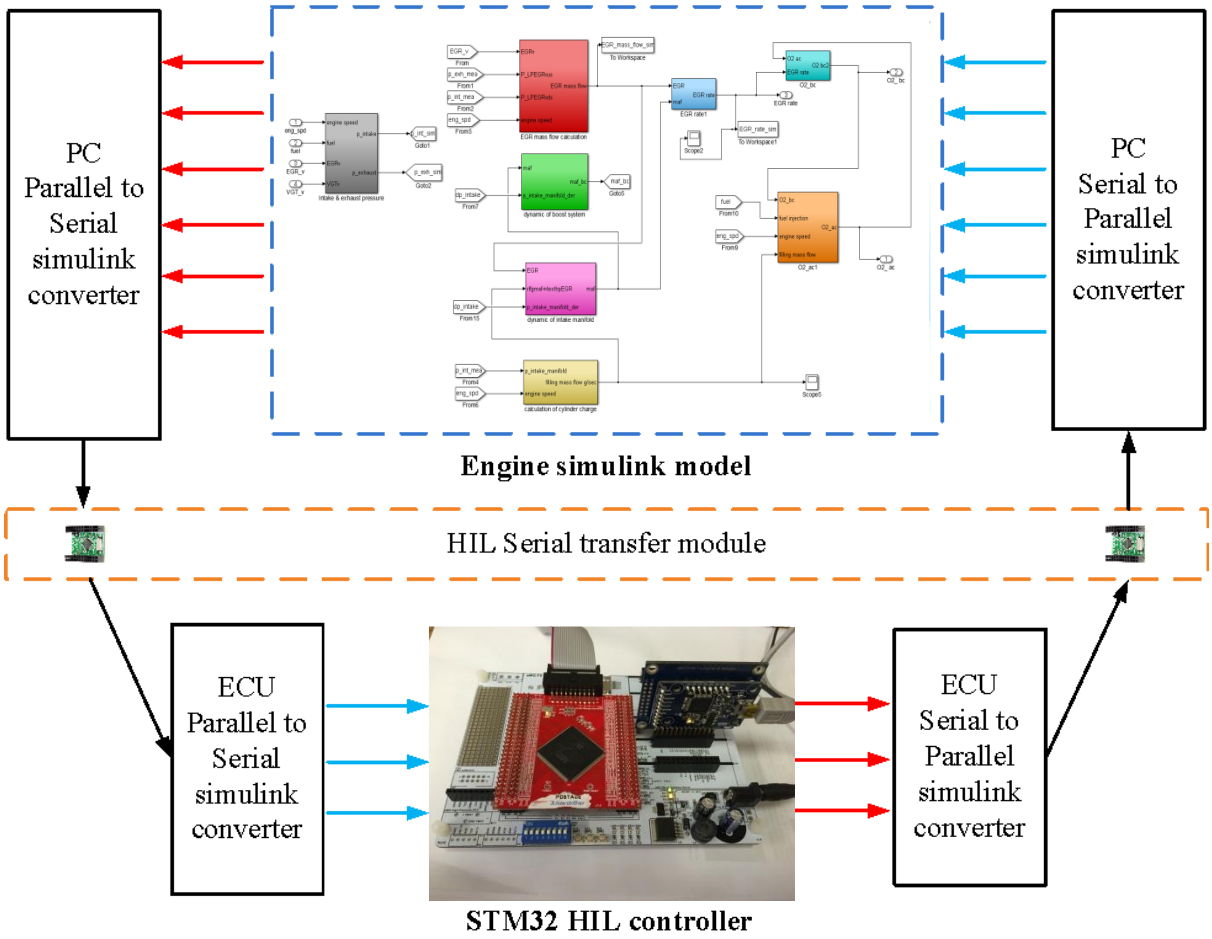

Figure 7-12 Block Diagram of HIL Simulation Setup

Figure 7-12 shows the setup of a HIL simulation platform for EGR-VGT control with an external hardware controller and engine Simulink model. A personal computer is used as the target PC to operate the Simulink model and real-time signal convertor. With the real-time diesel engine model, the target PC can provide the real-time value of the oxygen concentration and intake pressure, which works similarly as in a real diesel engine. The HIL serial transfer module acts as a bridge between the physical variables from the Simulink model and the signals from the hardware controller. Most importantly, the EGR-VGT management strategy is implemented in the hardware controller ARM STM32F417Ix. The detailed specification of the controller is listed in Table 7-5.

Table 7-5 Specification of ARM STM32F417Ix

Peripherals	STM32F417Ix	
Flash memory in Kbytes	512	1024
SRAM in Kbytes	192(112+16+64)	
FSMC memory controller	Yes(1)	
GPIOs	140	
Channel 12-bit ADC	24	
Maximum CPU frequency	168 MHz	
Ambient temperature	–40 to +105 °C	
Package	LQFP176	

The detailed work flow is illustrated in Figure 7-12 also. Firstly, the variables from the Simulink model, including set points and measured values, are processed to serial signals through a PC parallel to serial convertor. Then, the serial signal is sent to the ECU serial to parallel convertor through a HIL serial transfer module. After the controller receives the parallel signal, the control algorithm is executed and the control signals such as the EGR valve and VGT position are converted to serial signals and sent back to the Simulink model. Thus, a closed HIL simulation loop is implemented.

7.4.2 Parameters Configuration of the Platform

In order to flash the Simulink model into the ARM controller, the STM32 toolbox of the real-time workshop (RTW) in MATLAB is employed to generate the C-code directly from Simulink and convert the C code to a hex file. Then the hex file is downloaded to the ARM controller.

Basically, there are two models used in the HIL platform. The first is the controller model for code generating, including the PID and MPC controller; while the other is the real-time diesel engine model, which predicts the outputs such as oxygen concentration, intake pressure and emissions based on four variables as introduced in Chapter 6.

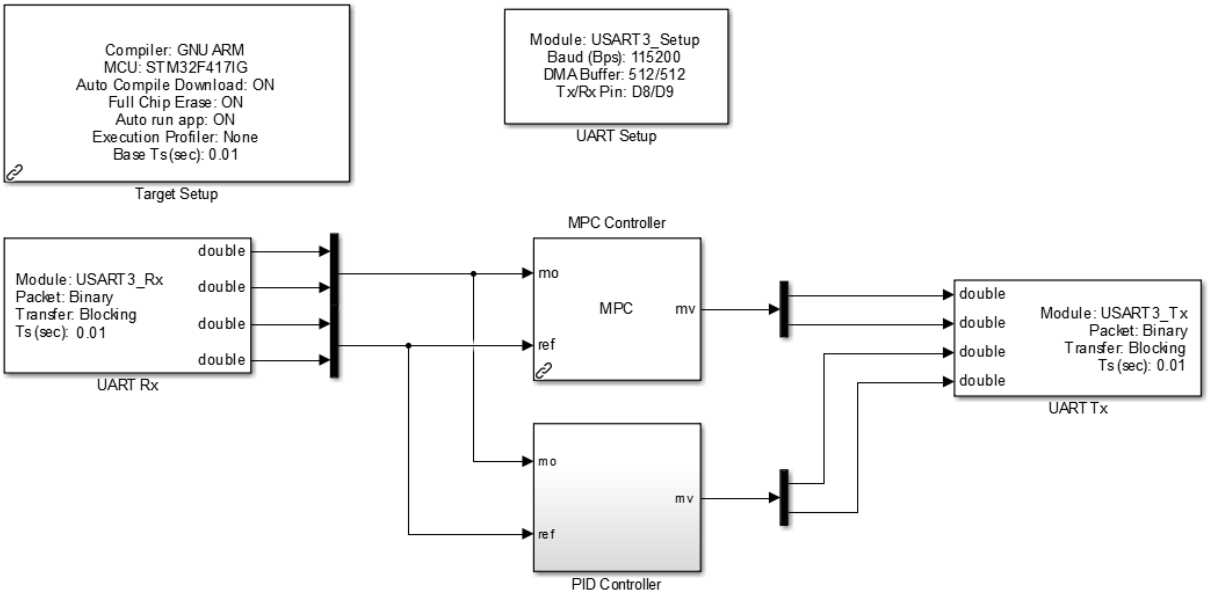

Figure 7-13 Simulink Structure of Controller Model for Code Generating

Figure 7-13 presents the Simulink structure of the controller model. A discrete MPC controller, introduced in the previous section, is included in the model. Also, to compare the results of the MPC, the PID controller is embedded as well. Due to the low cost of the hardware and easy implementation, the serial signal is widely used for data transmission. In this study, the control signals are converted to serial type via UART Tx module. Similarly, the measured values from the engine model are converted to a parallel type via the UART Rx module. To realize the real-time action in the VGT-EGR controller, the ECU sample time is defined as 0.01 s. The UART sample time is set as 0.1 s to ensure the capture of this data

from the ECU. Since the engine model is developed with the sample time at 0.1 s, the sample time of the MPC and PID controller is kept as 0.1 s.

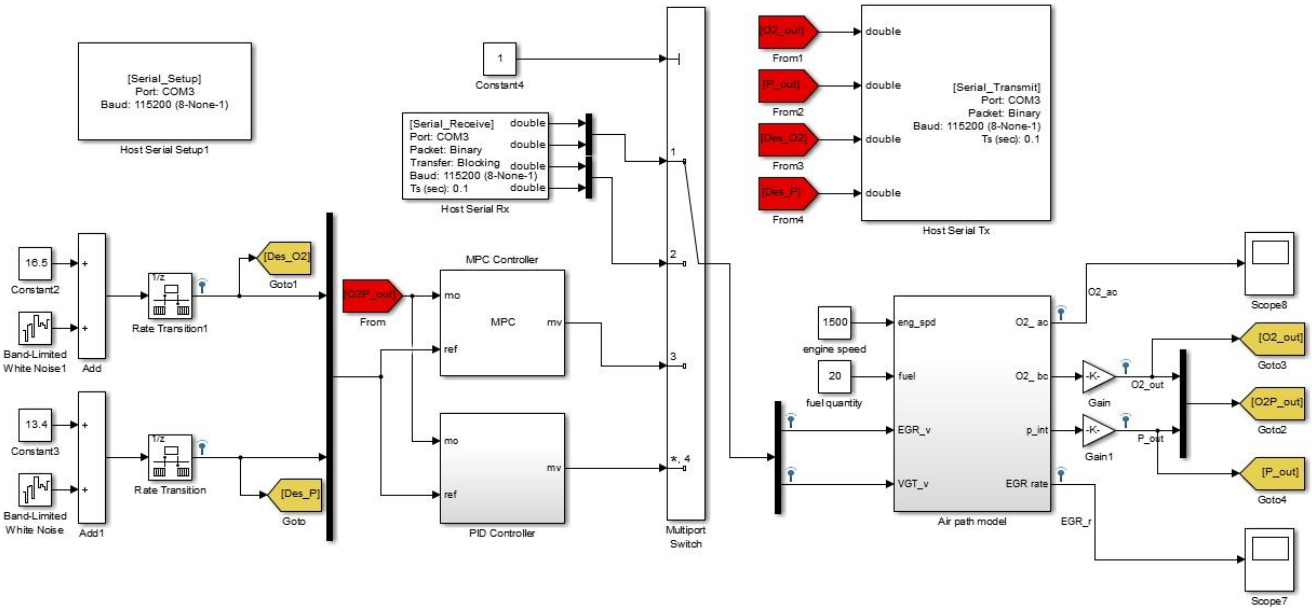

Figure 7-14 Simulink Structure of PC Model

Figure 7-14 shows the Simulink structure of the PC model. The PC is operated under the Windows 7 system, communicating with the ARM controller through the R232 serial port. In order to realize the real-time simulation, the baud rate of the serial is set as the maximum, 115200 bps. To compare the reaction of the HIL and Simulink, a multiport switch is implemented to change the control mode. Similarly to the controller model in the ECU, the sample time of the PC model is set as 0.1 s.

7.4.3 Validation of MPC on HIL Platform

Based on the development of the HIL platform and parameters configuration introduced above, the performance of both the MPC and PID control of a diesel engine air system is

tested on a HIL simulation platform. In order to validate the capability of real-time HIL simulation, the response of pure simulation on a model, model-in-the-loop (MIL) and the actual ECU responses, HIL, are compared with the same step of reference value designed. The comparison of the profiles is shown in Figure 7-15.

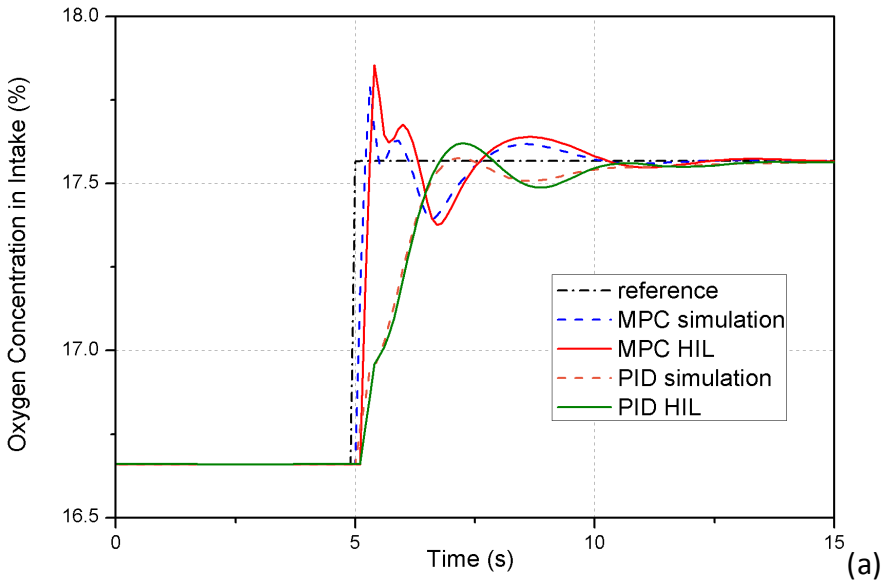

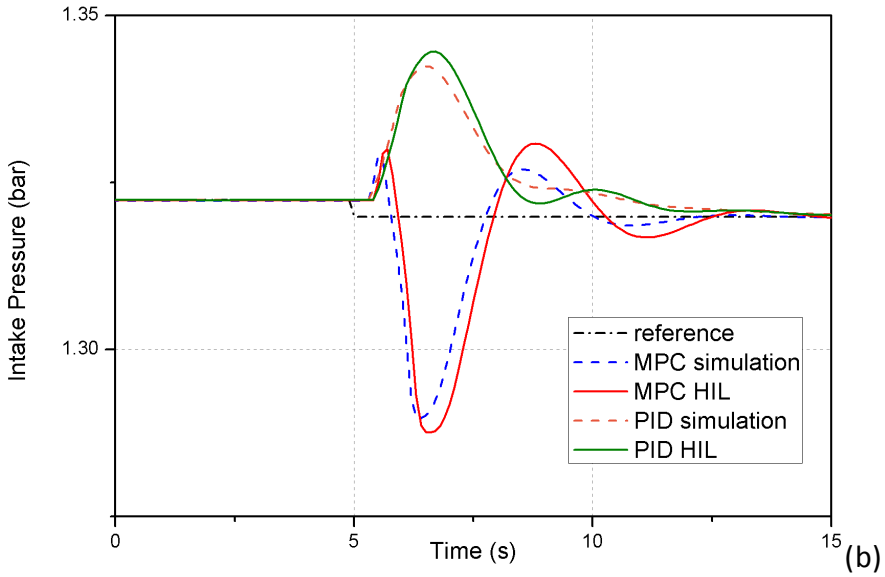

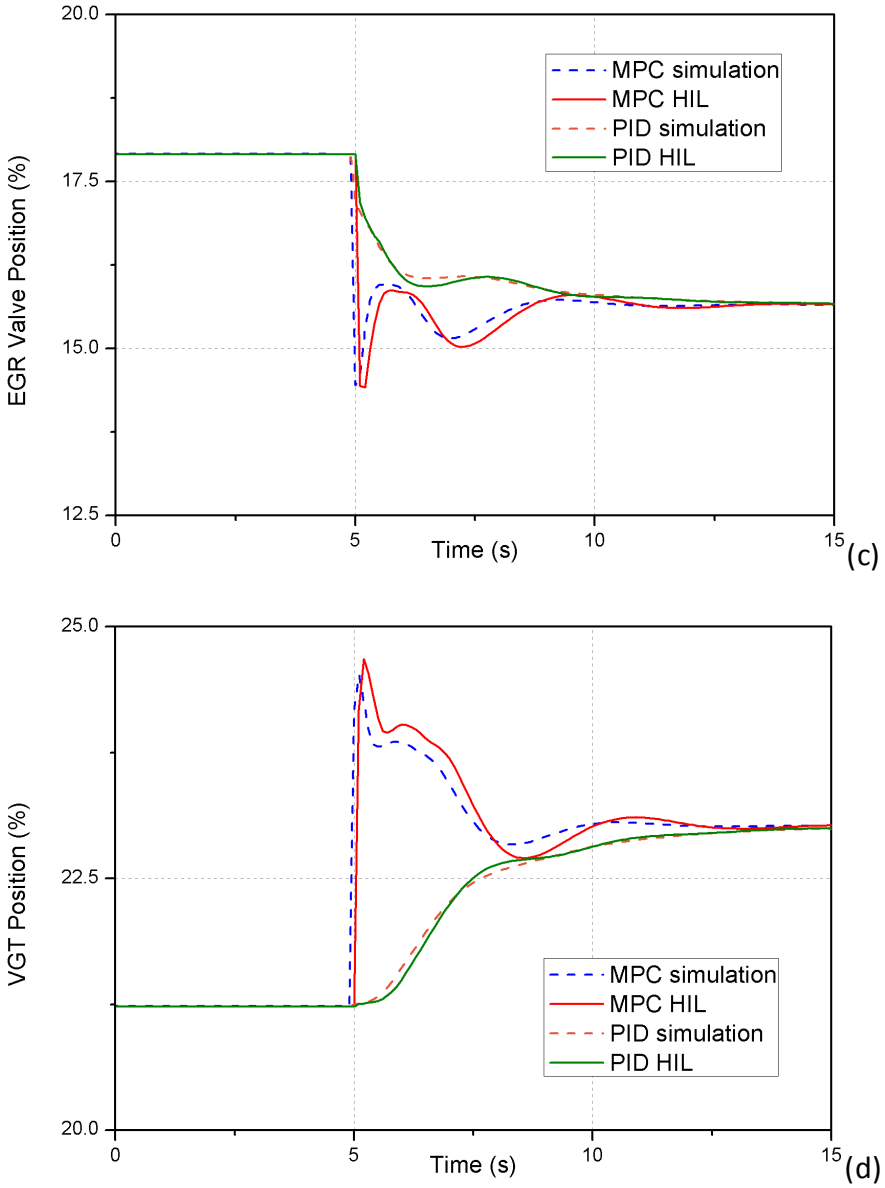

Figure 7-15 Comparison of Simulation Results with HIL; (a) Oxygen Concentration in Intake; (b) Intake Pressure; (c) EGR Valve Position; (d) VGT Position

In Figure 7-15, it is observed that with the step of the oxygen concentration set points, both MPC and PID controllers are able to track the step and settle at a steady value in the HIL platform. It is clearly shown that the response time of the MPC is shorter than the PID control as discussed in the previous section. Also, small lags of both measured values and actuator positions are found. There are two factors for this phenomenon. First, although the signal transmission between the hardware is rather fast, the time cost still has an influence

on the actuators' behaviour. When the PC outputs signal, the ARM controller must receive the step of the signal behind one sample time (0.1 second in this case). The other factor lies in the computation of the ARM controller. Due to the requirement of on-line prediction and calculation of MPC based on an identified model, the difference of computation speed between an ARM controller and PC is non-negligible. This also explains why the deviation of the MPC is slightly larger than PID.

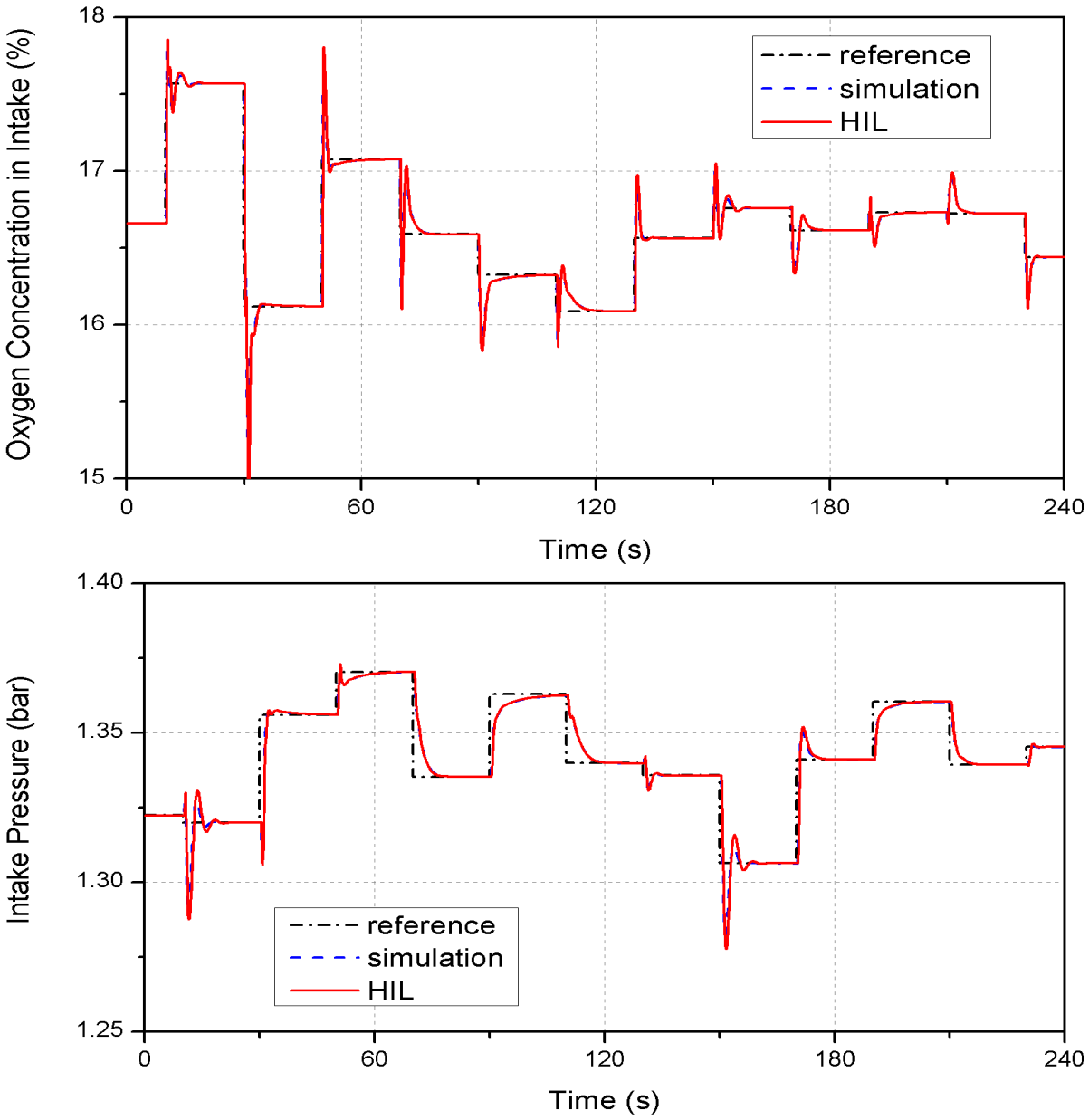

Figure 7-16 Validation of MPC on HIL Platform

To verify the controller at the variety of set points, various step reference values of oxygen concentration and intake pressure are applied. As shown in Figure 7-16, the results on the HIL platform present good tracking of the set points in most steps. Also, the deviation of simulation and HIL is acceptable, which proves the capability of real-time control on the developed HIL platform.

7.5 Summary

In this chapter, an advanced fast predictive approach to control the air system of a turbocharged diesel engine is developed and introduced. The state-space models are obtained by the system identification technique based on the dynamic engine model introduced in Chapter 6. Then, the linear model is utilized in an MPC controller as the model plant for the development of the control strategy. The primary advantage of the MPC lies in the capability of handling a highly coupled MIMO system. Two essential parameters, EGR valve and VGT position are properly controlled by the developed MPC approach. Compared with the conventional PID control method, the main control target of oxygen concentration in the MPC method has a rapid response with a maintained boost pressure profile; thereby showing a great potential for emission abatement. Furthermore, a comparison of MPC approaches with different references is conducted between oxygen concentration oriented and EGR rate oriented. It is proved that both control strategies are able to follow the reference value without large errors and reach steady state within an acceptable period. Considering the advantage of the direct measurement of the oxygen concentration by a lambda sensor, the oxygen oriented control strategy is feasible and promising for real application in turbocharged diesel engines.

One HIL simulation platform is developed to present the real-time capability of the model-based control strategy. The validation results on the HIL platform show good tracking of the set points and the difference between the pure model and actual ECU response is tiny and acceptable. It means that the developed MPC control can be implemented in real vehicle application.

CHAPTER 8 CONCLUSIONS AND FUTURE WORK

The research work in this thesis has focused on the dynamic performance of a turbocharged diesel engine during transient operation and the study of an advanced fast predictive control approach with a novel real-time diesel engine model. In addition, the techniques for processing the experimental data from engine transient tests are developed to facilitate the investigation and model construction. The main conclusions of the thesis are presented, followed by suggestions for future work.

8.1 Conclusions

The conclusions in this study are divided into four parts and presented below, in the order that the chapters appear.

Methodology for Engine Transient Analysis

Measurement and processing methods of instantaneous data during engine transient tests have been developed. For combustion diagnostic data processing, four alternative automated filtering methods, namely FFT, low-pass, linear and zero-phase filtering are implemented on cycle-by-cycle in-cylinder pressure data obtained from gasoline engine and diesel engine transient tests. FFT filtering is the best suited method for gasoline engine tests

since it eliminates most pressure fluctuation and provides smooth RoHR profiles; whilst retaining the significant information of the engine combustion. In diesel engine tests, due to the multiple injection strategy, the noise and combustion instability cannot be recognized through FFT or low-pass filtering with the original sampling frequency. A moving average filter such as a zero-phase filter presents the best performance on balance, considering the advantages of its convenient implementation and preservation of information.

The high-frequency instantaneous emission data has been properly processed through FFT filtering and cycle-based averaging. The filtered emission data presents high suitability for data analysis of engine transient performances. A method to compensate for measurement facilities with a long response time has been developed and tested. Furthermore, the peak-to-trough method has been successfully applied to the experimental data for time-alignment.

Engine Dynamic Performance during Transient Operation

For the experimental study of engine dynamic performance, various transient experiments were designed and conducted. The effects of engine speed and EGR are investigated through load increase tests at a constant engine speed between 1000 rpm to 2000 rpm with different EGR calibrations. In addition, the sensitivity of dynamic performance to fuel properties is studied using alternative fuels. The main conclusions are summarized as follows:

1. During the load increase tests, apparent spikes of pressure drop are found, derived from the delay of the energy at the turbocharger to boost the intake pressure. Meanwhile, due to the slow response of the EGR flow, a serious deficiency of oxygen in the cylinder is observed, resulting in incomplete combustion and excessive HC and PM emissions.

2. At higher engine speed, the faster growth of boost pressure with larger amplitude is present at the load transition, along with lower oxygen concentration and larger delays of the combustion phase, due to the increased exhaust gas energy. From the control point of view, the VGT position has a more significant influence at high engine speed. Also, the overshoot of HC emissions is more serious when the engine speed increases, but the value in steady state is close in different cases.

3. As the EGR calibration is modified, spikes of pressure drop can be found in each case. Nevertheless, the low EGR valve position facilitates the faster rise of boost pressure and abates the drop of oxygen concentration at load transition. As regards the emission behaviour, the NOx-PM trade-off still exists within the transient period and an optimal control strategy is necessary to minimize both NOx and PM.

4. When fuelled with alternative fuels, the trend of the emission behaviour is similar compared with conventional diesel. In conclusion, more NO emissions and lower HC emissions with a shorter recovery period were observed with the increase of the HVO ratio. Also, the total PN and PM of the HVO blends are less than diesel, up to 40%; higher particulate concentrations in the nucleation mode and fewer particles which are of a smaller size are produced by the HVO blends during the transient tests.

Control-oriented Diesel Engine Modelling

A control-oriented turbocharged diesel engine model including the air path, combustion and dynamic emission behaviour has been developed. The detailed conclusions of the model are presented below:

1. The developed model is able to simulate the main engine parameters such as the oxygen concentration, EGR mass flow, intake air mass flow, maximum in-cylinder temperature and IMEP. During transient operation, the fit of the EGR mass flow and oxygen concentration in the intake and exhaust manifold are 80%, 73% and 67% respectively. In addition, two important emissions of a diesel engine, NOx and particulate matter can be predicted with reasonable accuracy.
2. The dynamic model is capable of capturing most peaks and troughs of important air path parameters during engine transient operation. The main trends of the instantaneous emission behaviour following the change of engine parameters can be reflected.
3. Due to the simple structure, this model can run as a real-time simulator for engine control strategy development, reducing the experimental time and cost on real engine testing. Combined with the RCP facility, the model can be implemented in the ECU for vehicle application.
4. The model has high genericity and can be modified to match different engines. With the basic physics insight, it is easy to update the parameters and train the networks based on limited experimental data.

Model-based Fast Predictive Control

The advanced fast predictive control approach of MPC is developed and implemented in the air system of a turbocharged diesel engine for EGR and VGT control. The approach mainly includes the state space model development through system identification; the controller structure build up; and the development of a control strategy based on the linear model plant. In the varied step cases, the MPC control strategy presents a good tracking performance of the reference value. Compared with the conventional PID control method, the main control target of the oxygen concentration in the MPC method has a rapid response with a maintained boost pressure profile; thereby showing a great potential for emission abatement. Furthermore, oxygen concentration oriented and EGR rate oriented MPC strategies are compared and this shows the feasibility of new oxygen concentration oriented control, considering the advantage of direct measurement of the oxygen concentration by a lambda sensor.

One HIL simulation platform is developed to present the real-time capability of the model-based control strategy. The validation results on the HIL platform show good tracking of the set points and the difference between a pure model's and the actual control unit's response is tiny and acceptable. This means that the MPC control which was developed can be implemented in real vehicle application.

8.2 Future Work

Supported by the JLR project “advanced control of diesel engines”, the test bench used in this study will be updated with a Pi Innovo Open ECU which provides the full capability of rapid prototype control including the modification of maps and embedded control strategies. Based on the research in this thesis, some recommendations for future work are outlined.

Identification of Engine Air Path Transient Performance

Restricted by the conventional ECU, it is noticed that the original control strategy and calibration have inevitable influence on the investigation of engine transient performance. With the advanced Open ECU, the control parameters of interest can be easily manipulated and meanwhile the remaining parameters are well maintained. Due to the complicated and inter-coupled air path of a diesel engine, the proper control of the actuators is rather essential and the detailed dynamic characteristics can be identified in this approach. As a result, researchers are able to develop more accurate and reliable engine models.

Integration of Air Path and Fuel Injection System Control Strategies

The MPC approach has been successfully applied to a diesel engine air path control in this study. It would be interesting to develop the control strategy for the fuel injection system. Currently, the fuel injection in diesel engines is feedforward controlled and there is great potential to improve the combustion efficiency with an advanced strategy. In addition, the control of the air path and fuel injection system can be integrated for further investigation.

Development of Fast MPC Approach

As the engine management becomes increasingly complicated, there is always a need to improve the computation speed of models and controllers. Based on the standard MPC approach developed in this thesis, the parameters in the MPC controller can be modified and optimized to achieve a faster speed. Moreover, it is suggested that some alternative MPC approaches such as explicit MPC or nonlinear MPC can be tested.

On-board Implementation of MPC Control

With the Open ECU, it is achievable to implement the developed control strategy on a real engine through the complier. As a result, the model-based controller can not only be tuned based on off-line experimental data and an engine model, but also be optimized with the on-board realization. In this method, the engine control environment would be close to the real application and further validation could be conducted for the MPC approach.

APPENDIX

Experimental Setup for Gasoline Engine Test Bench

Engine

The gasoline engine used as reference for engine transient analysis was a Jaguar SI/HCCI Dual Mode V6 Research gasoline Engine.

Table A1 Technical Data of the Gasoline Engine

Engine Type	Jaguar V6 GDI
Displacement Volume	3.0 Litres
Bore	89 mm
Stroke	79.5 mm
Rod	138mm
Fuel	ULG95
Compression ratio	11.3
Max Valve Lift (SI/HCCI)	9/3 mm
Valve Duration (SI/HCCI)	260/160 CAD
Intake valve timing	Variable
Exhaust valve timing	Variable
Air/Fuel ratio	Variable

The engine was operated on SI mode in these experiments.

dSPACE Engine Control System

The dSPACE real-time control system was developed by dSPACE Ltd. The processor of the dSPACE hardware has very high computational capability and is assembled with many I/O supports which help the customers with configuration depending on their needs.

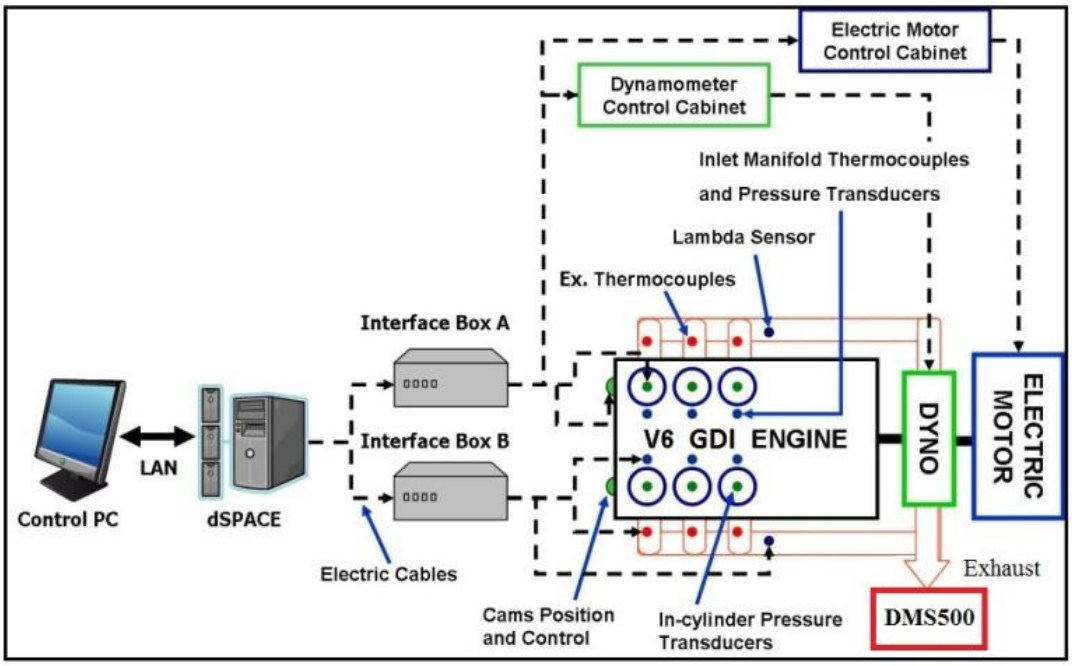

Figure A1 Schematic Diagram of the Gasoline Test Bench

REFERENCES

Aatola, Hannu, Martti Larmi, Teemu Sarjovaara, and Seppo Mikkonen. 2008. "Hydrotreated Vegetable Oil (HVO) as a Renewable Diesel Fuel: Trade-off between NOx, Particulate Emission, and Fuel Consumption of a Heavy Duty Engine. SAE Technical Paper 2008-01-2500." *SAE Technical Papers* 1 (1): 12. doi:10.4271/2008-01-2500.

Akihama, K., Y. Takatori, K. Inagaki, a.M. Dean, and S. Sasaki. 2001. "Mechanism of the Smokeless Rich Diesel Combustion by Reducing Temperature." *SAE Technical Paper* 2001 (2001-01-0655): 2001–01–0655. doi:10.4271/2001-01-0655. http://papers.sae.org/2001-01-0655/.

Alagumalai, Avinash. 2014. "Internal Combustion Engines: Progress and Prospects." *Renewable and Sustainable Energy Reviews*. doi:10.1016/j.rser.2014.06.014.

Alberer, Daniel, and Luigi del Re. 2009. "Fast Oxygen Based Transient Diesel Engine Operation." *SAE* 2 (1): 405–413.

Alberer, Daniel, and Luigi Re. 2010. "Fast Oxygen Based Transient Diesel Engine Operation." *SAE International Journal* 2 (1): 405–413.

Alonso, José M, Fernando Alvarruiz, José M Desantes, Leonor Hernández, and Vicente Hernández. 2007. "Combining Neural Networks and Genetic Algorithms to Predict and Reduce Diesel Engine Emissions." *IEEE Transactions on Evolutionary Computation* 11 (1): 46–55.

Ambs, J L, and B T McClure. 1993. "The Influence of Oxidation Catalysts on NO2 in Diesel Exhaust." *Society of Automotive Engineers*. doi:10.4271/932494.

Anderson, David, Justin Callies, Baitao Xiao, and Robert Gary Prucka. 2012. "In-Cylinder Thermodynamic Analysis for Performance Engine Development" (April). doi:10.4271/2012-01-1170. http://www.sae.org/technical/papers/2012-01-1170.

Arcoumainis, C, and C.S. Jou. 1992. "Measurement and Prediction of Transient NOx Emissions in DI Diesel Engines." *IMechE Conference* (paper C448/039).

Arnold, J F, N Langlois, H Chafouk, and G Tr. 2006. "Control of the Air System of a Diesel Engine : A Fuzzy Multivariable Approach." In *International Conference on Control Applications*, 2132–2137. Munich, Germany.

Arnold, Jean-François, Nicolas Langlois, and Houcine Chafouk. 2009. "Fuzzy Controller of the Air System of a Diesel Engine: Real-Time Simulation." *European Journal of Operational Research* 193 (1) (February): 282–288. doi:10.1016/j.ejor.2007.08.046. http://linkinghub.elsevier.com/retrieve/pii/S0377221707010570.

Assanis, Dennis N, Zoran S Filipi, Scott B Fiveland, and Michalis Syrimis. 2000. "A Methodology for Cycle-By-Cycle Transient Heat Release Analysis in a Turbocharged Direct Injection Diesel Engine." *SAE*: 1–14.

Atkinson, Chris, and Gregory Mott. 2005. "Dynamic Model-Based Calibration Optimization : An Introduction and Application to Diesel Engines." *SAE International*.

Atkinson, Christopher M, Marc Allain, Yury Kalish, and Houshun Zhang. 2009. "Model-Based Control of Diesel Engines for Fuel Efficiency Optimization." *SAE International*.

August, Recei V, V Re, Manuscript Recei, and V No. 2008. "Complex Diesel Engine Simulation with Focus on Transient Operation." *Energy & Fuels*: 1411–1417.

Beattie, Tim, Richard P. Osborne, and Wilhelm Graupner. 2013. "Engine Test Data Quality Requirements for Model Based Calibration: A Testing and Development Efficiency Opportunity" (April). doi:10.4271/2013-01-0351. http://www.sae.org/technical/papers/2013-01-0351.

Bemporad, Alberto. 2001. "The Explicit Linear Quadratic Regulator for Constrained System." *Automatica* 38: 3–20.

Bemporad, Alberto, Manfred Morari, and N Lawrence Ricker. 2014. *Model Predictive Control Toolbox™ User ' S Guide*.

Benajes, J, S Molina, R Novella, and K DeRudder. 2008. "Influence of Injection Conditions and Exhaust Gas Recirculation in a High-Speed Direct-Injection Diesel Engine Operating with a Late Split Injection." *Proceedings of the Institution of Mechanical Engineers, Part D: Journal of Automobile Engineering* 222 (4): 629–641. doi:10.1243/09544070JAUTO657.

Benz, Michael, Christopher H. Onder, and Lino Guzzella. 2010. "Engine Emission Modeling Using a Mixed Physics and Regression Approach." *Journal of Engineering for Gas Turbines and Power* 132 (4). http://cat.inist.fr/?aModele=afficheN&cpsidt=22453158.

Billings, S.A., S Chen, and R.J. Backhouse. 1989. "The Identification of Linear and Non-Linear Models of Turbocharged Automotive Diesel Engine." *Mechanical Systems and Signal Processing* 3: 123–142.

Black, J, P G Eastwood, K Tufail, T Winstanley, Ford Motor Company, Y Hardalupas, and A M K P Taylor. 2010a. "The Effect of VGT Vane Control on Pumping Losses during Full-Load Transient Operation of a Common-Rail Diesel Engine The Effect of VGT Vane Control on Pumping Losses during Full- Load Transient Operation of a Common-Rail Diesel Engine."

———. 2010b. "Diesel Engine Transient Control and Emissions Response during a European Extra-Urban Drive Cycle (EUDC):" 1015–1030.

Boehner, Wolfgang, and Karsten Hummel. 1997. "Common Rail Injection System for Commercial Diesel Vehicles." *SAE TECHNICAL PAPER SERIES* (412). doi:10.4271/970345.

Bonilla, David, Justin D K Bishop, Colin J. Axon, and David Banister. 2014. "Innovation, the Diesel Engine and Vehicle Markets: Evidence from OECD Engine Patents." *Transportation Research Part D: Transport and Environment* 27: 51–58. doi:10.1016/j.trd.2013.12.012. http://dx.doi.org/10.1016/j.trd.2013.12.012.

Boretti, Alberto A. 2012. "Stochastic Reactor Modelling of Multi Modes Combustion with Diesel Direct Injection or Hydrogen Jet Ignition Start of Combustion." *International Journal of Hydrogen Energy* 37 (18): 13555–13563. doi:10.1016/j.ijhydene.2012.06.055.

Bosch. 2014. "Lambda Sensor LSU4.9."

Brahma, I., and J. N. Chi. 2011a. "Development of a Model-Based Transient Calibration Process for Diesel Engine Electronic Control Module Tables - Part 1: Data Requirements, Processing, and Analysis." *International Journal of Engine Research* 13 (1) (November 7): 77–96. doi:10.1177/1468087411424376. http://jer.sagepub.com/lookup/doi/10.1177/1468087411424376.

———. 2011b. "Development of a Model-Based Transient Calibration Process for Diesel Engine Electronic Control Module Tables - Part 2: Modelling and Optimization." *International Journal of Engine Research* 13 (2) (December 7): 147–168. doi:10.1177/1468087411424377. http://jer.sagepub.com/lookup/doi/10.1177/1468087411424377.

Brahma, Indranil, Mike C Sharp, and Tim R Frazier. 2010. "Empirical Modeling of Transient Emissions and Transient Response for Transient Optimization" 2 (1): 1433–1443.

Bullock, Darcy, Brian Johnson, Richard B Wells, Michael Kyte, and Zhen Li. 2004. "Hardware - in-the-Loop Simulation." *Tramsportation Research Part C: Emerging Technologies* 12 (1): 73–89. doi:10.1016/j.trc.2002.10.002. http://linkinghub.elsevier.com/retrieve/pii/S0968090X03000792.

Burtscher, H. 2005. "Physical Characterization of Particulate Emissions from Diesel Engines: A Review." *Journal of Aerosol Science* 36 (7) (July): 896–932. doi:10.1016/j.jaerosci.2004.12.001. http://linkinghub.elsevier.com/retrieve/pii/S0021850204004124.

Camacho, Eduardo, and Carlos Bordons. 2005. *Model Predictive Control. Advanced Textbooks in Control and Signal Processing*. Berlin: Springer.

Cambustion. 2011. "DMS500 Fast Engine Particulate Analyzer. See Also, <www.cambustion.co.uk>."

———. 2012. "HFR500 Fast FID Analyzer. See Also, <www.cambustion .co.uk>."

———. 2013. "CLD500 Fast NOx Analyzer. See Also, <www.cambustion .co.uk>."

Canakci, M. 2005. "Performance and Emissions Characteristics of Biodiesel from Soybean Oil." *Proceedings of the Institution of Mechanical Engineers, Part D: Journal of Automobile Engineering*. doi:10.1243/095440705X28736.

Cardone, Massimo, Maria Vittoria Prati, Vittorio Rocco, Maurizia Seggiani, Adolfo Senatore, and Sandra Vitolo. 2002. "Brassica Carinata as an Alternative Oil Crop for the Production of Biodiesel in Italy: Engine Performance and Regulated and Unregulated Exhaust Emissions." *Environmental Science and Technology* 36 (21): 4656–4662. doi:10.1021/es011078y.

Carlucci, P, P Carlucci, a Ficarella, a Ficarella, D Laforgia, and D Laforgia. 2003. "Effects of Pilot Injection Parameters on Combustion for Common Rail Diesel Engines" (x): 29–40. doi:10.4271/2003-01-0700. http://www.sae.org/technical/papers/2003-01-0700.

Catania, Andrea Emilio, Claudio Dongiovanni, Antonio Mittica, Claudio Negri, and Ezio Spessa. 1996. "Study of Automotive Diesel Injection-System Dynamics Under Control." *SAE Technical Paper Series*.

Catania, Andrea Emilio, Roberto Finesso, and Ezio Spessa. 2011. "Predictive Zero-Dimensional Combustion Model for DI Diesel Engine Feed-Forward Control." *Energy Conversion and Management* 52 (10) (September): 3159–3175. doi:10.1016/j.enconman.2011.05.003. http://linkinghub.elsevier.com/retrieve/pii/S0196890411001609.

Çetinkaya, Merve, Yahya Ulusoy, Yücel Tekìn, and Fìlìz Karaosmanoğlu. 2005. "Engine and Winter Road Test Performances of Used Cooking Oil Originated Biodiesel." *Energy Conversion and Management* 46 (7-8): 1279–1291. doi:10.1016/j.enconman.2004.06.022.

Chadwell, Christopher James, and Mark Walls. 2010. "Analysis of a SuperTurbocharged Downsized Engine Using 1-D CFD Simulation." *SAE International Journal*. doi:10.4271/2010-01-1231.

Chan, S.H. 1996. "Measurement of Concentrations of Transient Gases Using a Conventional NDIR Analyser." *Proc. Inst. Phys., J. Measmt Sci. Technol* 7: 1–11.

Chiara, F, and M Canova. 2009. "Mixed-Mode Homogeneous Charge Compression Ignition–direct Injection Combustion on Common Rail Diesel Engines: An Experimental Characterization." *International Journal of Engine Research*. doi:10.1243/14680874JER02609.

Choi, Dae, Paul C. Miles, Hanho Yun, and Rolf D. Reitz. 2005. "A Parametric Study of Low-Temperature, Late-Injection Combustion in a HSDI Diesel Engine." *JSME International Journal Series B* 48 (4): 656–664. doi:10.1299/jsmeb.48.656.

Chuepeng, Sathaporn, Hongming Xu, Athanasios Tsolakis, Miroslaw Wyszynski, and Philip Price. 2011. "Particulate Matter Size Distribution in the Exhaust Gas of a Modern Diesel Engine Fuelled with a Biodiesel Blend." *Biomass and Bioenergy* 35 (10): 4280–4289.

doi:10.1016/j.biombioe.2011.07.017.
http://dx.doi.org/10.1016/j.biombioe.2011.07.017.

Chung, Namhoon, Sunwoo Kim, and Myoungho Sunwoo. 2005. "Nonlinear Dynamic Model of a Turbocharged Diesel Engine." *SAE Technical Paper Series* (724).

Cieslar, Dariusz, Paul Dickinson, Alex Darlington, Keith Glover, and Nick Collings. 2014. "Model Based Approach to Closed Loop Control of 1-D Engine Simulation Models." *Control Engineering Practice* 29: 212–224. doi:10.1016/j.conengprac.2014.01.021.
http://dx.doi.org/10.1016/j.conengprac.2014.01.021.

Cong, S., G. P. McTaggart-Cowan, C. P. Garner, E. Wahab, and M. Peckham. 2011. "Experimental Investigation of Low Temperature Diesel Combustion Processes." *Combustion Science and Technology*. doi:10.1080/00102202.2011.600740.

D'Ambrosio, Stefano, Roberto Finesso, Lezhong Fu, Antonio Mittica, and Ezio Spessa. 2014. "A Control-Oriented Real-Time Semi-Empirical Model for the Prediction of NOx Emissions in Diesel Engines." *Applied Energy* 130: 265–279.
doi:10.1016/j.apenergy.2014.05.046.

Davis, Paul, and Mark Peckham. 2007. "The Analysis of Gasoline Transient Emissions Behaviour Using Fast Response Gas Analysers."

Dec, John E, and Peter L Kelly-Zion. 2000. "The Effects of Injection Timing and Diluent Addition on Late-Combustion Soot Burnout in a DI Diesel Engine Based on Simultaneous 2-D Imaging of OH and Soot." *SAE Technical Paper Series* (724).
doi:10.4271/2000-01-0238. http://dx.doi.org/10.4271/2000-01-0238.

Dec, John E. 2009. "Advanced Compression-Ignition Engines—understanding the in-Cylinder Processes." *Proceedings of the Combustion Institute*. doi:10.1016/j.proci.2008.08.008.

Fernando, Sandun, Chris Hall, and Saroj Jha. 2006. "NO X Reduction from Biodiesel Fuels." *Energy & Fuels*: 376–382. doi:10.1021/ef050202m.

Filipi, Zoran, Yongsheng Wang, and Dennis Assanis. 2001. "Effect of Variable Geometry Turbine (VGT) on Diesel Engine and Vehicle System Transient Response." *SAE 2001 World Congress* (724). doi:10.4271/2001-01-1247.

Finesso, Roberto, Daniela Misul, and Ezio Spessa. 2014. "Development and Validation of a Semi-Empirical Model for the Estimation of Particulate Matter in Diesel Engines." *Energy Conversion and Management* 84: 374–389.
doi:10.1016/j.enconman.2014.04.053.
http://dx.doi.org/10.1016/j.enconman.2014.04.053.

Frijters, P.J.M., and R.S.G. Baert. 2006. "Oxygenated Fuels for Clean Heavy-Duty Diesel Engines." *International Journal of Vehicle Design*. doi:10.1504/IJVD.2006.009671.

García-Nieto, S., M. Martínez, X. Blasco, and J. Sanchis. 2008. "Nonlinear Predictive Control Based on Local Model Networks for Air Management in Diesel Engines." *Control Engineering Practice* 16 (12): 1399–1413. doi:10.1016/j.conengprac.2008.03.010.

Garcia-Ortiz, J.V., P. Langthaler, and L. Del Re. 2006. "GPC Control of the Airpath of High Speed Diesel Engines." *2006 IEEE Conference on Computer Aided Control System Design, 2006 IEEE International Conference on Control Applications, 2006 IEEE International Symposium on Intelligent Control* (October): 2772–2777. doi:10.1109/CACSD-CCA-ISIC.2006.4777077. http://ieeexplore.ieee.org/lpdocs/epic03/wrapper.htm?arnumber=4777077.

Garg, a. G., P. Diwan, and M. Saxena. 2012. "Artificial Neural Networks Based Methodologies Fo Optimization of Engine Operations." *International Journal of Scientific & Engineering Research* 3 (5): 2–7.

Giakoumis, Evangelos G., Constantine D. Rakopoulos, Athanasios M. Dimaratos, and Dimitrios C. Rakopoulos. 2012. "Exhaust Emissions of Diesel Engines Operating under Transient Conditions with Biodiesel Fuel Blends." *Progress in Energy and Combustion Science* 38 (5) (October): 691–715. doi:10.1016/j.pecs.2012.05.002. http://linkinghub.elsevier.com/retrieve/pii/S0360128512000342.

Glewen, William, Christopher Meyer, David Foster, Michael Andrie, and Roger Krieger. 2011. "Sources and Tradeoffs for Transient NO and UHC Emissions with Low Temperature Diesel Combustion" (x) (April). doi:10.4271/2011-01-1356. http://www.sae.org/technical/papers/2011-01-1356.

Grahn, Markus, Krister Johansson, Christian Vartia, and Tomas McKelvey. 2012. "A Structure and Calibration Method for Data-Driven Modeling of NO X and Soot Emissions from a Diesel Engine." *SAE International* (April). doi:10.4271/2012-01-0355. http://www.sae.org/technical/papers/2012-01-0355.

Grahn, Markus, and Jan-ola Olsson Tomas. 2011. "A Diesel Engine Model for Dynamic Drive Cycle Simulations:" 11833–11838.

Grondin, Olivier, Richard Stobart, Houcine Chafouk, and Jean Maquet. 2004. "Modelling the Compression Ignition Engine for Control : Review and Future Trends." *SAE* (724).

Gurney, Andrew, Helal Ahammad, and Melanie Ford. 2009. "The Economics of Greenhouse Gas Mitigation: Insights from Illustrative Global Abatement Scenarios Modelling." *Energy Economics* 31 (SUPPL. 2). doi:10.1016/j.eneco.2009.08.016.

Guzzella, Lino. 2010. *Introduction to Modeling and Control of Internal Combustion Engine Systems*.

Guzzella, Lino, and Christopher H. Onder. 2010. *Introduction to Modeling and Control of Internal Combustion Engine Systems*. Springer.

Hagena, Jonathan R, Zoran S Filipi, and Dennis N Assanis. 2010. "Transient Diesel Emissions : Analysis of Engine Operation During a Tip-In" 2006 (724).

Haiyan, Wang Haiyan Wang. 2006. *Control Oriented Dynamic Modeling of a Turbocharged Diesel Engine*. *Sixth International Conference on Intelligent Systems Design and Applications*. Vol. 2. Ieee. doi:10.1109/ISDA.2006.253821. http://ieeexplore.ieee.org/lpdocs/epic03/wrapper.htm?arnumber=4021648.

Hannan, M. A., F. A. Azidin, and A. Mohamed. 2014. "Hybrid Electric Vehicles and Their Challenges: A Review." *Renewable and Sustainable Energy Reviews*. doi:10.1016/j.rser.2013.08.097.

Hansen, Alan C., Dimitrios c. Kyritsis, and Chiafon F. Lee. 2009. *Characteristics of Biofuels and Renewable Fuel Standards*. Oxford: Blackwell Publishing.

He, Y, and C J Rutland. 2002. "Modeling of a Turbocharged Di Diesel Engine Using Artificial Neural Networks." *SAE Technical Papers* (724). http://www.scopus.com/inward/record.url?eid=2-s2.0-79959550080&partnerID=40&md5=0dbc2cff632edcae7adfea88aa305e75.

Herceg, Martin, Tobias Raff, Rolf Findeisen, and Frank Allgowe. 2006. "Nonlinear Model Predictive Control of a Turbocharged Diesel Engine." *2006 IEEE Conference on Computer Aided Control System Design, 2006 IEEE International Conference on Control Applications, 2006 IEEE International Symposium on Intelligent Control*. doi:10.1109/CACSD-CCA-ISIC.2006.4777076.

Heuwetter, David, William Glewen, Christopher Meyer, David Foster, Michael Andrie, and Roger Krieger. 2011. "Effects of Low Pressure EGR on Transient Air System Performance and Emissions for Low Temperature Diesel Combustion" (x) (September). doi:10.4271/2011-24-0062. http://www.sae.org/technical/papers/2011-24-0062.

Heywood, John B. 1988. *Internal Combustion Engine Fundamentals*. New York: McGraw-Hill, Inc.

Iida, Norimasa, and Tetsuya Igarashi. 2000. "Auto-Ignition and Combustion of N-Butane and DME / Air Mixtures in a Homogeneous Charge Compression Ignition Engine." *SAE TECHNICAL PAPER SERIES* (724).

Jacobs, Timothy, Dennis Assanis, and Zoran Filipi. 2003. "The Impact of Exhaust Gas Recirculation on Performance and Emissions of a Heavy-Duty Diesel Engine" (724).

Jankovic, Mrdjan, Miroslava Jankovic, and Ilya Kolmanovsky. 2000. "Constructive Lyapunov Control Design for Turbocharged Diesel Engines." *IEEE Transactions on Control Systems Technology* 8 (2): 288–299. doi:10.1109/87.826800.

Jiang, J. 1994. "Optimal Gain Scheduling Controller for a Diesel Engine." *IEEE Control System Magazine* 14 (4): 42–48.

Jindal, S., B. P. Nandwana, N. S. Rathore, and V. Vashistha. 2010. "Experimental Investigation of the Effect of Compression Ratio and Injection Pressure in a Direct Injection Diesel Engine Running on Jatropha Methyl Ester." *Applied Thermal Engineering* 30 (5): 442–448. doi:10.1016/j.applthermaleng.2009.10.004. http://dx.doi.org/10.1016/j.applthermaleng.2009.10.004.

Johnson, Tim. 2008. "Diesel Engine Emissions and Their Control: An Overview." *Platinum Metals Review* 52 (1): 23–37. doi:10.1595/147106708X248750.

Johnson, T V. 2009. "Review of Diesel Emissions and Control." *International Journal of Engine Research*. doi:10.1243/14680874JER04009.

Jung, M. 2003. "Mean-Value Modelling and Robust Control of the Airpath of a Turbocharged Diesel Engine." University of Cambridge.

Kang, Hyungsuk, and Patrick V Farrell. 2010. "Experimental Investigation of Transient Emissions (HC and NOx) in a High Speed Direct Injection (HSDI) Diesel Engine" (724).

Kao, M., and John J Moskwa. 1995. "Turbocharged Diesel Engine Modeling for Nonlinear Engine Control and State Estimation." *ASME Journal of Dynamic Systems, Measurement and Control* (117): 20–30.

Kaplan, Cafer, Ridvan Arslan, and Ali Sürmen. 2006. "Performance Characteristics of Sunflower Methyl Esters as Biodiesel." *Energy Sources, Part A: Recovery, Utilization, and Environmental Effects*. doi:10.1080/009083190523415.

Kessel, Martin Schmidt Jens-achim. 1999. "CASMA - Crank Angle Synchronous Moving Average Filtering." In *Proceedings of the 1999 American Control Conference , San Diego, CA, USA, 1999*, 1339–1340.

Kim, Duksang, Isaac Ekoto, William F Colban, and Paul C Miles. 2008. "In-Cylinder CO and UHC Imaging in a Light-Duty Diesel Engine during PPCI Low-Temperature Combustion." *SAE Int. J. Fuels Lubr.* 1 (1): 933–956. doi:10.4271/2008-01-1602.

Kirchen, Patrick, Peter Obrecht, and Konstantinos Boulouchos. 2009. "Soot Emission Measurements and Validation of a Mean Value Soot Model for Common-Rail Diesel Engines during Transient Operation." *SAE Int. J. Engines* 2 (1): 1663–1678.

Kistler. 2007. "High-Temperature Pressure Sensor." *From http://www.intertechnology.com/Kistler/pdfs/Pressure_Model_6052B1.pdf.*

Kokjohn, S. L., R. M. Hanson, D. a. Splitter, and R. D. Reitz. 2011. "Fuel Reactivity Controlled Compression Ignition (RCCI): A Pathway to Controlled High-Efficiency Clean Combustion." *International Journal of Engine Research* 12 (3): 209–226. doi:10.1177/1468087411401548.

Kopperoinen, Aaro, Matti Kytö, and Seppo Mikkonen. 2011. "Effect of Hydrotreated Vegetable Oil (HVO) on Particulate Filters of Diesel Cars." *SAE Paper*: 1210–1218. doi:10.4271/2011-01-2096.

Kouremenos, D.A., C.D. Rakopolous, and E Karvounis. 1987. "Thermodynamic Analysis of Direct Injection Diesel Engines by Multi-Zone Modelling." *In: Proceedings of the ASME-WA Meeting,* 3: 67–77.

Kuleshov, A.S. 2009. "Multi-Zone DI Diesel Spray Combustion Model for Thermo- Dynamic Simulation of Engine with PCCI and High EGR Level." *SAE International* (2009-01-1056).

Kumar, Suneel, Manish Kumar Chauhan, and Varun. 2013. "Numerical Modeling of Compression Ignition Engine: A Review." *Renewable and Sustainable Energy Reviews* 19: 517–530. doi:10.1016/j.rser.2012.11.043. http://dx.doi.org/10.1016/j.rser.2012.11.043.

L.Eriksson. 2007. "Modeling and Control of Turbocharged SI and DI Engines." *Oil & Gas Science and Technology* 62. http://ogst.ifpenergiesnouvelles.fr/articles/ogst/pdf/2007/04/ogst06101.pdf.

Ladommatos, L, S Abdelhalim, and H Zhao. 2000. "The Effects of Exhaust Gas Recirculation on Diesel Combustion and Emissions." *International Journal of Engine Research* 1. doi:10.1243/1468087001545290.

Lapuerta, Magín, Octavio Armas, and Rosario Ballesteros. 2002. "Diesel Particulate Emissions from Biofuels Derived from Spanish Vegetable Oils." *SAE Technical Paper Series*. doi:10.4271/2002-01-1657.

Lapuerta, Magín, Octavio Armas, Rosario Ballesteros, and Jesús Fernández. 2005. "Diesel Emissions from Biofuels Derived from Spanish Potential Vegetable Oils." *Fuel* 84 (6 SPEC. ISS.): 773–780. doi:10.1016/j.fuel.2004.11.010.

Ledger, J. D., R.S. Benson, and H Furukawa. 1973. "Improvement in Transient Performance of a Turbocharged Diesel Engine by Air Injection into the Compressor." *SAE Technical Paper*.

Liu, Dai. 2014. "THE COMBUSTION AND EMISSIONS USING ALTERNATIVE FUELS IN AN AUTOMOTIVE DIESEL ENGINE UNDER STEADY AND START CONDITIONS." University of Birmingham.

Liu, Derong, Hossein Javaherian, Olesia Kovalenko, and Ting Huang. 2008. "Adaptive Critic Learning Techniques for Engine Torque and Air-Fuel Ratio Control." *IEEE Transactions on Systems* 38 (4) (August): 988–93. doi:10.1109/TSMCB.2008.922019. http://www.ncbi.nlm.nih.gov/pubmed/18632389.

Ljung, Lennart. 1999. *System Identification: Theory for the User*. Second. Prentice Hall PTR.

———. 2014. "System Identification Toolbox ™ User ' S Guide."

Lu, Xingcai, Dong Han, and Zhen Huang. 2011. "Fuel Design and Management for the Control of Advanced Compression-Ignition Combustion Modes." *Progress in Energy and Combustion Science*. doi:10.1016/j.pecs.2011.03.003.

Maciejowski, J M. 2001. *Predictive Control with Constraints*. *Printice Hall*. doi:10.1016/j.compag.2008.03.003. http://books.google.be/books?hl=nl&lr=&id=HV_Y58c7KiwC&oi=fnd&pg=PR11&dq=maciejowski&ots=Cr8Z_h7wLm&sig=9YpVQljqvtEjG1MJDXkgyg7tTAA#v=onepage&q&f=false.

Maiboom, Alain, Xavier Tauzia, and Jean-François Hétet. 2008. "Experimental Study of Various Effects of Exhaust Gas Recirculation (EGR) on Combustion and Emissions of an Automotive Direct Injection Diesel Engine." *Energy*. doi:10.1016/j.energy.2007.08.010.

Mancaruso, E, S S Merola, and B M Vaglieco. 2008. "Study of the Multi-Injection Combustion Process in a Transparent Direct Injection Common Rail Diesel Engine by Means of Optical Techniques." *International Journal of Engine Research*. doi:10.1243/14680874JER01308.

Maroteaux, Fadila, and Charbel Saad. 2013. "Diesel Engine Combustion Modeling for Hardware in the Loop Applications: Effects of Ignition Delay Time Model." *Energy* 57: 641–652. doi:10.1016/j.energy.2013.03.098. http://dx.doi.org/10.1016/j.energy.2013.03.098.

Mathworks. 2014. "System Identification Toolbox User Guide - Identifying Nonlinear ARX Models." http://uk.mathworks.com/help/ident/ug/identifying-nonlinear-arx-models.html#bq5906d-1.

Millo, Federico, Luciano Rolando, and Maurizio Andreata. 2011. "Numerical Simulation for Vehicle Powertrain Development." In *Numerical Analysis - Theory and Application*.

Monyem, Abdul, and Jon H. Van Gerpen. 2001. "The Effect of Biodiesel Oxidation on Engine Performance and Emissions." *Biomass and Bioenergy* 20 (4): 317–325. doi:10.1016/S0961-9534(00)00095-7.

Murata, Y., J. Kusaka, M. Odaka, Y. Daisho, D. Kawano, H. Suzuki, H. Ishii, and Y. Goto. 2006. "Achievement of Medium Engine Speed and Load Premixed Diesel Combustion with Variable Valve Timing." *SAE Technical Paper* 2006 (724): 01–0203. doi:2006-01-0203. http://subscriptions.sae.org/content/2006-01-0203/.

Murata, Yutaka, Jin Kusaka, Yasuhiro Daisho, Daisuke Kawano, Hisakazu Suzuki, Hajime Ishii, and Yuichi Goto. 2008. "Miller-PCCI Combustion in an HSDI Diesel Engine with VVT." *SAE Int. J. Engines* 1 (1): 444–456. doi:10.4271/2008-01-0644. http://dx.doi.org/10.4271/2008-01-0644.

Nabi, Md Nurun, Md Shamim Akhter, and M. Md Z Shahadat. 2006. "Improvement of Engine Emissions with Conventional Diesel Fuel and Diesel-Biodiesel Blends." *Bioresource Technology* 97 (3): 372–378. doi:10.1016/j.biortech.2005.03.013.

Nakayama, Shigeki, Taku Ibuki, Hitoshi Hosaki, and Hiroyuki Tominaga. 2008. "An Application of Model Based Combustion Control to Transient Cycle-by-Cycle Diesel Combustion." *SAE International* 1 (1).

Nam, Kihoon, Jun Yu, and Sunghwan Cho. 2011. "Improvement of Fuel Economy and Transient Control in a Passenger Diesel Engine Using LP(Low Pressure)-EGR" (April). doi:10.4271/2011-01-0400. http://www.sae.org/technical/papers/2011-01-0400.

Nanjundaswamy, Harsha, Marek Tatur, Dean Tomazic, Mufaddel Dahodwala, Thomas Eping, Lukas Virnich, Qianfan (Harry) Xin, Walter Gorczowski, and Michael Read. 2011. "Development and Calibration of On-Board-Diagnostic Strategies Using a Micro-HiL Approach." *SAE Technical Paper 2011-01-0703*. doi:10.4271/2011-01-0703. http://www.sae.org/technical/papers/2011-01-0703.

Natti, Krishna C, and Naeim a Henein. 2012. "Particulate Matter Characterization Studies in an HSDI Diesel Engine under Conventional and LTC Regime" 1 (1): 735–745. doi:10.4271/2008-01-1086.

Navigant, and Research. 2014. "Transportation Forecast : Global Fuel Consumption." *Road Transportation Sector Consumption of Gasoline, Diesel, Biofuels, Natural Gas, Liquiefied Petroleum Gas, Electricity and Hydrogen: Global Market Forecasts, 2014-2035*: 2014–2016.

Nishio, Yui, Mamoru Hasegawa, Kojiro Tsutsumi, Junji Goto, and Norihiro Iizuka. 2013. "Model Based Control for Dual EGR System with Intake Throttlein New Generation 1.6L Diesel Engine." doi:10.4271/2013-24-0133. http://www.sae.org/technical/papers/2013-24-0133.

Omran, R, R Younes, and J C Champoussin. 2009. *Optimal Control of a Variable Geometry Turbocharged Diesel Engine Using Neural Networks: Applications on the ETC Test Cycle*. *IEEE Transactions on Control Systems Technology*. Vol. 17. doi:10.1109/TCST.2008.2001049. http://ieeexplore.ieee.org/lpdocs/epic03/wrapper.htm?arnumber=4682656.

Ortner, P, R Bergmann, H.J. Ferreau, and Luigi del Re. 2009. "Nonlinear Model Predictive Control of a Diesel Engine Airpath." In *In Proceedings of the IFAC Workshop on Control Applications of Optimisation (CAO)*, 91–96. doi:10.3182/20090506-3-SF-4003.00017. ftp://ftp.esat.kuleuven.be/pub/SISTA/ida/reports/09-89.pdf\nftp://ftp.esat.kuleuven.ac.be/pub/pub/stadius/ida/reports/09-89.pdf\nhttp://www.ifac-papersonline.net/Detailed/41888.html.

Ortner, Peter, and Luigi Re. 2007. "Predictive Control of a Diesel Engine Air Path." *IEEE Transactions on Control Systems Technology* 15 (3): 449–456.

Park, Cheolwoong, Sanghoon Kook, and Choongsik Bae. 2004. "Effects of Multiple Injections in a HSDI Diesel Engine Equipped With Common Rail Injection System." *SAE TECHNICAL PAPER SERIES*. doi:10.4271/2004-01-0127. http://cat.inist.fr/?aModele=afficheN&cpsidt=16124787.

Park, W., J. Lee, K. Min, J. Yu, S. Park, and S Cho. 2013. "Prediction of Real-Time NO Based on the in-Cylinder Pressure in Diesel Engines." *Proceedings of the Combustion Institute* 34 (2): 3075–3082.

Pedrycz, W. 1989. *Fuzzy Control and Fuzzy Systems*. Research Studies Press Ltd.

Pflaum, Heiko, Peter Hofmann, Bernhard Geringer, and Werner Weissel. 2010. "Potential of Hydrogenated Vegetable Oil (HVO) in a Modern Diesel Engine." *Fuel*. doi:10.4271/2010-32-0081.

Pickering, S G, and C J Brace. 2007. "Automated Data Processing and Metric Generation for Driveability Analysis." *Proceedings of the Institution of Mechanical Engineers, Part D: Journal of Automobile Engineering* 221 (4) (January 1): 429–441. doi:10.1243/09544070JAUTO347. http://pid.sagepub.com/lookup/doi/10.1243/09544070JAUTO347.

Quérel, C, A Bonfils, O Grondin, and Y Creff. 2013. "Control of a SCR System Using a Virtual NOx Sensor." In *In Proceedings of the 7th IFAC Symposium on Advances in Automotive Control*. Tokyo, Japan.

Quérel, C., O. Grondin, and C. Letellier. 2015. "Semi-Physical Mean-Value NOx Model for Diesel Engine Control." *Control Engineering Practice* 40 (x): 27–44. doi:10.1016/j.conengprac.2015.02.005. http://www.sciencedirect.com/science/article/pii/S0967066115000386.

R.S.Wijetunge, C.J.Brace, J.G.Hawley, and N.D.Vaughan. 2000. "Fuzzy Logic Control of Diesel Engine Turbocharging and Exhaust Gas Recirculation." In *CONTROL 2000 UKACC Inernational Conference on Control University of Cambridge*.

Rakopoulos, C D, C N Michos, and E G Giakoumis. 2005. "Study of the Transient Behavior of Turbocharged Diesel Engines Including Compressor Surging Using a Linearized Quasi-Steady Analysis." *Mechanical Engineering* 2005 (724). doi:10.4271/2005-01-0225.

Rakopoulos, C. D., and E. G. Giakoumis. 2006. "Review of Thermodynamic Diesel Engine Simulations under Transient Operating Conditions." In *SAE*. http://digitallibrary.sae.org/content/2006-01-0884.

Rakopoulos, C.D., and E.G. Giakoumis. 2006. "Review of Thermodynamic Diesel Engine Simulations under Transient Operating Conditions in Thermal Fluid Sciences 2006." *SAE Technical Paper Series*. doi:10.4271/2006-01-0884.

Rakopoulos, Constantine D., Athanasios M. Dimaratos, Evangelos G. Giakoumis, and Dimitrios C. Rakopoulos. 2010. "Investigating the Emissions during Acceleration of a Turbocharged Diesel Engine Operating with Bio-Diesel or N-Butanol Diesel Fuel Blends." *Energy* 35 (12) (December): 5173–5184. doi:10.1016/j.energy.2010.07.049. http://linkinghub.elsevier.com/retrieve/pii/S036054421000424X.

Rakopoulos, Constantine D., and Evangelos G. Giakoumis. 2009a. *Diesel Engine Transient Operation*. Springer. doi:10.1007/978-1-84882-375-4.

———. 2009b. *Diesel Engine Transient Operation*.

Rawlings, James B. 1999. "Tutorial: Model Predictive Control Technology." In *Proceedings of the American Control Conference*, 662–676. San Diego, California. doi:10.1109/ACC.1999.782911. http://ieeexplore.ieee.org/lpdocs/epic03/wrapper.htm?arnumber=782911.

Saad, Charbel, Fadila Maroteaux, Jean-Baptiste Millet, and Fabrice Aubertin. 2011. "Combustion Modeling of a Direct Injection Diesel Engine Using Double Wiebe Functions: Application to HiL Real-Time Simulations." *SAE International*. doi:10.4271/2011-24-0143. http://www.sae.org/technical/papers/2011-24-0143.

Splitter, Derek a., Reed Hanson, Sage L. Kokjohn, and Rolf D. Reitz. 2011. "Reactivity Controlled Compression Ignition (RCCI) Heavy-Duty Engine Operation at Mid-and High-Loads with Conventional and Alternative Fuels." *SAE Technical Paper Series* 1 (Ci): 0363. doi:10.4271/2011-01-0363. http://www.sae.org/technical/papers/2011-01-0363.

Splitter, Derek a., Rolf D. Reitz, and Reed Hanson. 2010. "High Efficiency , Low Emissions RCCI Combustion by Use of a Fuel Additive." *SAE Technical Paper Series* 1 (2): 2167. doi:10.4271/2010-01-2167.

Stanglmaier, Rudolf H, and Charles E Roberts. 1999. "Homogeneous Charge Compression Ignition (HCCI): Benefits , Compromises , and Future Engine Applications." *SAE TECHNICAL PAPER SERIES* (1999-01-3682).

Stewart, G., and F. Borrelli. 2008. "A Model Predictive Control Framework for Industrial Turbodiesel Engine Control." *2008 47th IEEE Conference on Decision and Control*. doi:10.1109/CDC.2008.4739384.

Stone, Richard. 1999. *Introduction to Internal Combustion Engines*. doi:10.1007/978-1-4471-4468-7_1.

Sugiyama, Kouseki, Isamu Goto, Koji Kitano, Kazuhisa Mogi, and Markku Honkanen. 2011. "Effects of Hydrotreated Vegetable Oil (HVO) as Renewable Diesel Fuel on Combustion and Exhaust Emissions in Diesel Engine." *SAE Paper* 5 (1): 2138–2150. doi:10.4271/2011-01-1954.

Suzuki, Hisakazu, Rahman Montajir, Terunao Kawai, Hajime Ishii, and Yuichi Goto. 2003. "Exhaust Emission Behavior of Mixed Fuels Having Different Component Cetane Number and Boiling Point." *JSAE/SAE*.

Syrimis, M., and D. N. Assanis. 2003. "Knocking Cylinder Pressure Data Characteristics in a Spark-Ignition Engine." *Journal of Engineering for Gas Turbines and Power* 125 (2): 494. doi:10.1115/1.1560709.

http://gasturbinespower.asmedigitalcollection.asme.org/article.aspx?articleid=1421618.

Systems, Mechatronical, Johannes Kepler, D Alberer, L Re, S Winkler, P Langthaler, Daniel Alberer, Luigi Re, Stephan Winkler, and Peter Langthaler. 2005. "Virtual Sensor Design of Particulate and Nitric Oxide Emissions in a DI Diesel Engine Virtual Sensor Design of Particulate and Nitric Oxide Emissions in a DI Diesel Engine."

Tesfa, B, R Mishra, F Gu, and A D Ball. 2014. "NOx Emission Prediction Based on Measurement of in-Cylinder Pressure for CI Engine Running with Diesel and Biodiesel."

Turner, J.W.G., a. Popplewell, R. Patel, T.R. Johnson, N.J. Darnton, S. Richardson, S.W. Bredda, et al. 2014. "Ultra Boost for Economy: Extending the Limits of Extreme Engine Downsizing." *SAE International* 7 (1): 387–417. doi:10.4271/2014-01-1185. http://www.sae.org/technical/papers/2014-01-1185.

Tutuianu, Monica, Alessandro Marotta, Heinz Steven, Eva Ericsson, Takahiro Haniu, Noriyuki Ichikawa, and Hajime Ishii. 2013. "Development of a World-Wide Worldwide Harmonized Light Duty Driving Test Cycle (WLTC)." In *68th GRPE*. https://www2.unece.org/wiki/download/attachments/9798086/WLTP-DHC-18-06e.doc?api=v2.

Visakhamoorthy, S, T Tzanetakis, D Haggith, A Sobiesiak, and J Z Wen. 2012. "Numerical Study of a Homogeneous Charge Compression Ignition (HCCI) Engine Fueled with Biogas." *Applied Energy* 92: 437–446.

Wahlstrom, J., and L. Eriksson. 2011. "Modelling Diesel Engines with a Variable-Geometry Turbocharger and Exhaust Gas Recirculation by Optimization of Model Parameters for Capturing Non-Linear System Dynamics." *Proceedings of the Institution of Mechanical Engineers, Part D: Journal of Automobile Engineering* 225 (x): 960–986. doi:10.1177/0954407011398177.

Watson, N, and M.S. Janota. 1982. *Turbocharging the Internal Combustion Engine*. *London: MacMillan*. Vol. 130. doi:10.1038/130259a0.

Watson, N, and M Marzouk. 1977. "A Non-Linear Digital Simulation of Turbocharged Diesel Engines under Transient Conditions." *SAE Technical Paper*.

Wijetunge, R S, C J Brace, J G Hawley, and N D Vaughan. 1999. "Dynamic Behaviour of a High Speed Direct Injection Diesel Engine." *SAE* (724).

Winterborne, D.E., C Thiruarooran, and P.E. Wellstead. 1977. "A Wholly Dynamical Model of a Turbocharged Diesel Engine for Transfer Function Evaluation." *SAE Technical Paper*.

Yao, Mingfa, Zhaolei Zheng, and Haifeng Liu. 2009. "Progress and Recent Trends in Homogeneous Charge Compression Ignition (HCCI) Engines." *Progress in Energy and Combustion Science* 35 (5): 398–437. doi:10.1016/j.pecs.2009.05.001. http://dx.doi.org/10.1016/j.pecs.2009.05.001.

Yokomura, Hitoshi, Susumu Kouketsu, Seijiro Kotooka, and Yoshiyuki Akao. 2004. "Transient EGR Control for a Turbocharged Heavy Duty Diesel Engine." *SAE Technical Paper 2011-01-0703*. doi:10.4271/2004-01-0120.

York, a P E, a Tsolakis, K H Jürgen Buschow, W Cahn Robert, C Flemings Merton, Ilschner Bernard, J Kramer Edward, Mahajan Subhash, and Veyssière Patrick. 2010. "Cleaner Vehicle Emissions." *Encyclopedia of Materials: Science and Technology*. http://www.sciencedirect.com/science/article/pii/B9780080431529022533.

Yunyu, Hu, Korfer Thomas, Thorsten Schnorbus, Michele Miccio, and Joschka Schaub. 2014. "Reduction of Engine-out Emission and Fuel Consumption by Variable EGR Distribution in Diesel and Multi Fuel Engines." In *Internationales Stuttgarter Symposium*.

Zhang, Fan. 2013. "Spray , Combustion and Emission Characteristics of Dieseline Fuel." PhD thesis, University of Birmingham.

Zhao, Dezong, Cunjia Liu, Richard Stobart, Jiamei Deng, Senior Member, Edward Winward, and Guangyu Dong. 2014. "An Explicit Model Predictive Control Framework for Turbocharged Diesel Engines." *IEEE Transaction on Industrial Electronics* 61 (7): 3540–3552.

Zwaanenbug, Koos. 2008. "Next-Generation Hardware-in-the-Loop Systems for Commercial Vehicle Applications." *SAE Technical Paper Series* (724).